Clin Neuroradiol
https://doi.org/10.1007/s00062-021-01075-5

ABSTRACTS

56. Jahrestagung der Deutschen Gesellschaft für Neuroradiologie e. V.

Virtuelle Konferenz

Wissenschaftliche Leitung

Prof. Dr. med. Jennifer Linn (Dresden)

Dieses Supplement wurde von der Deutschen Gesellschaft für Neuroradiologie finanziert.

Published online: 20 September 2021

Inhaltsverzeichnis

Abstracts

Bei den mit * gekennzeichneten Autoren handelt es sich um die präsentierenden Autoren.

[19] Einfluss der Charakteristika von Vergleichskollektiven auf die automatische Hirnatrophieschätzung – wie viele Vergleichssubjekte sind notwendig?

Christian Rubbert[1*], Luisa Wolf[1], Bernd Turowski[1], Dennis Hedderich[2], Christian Gaser[3], Robert Dahnke[3, 4, 5], Julian Caspers[1]

[1]Heinrich-Heine-Universität Düsseldorf, Medizinische Fakultät, Institut für Diagnostische und Interventionelle Radiologie, Düsseldorf, Deutschland
[2]Abteilung für Diagnostische und Interventionelle Neuroradiologie, Klinikum rechts der Isar der Technischen Universität München, München, Deutschland
[3]Klinik für Neurologie, Klinik für Psychiatrie, Universitätsklinikum Jena, Jena, Deutschland
[4]Lehrstuhl für Psychologie, Friedrich-Schiller-Universität Jena, Jena, Deutschland
[5]Center of Functionally Integrative Neuroscience, Aarhus University, Aarhus, Dänemark

Hintergrund: Softwarebasierte Ansätze zur Hirnatrophieschätzung halten zunehmend Einzug in die neuroradiologische Diagnostik. Hierbei werden MRTs mit einem Normalkollektiv (NK) verglichen. Der Einfluss des NK auf die Ergebnisse ist nicht hinreichend untersucht. Wir untersuchten die folgenden Fragen: 1) Wie viele Vergleichssubjekte sind für eine konsistente Atrophieschätzung notwendig? 2) Führen unterschiedliche NKs bei der Abschätzung regionaler Atrophie zu unterschiedlichen Ergebnissen?

Methoden: Im ersten Schritt wurden die folgenden NK in einem NK_{komb} kombiniert: HCP-A, IXI, Rockland sowie die gesunden Kontrollen (GK) von PPMI und ADNI ($n=3579$). Als Probanden für die Atrophieschätzung wurden 43 Patienten mit Morbus Alzheimer (AD) aus ADNI selektiert (T1 3-D-Schichtdicke ≤1 mm sowie ≥100 alters- und geschlechtsspezifische Vergleichssubjekte im NK_{komb} verfügbar). Die voxelweise Abweichung des Volumens der grauen Substanz wurde anhand von Vergleichskollektiven mit 2–100 zufällig aus NK_{komb} ausgewählten Vergleichssubjekten mittels der automatisierten und frei verfügbaren Software veganbagel unter Einsatz von CAT12/SPM12 errechnet. Der Mittelwert der voxelweisen Standardabweichung (mSD) dieser z-Werte wurde über 100 Wiederholungen berechnet (Abb. 1). Die mSD wurde gegen die Anzahl der Vergleichssubjekte aufgetragen. Die Kniepunkte dieser Kurven wurden als die Minimalanzahl notwendiger Vergleichssubjekte in einem NK definiert. Abschließend wurden alle AD-Patienten und zusätzlich aus ADNI gematchten GK bestimmt, für die in den einzelnen NK mindestens die etablierte Minimalanzahl an Vergleichssubjekten vorlag. Für diese wurden mittels jedem einzelnen NK Atrophiekarten berechnet, und die mesiotemporale Atrophie wurde qualitativ durch 2 Radiologen bestimmt, um AD und GK zu differenzieren.
Ergebnisse: Der mittlere Kniepunkt lag über alle Altersstufen bei 11,5 ± 0,9 Vergleichssubjekten (Abb. 2).
Für 18 AD/18 GK lagen in den NK genügend Vergleichssubjekte vor. Die beiden Radiologen stimmten in allen Fällen in der Diagnose AD/GK überein (Kappa für das Ausmaß der Atrophie: 0,98). Sensitivität und Spezifität betrugen für HCP-A: 92,3 %/72,7 %, IXI: 91,7 %/69,6 %, PPMI: 92,3 %/72,7 % und Rockland: 100 %/73,9 %.
Fazit: Für eine konsistente Atrophieschätzung müssen mindestens 12 alters- und geschlechtsspezifische Vergleichssubjekte vorliegen. Eine qualitative Abschätzung regionaler Atrophie ist verlässlich und mit ei-

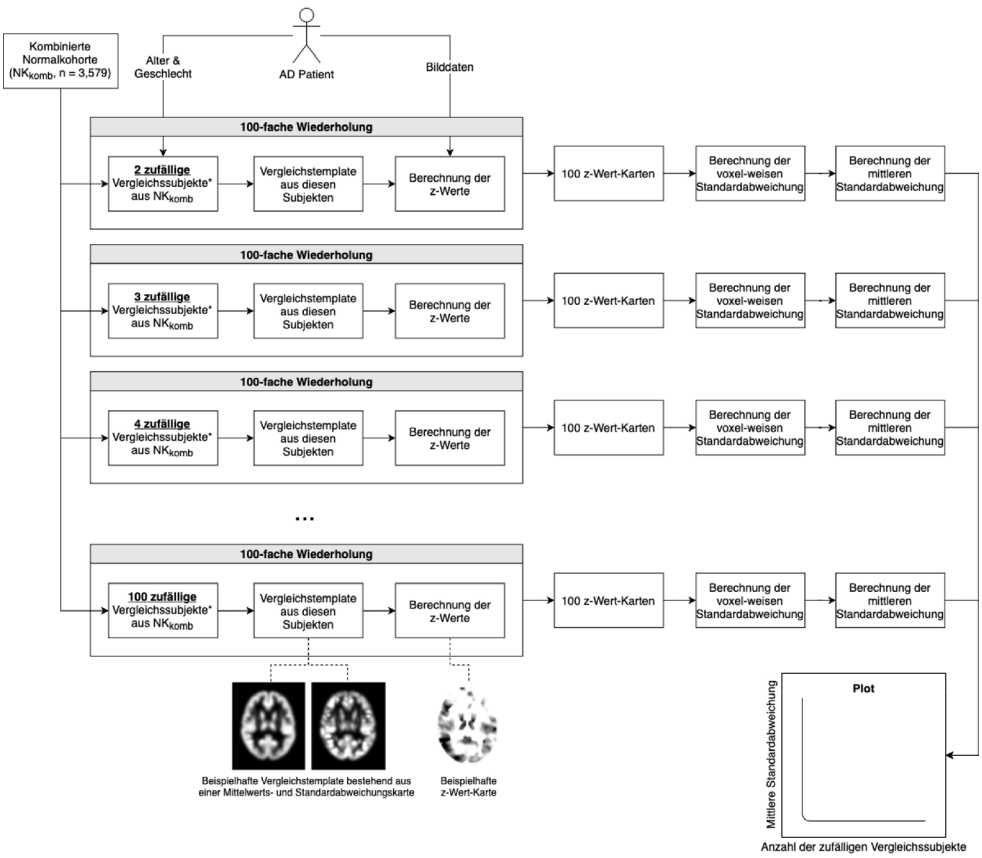

Abb. 1 | 19 Flowchart der Analyse zur Bestimmung der notwendigen Minimalanzahl von Vergleichssuhletden in einem Normkollektiv zur automatisierten Abschätzung der Hirnatrophie*. Gleiches Geschlecht wie der AD-Patient sowie Alter ±2 Jahre

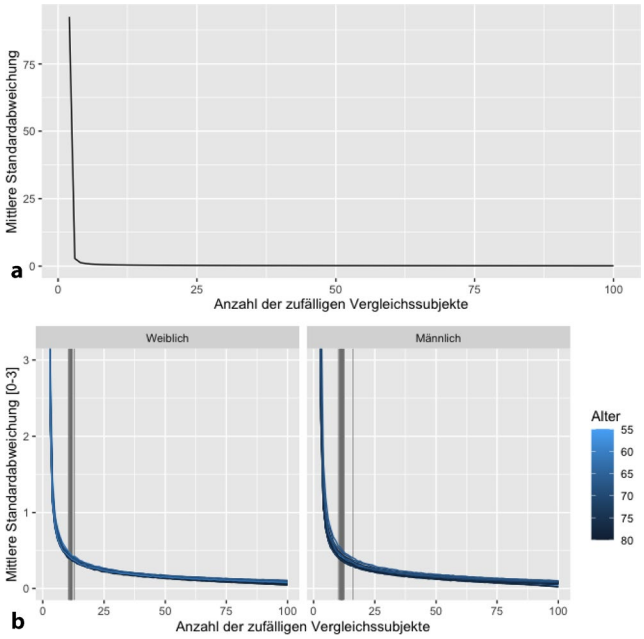

Abb. 2 | 19 **a** Mittlere Standardabweichung der voxd-weisen z-Werte über alle Wiederholungen aufgetragen gegen die Anzahl der zufälligen Vergleichssubjekte für einen 67-jährigen AD-Patienten aus der ADN I-Datenbank. Der Kniepunkt für diesen Patienten lag bei 11 Vergleichssubjekten, **b** Entsprechende Kurven aller AD-Patienten (mit verkürzter y-Achse). Die Kniepunkte sind durch *vertikale graue Linien* markiert

ner exzellenten Übereinstimmung unabhängig von der zugrundeliegenden NK möglich.

[20] Improved detection of cavernous sinus invasion of pituitary macroadenomas via ultra-high-field 7 T MRI

Felix Eisenhut[1*], Manuel Schmidt[1], Elisabeth Heynold[2], Soheil Arinrad[2], Sven-Martin Schlaffer[2], Michael Buchfelder[2], Arnd Dörfler[1]

[1]Radiologisches Institut, Universitätsklinikum Erlangen, Abteilung für Neuroradiologie, Erlangen, Germany
[2]Abteilung für Neurochirurgie, Universitätsklinikum Erlangen, Erlangen, Germany

Background: To compare 7 T magnetic resonance imaging (MRI) of pituitary gland (PG) macroadenomas with standard MRI and intraoperative findings regarding lesion detection, intrasellar adenoma localization and invasion of the cavernous sinus (CS).
Methods: Patients with a clinically suspected PG lesion (e. g. due to bitemporal hemianopsia) underwent preoperative 1.5 T or 3 T and 7 T MRI. Evaluation of image quality (IQ) regarding overall IQ, anatomical parameters (border between the PG and the CS; border between anterior and posterior PG; optic nerve/oculomotor and trigeminal nerve differentiation) and artefacts as well as a qualitative (lesion detection, lesion location, CS invasion) and quantitative (lesion size, extent of cavernous sinus invasion using the Knosp score) analysis of the datasets was performed and compared to intraoperative findings.
Results: A total of 39 patients underwent preoperative 1.5 or 3 T and 7 T MRI; in 9 patients both 1.5 or 3 T and 7 T MRI allowed the detection of a macroadenoma. Overall IQ of 7 T MRI was rated higher than IQ of 1.5 and equal to 3 T MRI ($IQ_{overall\ 1.5T} = 2.00 \pm 0.71$, $IQ_{overall\ 7T} = 2.80 \pm 0.45$; $IQ_{overall\ 3T} = 3.00 \pm 0.0$, $IQ_{overall\ 7T} = 3.0 \pm 0.0$). IQ of each evaluated anatomical parameter was rated higher in 7 T MRI than in 1.5 T and higher or equal than in 3 T MRI. There was no significant image IQ difference regarding susceptibility or motion artefacts. There was complete congruence regarding intrasellar lesion localization between 1.5/3 T and 7 T MRI ($n_{right} = 3$; $n_{medial} = 3$; $n_{left} = 3$) and a strong correlation regarding lesion size determination. 7 T MRI showed better agreement with intraoperative findings than 1.5 or 3 T MRI regarding a CS invasion with a correct radiologic assessment in 66,6 % of all patients via 7 T MRI versus a correct radiologic assessment in 55,6 % of all patients via 1.5/3 T MRI.
Discussion: Whereas both standard 1.5 or 3 T MRI and 7 T MRI equally allowed macroadenoma detection and correct intrasellar localization with a strong correlation regarding intra- and suprasellar lesion size determination, ultra-high-field 7 T MRI depicts significantly better the invasion of the CS with high correlation to intraoperative findings. In consequence, 7 T MRI can help to improve neurosurgical resection because of its detailed delineation of tumour boundaries with possible preservation of healthy tissue.
Conclusion: In addition to granting exact localization and size of PG macroadenomas, 7 T MRI yields more accurate information regarding a CS invasion with better agreement with intraoperative findings than 1.5 or 3 T MRI.

[22] Diffusion microstructure imaging in progressive supranuclear palsy: reduced axonal volumes in the superior cerebellar peduncles, dentatorubrothalamic crossing, ventromedial thalami and frontomesial white matter

Alexander Rau[1*], Wolfgang Jost[1], Elias Kellner[2], Theo Demerath[1], Marco Reisert[2], Horst Urbach[1]

[1]Universitätsklinikum Freiburg, Klinik für Neuroradiologie, Freiburg im Breisgau, Germany
[2]Universitätsklinikum Freiburg, Medizinphysik, Freiburg im Breisgau, Germany

Background: The differentiation between Parkinson's disease (PD) and atypical Parkinson syndromes such as progressive supranuclear palsy (PSP), multiple system atrophy (MSA) and corticobasal degeneration is challenging in clinical practice. We evaluated whether diffusion microstructure imaging (DMI; calculation of diffusivities and volume fractions of intra- and extra-axonal and csf-compartments based on multishell-DWI) enables the identification of PSP patients within a cohort of suspected atypical parkinsonism.
Methods: In a retrospective study, DMI parameters were analyzed in patients with clinically suspected atypical parkinsonism syndromes and healthy controls (HC). Between 2018 and 2020, an exploration cohort was used to identify voxel- and region-based differences and to calculate cut-off values in a receiver operating characteristic analysis. Afterwards, the accuracy was tested on a single subject level.
Results: In the exploration cohort, 52 PSP patients were compared to 20 PD, 26 MSA, and 7 corticobasal syndrome patients, as well as 25 HC. PSP patients showed widespread intraaxonal volume loss in the superior cerebellar peduncles, the dentatorubrothalamic tracts, the ventromedial thalami and the frontal white matter (each $p < 0.001$). Especially the ventromedial thalami showed a high area under the curve of 0.899 between PSP and others. The validation cohort ($n = 25$) consisted of 12 PSP patients, eight with PD, four with MSA, while one patient had no final diagnosis of parkinsonism. The accuracy of the DMI approach in identifying PSP patients was confirmed in the thalamus and the frontal white matter (accuracy 0.96 each).
Discussion: DMI reveals a characteristic regional pattern of axonal degeneration in PSP patients. This fits well with published regions of specific changes in PSP in terms of atrophy and alterations in diffusion weighted imaging.
Conclusion: DMI might be used to identify PSP patients on an individual level in a collective with suspected atypical Parkinson syndromes.

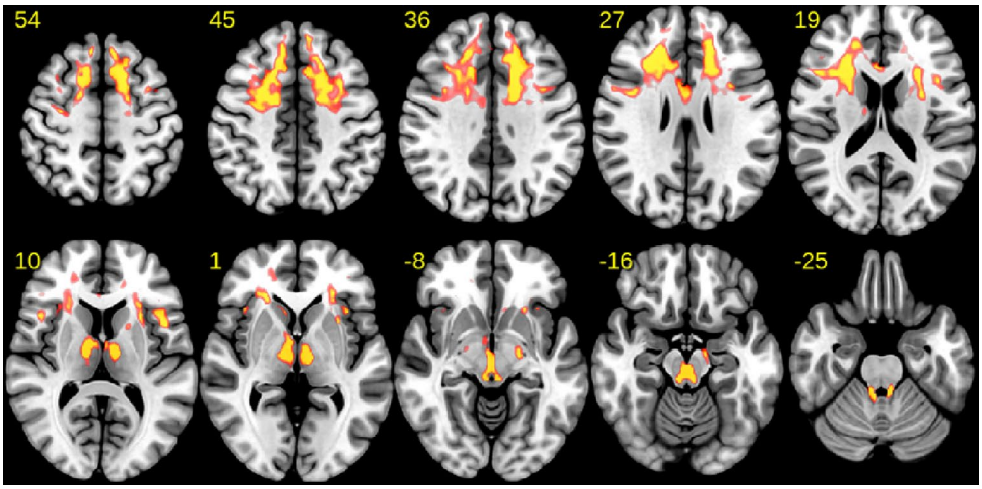

Fig. 1 | 22 Voxel-wise comparisons of the intra-axonal volume between PSP and a pooled comparison group of PD, MSA, corticobasal syndrome and healthy controls.

[23] Regionale Signatur des Normaldruckhydrozephalus in der [18F]FDG-PET

Alexander Rau[1*], Lars Frings[2], Ganna Blazhenets[2], Nils Schröter[3], Philipp Tobias Meyer[2], Horst Urbach[1]

[1]Universitätsklinikum Freiburg, Klinik für Neuroradiologie, Freiburg im Breisgau, Deutschland
[2]Universitätsklinikum Freiburg, Klinik für Nuklearmedizin, Freiburg im Breisgau, Deutschland
[3]Universitätsklinikum Freiburg, Klinik für Neurologie und Neurophysiologie, Freiburg im Breisgau, Deutschland

Hintergrund: Erweiterte Ventrikel und enge vertexnahe Subarachnoidalräume in der MRT (NPH-Aspekt) sind Zeichen des idiopathischen Normaldruckhydrozephalus (iNPH) in der radiologischen Diagnostik. Für die FDG-PET wurde bisher keine diagnostische regionale Signatur etabliert. Wir gingen der Frage nach, ob sich der zerebrale Glukosemetabolismus bei Patienten mit und ohne NPH-Aspekt unterscheidet.

Methoden: Wir werteten retrospektiv FDG-PET-Daten von Patienten aus, die hausintern sowohl mittels FDG-PET als auch MRT zur Abklärung einer neurodegenerativen Erkrankung im Zeitraum 2010 bis 2020 untersucht wurden. Anhand visueller und SVM-gestützter Expertenbegutachtung wurden die Gruppen „NPH-Aspekt“ ($N=88$) versus „kein NPH-Aspekt“ ($N=258$) definiert. Bei den Patienten mit NPH-Aspekt wurden zudem diejenigen mit entsprechenden klinischen Symptomen ($N=46$; möglicher iNPH) und einem positiven Tap-Test ($N=13$; wahrscheinlicher iNPH) identifiziert. Zudem wurde eine neuronorme Kontrollgruppe ($N=45$) zum Vergleich genutzt. Die FDG-PET-Daten wurden räumlich normalisiert, geglättet und skaliert (Referenz: Hirnparenchym) sowie mittels SPM12 verglichen (ANCOVA mit Covariate Alter; $p<0{,}05$, FWE-korrigiert, $k>100$ Voxel). In einer konfirmatorischen Subgruppenanalyse wurden die FDG-PET von Patienten mit möglichem oder wahrscheinlichem iNPH mit jenen ohne NPH-Aspekt verglichen.
Ergebnisse: Patienten mit NPH-Aspekt zeigten eine höhere relative FDG-Aufnahme beidseits parazentral im Bereich der Mantelkante. Dies wurde bestätigt in der Subgruppenanalyse von Patienten mit der klinischen Bild eines iNPH. Eine Verminderung der FDG-Aufnahme

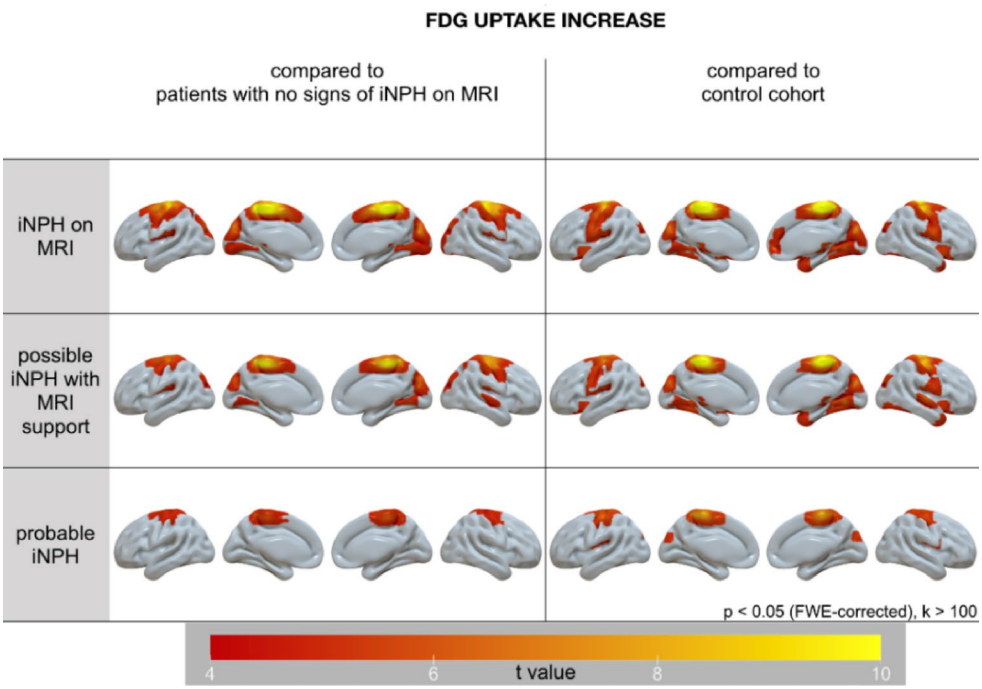

Abb. 1 | 23

zeigte sich hingegen lediglich im Bereich der Seitenventrikel (in erster Linie Partialvolumeneffekt).
Diskussion: Die vertexnahe Enge des Hirngewebes beim iNPH in der MRT findet ihre Entsprechung in der FDG-PET als dort lokalisierter relativer Hypermetabolismus (insbesondere im Vergleich zu Patienten mit möglicher Neurodegeneration, als wichtigste Differenzialdiagnose). Die diagnostische Wertigkeit dieser Signatur ist in einer prospektiven Studie zu validieren.
Fazit: Patienten mit NPH weisen einen relativen vertexnahen Hypermetabolismus auf.

[28] Serielle CT-Perfusion zum Vasospasmus-Monitoring bei Patienten mit aneurysmatischer Subarachnoidalblutung

Ole Bettinger[1*], Olav Jansen[1], Michael Synowitz[2], Charlotte Flüh[2], Nikolas Hagen[2], Friederike Austein[1], Naomi Larsen[1]

[1]Klinik für Radiologie und Neuroradiologie, Universitätsklinikum Schleswig-Holstein, Campus Kiel, Kiel, Deutschland
[2]Klinik für Neurochirurgie, Universitätsklinikum Schleswig-Holstein, Campus Kiel, Kiel, Deutschland

Hintergrund: Zerebrale Vasospasmen nach aneurysmatischer Subarachnoidalblutung (SAB) sind mit einer hohen Morbidität und Mortalität assoziiert. Bei beatmeten Patienten stützt sich das Monitoring hauptsächlich auf die transkranielle Dopplersonographie (TCD). Ziel dieser Studie war die Evaluation zusätzlich durchgeführter serieller CT-Perfusionen hinsichtlich eines diagnostischen Mehrwerts für die Detektion von Vasospasmen.
Methoden: Retrospektiv wurden alle Patienten eingeschlossen, bei denen gemäß der klinikeigenen SOP zusätzlich zur täglichen TCD eine CTP an standardisierten Tagen nach SAB (1, 5, 7, 10) durchgeführt wurde. Die Sensitivität und Spezifität der TCD und des CTP-Parameters Tmax mit 4 Schwellenwerten (4 s, 6 s, 8 s, und 10 s) wurden berechnet, und die beiden Monitoringmethoden TCD alleine vs. TCD + CTP verglichen. Als Goldstandard diente die DSA und CT- oder MR-Verlaufskontrollen.
Ergebnisse: Es entsprachen 29 Patienten mit insgesamt 106 Perfusionszeitpunkten den Einschlusskriterien. An 25/106 Messzeitpunkten bei 10/29 Patienten lagen Vasospasmen vor. Durch die seriellen CTPs wurden 9/25 Vasospasmen (36 %) bei 6/29 Patienten detektiert, die im TCD-Monitoring nicht erkannt wurden. TCD zeigte eine Sensitivität von 0,6 und Spezifität von 0,63 (AUC 0,615). Tmax >4 s wies eine Sensitivität von 0,927 und Spezifität von 0,8 auf (AUC 0,863), Tmax >6 s eine Sensitivität von 0,439 und Spezifität von 0,975 (AUC 0,707). Die kombinierte Monitoringmethode TCD + CTP wies eine signifikant bessere Detektion von Vasospasmen auf im Vergleich zu TCD alleine ($p=0{,}008$).
Diskussion: CD zeigt in dieser Studie eine mit vormals publizierten Daten vergleichbare geringe Sensitivität [1]. Die Erweiterung des Monitorings um serielle CTPs in der Phase mit der höchsten Vasospasmus-Inzidenz erhöht die diagnostische Genauigkeit signifikant, geht aber mit einer erhöhten Dosis ionisierender Strahlung einher.
Fazit: Das Monitoring mit TCD und serieller CTP detektiert signifikant mehr Vasospasmen als TCD alleine und kann das Outcome schwerbetroffener SAB-Patienten potenziell verbessern. Der Schwellenwert Tmax >4 s liefert die höchste diagnostische Genauigkeit.

Literatur

1. Lysakowski C, Walder BC, MC, et al. Transcranial Doppler versus angiography in patients with vasospasm due to a ruptured cerebral aneurysm: A systematic review. Stroke. 2001;32:2292–8.

[33] Support vector machine(SVM)-based spontaneous intracranial hypotension (SIH) detection

Philipp Arnold[1*], Emre Kaya[1], Marco Reisert[2], Niklas Lützen[1], Philippe Dovi-Akue[1], Christian Fung[3], Jürgen Beck[3], Horst Urbach[1]

[1]Uniklinik Freiburg, Klinik für Neuroradiologie, Freiburg im Breisgau, Germany
[2]Uniklinik Freiburg, Medizinphysik, Freiburg im Breisgau, Germany
[3]Uniklinik Freiburg, Klinik für Neurochirurgie, Freiburg im Breisgau, Germany

Background and purpose: To develop a fully automatic algorithm for the MRI identification of patients with spontaneous intracranial hypotension (SIH).
Material and methods: A support vector machine (SVM) was trained with structured reports of 140 patients with suspected SIH. Venous sinuses and basal cisterns were segmented on contrast-enhanced T1-weighted MPRAGE sequences using a convolutional neural network (CNN). For the segmented sinuses and cisterns, 56 radiomic features were extracted which served as input data for the SVM. The algorithm was validated with an independent cohort of 34 patients with proven CSF leaks and 27 patients who had MPRAGE scans for other reasons.
Results: The venous sinuses and the suprasellar cistern had the best discriminative power to separate SIH and non-SIH patients. On a combined score with 2 points, mean SVM-score was 1.41 (± 0.60) for the SIH and 0.30 (±0.53) for the non-SIH patients, respectively ($p<0.001$). AUC was 0.91.
Conclusion: A fully automatic algorithm analyzing a single MRI sequence separates SIH and non-SIH patients with a high diagnostic accuracy. It may help to consider the need of invasive diagnostics and transfer to a SIH center.

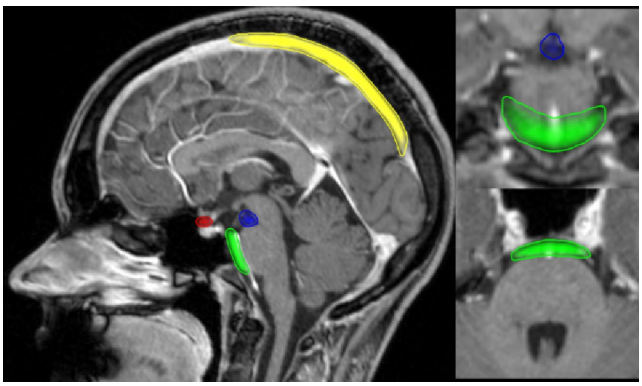

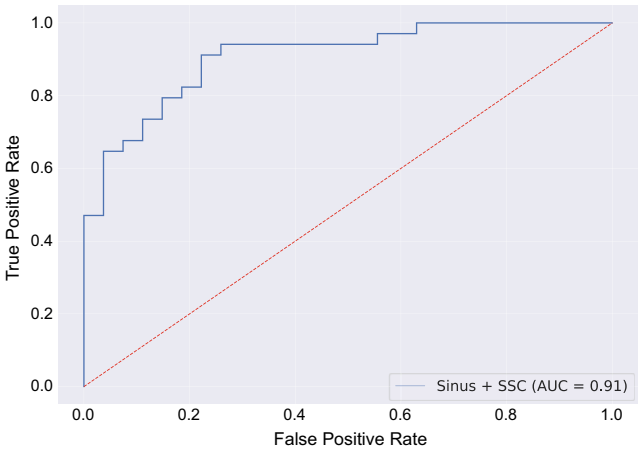

Abb. 1 | 33

[39] Complete One-Stop-Shopping im Angioraum

Philip Hölter[1*], Stefan Lang[1], Vanessa Beuscher[2], Bernd Kallmünzer[2], Michael Manhart[3], Stefan Schwab[2], Arnd Dörfler[1]

[1]Friedrich-Alexander-Universität Erlangen-Nürnberg, Neuroradiologische Abteilung, Erlangen, Deutschland
[2]Friedrich-Alexander-Universität Erlangen-Nürnberg, Neurologische Abteilung, Erlangen, Deutschland
[3]Siemens Healthcare GmbH Advanced Therapies Innovation SHS AT IN PRJ2, Forchheim, Deutschland

Hintergrund: Flachdetektor-Computertomographie (FDCT) ermöglicht „one-stop shopping" bei akutem ischämischem Schlaganfall (AIS). Obwohl der zervikale Gefäßstatus entscheidend für das weitere Prozedere ist, fehlen derzeit hierfür ausgelegte FDCT-Protokolle. Ziel dieser prospektiven Studie war die Implementierung eines neuen multimodalen FDCT-Protokolls, das um die Bildgebung von Halsgefäßen bei AIS-Patienten erweitert wurde. Ferner sollten mögliche zeitsparende Effekte dieses neuen multimodalen FDCT-Ansatzes evaluiert werden.
Methoden: Insgesamt 16 Patienten wurden eingeschlossen. Acht Patienten mit AIS aufgrund eines großen Gefäßverschlusses (LVO) wurden prospektiv analysiert und erhielten eine erweiterte FDCT-Bildgebung (native Flachdetektor-Computertomographie [NE-FDCT], Flachdetektor-Computertomographie-Perfusion [FDCTP], Flachdetektor-Computertomographie-Angiographie [FDCTA]). Zeitpunkte des Workflows wurden registriert und Zeitintervalle berechnet. Zum Vergleich wurden 8 AIS-Patienten mit multimodaler CT-Bildgebung (native Computertomographie [NE-CT], Computertomographie-Perfusion [CTP] und Computertomographie-Angiographie [CTA]) retrospektiv evaluiert.
Ergebnisse: Alle FDCT-Datensätze waren von diagnostischer Qualität. LVO-Nachweis und Ausschluss einer intrazerebralen Blutung sowie die Quantifizierung des Perfusionsdefizits waren zuverlässig möglich. Die mittlere „door-to-image time" war für die FDCT-Gruppe und die Kontrollgruppe vergleichbar (CT: 30 min, IQR 27–58; FDCT: 44,5 min, IQR 31–55, $p=0{,}491$). „Door-to-puncture time" (CT: 79,5 min, IQR 65–90; FDCT: 59,5 min, IQR 51–67; $p=0{,}016$) und „image-to-puncture time" (CT: 44 min, IQR 30–50; FDCT: 14 min, IQR 12–18; $p<0{,}001$) waren signifikant kürzer, wenn Patienten direkt FDCT-Bildgebung erhielten.
Diskussion: Die Verwendung eines neuen, erweiterten multimodalen FDCT-Protokolls als First-line-imaging-Ansatz bei AIS-Patienten ist möglich und mit der multimodalen CT-Bildgebung vergleichbar. FDCT-Bildgebung könnte so den Workflow straffen, da sich der Patiententransport auf die Richtung von der Notaufnahme zur Angiosuite konzentriert.
Fazit: Das neue erweiterte FDCT-Protokoll ermöglicht eine diagnostische Bildgebung innerhalb der Angiosuite, einschließlich der Darstellung der zervikalen Gefäße. Die Zeitspanne von der ersten Bildgebung bis zur Schlaganfallbehandlung kann somit verkürzt werden.

[45] A lesion-level deep learning approach to predict enhancing lesions from nonenhanced images in multiple sclerosis

Nikhil Sasidharan[1], Timo Loehr[1,2], Matthias Bussas[3], Dominik Sepp[1], Lioba Grundl[1], Daria Bischl[1], Isabelle Riederer[1], Karolin Paprottka[1], Marie Metz[1], David Schinz[1], Christiane Gasperi[3], Achim Berthele[3], Sophia Grahl[3], Bernhard Hemmer[3], Claus Zimmer[1], Björn Menze[2], Mark Mühlau[3], Jan Kirschke[1], Benedikt Wiestler[1*]

[1]Klinikum rechts der Isar, Technical University of Munich, Neuroradiology, München, Germany
[2]Technische Universität München, Department of Informatics, München, Germany
[3]Klinikum rechts der Isar der Technischen Universität München, Technical University of Munich, Neurology, München, Germany

Background: In patients with multiple sclerosis (MS), contrast enhancing lesions are an important marker of disease activity. Identifying these on non-enhanced images would potentially allow omitting contrast agents in MR examinations of MS patients.
Methods: In total, 485 consecutive patients with 1034 exams from a prospective observational cohort of multiple sclerosis patients were included in this analysis (scanned between 01/2008 and 09/2017). 10,311 lesion-level patches were generated from 297 patients to train a deep convolutional neural network (85 % training, 15 % validation) to discriminate between enhancing and non-enhancing lesions. Manual annotation of individual lesions enhancement on T1-weighted images after contrast administration served as the ground truth. This network was then tested on the remaining 188 patients. An external data set of 29 patients was additionally used to validate results. Network performance was statistically assessed by AUC, sensitivity, specificity and accuracy analysis.
Results: MR examinations of 485 patients were analyzed. Out of this dataset, 297 patients (mean age: 34.8 years ±9.7, ratio female:male 196:101) were used for training and validating the network and 188 patients (mean age: 33.9 years ±9.1, ratio female:male 130:58) were used for testing. On the lesion level, an AUC of 0.905 was observed. A prespecified probability threshold of 0.75 allowed for identification of enhancing lesions with a sensitivity of 47.65 %, specificity of 97.27 % and accuracy of 95.27 %. On patient level, the network exhibited a sensitivity of 82.76 %, specificity of 66.15 % and accuracy of 71.28 %. Data from an external center confirmed these results.
Conclusions: A deep learning approach at the lesion level is effective in predicting contrast-enhancing lesions from nonenhanced MRI images of patients with MS.

References

1. Huang G, Liu Z, Van Der Maaten L, Weinberger KQ. Densely Connected Convolutional Networks. 2017 IEEE Conf Comput Vis Pattern Recognit CVPR. Honolulu, HI IEEE. 2017; https://doi.org/10.1109/CVPR.2017.243.
2. Narayana PA, Coronado I, SJ S, Wolinsky JS, Lublin FD, Gabr RE. Deep Learning for Predicting Enhancing Lesions in Multiple Sclerosis from Noncontrast MRI. Radiology. 2020;294(2):398–404. https://doi.org/10.1148/radiol.2019191061.
3. Lesjak Ž, Galimzianova A, Koren A, et al. A novel public MR image dataset of multiple sclerosis patients with lesion segmentations based on multi-rater consensus. Neuroinform. 2018;16(1):51–63. https://doi.org/10.1007/s12021-017-9348-7.

Fig. 1 | 45

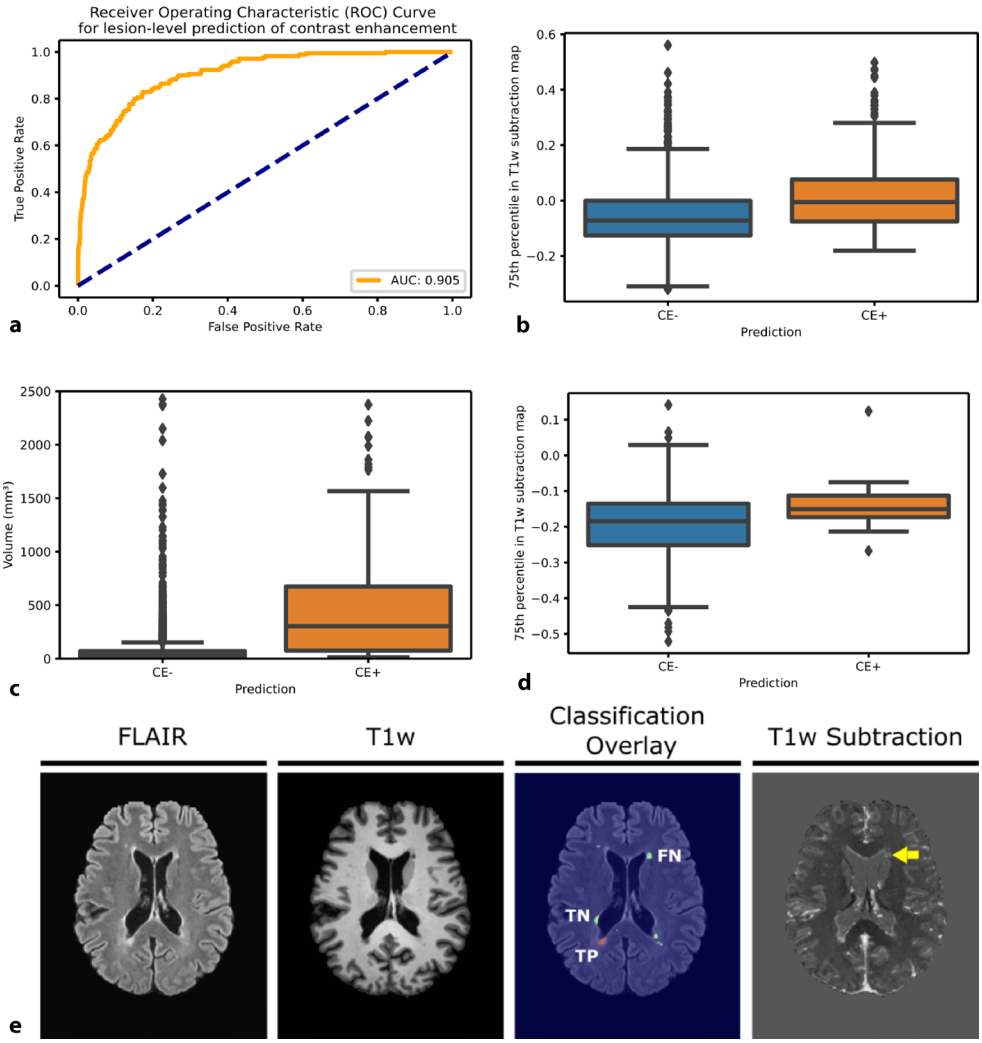

[48] Additional use of a deep learning algorithm in detecting intracranial hemorrhages on emergency computed tomographies of a radiology and neuroradiology department with teleradiology

Almut Kundisch[1], Alexander Hönning[2], Sven Mutze[3,4], Lutz Kreissl[3], Johannes Lemcke[5], Maximilian Sitz[5], Paul Sparenberg[6], Leonie Gölz[3*,4]

[1]Zentrum für Notfalltraining, BG Klinikum Unfallkrankenhaus Berlin gGmbH, Berlin, Germany
[2]Zentrum für klinische Forschung, BG Klinikum Unfallkrankenhaus Berlin gGmbH, Berlin, Germany
[3]Institut für Radiologie und Neuroradiologie, BG Klinikum Unfallkrankenhaus Berlin gGmbH, Berlin, Germany
[4]Institut für diagnostische Radiologie und Neuroradiologie, Universitätsmedizin Greifswald, Greifswald, Germany
[5]Klinik für Neurochirurgie, BG Klinikum Unfallkrankenhaus Berlin gGmbH, Berlin, Germany
[6]Klinik für Neurologie, BG Klinikum Unfallkrankenhaus Berlin gGmbH, Berlin, Germany

Background: As teleradiology continues to spread, diagnostic imaging of varying quality is increasingly bundled at big centers during any time of the day. This trend demands for prioritization and speediness of reporting in radiology. Deep learning algorithms could support radiologists in meeting these challenges [1]. This study analyzes the number of additionally detectable intracranial hemorrhages (ICH) by an approved artificial intelligence (AI) analysis software and evaluates reasons for false results at a (neuro)radiology department of a level 1 trauma center with teleradiology.

Methods: Retrospective cohort-study. (1) Analysis of consecutive emergency non-contrast head computed tomographies (hCT) by the AI. (2) Review of hCT with deviating results of the AI and the initial radiology report (RR) by a neuroradiologist (NR). (3) Evaluation of the number of additionally detected ICH using the AI and of reasons for false results.

Results: A total of 4946 hCT were included between 05/2020 and 09/2020 from 19 different CT scanners (Fig. 1). 205 reports (4.1 %) were classified as bleedings both by the RR and the AI. 162 (3.3 %) diverging reports were identified, 62 of these were confirmed as bleedings by a NR. The RR identified 33 ICH, analysis by the AI detected 29 ICH. 88 (1.8 %) hCT flagged by the AI as bleedings and 10 (0.2 %) positive RR were evaluated as incorrect findings by the NR. ICH missed by the AI were often located in the subarachnoid (SA) space (41.2 %) and immediately underneath the calvaria (47.1 %). 85 % of ICH missed by the RR but detected by AI occurred beyond regular working hours. Calcifications (39.3 %), beam hardening artifacts (18 %), tumors (15.7 %), and vessels (7.9 %) were the most common reasons for incorrectly positive flagged hCT. There was no significant

Fig. 1 | 48

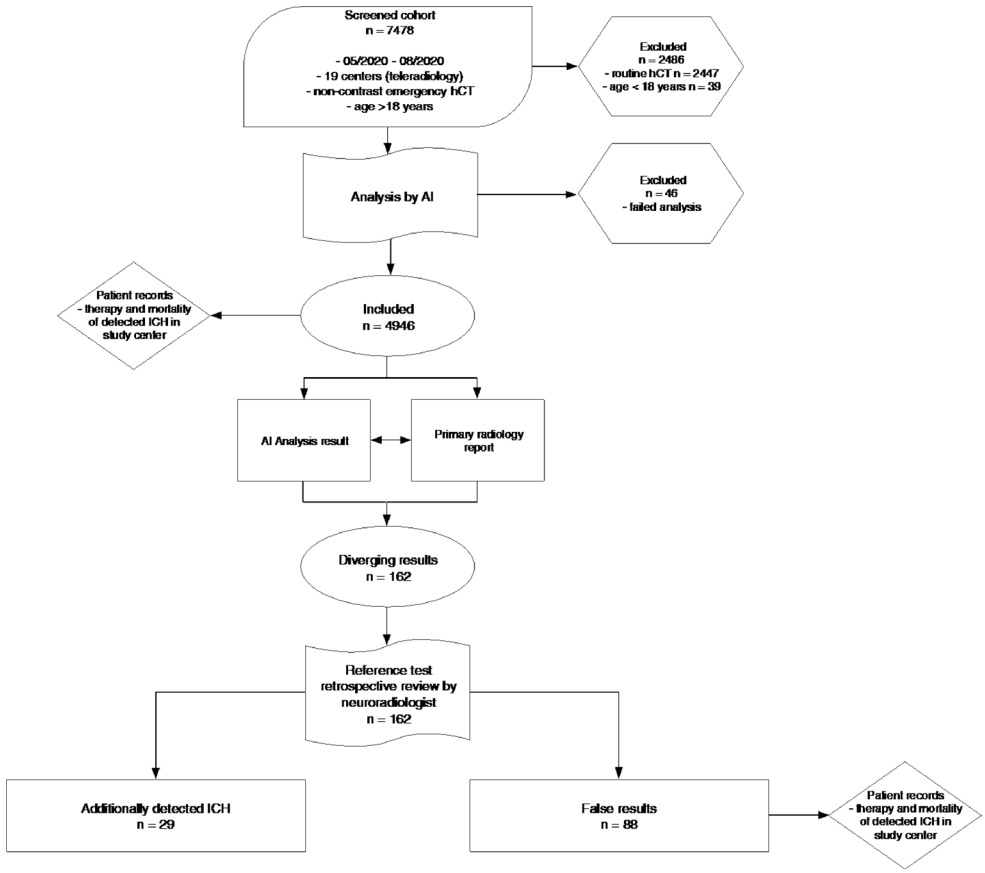

association between size of the ICH or image quality and probability of incorrect AI results.
Discussion: The disagreement rate between AI analysis and primary RR was 3.3 %. 12.2 % ICH were identified additionally by the AI. 1.8 % hCT were falsely flagged by the AI often caused by calcifications. ICH missed by the AI were mainly located in the SA space or underneath the calvaria.
Conclusion: Combining radiological experience and an AI algorithm is a promising strategy for maximizing detection of ICH in high-volume radiology departments with teleradiology, especially during on-call duty.

References

1. Ginat DT. Ginat -DT. Analysis of head -CT scans flagged by deep learning software for acute intracranial hemorrhage. Neuroradiology. 2020;62(3):335–40. https://doi.org/10.1007/s00234-019-02330-w.

[51] Hämodynamische Evaluation von Moyamoya-Patienten: Analyse von Resting-state-fMRT zur Abschätzung der zerebrovaskulären Reaktivität

Leonie Zerweck[1*], Constantin Roder[2], Till-Karsten Hauser[1], Johannes Thurow[3], Annerose Mengel[4], Marcos Tatagiba[2], Nadia Khan[2, 5], Philipp T. Meyer[3], Ulrike Ernemann[1], Uwe Klose[1]

[1]Universitätsklinikum Tübingen, Abteilung für Diagnostische und Interventionelle Neuroradiologie, Tübingen, Deutschland
[2]Universitätsklinikum Tübingen, Abteilung für Neurochirurgie, Tübingen, Deutschland
[3]Universitätsklinikum Freiburg, Abteilung für Nuklearmedizin, Freiburg, Deutschland
[4]Universitätsklinikum Tübingen, Abteilung für Neurologie, Tübingen, Deutschland
[5]Universitäts-Kinderspital Zürich, Moyamoya-Center, Zürich, Schweiz

Hintergrund: Für die Beurteilung des Schlaganfallrisikos bei Moyamoya-Patienten ist die Abschätzung der zerebralen Perfusionsreserve (CPR) notwendig. Als diagnostischer Standard gilt hierfür [^{15}O]water PET. Die Ermittlung der zerebrovaskulären Reaktivität (CVR) als Index der CPR mittels Breath-hold-fMRT (bh-fMRT) scheint eine besser verfügbare und zuverlässige Alternative zu sein [1]. Als weitere Option, die CVR zu untersuchen, wird Resting-state-fMRT (rs-fMRT) diskutiert [2]. Ziel dieser Studie war die Analyse von rs-fMRT zur Abschätzung der CVR bei Moyamoya-Patienten.
Methoden: Die rs-fMRT-Datensätze von 25 Moyamoya-Patienten wurden analysiert und mit den zugehörigen bh-fMRT-Datensätzen sowie in einer Subgruppe von 7 Patienten mit [^{15}O]water PET-Datensätzen verglichen. Die rs-fMRT-Datensätze wurden bewegungskorrigiert, normalisiert, räumlich geglättet und frequenzgefiltert. Ein Kleinhirn-Template wurde angewandt, um den Signalverlauf des Kleinhirns zu bestimmen. Als Parameter für die CVR wurde die Kreuzkorrelation des Zeitverlaufs jedes Voxels mit dem Zeitverlauf des Kleinhirns berechnet. Für den Vergleich zwischen rs-fMRT und bh-fMRT, bzw. [^{15}O]water PET wurden die durchschnittlichen CVR- bzw. CPR-Werte aller Modalitäten in 12 standardisierten VOIs [3] ermittelt und die Korrelation berechnet [4].
Ergebnisse: Sowohl beim Vergleich der 25 rs-fMRT- und bh-fMRT-Datensätze (Pearson's $r = 0{,}71 \pm 0{,}13$ [0,35–0,95]), als auch der 7 rs-fMRT- und [^{15}O]water PET-Datensätzen (Pearson's $r = 0{,}80 \pm 0{,}19$ [0,41–0,95]) zeigte sich eine gute Korrelation [4]. Die Maps eines Patienten mit hoher Korrelation und die zugehörigen Scatterplots sind in Abb. 1 und 2 dargestellt.

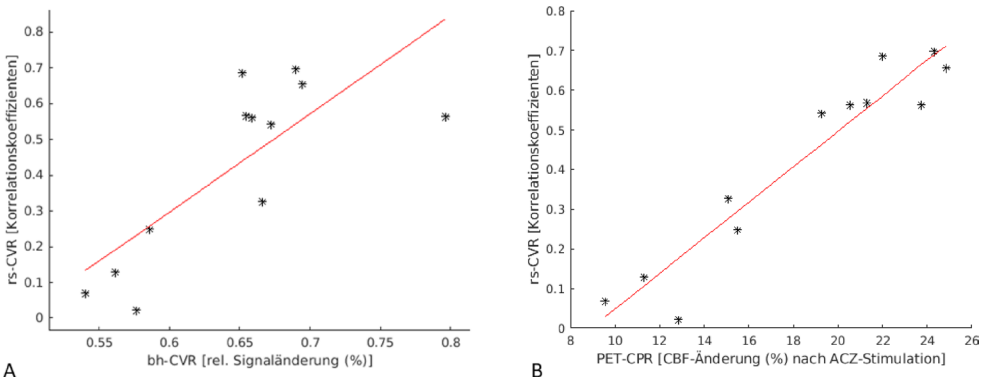

Abb. 1 | 51 Korrelation zwischen rs-fMRT und bh-fMRT (**a;** $r=0{,}78$) und zwischen rs-fMRT und [^{15}O]water PET (**b;** $r=0{,}95$) eines Patienten

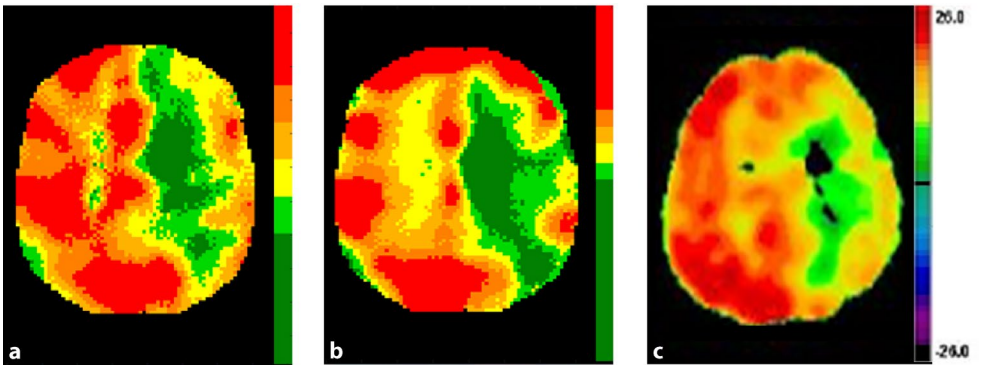

Abb. 2 | 51 Exemplarische rs-fMRT- (**a**), bh-fMRT- (**b**) und [^{15}O]water PET-Maps (**c**) eines Patienten

Fazit: rs-fMRT scheint eine vielversprechende Methodik für die hämodynamische Evaluation in der Moyamoya-Diagnostik zu sein, die gut verfügbar ist und kaum Mitarbeit der Patienten voraussetzt. Weitere Studien sind erforderlich.

Literatur

1. Hauser TK, et al. Neuroimage Clin. 2019;22:101713.
2. Liu P, et al. Neuroimage. 2017;146:320–6.
3. Tatu L, et al. Neurology. 1998;50(6):1699–708.
4. Zerweck et al. (2021) AJNR Submitted.

[54] Diversion-p64–results from an international, prospective, multicentre, single-arm post-market clinical follow-up study to assess the safety and effectiveness of the p64 flow modulation device

Alain Bonafé[1], Marta Aguilar-Pérez[2], Hans Henkes[2], Pedro Lylyk[3], Carlos Bleise[3], Grégory Gascou[1], Stanimir Sirakov[4], Alexander Sirakov[4], Luc Stockx[5], Francis Turjman[6], Andrey Petrov[7], Christian Roth[8], Ana Paula Narata[9], Xavier Barreau[10], Christian Loehr[11], Ansgar Berlis[12], Laurent Pierot[13], Marcin Miś[14], Antony Goddard[15], Peter Schramm[16*]

[1]Hôpital Gui de Chauliac (CHU Montpellier), France
[2]Klinikum Stuttgart Katharinenhospital, Germany
[3]Clínica La Sagrada Familia, Argentina
[4]University Hospital St. Ivan Rilski, Bulgaria
[5]Ziekenhuis Oost-Limburg, Belgium
[6]Hôpital Pierre Wertheimer, France
[7]Federal Almazov North-West Medical Research Centre, Russian Federation
[8]Klinikum Bremen-Mitte, Germany
[9]Hôpital Bretonneau (CHRU de Tours), France
[10]Groupe Hospitalier Pellegrin, France
[11]Knappschaftskrankenhaus Recklinghausen, Germany
[12]Klinikum Augsburg, Germany
[13]Hôpital Maison Blanche, France
[14]Zakład Radiologii Ogólnej, Zabiegowej i Neuroradiologii, Poland
[15]Leeds Teaching Hospitals NHS TRUST, United Kingdom
[16]Institut für Neuroradiologie, UKSH Universitätsklinikum Schleswig-Holstein Campus Lübeck, Lübeck, Germany

Background: The use of flow diversion to treat intracranial aneurysms has increased in recent years. We sought to assess the safety and angiographic efficacy of the p64 Flow Modulation Device.
Methods: Diversion-p64 is an international, prospective, multicentre, single arm, study conducted at 26 centres. The p64 device was used to treat anterior circulation aneurysms between December 2015 and January 2019. The primary safety endpoint was the incidence of major stroke or neurologic death at 3–6 months with the primary efficacy endpoint being complete aneurysm occlusion on follow-up angiography.
Results: A total of 420 patients met the eligibility criteria and underwent treatment with the p64 Flow Modulation Device (mean age 55 ± 12.0 years, 86.2 % female). Mean aneurysm dome width was 6.99 ± 5.28 mm and neck width 4.47 ± 2.28 mm. Mean number of p64s implanted per patient was 1.06 ± 0.47 with adjunctive coiling performed in 14.0 % of the cases. At 1-year angiography (mean 375 ± 73 days), available for 343 patients (81.7 %), complete aneurysm occlusion was seen in 83.7 % ($n=287$) of patients. Safety data was available for 413 patients (98.3 %) at the first follow-up (mean 145 ± 45 days) with a composite morbi-mortality rate of 2.42 % ($n=10$).
Discussion: Diversion-p64 is the largest prospective study using the p64 Flow Modulation Device. The results of this study will be compared with similar devices available on the US and EU market. The results of Diversion-p64 demonstrate one of the lowest rates of morbi-mortality seen in any prospective study on flow diversion. Furthermore, the results seen in Diversion-p64 are better than those seen using more traditional techniques such as endovascular coiling or balloon assisted coiling.

Conclusion: The results of Diversion-p64 demonstrate that the device has a high efficacy and excellent safety profile that is comparable to other devices.

References

1. Aguilar Pérez M, Henkes E, Hellstern V, et al. Endovascular treatment of anterior circulation aneurysms with the p64 Flow Modulation Device: mid- and long-term results in 617 aneurysms from a single center. Oper Neurosurg Hagerstown Md.. https://doi.org/10.1093/ons/opaa425 (Erstellt: 19. Jan. 2021).
2. Hanel RA, Kallmes DF, Lopes DK, et al. Prospective study on embolization of intracranial aneurysms with the pipeline device: the -PREMIER study 1 year results. J Neurointerventional Surg. 2020;12:62–6. https://doi.org/10.1136/neurintsurg-2019-015091.

[57] Visual analysis of brain lesion load in patients with cerebral small vessel disease

Sarah Mittenentzwei[1*], Alessandro Sciarra[2], Falk Lüsebrink[2 3], Merita Aruci[3], Philipp Ulbrich[2 4], Frank Schreiber[2 4], Andreas Lemke[5], Monique Meuschke[1], Bernhard Preim[1], Stefanie Schreiber[2 4 6], Steffen Oeltze-Jafra[1 2 6]

[1]Institute for Simulation and Graphics, Otto von Guericke University, Magdeburg, Germany
[2]Department of Neurology, Otto von Guericke University, Magdeburg, Germany
[3]Faculty of Natural Sciences, Otto von Guericke University, Magdeburg, Germany
[4]German Center for Neurodegenerative Diseases (DZNE), Magdeburg, Germany
[5]Mediaire GmbH, Berlin, Germany
[6]Center for Behavioral Brain Sciences (CBBS), Magdeburg, Germany

Background: Sporadic cerebral small vessel disease (CSVD) refers to microvascular brain pathologies leading to various types of tissue lesions. Typically, two main CSVD subtypes are differentiated based on the localization of hemorrhages in either strictly lobar (cerebral amyloid angiopathy, CAA) or deep regions (hypertensive arteriopathy, HA). Assignment of patients with hemorrhages in mixed (lobar and deep) regions to one or–simultaneously–both diagnoses is currently impossible. An analysis of (additional) hemorrhagic and nonhemorrhagic brain lesions (load, co-occurrence, localization, patterns) in these mixed cases may aid in a (better) classification.
Methods: We propose a web-based tool for an interactive visual analysis of individual and cohort CSVD lesion load. The tool supports three lesion types: white matter hyperintensities (WMH), enlarged perivascular spaces (ePVS) and cerebral microbleeds (CMB). In a pre-processing step, the lesions must be segmented in different MRI sequences and the image data as well as the masks must be co-registered.

The tool integrates multiple views for cohort specification [1] and visualization of lesion load (Fig. 1). It supports the comparison of several subcohorts, e. g., CAA, HA, mixed cases. A detailed representation of individual lesions and lesion co-occurrence are shown in 2D/3D. Since the cohort representation can quickly become cluttered due to many (overlapping) lesions, we included a more abstract visualization of the lesion load distribution using the bullseye brain parcellation [2].
Results: We evaluated the tool in a pilot study with 10 cases from clinical routine. Lesions were segmented using *mdbrain* (Mediaire GmbH) and *Mango* (RII, UT Health). Three CSVD experts tested the tool. They stated that it is very useful in detecting lesion patterns that may be characteristic for CAA or HA and support a better differentiation of mixed cases. They found for instance, that some cases had an asymmetrical lesion load in the frontal lobes deserving further investigation.
Discussion: The tool provides new insights about the lesion load and pattern of CSVD patients. To improve the analysis process, more statistical evaluation should be included in the tool. A follow-up study of 240 clinical cases is in progress.
Conclusion: The general principle of an interactive visual analysis of CSVD lesion load is a very promising approach to further research in CAA-HA-differentiation.

References

1. Müller, J., et al. IEEE Trans. Vis. Comput. Graph. 27.6 (2021)
2. Sudre, C. H., et al. J Neuroradiol. 45.2 (2018)

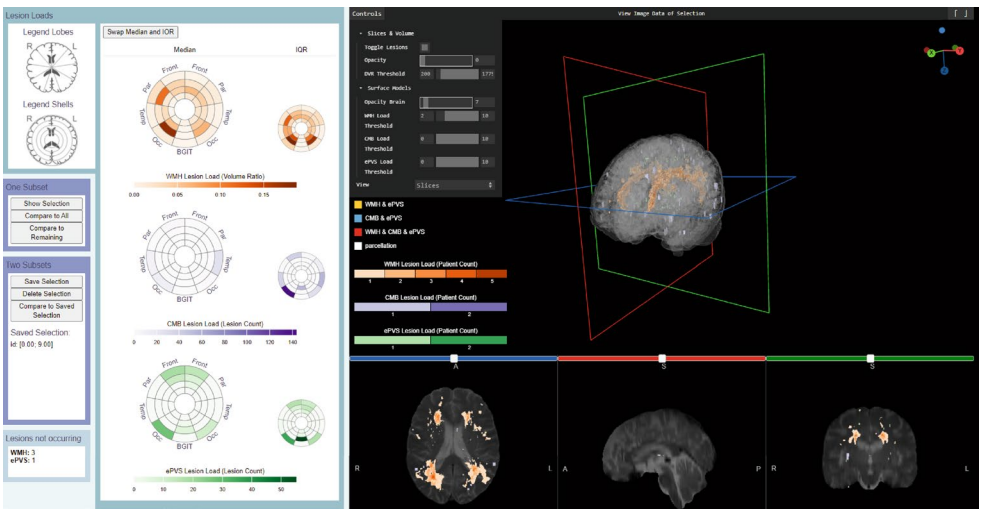

Fig. 1 | 57 Web-based tool for the analysis of CSVD lesion load. Linked 2D-, 3D- and bullseye plot views show the spatial distribution of various lesion types

[61] Venous outflow profiles are associated with early edema progression rate on noncontrast computed tomography in ischemic stroke patients

Noel van Horn[1*], Reza Kabiri[1], Soren Christensen[2], Michael Mlynash[2], Gabriel Broocks[1], Lukas Meyer[1], Maarten Lansberg[2], Gregory Albers[2], Jens Fiehler[1], Max Wintermark[3], Jeremy Heit[3], Tobias Faizy[1]

[1]Institut für Diagnostische und Interventionelle Neuroradiologie, Universitätsklinikum Hamburg-Eppendorf, Hamburg, Germany
[2]Stanford University, Department of Neurology and Neurological Sciences, USA
[3]Stanford University, Department of Radiology, USA

Background: Robust cortical venous outflow (VO) profiles correlate with favorable tissue perfusion in patients with acute ischemic stroke due to large vessel occlusion (AIS-LVO). In these patients, development of extensive early ischemic brain edema is associated with poor functional outcome, despite (after) treatment. We hypothesized that favorable VO profiles correlate with less early edema progression rate (EPR).
Methods: In this multicenter analysis we retrospectively investigated AIS-LVO patients treated by mechanical thrombectomy between January 2013 and December 2020. Baseline CT angiography (CTA) was used to determine VO using the cortical vein opacification score (COVES); favorable VO was defined as COVES ≥3. EPR was determined as the ratio of net water uptake (NWU) on baseline non-contrast CT and time from symptom onset to admission imaging. Multivariable regression analysis was used to assess the primary outcome (EPR).
Results: A total of 728 patients were included in this study. In univariable regression analysis lower COVES ($p=0.002$), lower Maas collateral score ($p=0.005$), a higher infarct core volume ($p<0.001$) and the location of vessel occlusion ($p=0.003$). Multivariable logistic regression analysis showed that higher COVES (OR: –0.01, 95 % CI –0.021 to 0.004, $p<0.003$) is associated with EPR.
Conclusion: A more favorable VO profile defined by a higher COVES is associated with lower EPR in AIS-LVO patients treated by endovascular thrombectomy.

References

1. Galego O, et al. Collateral pial circulation relates to the degree of brain edema on ct 24 hours after ischemic stroke. Neuroradiol J. 2018.
2. Broocks G, et al. Computed tomography angiography collateral profile is directly linked to early edema progression rate in acute ischemic stroke. Stroke. 2019.

[64] Cerebral venous outflow profiles are associated with first-pass effect in endovascular thrombectomy

Noel van Horn[1*], Reza Kabiri[1], Marius Mader[2], Sören Christensen[3], Michael Mlynash[3], Gabriel Broocks[1], Jawed Nawabi[4], Maarten Lansberg[3], Gregory Albers[3], Jens Fiehler[1], Max Wintermark[5], Jeremy Heit[5], Tobias D. Faizy[1]

[1]Institut für Diagnostische und Interventionelle Neuroradiologie, Universitätsklinikum Hamburg-Eppendorf, Hamburg, Germany
[2]Klinik und Poliklinik für Neurochirurgie, Universitätsklinikum Hamburg-Eppendorf, Hamburg, Germany
[3]Stanford University, Department of Neurology and Neurological Sciences, USA
[4]Institut für Diagnostische und Interventionelle Radiologie, Universitätsklinikum Berlin, Charité, Germany
[5]Stanford University, Department of Radiology, USA

Background: Recent studies found that favorable venous outflow (VO) profiles are associated with higher reperfusion rates after mechanical thrombectomy (MT) in patients with acute ischemic stroke due to large vessel occlusion (AIS-LVO). Fewer retrieval attempts during MT lead to better functional outcomes, also due to the first-pass effect. We hypothesized that favorable VO profiles assessed on baseline computed tomography angiography (CTA) images correlate with successful vessel reperfusion after the first retrieval attempt.
Methods: Multicenter retrospective cohort study of AIS-LVO patients treated by MT. Baseline CTA was used to determine the cortical vein opacification score (COVES). Favorable VO was defined as COVES ≥3. Primary outcome was successful vessel reperfusion defined as Thrombolysis in Cerebral Infarction (TICI) 2b–3 after first retrieval attempt.
Results: A total of 617 patients were included in this study, of which 205 (33.2 %) experienced first-pass reperfusion. In univariate analysis, higher COVES ($p=0.011$) and shorter interval from symptom onset to groin puncture ($p=0.003$) were independently associated with first-pass reperfusion after MT. In multivariable logistic regression analysis, higher COVES (OR = 0.84, 95 % CI 0.73–0.98, $p=0.027$) and higher Maas score (OR 1.28, 95 % CI 1.08–1.53, $p=0.005$) were associated with first-pass reperfusion, while intravenous application of alteplase indicated no independent correlation.
Conclusion: A robust cerebral VO profile classified as higher COVES is associated with first-pass reperfusion in patients with AIS-LVO treated by endovascular thrombectomy.

References

1. Zaidat OO, Castonguay AC, Linfante I, et al. First pass effect. Stroke. 2018.
2. Faizy TD, Kabiri R, Christensen S, et al. Favorable venous outflow profiles correlate with favorable tissue-level collaterals and clinical outcome. Stroke. 2021.

[65] Tract-based inflammatory and neurodegenerative Multiple Sclerosis measurements of disease progression using quantitative MR

Paul Kuntke[1*], Caroline Koehler[1], Hannes Wahl[1], Hagen H. Kitzler[1]

[1]Institut für Diagnostische und Interventionelle Neuroradiologie, Universitätsklinikum Carl Gustav Carus Dresden, Dresden, Deutschland

Hintergrund: Multiple Sklerose (MS) ist eine Erkrankung, die mit Demyelinisierung und axonaler Degeneration einhergeht. Diese können mittels Diffusionstensorbildgebung (DTI) und Myelin-Wasser-Bildgebung (MWI) quantifiziert werden, indem der Einfluss der MS-Läsionen (T2L) auf das umgebende Traktgewebe („normal appearing tract tissue“, NATT) bestimmt wird.
Methoden: Bei 28 MS-Patienten sowie 26 gesunde Probanden wurden Myelin-Wasser-Fraktion (MWF; [1]) sowie die DTI-Messwerte (FA, RD, MD, AD) in T2L und NATT bestimmt. Atlasbasiert [2] wurden Fasertrakte selektiert und die relative Läsionsbelastung (rLB) der Trakte berechnet, um die Läsionslast unabhängig vom Traktvolumen zu vergleichen.
Ergebnisse: Es wurde ein signifikanter Unterschied von MWF und FA zwischen Kontrollen und Patienten gefunden (MWF; $p<0{,}001$; FA: $p=0{,}0018$). Des Weiteren zeigte sich eine moderate Korrelation zwischen MWF_{Lesion} u. MW_{FNATT} ($r=0{,}62$) und FA_{Lesion} und F_{ANATT} ($r=0{,}60$; Abb. 1). Es bestand demgegenüber keine Korrelation zwischen MWF_{Lesion} und FA_{Lesion} ($r=0{,}18$) und eine schwache, aber nahezu moderate Korrelation zwischen MW_{FNATT} und F_{ANATT} ($r=0{,}48$).
Diskussion: Die moderate Korrelation zwischen der Schädigung des Läsionsgewebes und der NATT zeigt, dass Läsionen bei MS einen Einfluss auf das sie umgebende Traktgewebe haben. Dieser Effekt verstärkt sich in Abhängigkeit vom Grad der Schädigung der Läsionen.
Fazit: Unsere Ergebnisse stützen die Hypothese, dass die Waller-Degeneration von Axonen vom Ausmaß der inflammatorischen Schädi-

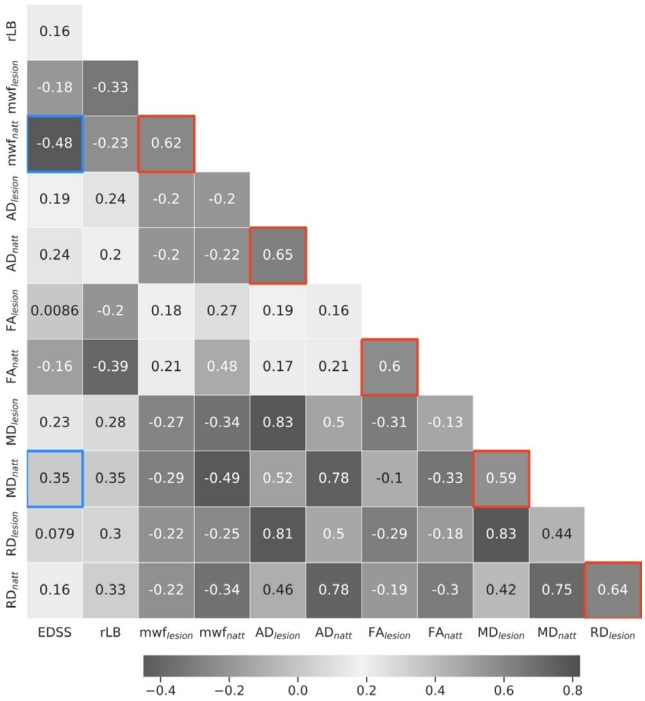

Abb. 1 | 65

gung der fokalen Läsion abhängt. Unsere Ergebnisse weisen darauf hin, dass der axonale Verlust innerhalb der Läsionen nicht parallel mit der inflammatorischen Demyelinisierung entsteht, was hypothetisch auf teilweise axonal schützende Remyelinisierung zurückzuführen ist. Gleichzeitig verlaufen aber Demyelinisierung und axonaler Verlust außerhalb der Läsionen im NATT parallel, hinweisend auf einen möglicherweise langsam progredienten, homogenen degenerativen Prozess.

Literatur

1. Deoni SC, et al. One component? Two components? Three? The effect of including a nonexchanging „free“ water component in multicomponent driven equilibrium single pulse observation of T1 and T2.
2. Wakana, et al. Reproducibility of quantitative tractography methods applied to cerebral white matter. Neuroimage. 2007;36:630–44.

[80] Vergleich zweier Thrombektomie-Versorgungskonzepte beim akuten Schlaganfall: „drip and ship“ vs. „drive the doctor“

Fatih Seker[1], Christian Urbanek[2], Jasmin Jung[1]*, Martin Bendszus[1], Markus Möhlenbruch[1]

[1]Neuroradiologie, Universitätsklinikum Heidelberg, Deutschland
[2]Neurologie, Klinikum Ludwigshafen, Deutschland

Hintergrund: Die flächendeckende Versorgung mit der Thrombektomie beim akuten Schlaganfall ist weiterhin eine Herausforderung. Neben der Primäreinweisung in Thrombektomie-Zentren („mothership“) und der Sekundärverlegung an Thrombektomie-Zentren („drip and ship“, DS) wird in manchen Schlaganfallnetzwerken ein weiteres Konzept angeboten. Hierbei fahren Neurointerventionslisten aus Thrombektomie-Zentren an externe Krankenhäuser, um dort eine Thrombektomie durchzuführen, anstatt die Patienten an ein Thrombektomie-Zentrum zu verlegen („drive the doctor“, DD). Ziel der vorliegenden retrospektiven Studie war der Vergleich des klinischen Outcomes bei „drip and ship“ und „drive the doctor“.

Methoden: In dieser retrospektiven Arbeit wurden alle Schlaganfallpatienten untersucht, die von 2015 bis 2019 im Rahmen einer Kooperationsvereinbarung zwischen einem Universitätsklinikum und einem städtischen Krankenhaus (ca. 30 km Entfernung) thrombektomiert worden sind. Die Patienten wurden je nach personeller bzw. technischer Kapazität entweder vom städtischen Krankenhaus an das Universitätsklinikum zwecks Thrombektomie verlegt (DS) oder vor Ort am städtischen Krankenhaus durch Anfahrt eines Neuroradiologen aus dem Universitätsklinikum thrombektomiert (DD). Gutes Outcome wurde definiert als mRS-Score bei Entlassung 0–2 bzw. unverändert gegenüber dem prämorbiden mRS.

Ergebnisse: Insgesamt wurden 114 Patienten im Rahmen von DS und 179 Patienten im Rahmen von DD thrombektomiert. Gutes Outcome wurde ähnlich häufig in DS und DD erreicht (DS 26,3 % vs. DD 31,3 %; $p=0{,}43$). Auch hinsichtlich mRS bei Entlassung (DS median 4 [IQR 3–5], DD median 4 [IQR 2–5]; $p=0{,}686$) und NIHSS bei Entlassung (DS median 9 [IQR 3–21], DD median 7 [IQR 2–19]; $p=0{,}208$) gab es keinen signifikanten Unterschied zwischen beiden Gruppen.

Diskussion: In dieser retrospektiven Studie, in welcher „drip and ship“ und „drive the doctor“ direkt miteinander verglichen worden sind, konnte gezeigt werden, dass „drive the doctor“ hinsichtlich des klinischen Outcomes dem bereits etablierten „Drip and ship“-Konzept nicht unterlegen ist.

Fazit: Das „Drive-the-doctor“-Konzept, welches von anderen Schlaganfallnetzwerken auch unter diversen Namen publiziert worden ist, liefert gute klinische Ergebnisse und kann neben „mothership“ und „drip and ship“ als weiteres Konzept zur flächendeckenden Schlaganfallversorgung berücksichtigt werden.

[82] Diagnostic value of DW-MRI and 18F-FDG PET/CT in detection of residual/recurrent tumors after (chemo) radiotherapy for head and neck squamous cell carcinoma

Christophe Schroeder[2], Jung-Hyun Lee[3], Johannes Roßkopf[4], Soung Yung Kim[1]*

[1]Department of Diagnostic and Interventional Radiology, Neu-Ulm, Germany
[2]Hospital Center Luxembourg–Center, Department of Diagnostic and Interventional Radiology, Luxembourg, Luxemburg
[3]Institute of Molecular Virology, Neu-Ulm, Germany
[4]Bezirkskrankenhaus Günzburg, Department of Neuroradiology, Günzburg, Germany

Background: Detection of residual or recurrent tumors in patients treated for head and neck squamous cell carcinoma (HNSCC) can be very challenging. This retrospective study compares the diagnostic accuracy of diffusion-weighted MR imaging (DW-MRI) and fluorine 18F-fluorodeoxyglucose (18F-FDG) PET/CT in detection residual or recurrent tumors and their local extension, in patients with HNSCC after treatment with (chemo)radiotherapy (CRT).

Methods: Twenty-five patients (17 men, 8 women, median age: 64 years, range: 53–86) who underwent surgical salvage for residual or recurrent tumors after CRT were included. The DW-MRI and PET/CT images were anonymized and reviewed retrospectively. The results were compared to the gold standard of histopathology.

Results: Both DW-MRI and18F-FDG PET/CT had a sensitivity of 92 % (23/25) in the detection of residual or recurrent tumors. MRI had a sensitivity, specificity, positive predictive value (PPV) and negative predictive value (NPV) for detecting perineural spread of 62 % (5/8), 88 % (15/17), 71 % (5/7) and 83 % (15/18), respectively; in comparison, PET/CT did not detect any cases of perineural spread. The sensitivity, specificity, PPV and NPV of MRI in detecting muscle infiltration was 75 % (9/12), 77 % (10/13), 75 % (9/12) and 77 % (10/13) respectively, while the values for 18F-FDG PET/CT were 58 % (7/12), 69 % (9/13), 64 % (7/11) and 64 % (9/14).

Discussion: The detection rate of residual or recurrent tumor was equally high in DW-MRI- and 18F FDG PET/CT with 92 % (23/25). Prior studies in patients with HNSCC have shown that 18F FDG PET/CT has a higher diagnostic accuracy compared to MRI for assessment of untreated HNSCC or treated HNSCC. However, these studies did not include MRI with DWI, which obviously influences the diagnostic performance. In addition, DW-MRI can pinpoint suspicious areas where biopsy should be taken if needed. Therefore, we have assessed to measure the ability of DW-MRI and PET/CT in detecting of perineural spread (PNS) and muscle infiltration.
Conclusion: DW-MRI and 18F-FDG PET/CT have an identical detection rate of residual or recurrent tumors after CRT. MRI has a higher sensitivity in detecting local perineural spread, has a better accuracy in the detection of muscle infiltration and more accurately correlates the lesion size to the histopathologic specimen.

[88] Multi-parametric quantitative mapping of R1, R2*, PD, and MTsat is reproducible when accelerated with Compressed SENSE

Ronja Berg[1*], Tobias Leutritz[2], Nikolaus Weiskopf[2], Christine Preibisch[1]

[1]Technische Universität München, Klinikum rechts der Isar, Abteilung für Neuroradiologie, Fakultät für Medizin, München, Germany
[2]Max Planck Institut für Kognitions- und Neurowissenschaften, Abteilung Neurophysik, Leipzig, Germany

Introduction: Conventional clinical routines use qualitative magnetic resonance imaging (MRI) to assess diseased tissue. Multiparametric mapping (MPM) of R1, R2*, PD, and MTsat is a quantitative MRI method that promises better comparability across sites and higher sensitivity to systemic tissue changes. For clinical applications of MPM, the sequences need to be accelerated and their accuracy verified. Therefore, we investigated the reproducibility of MPM using Compressed SENSE acceleration.
Methods: Five healthy subjects were scanned three times on a Philips 3T Ingenia Elition. MPM comprised B1 mapping and gradient echo sequences with T1w: TR = 18 ms, $\alpha = 25°$; PDw: TR = 18 ms, $\alpha = 4°$; and MTw: TR = 48 ms, $\alpha = 6°$, $\alpha_{MT} = 220°$, $t_{MT} = 8$ ms, $f_{MT} = 1000$ Hz; with 6 echoes each (TE1/ΔTE = 2.4/2.4 ms) and (1 mm)^3 resolution. In each scan session, SENSE (20 min) and Compressed SENSE (CS) with acceleration factors CS = 4 (15:40 min) and CS = 6 (10:30 min) were used. Quantitative parameter maps (qMaps) were calculated using the hMRI toolbox [1, 2]. Coefficients of variation (CoV) were calculated across both scan sessions ("repeatability") and accelerations ("reproducibility" with different acceleration parameters) and were compared in whole-brain GM and WM.
Results: R1, R2*, PD and MTsat parameter maps appeared visually similar across different accelerations (Fig. 1a) and scan sessions (Fig. 2a). Repeatability-based CoV values of qMaps acquired with the same acceleration across scan sessions were comparable for SENSE, CS = 4, and CS = 6 (Fig. 1b). Likewise, reproducibility-based CoV values of qMaps acquired with different accelerations were comparable for scans A, B, and C (Fig. 2b). In GM and WM, subject-mean reproducibility-based

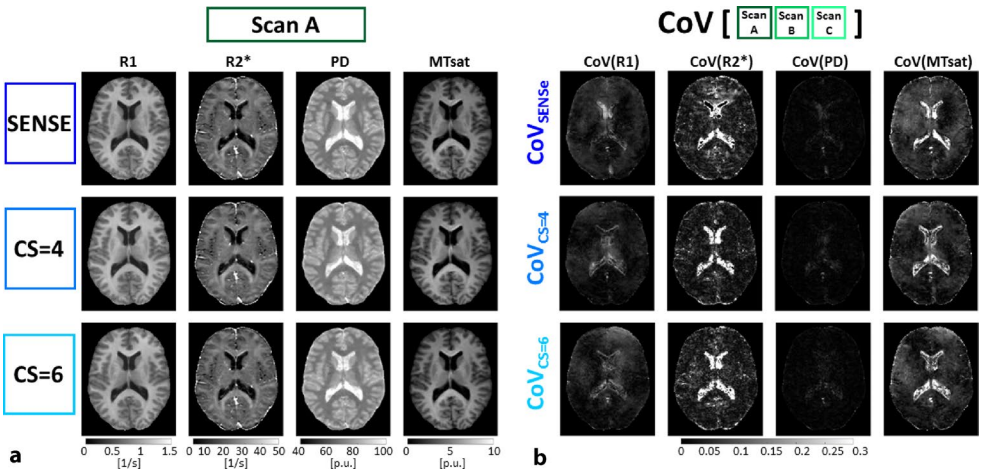

Fig. 1 | 88 Repeatability evaluation: Exemplary maps of quantitative parameters (**a**) and coefficients of Variation (CoV) (**b**) from a healthy volunteer for different acceleration methods. The quantitative parameter maps in **a**) were acquired in Scan A with different accelerations and the CoV maps were calculated from the three scans with the same acceleration method acquired in different scan sessions (Scan A, Scan B, and Scan C)

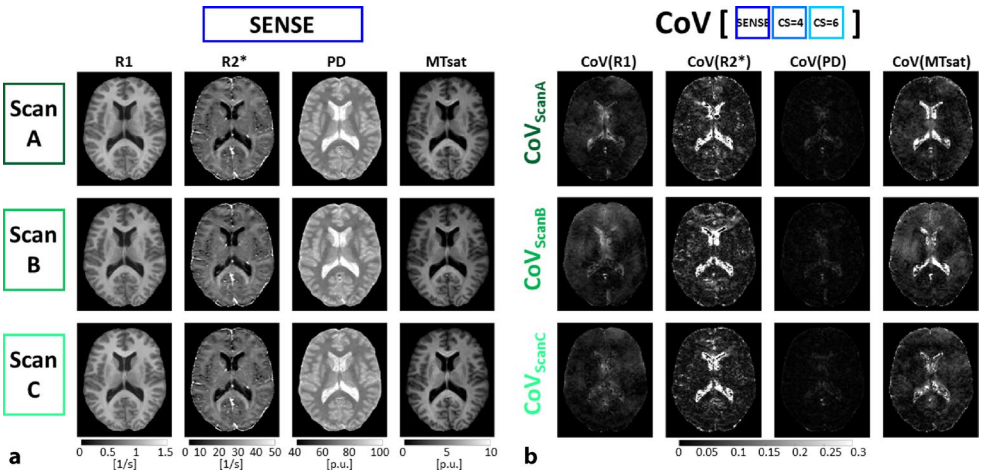

Fig. 2 | 88 Reproducibility evaluation: Exemplary maps of quantitative parameters (**a**) and coefficients of variation (CoV) maps (**b**) from the healthy volunteer shown in Fig. 1 for different scan sessions. The quantitative parameter maps in **a**) were acquired with SENSE in different scan sessions and the CoV maps were calculated from the three sequences within the same scan session and with different accelerations (SENSE, CS = 4, CS = 6)

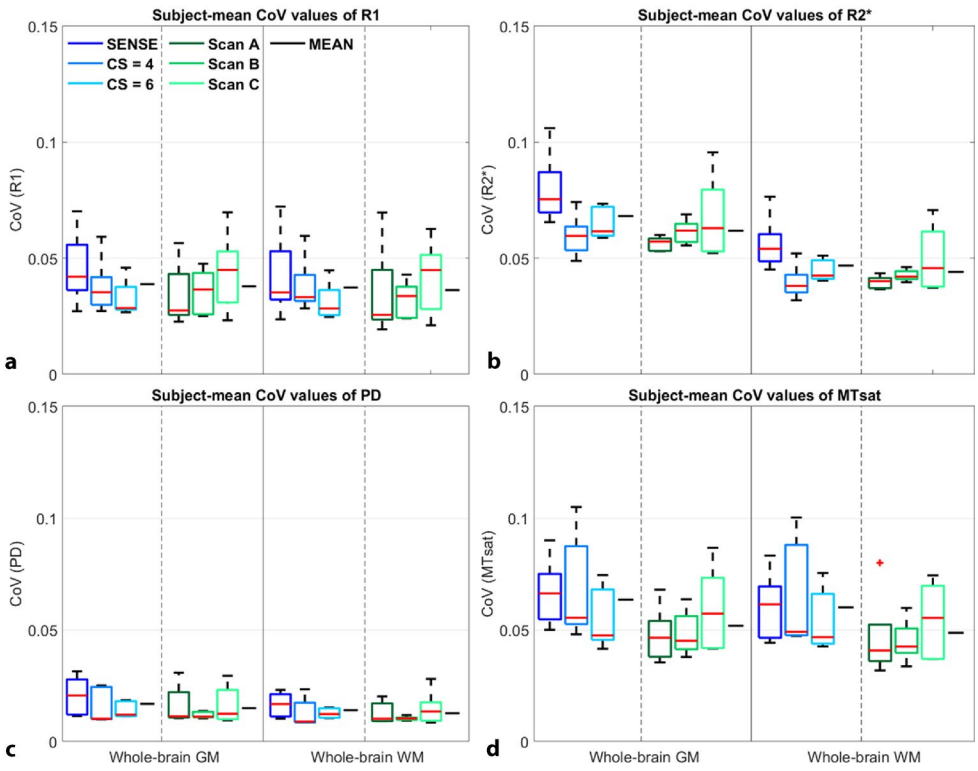

Fig. 3 | 88 Boxplots of coefficients of variation (CoV) of quantitative parameter maps from the repeatability (*blue*) and reproducibility (*green*) measurements. In each panel, the subject-mean CoV values of R1 (**a**), R2* (**b**), PD (**c**), and MTsat (**d**) are shown for whole-brain GM and whole-brain WM segmentations. The average of repeatability (SENSE, CS = 4, and CS = 6) and reproducibility data points (Scan A, Scan B, and Scan C) is shown in *black*

CoVs (green) were comparable to repeatability-based CoVs (blue) for R1 and PD and even slightly lower for R2* and MTsat (Fig. 3).
Discussion: Average R1 and PD showed similar variability across either scan sessions or accelerations, and average R2* and MTsat were even more stable (lower CoV) across accelerations than scan sessions. Together with the high visual similarity between qMaps acquired with different accelerations, this suggests that the highest investigated acceleration, CS with acceleration factor of 6, provides accurate MPM results.
Conclusion: As Compressed SENSE allows considerably reducing scan durations while providing accurate quantitative parameter maps, if facilitates MPM in clinical routines.

References

1. Tabelow 2019 NeuroImage
2. Weiskopf 2015 CurrOpinNeurol

[89] Perfusion imaging-based tissue-level collaterals are associated with early edema progression rate in ischemic stroke

Noel van Horn[1*], Soren Christensen[2], Michael Mlynash[2], Reza Kabiri[1], Gabriel Broocks[1], Maarten Lansberg[2], Gregory Albers[2], Jens Fiehler[1], Max Wintermark[3], Jeremy Heit[3], Tobias Faizy[1, 3]

[1]Institut für Diagnostische und Interventionelle Neuroradiologie, Universitätsklinikum Hamburg-Eppendorf, Hamburg, Germany
[2]Department of Neurology and Neurological Sciences, Stanford University, USA
[3]Stanford University, Department of Radiology, USA

Background: Hypoperfusion intensity ratio (HIR) is an automated perfusion imaging-based assessment tool that quantifies tissue-level collaterals (TLC) and microperfusion in patients with acute ischemic stroke due to large vessel occlusion (AIS-LVO). Poor TLC status may be correlated with infarct growth and edema progression. To investigate the relationship between TLC and edema progression, reflected by ischemic lesion Net Water Uptake (NWU) on non-contrast head CT (NCCT). We hypothesized that favorable HIR is correlated with early edema progression rate (EPR) prior to treatment in AIS-LVO.
Methods: Multicenter retrospective analysis of AIS-LVO patients who underwent mechanical thrombectomy (MT). HIR was assessed on baseline CTP (defined as time-to-maximum [TMax]>10 s/[TMax]>6 s). Ischemic lesion NWU and EPR (quantitative NWU/time from symptom onset to baseline imaging) were assessed on baseline NCCT. Arterial collaterals were assessed by the Maas Score. Primary Outcome was EPR. Secondary outcome was poor outcome defined as a modified Rankin scale at 90-days (mRS90) of 3–6.
Results: A total of 718 patients were included. Multivariable logistic regression analysis showed higher (unfavorable) HIR (OR 0.06, 95 % CI 0.23–0.10; $p<0.002$) and lower Maas collateral score (OR –0.18, 95 % CI –0.03 to –0.005, p) were associated with higher EPR. Higher (unfavorable) HIR (OR 20.56, 95 % CI 9.65–43.79, $p<0.001$) was also associated with mRS90 of 3–6.
Conclusion: A favorable cerebral collateral status at a tissue level (TLC) was associated with a lower early edema progression rate and decreased total NWU on baseline non contrast head CT as well as good functional outcome in AIS-LVO patients.

References

1. Faizy TD, Kabiri R, Christensen S, et al. Perfusion imaging-based tissue-level collaterals predict ischemic lesion net water uptake in patients with acute ischemic stroke and large vessel occlusion. J Cereb Blood Flow Metab. 2021; https://doi.org/10.1177/0271678X21992200.
2. Broocks G, Kemmling A, Meyer L, et al. Computed Tomography Angiography Collateral Profile Is Directly Linked to Early Edema Progression Rate in Acute Ischemic Stroke. 2019 Dec. https://doi.org/10.1161/STROKEAHA.119.027062.

[90] „Chemical exchange saturation transfer"(CEST)-MRT-Sequenz in der klinischen 3-Tesla-Magnetresonanztomographie – Anwendungs- und Signalanalyse

Julia Petra Lingl[1*], Arthur Peter Wunderlich[2], Soung Yung Kim[2], Meinrad Beer[2], Johannes Roßkopf[3]

[1]Universität Ulm, Medizinische Fakultät, Ulm, Deutschland
[2]Universitätsklinikum Ulm, Klinik für diagnostische und interventionelle Radiologie, Ulm, Deutschland
[3]Bezirkskrankenhaus Günzburg, Sektion für Neuroradiologie, Günzburg, Deutschland

Hintergrund: „Chemical exchange saturation transfer"(CEST)-MRT-Bildgebung ermöglicht *in vivo* die Quantifizierung körpereigener Metabolite von z. B. in Proteinen gebundenen Amidgruppen (Amid-Protonen-Transfer-CEST, APT-CEST), wie sie beispielsweise in Hirntumoren vorkommen [1, 2].
Methoden: Es wurden APT-CEST-Asymmetriedaten am 3-T-MRT (Skyra, Siemens) an einer Kohorte von Hirntumorpatienten unter Therapie erhoben ($n=27$; 6 Glioblastome multiforme, 6 Meningeome, 4 Lymphome, 11 intrazerebrale Metastasen). Mittels ROI-basierten Analysen wurden Sensitivtäten (Sens) und Spezifitäten (Spez) über ROC-Kurven bestimmt. Als Vergleich wurden Diffusions-(ADC-) und Perfusionsbildgebung (rCBV, relatives Blutvolumen) als weitere fortgeschrittene MRT-Sequenzen herangezogen.
Ergebnisse: Die kontrastmittelaufnehmenden Tumoranteile zeigten statistisch signifikant höhere APT-CEST-Werte als die normal erscheinende weiße Hirnsubstanz (NAWM) bei einer Sensitivität von 89 % und einer Spezifität von 78 % (0,32 vs. –0,64; $p<0,05$). Hirneigene Tumoren wiesen im Durchschnitt höhere CEST-Signale als Metastasen auf (–0,67 vs. –0,20; $p<0,05$; Sens/Spez 81 %/55 %). Die Perfusionsbildgebung bei Glioblastomen liefert zu CEST vergleichbare Ergebnisse. ADC ergab keine Signifikanz hinsichtlich Differenzierung zwischen Tumor und NAWM oder zwischen hirneigenen Tumoren und Metastasen.
Diskussion: CEST-MRT ermöglichte auf Gruppenniveau *in vivo* eine statistisch signifikante Unterscheidung zwischen Tumor und NAWM sowie eine Einordnung in hirneigenen Tumor vs. Metastase. Die Diffusionsbildgebung zeigte sich im Vergleich zur CEST-Bildgebung unterlegen hinsichtlich Sensitivität, Spezifität und Signifikanz. MR-Perfusion hingegen lieferte vergleichbare Ergebnisse zur Differenzierung zwischen Hirntumor und NAWM.
Fazit: Die Ergebnisse dieser Studie zeigten, dass CEST in der Hirntumordiagnostik bezüglich Diagnosestellung und Entitätsbestimmung einen wertvollen Beitrag leisten kann. Studien mit größerem Stichprobenumfang sind jedoch zur Verifizierung nötig.

Literatur

1. KM J, Pollard AC, Pagel MD. Clinical applications of chemical exchange saturation transfer (CEST) MRI. J Magn Reson Imaging. 2018;47:11–27.
2. Jiang S, et al. Identifying Recurrent Malignant Glioma after Treatment Using Amide Proton Transfer-Weighted MR Imaging: A Validation Study with Image-Guided Stereotactic Biopsy'. Clin Cancer Res. 2019;25:552–61.

[98] Automated detection and quantification of brain metastases on clinical MRI data using artificial neural networks: improving the assessment accuracy of disease burden

Irada Pflüger[1*], Fabian Isensee[2], Tassilo Wald[2], Marianne Schell[1], Hagen Meredig[1], Kai Schlamp[3], Claus Peter Heußel[3, 4], Denise Bernhardt[5], Wolfgang Wick[6, 7], Klaus H Maier-Hein[2], Martin Bendszus[1], Philipp Vollmuth[1]

[1]University of Heidelberg Medical Center, Department of Neuroradiology, Heidelberg, Germany
[2]German Cancer Research Center (DKFZ), Medical Image Computing, Heidelberg, Germany
[3]Clinic for Thoracic Diseases (Thoraxklinik), Department of Diagnostic and Interventional Radiology with Nuclear Medicine, Heidelberg, Germany
[4]Translational Lung Research Center Heidelberg (TLRC), Heidelberg, Germany
[5]Klinikum rechts der Isar, Technical University Munich, Department of Radiation Oncology, München, Germany
[6]University of Heidelberg Medical Center, Department of Neurology, Heidelberg, Germany
[7]German Cancer Research Center (DKFZ), Clinical Cooperation Unit Neurooncology, Heidelberg, Germany

Background: The growth dynamic of brain metastases (BM) is an essential criterium for the assessment of the efficiency of a therapy. It is mainly determined by MRI by manual measurements of the targeted lesions according to the Response Assessment in Neuro-Oncology [1]. This is potentially less accurate and reproducible than volumetric measurements. Therefore, we evaluate the potential of artificial neural networks (ANN) for automated volumetric assessment of BM burden.
Methods: The development and testing of the ANN for automated detection and segmentation of contrast-enhancing tumors (CE) and non-enhancing FLAIR signal abnormalities (NE) on MRI were performed on a single institutional cohort of 308 patients with BM from several primary cancer scanned on a 3T MRI. Independent testing was done in a dataset with 30 patients with BM from lung cancer scanned on a 1.5T MRI. The performance was assessed separately per scan for CE and NEC using case-wise DICE coefficient (C-DICE) and concordance correlation coefficient (CCC). Also, we evaluated performance for CE per lesion employing lesion detection performance (L-DICE), lesion-wise positive predictive value (LPPV) and lesion sensitivity (L.-Sensitivity).
Results: The ANN shows good performance for accurate detection and segmentation of CE and NEC in both test datasets per scan (median C-DICE for CE 0.91 and for NEC 0.96 in institutional test set, and for CE 0.84 and for NEC 0.83 in independent test set), and the CCC was ≥0.98 in each dataset. A similar good performance (mean L-DICE) was reached in both institutional (0.72) and independent (0.79) test sets. In institutional test set mean L-Sensitivity and LPPV for CE were 0.74 and 0.89 accordingly, as compared to 0.84 for L-Sensitivity and 0.76 for LPPV in independent test set.
Discussion: We showed that automated quantitative analysis of MRI using ANN could allow radiologist and clinicians to overcome the inherent limitations of manual assessment of tumor burden. This has important implications particularly in the context of longitudinal follow-up, because of intrinsic human variability e. g. small changes in disease burden may be overlooked.
Conclusion: Our results highlight the capability of ANN for reliable, automated volumetric quantification of BM and precise differentiation between CE and NEC on MRI. Our developments can improve the quantitative assessment of disease burden and disease progression on MRI in patients with BM.

References

1. Lin, et al. Response assessment criteria for brain metastases: proposal from the RANO group. Lancet Oncol. 2015.

[108] Application of augmented reality in percutaneous procedures–rhizotomy of the Gasserian Ganglion

Alexander Rau[1*], Roland Rölz[2], Horst Urbach[1], Volker Arnd Coenen[2], Theo Demerath[1], Peter Reinacher[2]

[1]Universitätsklinikum Freiburg, Klinik für Neuroradiologie, Freiburg im Breisgau, Germany

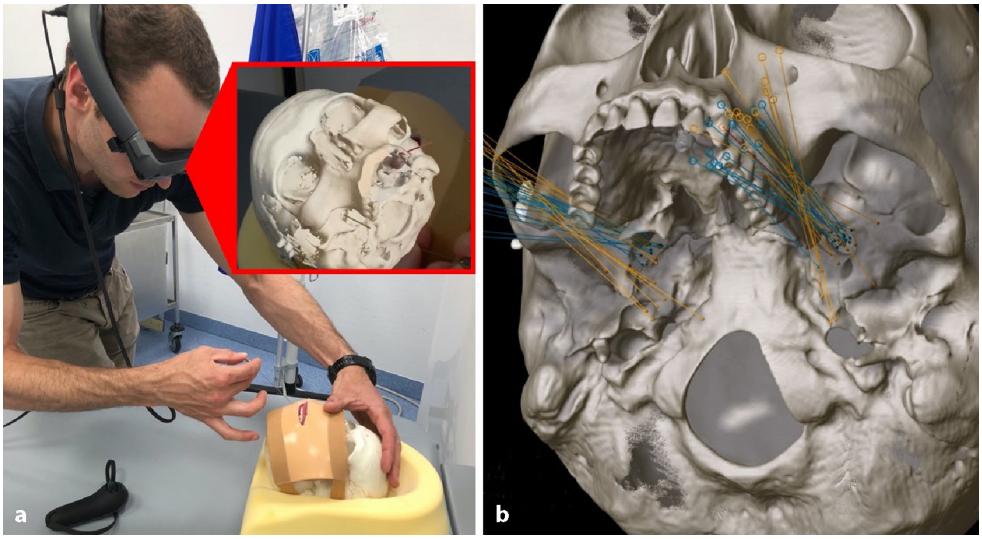

Fig. 1 | 108 **a** Experimental setup. **b** Reconstruction of the needle positions ($n=64$) in the postprocedural CT scan, *orange* trajectories carried out conventionally using landmarks, *blue* trajectories using augmented reality (AR) guidance

[2]Universitätsklinikum Freiburg, Abteilung Stereotaktische und Funktionelle Neurochirurgie, Freiburg, Germany

Background: Percutaneous rhizotomy of the Gasserian ganglion for trigeminal neuralgia is an effective therapeutic procedure. Yet, landmark-guided cannulation of the foramen ovale is manually challenging and difficult to learn. We sought to overcome these limitations and assessed the feasibility and accuracy of an augmented reality(AR)-guided puncture.
Methods: A head phantom with soft tissue structures of the facial area was built. A 3D dataset of the phantom was generated using a stereotactic planning workstation. An optimal trajectory to the foramen ovale was created and then transferred to an AR headset. Two neurosurgeons and two neuroradiologists independently performed eight augmented reality-guided and eight landmark-guided cannulations of the foramen ovale, respectively. For each AR–guided cannulation, the hologram was manually aligned with the phantom. Accuracy was evaluated using the Euclidean distance to the target point as well as the lateral deviation between the achieved trajectory from the planned trajectory at target point level.
Results: With the help of augmented reality, a successful cannulation of the foramen ovale was achieved in 90.6 % compared to the purely landmark-based method with 18.8 %. Euclidean distance and lateral deviation were significantly lower with AR guidance than landmark-guided ($p<0.01$).
Discussion: We see a great potential of AR-based planning and execution for minimizing risks of cannulation of the foramen ovale. This minimally invasive procedure is challenging and is subject to several considerable risks due to the proximity of the foramen ovale to critical structures. Beside CT guidance, intra- or perioperative imaging modalities such as MRI have also been established. However, these are usually resource intensive, include radiation exposure, or invasive head fixation.
Conclusion: Augmented reality greatly improved accuracy of simulated percutaneous rhizotomy of the Gasserian ganglion.

[109] Strukturiertes Reporting geometrischer und hämodynamischer Aneurysmaeigenschaften zur Stratifikation des Rupturrisikos

Daniel Behme[1*, 2], I Reinitz[2], Oliver Beuing[3], Maximilian Thormann[1], B Neyazi[4], Erol Sandalcioglu[4], Anastasios Mpotsaris[1], B Preim[5], Philipp Berg[2, 6], Sylvia Saalfeld[2, 5]

[1]Klinik für Neuroradiologie, Universitätsklinik Magdeburg, Magdeburg, Deutschland
[2]Forschungscampus STIMULATE, Magdeburg, Deutschland
[3]AMEOS Klinik Bernburg, Bernburg, Deutschland
[4]Klinik für Neurochirurgie, Universitätsklinik Magdeburg, Deutschland
[5]Department of Simulation and Graphics, Universität Magdeburg, Deutschland
[6]Department of Fluid Mechanics and Technical Flows, Universität Magdeburg, Deutschland

Hintergrund: Obwohl diverse Risikoscores für unrupturierte Aneurysmen bestehen, bleibt die Beratung von Patient*innen eine Herausforderung. Zudem werden in der alltäglichen Praxis nur sehr einfache geometrische (z. B. Größe) Faktoren herangezogen, hämodynamische Faktoren spielen in der Beratung aktuell keine Rolle, obwohl viele Forschungsergebnisse der letzten Jahre diverse hämodynamische Faktoren identifizieren konnten, welche mit dem Rupturrisiko assoziiert sind. Ziel unseres strukturierten Reportings ist es daher, diese Faktoren für die tägliche klinische Praxis nutzbar zu machen.
Methoden: Basierend aktueller State-of-the-Art-Forschungsergebnisse wurden je 5 morphologische und 5 hämodynamische Faktoren untersucht. Diese wurden in einem strukturierten Report so dargestellt, dass die anwendenden Ärzt*innen und Patienten den Report intuitiv verstehen können. Farbskalen zeigen auf Basis bereits publizierter Daten, ob ein Faktor eher für hohes oder niedriges Rupturrisiko spricht. Zudem werden die Aneurysmen graphisch dargestellt und ein Gesamtscore angegeben (Abb. 1).
Ergebnisse: Wir konnten ein strukturiertes Reporting für anspruchsvolle geometrische und hämodynamische Aneurysmaanalysen produzieren, welches ohne besondere Hardware semiautomatisch erzeugt werden kann.
Diskussion: Strukturierte Reports zu diversen relevanten Aneurysmarisikofaktoren existieren bisher nicht und ergänzen bestehende klinische Scores um wichtige Informationen.
Fazit: Strukturiertes Reporting hämodynamischer und geometrischer Aneurysmaeigenschaften ist praktisch durchführbar und kann die Beratung von Patient*innen mit unrupturierten intrakraniellen Aneurysmen in der Zukunft deutlich verbessern.

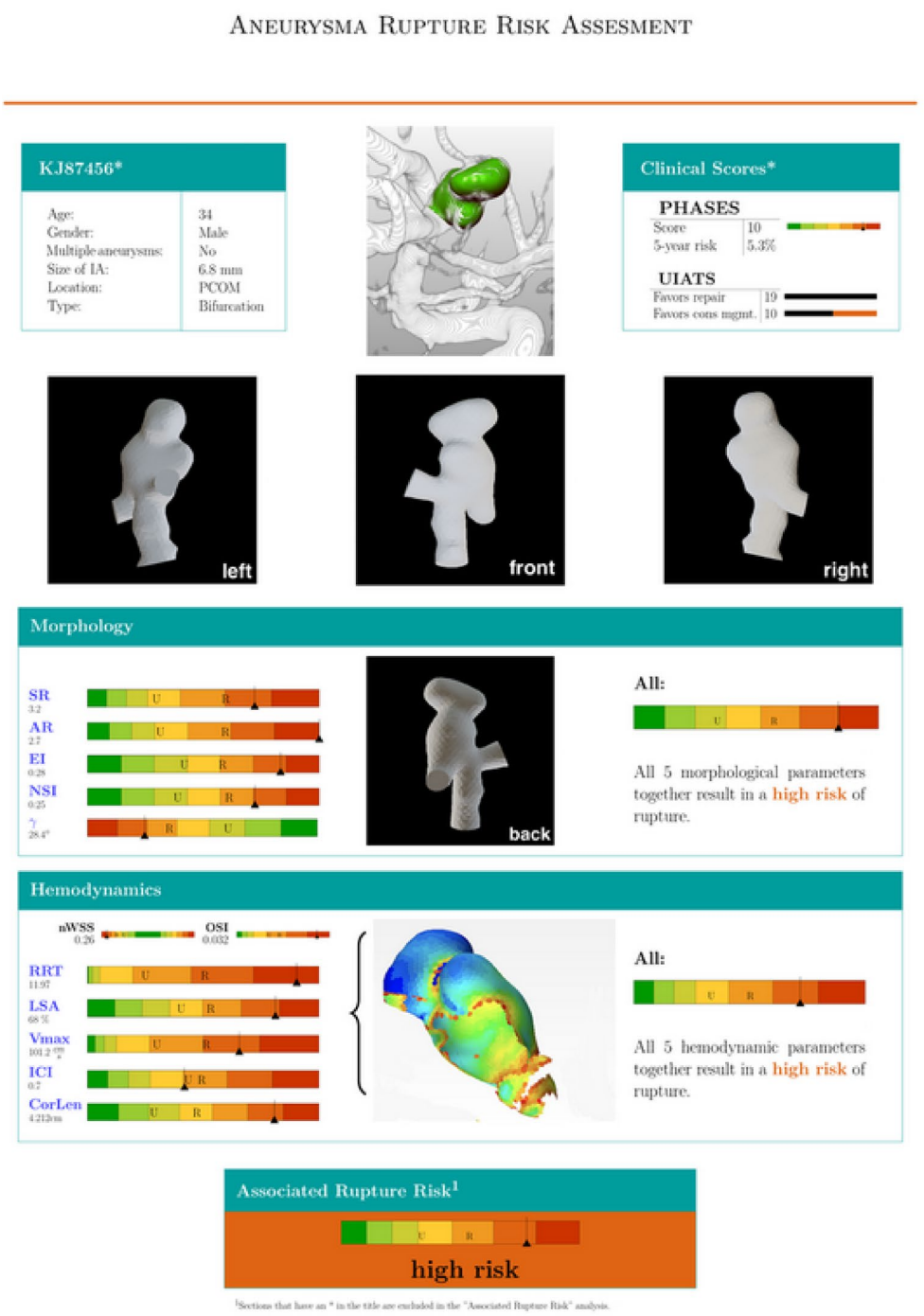
Aneurysma Rupture Risk Assesment
KJ87456*
Age: 34
Gender: Male
Multiple aneurysms: No
Size of IA: 6.8 mm
Location: PCOM
Type: Bifurcation
Clinical Scores*
PHASES
Score 10
5-year risk 5.3%
UIATS
Favors repair 19
Favors cons mgmt. 10
left
front
right
Morphology
SR
AR
EI
NSI
γ
back
All:
All 5 morphological parameters together result in a high risk of rupture.
Hemodynamics
nWSS 0.26
OSI 0.032
RRT
LSA
Vmax
ICI
CorLen
All:
All 5 hemodynamic parameters together result in a high risk of rupture.
Associated Rupture Risk[1]
high risk
[1]Sections that have an * in the title are excluded in the "Associated Rupture Risk" analysis.

Abb. 1 | 109

[110] Increased interstitial fluid in periventricular caps and deep white matter hyperintensities in patients with suspected iNPH

Theo Demerath[1*], Alexander Rau[1], Marco Reisert[2], Elias Kellner[2], Jonas Hosp[3], Horst Urbach[1]

[1]Neuroradiologie, Universitätsklinikum Freiburg, Deutschland
[2]Medizinphysik, Universitätsklinikum Freiburg, Deutschland
[3]Neurologie und Neurophysiologie, Universitätsklinikum Freiburg, Deutschland

Background: Periventricular white matter changes are common in patients with idiopathic normal pressure hydrocephalus (iNPH) and considered to represent focally elevated interstitial fluid. We compared diffusion measures in periventricular caps in patients with imaging features of iNPH to patients without. The hypothesis is that periventricular caps in patients with possible iNPH show higher water content than in patients without imaging features of iNPH.
Methods: A total of 21 patients with iNPH Radscale 7–12 ("high probability of iNPH") and 10 patients with iNPH Radscale 2–4 ("low probability of iNPH") were examined with a neurodegeneration imaging protocol including a diffusion microstructure imaging sequence. Periventricular caps and deep white matter hyperintensities were segmented and diffusion measures were compared.
Results: In patients with iNPH, the free water content in periventricular caps was significantly higher compared to the control group ($p<0.001$). This effect was also detectable in deep white matter hyperintensities ($p=0.002$). Total brain volumes and total gray or white matter volumes did not differ between the groups. Periventricular free cap water fraction was highly discriminative regarding iNPH patients and controls with an ROC AUC of 0.933.
Discussion: Quantitative diffusion microstructure imaging shows elevated water content in periventricular caps and deep white matter lesions in patients with iNPH, which could be the imaging correlate for pathologic fluid accumulation.
Conclusion: Advanced diffusion imaging may be suitable for measuring increased white matter free water in patients with iNPH.

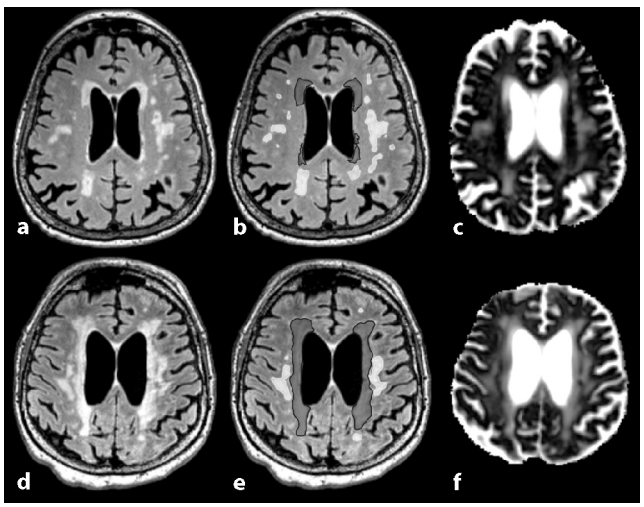

Fig. 1 | 110 Axial FLAIR reformats in Patients without (**a**) and with imaging features of iNPH (**d**) with corresponding superimposed segmentations (**b**, **e**) divided into periventricular caps (*dark grey*) and deep white matter lesions (*light grey*). Related parametric V-CSF-maps are shown in **c** and **f**

[111] „Within a minute" detection of focal cortical dysplasia (FCD)

Theo Demerath[1*], Marcel Heers[2], Dirk-Matthias Altenmüller[2], Andreas Schulze-Bonhage[2], Anke Maren Staack[3], Thomas Bast[4], Marco Reisert[5], Ralf Schwarzwald[1], Christoph Kaller[1], Hans-Jürgen Huppertz[6], Horst Urbach[1]

[1]Neuroradiologie, Universitätsklinikum Freiburg, Germany
[2]Neurochirurgie, Universitätsklinikum Freiburg, Germany
[3]Epileptologie, Epilepsiezentrum Kork, Deutschland
[4]Klinik für Kinder und Jugendliche, Epilepsiezentrum Kork, Germany
[5]Medizinphysik, Universitätsklinikum Freiburg, Germany
[6]Swiss Epilepsy Center, Klinik Lengg Zürich, Switzerland

Background: Focal cortical dysplasia (FCD) can be subtle and easily overlooked on MRI. Voxel-based morphometric analysis and automated FCD detection using a shallow artificial neural network (ANN) integrated in the Morphometric Analysis Program (MAP18) has been shown to facilitate FCD detection. The aim of our study was to evaluate ANN MAP using the MP2RAGE sequence for the enhanced and rapid FCD detection on MRI.
Methods: Prospective study including 40 consecutive, so far MRI-negative patients and 36 healthy controls. Post-processing of 3-Tesla MP2RAGE sequences to highlight typical FCD features. The resulting morphometric maps served as inputs for an artificial neural network generating FCD probability maps. The FCD probability maps were inversely normalized, co-registered to the MP2RAGE sequences and re-transferred into the PACS system. Co-registered images were scrolled through "within a minute" to determine whether a FCD was present or not.
Results: Fifteen FCD and three subcortical band heterotopias (SBH) were identified. Of those, four FCD and one SBH were only detected by MRI post-processing. False positive results occurred in 21 patients and 22 healthy controls. True positive cluster volumes were significantly larger than volumes of false positive clusters ($p<0.001$). The area under the curve of the receiver operating curve was 0.851 with a cut-off volume of 0.05 ml best indicating a FCD.
Discussion: Automated MRI post-processing and presentation of co-registered output maps in the PACS allowed for rapid (i. e. "within a minute") identification of FCDs. The presence of false-positive findings currently requires a careful comparison with conventional MR images but may be reduced in the future using a ANN better adapted to MP2RAGE images.
Conclusion: Morphometric Analysis Program (MAP18) post-processing of 3-Tesla MP2RAGE sequences using artificial neural networks facilitates the FCD detection and is a promising tool for radiologists less experienced with epilepsy imaging.

[113] Long-term epilepsy-associated tumors (LEATs): a voxel-based neuroimaging analysis

Urs Würtemberger[1*], Theo Demerath[1], Christoph Kaller[1], Niklas Lützen[1], Elias Kellner[1], Rösch Julie[2], Arnd Dörfler[2], Rössler Karl[3], Blümcke Ingmar[4], Horst Urbach[1]

[1]Klinik für Neuroradiologie, Uniklinik Freiburg, Freiburg, Germany
[2]Neuroradiologische Abteilung, Universitätsklinik Erlangen, Erlangen, Germany
[3]Universitätsklinik für Neurochirurgie des Allgemeinen Krankenhauses Wien, Universitätsklinikum AKH Wien, Wien, Austria
[4]Neuropathologisches Institut, Universitätsklinik Erlangen, Erlangen, Germany

Background: Long-term epilepsy-associated tumors (LEATs) are cortical-subcortical tumors in which preferential localization in the temporal lobe has been described (1). The aim of our work was to sta-

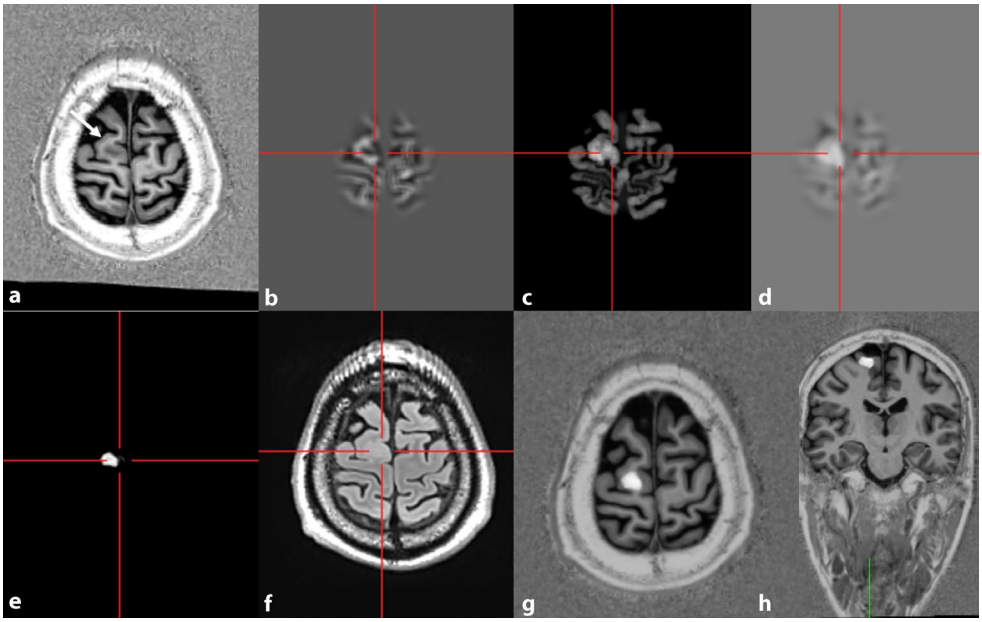

Fig. 1 | 111 Axial MP2RAGE image with a FCD IIB of the right superior frontal gyrus (**a**). Post-processing with a data base of 154 healthy controls results in the calculation of junction (**b**), thickness (**c**), and extension maps (**d**). These serve among others as input maps for an ANN that creates binary output maps (**e**). FLAIR images should be considered to separate the FCD and false positives (**f**). Finally, co-registered output and MP2RAGE maps are sent back to the PACS system (**g, h**)

tistically compare the spatial distribution of gangliogliomas (CD34+ and –), DNET, PXA, and ANET.
Methods: Preoperative MR images of 157 patients with histologically confirmed LEATs were retrospectively evaluated. All tumors were segmented semiautomatically and registered to MNI space. Based on the respective lesion center, standardized atlases were used to visualize and compare lesion localization.
Results: Four larger subgroups were identified: gangliogliomas ($n=100$) with (GG+) and without (GG–) CD34 immunoreactivity, DNETs ($n=32$), ANETs ($n=8$), and PXA ($n=17$). Gangliogliomas are significantly more likely temporally located than DNETs ($p=0.005$). Similarly, GG+ are significantly more often temporally localized than GG- gangliogliomas ($p=0.024$).
Discussion: Gangliogliomas, in contrast to DNET, differ significantly in their localization preference regarding the temporal lobe. The much more frequent extratemporal location of CD34 negative gangliogliomas supports the hypothesis that they may represent a separate tumor entity ("GNET"; [2]).
Conclusion: Voxel-based lesion analysis provides new aspects of preferential tumor localization in LEATs.

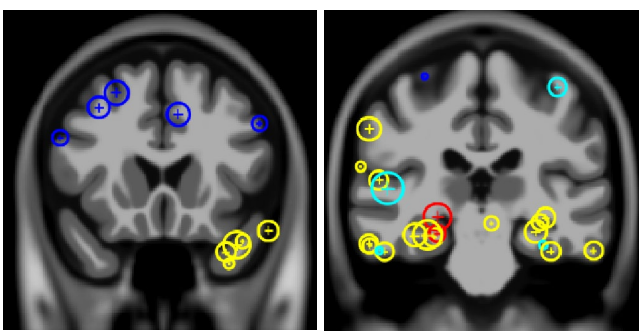

Fig. 1 | 113 Color map of LEAT tumor distribution in coronal view on MNI Space (*yellow* CD34+ GGL, *red* CD34– GGL, *blue* DNET, *cyan* PXA, *green* ANET)

References

1. Luyken C, et al. The spectrum of long-term epilepsy-associated tumors: long-term seizure and tumor outcome and neurosurgical aspects. Epilepsia. 2003;44:822–30.
2. Blumcke I, et al. A neuropathology-based approach to epilepsy surgery in brain tumors and proposal for a new terminology use for long-term epilepsy-associated brain tumors. Acta Neuropathol. 2014;128:39–54.

[117] Artificial intelligence substantially improves differential diagnosis of dementia–added diagnostic value of rapid brain volumetry

Jan Rudolph[1*], Johannes Rückel[1], Jörg Döpfert[2], Wen Xin Ling[2], Jens Opalka[2], Christian Brem[3], Nina Hesse[1], Boris Rauchmann[1], Maria Ingenerf[1], Vanessa Koliogiannis[1], Olga Solyanik[1], Hanna Zimmermann[3], Wilhelm Flatz[1], Robert Forbrig[3], Maximilian Patzig[3], Oliver Peters[4, 5], Josef Priller[4, 5, 6], Anja Schneider[7, 8], Klaus Fließbach[7, 8], Andreas Hermann[9, 10], Jens Wiltfang[11, 12, 13], Frank Jessen[7, 14, 15], Emrah Düzel[16, 17], Katharina Bürger[18, 19], Stefan Teipel[20, 21], Christoph Laske[22, 23], Matthis Synofzik[22, 24], A. Spottke[7, 25], Michael Ewers[18], Peter Dechent[26], John-Dylan Haynes[27], Klaus Scheffler[28], Jens Ricke[1], Michael Ingrisch[1], Sophia Stöcklein[1]

[1]Klinik und Poliklinik für Radiologie, München, Germany
[2]Mediaire GmbH, Berlin, Germany
[3]Institut für Diagnostische und Interventionelle Neuroradiologie, München, Germany
[4]Deutsches Zentrum für Neurodegenerative Erkrankungen (DZNE), Berlin, Germany
[5]Klinik für Psychiatrie und Psychotherapie, Charité–Universitätsmedizin Berlin, Berlin, Germany
[6]Klinik und Poliklinik für Psychiatrie und Psychotherapie, Klinikum rechts der Isar der Technischen Universität München, München, Germany
[7]Deutsches Zentrum für Neurodegenerative Erkrankungen (DZNE), Bonn, Germany
[8]Klinik für Neurodegenerative Erkrankungen und Gerontopsychiatrie, Universitätsklinikum Bonn, Bonn, Germany
[9]Deutsches Zentrum für Neurodegenerative Erkrankungen e. V. (DZNE), Dresden, Germany

Tab. 1 Spatial distribution of GG+ and GG- regarding the temporal lobe

	Other	TL	Total
GG–	8	7	15
GG+	21	64	85
Total	29	71	100

Tab. 2 Spatial distribution of GGL and DNET regarding the temporal lobe

	Other	TL	Total
GGL	29	71	100
DNET	18	14	32
Total	47	85	132

[10]Sektion für Translationale Neurodegeneration „Albrecht Kossel", Universitätsmedizin Rostock, Rostock, Germany
[11]Deutsches Zentrum für Neurodegenerative Erkrankungen e. V. (DZNE), Göttingen, Germany
[12]Klinik für Psychiatrie und Psychotherapie, Universitätsmedizin Göttingen, Göttingen, Germany
[13]Neurosciences and Signaling Group in Institut of Biomedicine (iBiMED), University of Aveiro, Aveiro, Portugal
[14]Klinik und Poliklinik für Psychiatrie und Psychotherapie, Uniklinik Köln, Köln, Germany
[15]Excellence Cluster on Cellular Stress Responses in Aging-Associated Diseases (CECAD), Universität Köln, Köln, Germany
[16]Deutsches Zentrum für Neurodegenerative Erkrankungen e. V. (DZNE), Magdeburg, Germany
[17]Institut für Kognitive Neurologie und Demenzforschung, Universität Magdeburg, Magdeburg, Germany
[18]Deutsches Zentrum für Neurodegenerative Erkrankungen (DZNE), München, Germany
[19]Institut für Schlaganfall- und Demenzforschung, München, Germany
[20]Deutsches Zentrum für Neurodegenerative Erkrankungen e. V. (DZNE), Standort Rostock, Rostock, Germany
[21]Klinik und Poliklinik für Psychosomatik und Psychotherapeutische Medizin, Rostock, Germany
[22]Deutsches Zentrum für Neurodegenerative Erkrankungen e. V. (DZNE), Tübingen, Germany
[23] Sektion für Demenzforschung und der Memory Clinic/ Gedächtnisambulanz, Universität Tübingen, Tübingen, Germany
[24]Zentrum für Neurologie, Neurodegenerative Erkrankungen, Uniklinik Tübingen, Tübingen, Germany
[25]Klinik und Poliklinik für Neurologie, Universitätsklinikum Bonn, Bonn, Germany
[26]MR-Forschung in der Neurologie und Psychiatrie, Abt. Kognitive Neurologie, Universitätsmedizin Göttingen, Göttingen, Germany
[27]Bernstein Zentrum für Computational Neuroscience Berlin, Charité–Universitätsmedizin Berlin, Berlin, Germany
[28]Department for Biomedical Magnetic Resonance, Universität Tübingen, Tübingen, Germany

Background: Brain volumetry is a key aspect in dementia diagnostics. We applied an artificial intelligence (AI) system based on a Convolutional Neural Network (CNN) which aims to perform lobe-separated rapid brain volumetry (< 1/2 h) of three-dimensional T1-weighted magnetic resonance imaging (MRI) with automated segmentation as well as comparison to age- and gender-adapted percentiles. Our aim was to quantify the added value in the differential diagnostics of dementia.
Methods: A total of 55 patients–17 with confirmed diagnosis of Alzheimer's disease (AD), 18 with confirmed diagnosis of frontotemporal dementia (FTD) and 20 healthy controls–received T1-weighted three-dimensional magnetization prepared–rapid gradient echo (MP-RAGE) MRI. Images were retrospectively assessed by one board-certified neuroradiologist (BCNR) and two radiology residents (RR)–one of whom had received 6 months of neuroradiology training (RR1). All cases were evaluated in a two-step reading process–beginning without AI-support and followed by an AI-supported reading (AI tool: mdbrain version 3.3.0). For each subject, the suspected diagnostic category (AD, FTD and healthy controls) was determined using a likelihood score (0–5), adding up to a sum of 5 for all three diagnostic categories. Individual reader performance with and without AI support was statistically evaluated using receiver operating characteristics (ROC).
Results: AI support substantially improved AD diagnosis in all three readers. The effect was most pronounced for RR2 who had not undergone neuroradiology training (area under the curve [AUC] without AI support [– AI]: 0.629, AI supported [+ AI]: 0.885). But, even for the BCNR, a substantial benefit was measurable (AUCs: BCNR—AI: 0.827, + AI: 0.882; RR1—AI: 0.713, + AI: 0.834). In diagnosing FTD RR2 improved with AI support (AUCs:—AI: 0.610, + AI: 0.754), while BCNR and RR1 had comparable reading performances with and without AI support (AUCs: BCNR—AI: 0.843, + AI: 0.828; RR1—AI: 0.865, + AI: 0.868).
Discussion: Even experienced BCNR can improve their diagnostic accuracy for AD by using AI based rapid brain volumetry and comparison with the age- and gender-matched reference cohorts. In diagnosing FTD, especially radiologists who are less experienced in dementia differential diagnosis can strongly benefit from AI support.
Conclusion: AI support in the radiological work-up of dementia patients is feasible and can substantially improve diagnostic accuracy, which might lead to earlier diagnosis and therefore optimized patient management.

[122] Virtuelle native Bildrekonstruktionen der Dual-Layer-Dual-Energy-CT: Verbesserung der Differenzierung von Enhancement und Verkalkungen in stereotaktischen Planungs-CT-Untersuchungen bei zystischen intrakraniellen Tumoren

Christian Nelles[1*], Kai Roman Laukamp[1], Charlotte Zaeske[1], Nils Große Hokamp[1], Simon Lennartz[1], Christoph Kabbasch[1], Marc Schlamann[1], David Zopfs[1]

[1]Institut für Diagnostische und Interventionelle Radiologie, Universitätsklinik Köln, Köln, Deutschland

Hintergrund: Vor stereotaktischer Biopsie von Hirnläsionen erfolgt häufig eine kontrastmittelgestützte CT des Kopfes zur Interventionsplanung, in der die Unterscheidung zwischen Enhancement und verkalkten Strukturen schwierig ist. Ziel der Studie war es, virtuell native Bilder (VNC) der Dual-Layer Dual-Energy-CT (dlDECT) im Vergleich zu konventionellen Bildern (CI) zur Differenzierung wandassoziierter Kontrastmittelaufnahme und Verkalkungen zystischer intrakranieller Tumoren zu untersuchen.
Methoden: Planungsuntersuchungen vor stereotaktischer Biopsie von 48 Patienten mit zystischen Hirntumoren, die sowohl eine wandassoziierte Kontrastmittelaufnahme als auch Verkalkungen aufwiesen, wurden retrospektiv eingeschlossen. Die Referenzdiagnosen wurden mittels MRT durch zwei Radiologen erstellt. Für jeden Patienten wurden zwei Läsionen in CI markiert, die durch zwei weitere, unabhängige Radiologen als Kontrastmittelaufnahme oder Verkalkung eingeordnet werden sollten; zunächst basierend auf CI, in einer zweiten Auswertung nach acht Wochen mit CI und VNC. Neben der Diagnose (Enhancement vs. Verkalkung) wurden die diagnostische Sicherheit und das Bildrauschen mittels 5-Punkte-Likert-Skalen bewertet.
Ergebnisse: Die diagnostische Genauigkeit stieg unter zusätzlicher Verwendung von VNC im Vergleich zu CI von 64 % auf 83 % ($p < 0{,}01$). Die diagnostische Sicherheit stieg von 3 (2–3) auf 4 (4–

5), während das Bildrauschen in VNC niedriger bewertet wurde: CI 5 (4–5) vs. VNC 4 (3–5), $p<0{,}01$. Während in CI die Unterschiede der Kontrast-zu-Rausch-Verhältnisse zwischen weißer Hirnsubstanz und randständiger Verkalkung bzw. Kontrastmittelaufnahme nicht signifikant waren (2,9 vs. 3,5; $p=0{,}07$), unterschieden sich diese in VNC signifikant (2,6 vs. 1,3; $p<0{,}01$).

Diskussion: Die zusätzliche Verwendung von VNC ergab gegenüber CI eine signifikant höhere diagnostische Genauigkeit und Sicherheit bei der Beurteilung von wandassoziierter Kontrastmittelaufnahme und Verkalkungen zystischer Hirnläsionen.

Fazit: VNC der dlDECT erleichtern eine Differenzierung randständiger Verkalkungen und randständigen Enhancements in stereotaktischen Planungs-CT-Untersuchungen bei Patienten mit zystischen Hirntumoren.

[126] Vermindertes Hypothalamusvolumen ist assoziiert mit vermindertem Körperwachstum bei sehr frühgeborenen Erwachsenen

Tobias Ruzok[1*, 2], Benita Schmitz-Koep[1, 2], Aurore Menegaux[1, 2], Robert Eves[3, 4], Dieter Wolke[3, 4], Peter Bartmann[5], Claus Zimmer[1, 2], Christian Sorg[1, 2, 6], Dennis Hedderich[1, 2]

[1]Abteilung für Diagnostische und Interventionelle Neuroradiologie, Klinikum rechts der Isar–Neuro-Kopf-Zentrum, Technische Universität München, München, Deutschland
[2]TUM-NIC Neuroimaging Center, Klinikum rechts der Isar, Technische Universität München, München, Deutschland
[3]Department of Psychology, Lifespan Health and Wellbeing Group, University of Warwick, Coventry, Vereinigtes Königreich
[4]Warwick Medical School, University of Warwick, Coventry, Vereinigtes Königreich
[5]Abteilung für Neonatologie, Universitätsklinikum Bonn, Bonn, Deutschland
[6]Abteilung für Psychiatrie und Psychotherapie, Klinikum rechts der Isar, Technische Universität München, München, Deutschland

Hintergrund: Nach Frühgeburt zeigen sich häufig eine verringerte Körpergröße und -gewicht bis ins Erwachsenenalter, allerdings ist noch nicht vollständig verstanden, welche Faktoren oder Mechanismen dies bedingen. Der Hypothalamus (HYP) und ausgewählte Kerngebiete (z. B. Ncl. paraventricularis und Ncl. infundibularis) regulieren u. a. Körperwachstumsprozesse. Neuartige Segmentierungsalgorithmen erlauben die Identifikation von HYP-Subsegmenten in strukturellen MRT-Untersuchungen des Gehirns. Wir vermuteten strukturelle HYP-

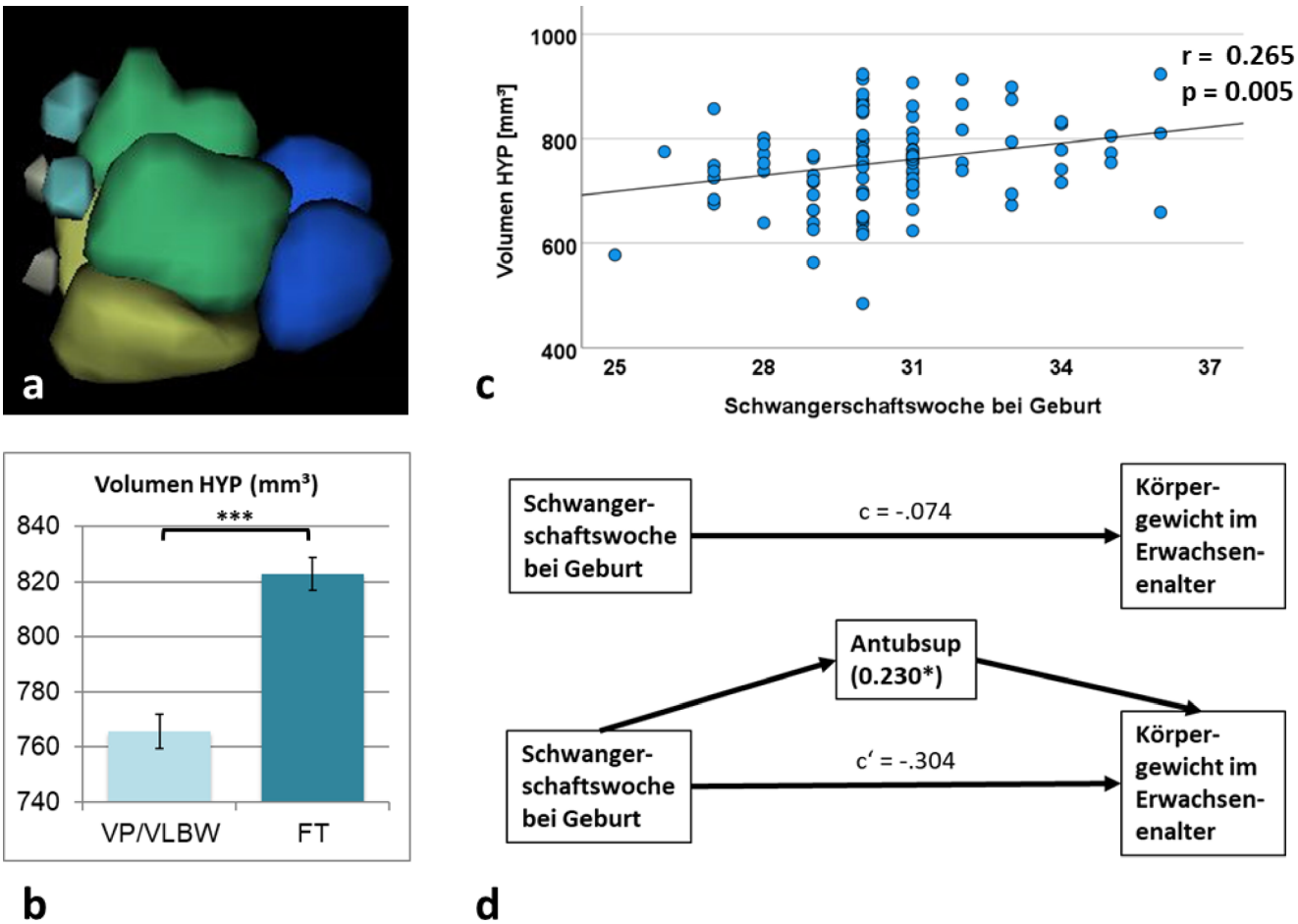

Abb. 1 | 126 (**a**) Der Hypothalamus und seine fünf Subsegmente (anterior – superior & inferior, tubular -superior & inferior und posterior) (**b**) Mittelwerte der HYP Volumina der Gruppen VP/VLBW (Very preterm and/or very low birthweight) vs. FT (Full term) aus allgemeinem linearem Modell; Fehlerbalken entsprechen den Standardfehlern (**c**) Assoziation zwischen Hypothalamusvolumen (in mm^3) und Schwangerschaftswoche bei Geburt (VP/VLBW Gruppe). Die lineare Regressionsgerade und die Regressionskoeffizienten der partiellen Korrelation sind ebenfalls eingezeichnet. (**d**) Mediationsmodell: Das „antubsup" Subsegment (= Summe der Subsegmente anterior superior & tubular superior) als sign. Mediator zwischen Schwangerschaftswoche bei Geburt und adultem Körpergewicht (in kg) in der VP/VLBW Gruppe (b-d jeweils kontrolliert für Geschlecht, totales intrakranielles Volumen und Typ des eingesetzten MR-Scanners)

Veränderungen nach Frühgeburt, die mit vermindertem Körperwachstum assoziiert sind.
Methoden: HYP-Subsegmentsegmentierung mittels Deep Convolutional Neural Network Algorithmus [1] anhand T1-gewichteter MRT (MPRAGE, 1 mm isotrop) von 101 sehr frühgeborenen Erwachsenen (Geburt vor der 32. Schwangerschaftswoche und/oder Geburtsgewicht <1500 g) und 110 Kontrollpersonen, als Teil der „Bayerischen Entwicklungsstudie".
Ergebnisse: Die Volumina des gesamten HYP und aller Subsegmente sind bei den frühgeborenen Erwachsenen vermindert ($p<0{,}05$, kontrolliert u. a. für intrakranielles Volumen und multiples Testen). Es zeigt sich eine signifikante Korrelation des HYP mit Variablen der Frühgeburtlichkeit (Schwangerschaftswoche bei Geburt, „Intensity of Neonatal Treatment Index"), insbesondere für mit Wachstumsvorgängen assoziierten Subsegmenten. Letztere sind nicht nur mit dem Körpergewicht im Erwachsenenalter assoziiert, sondern vermitteln auch die Beziehung von Frühgeburtsvariablen mit diesem. Hierbei tritt vorrangig das Subsegment „antubsup" als Mediator auf, welches sich durch Zusammenfügen zweier der fünf aus dem HYP segmentierten Untereinheiten ergibt und dadurch u. a. den Ncl. paraventricularis enthält (Abb. 1).
Diskussion: Die Volumina des HYP und seiner Kerngebiete hängen bei Frühgeburt mit Körperwachstum zusammen, wobei ursächlich auch andere ZNS-Ursachen und Komorbiditäten, maternale und genetische, umweltbezogene sowie endokrinologisch/metabolische Ursachen miteinbezogen werden müssen. Die Berücksichtigung individueller Wachstumstrajektorien und longitudinal erhobener MRT-Bilddaten könnte derartige Einflüsse weiter spezifizieren.
Fazit: Im Erwachsenenalter besteht eine Volumenverringerung des HYP nach Frühgeburt, die mutmaßlich den Einfluss von Frühgeburt auf das erwachsene Körpergewicht vermittelt.

Literatur

1. Billot B, et al. Automated segmentation of the hypothalamus and associated subunits in brain -MRI. Neuroimage. 2020.

[127] Improving automated glioma segmentation in routine clinical use through AI-based replacement of missing sequences with synthetic MR images

Marie Thomas[1*], Florian Kofler[1 2], Lioba Grundl[1], Tom Finck[1], Hongwei LI[2], Claus Zimmer[1], Björn Menze[2], Benedikt Wiestler[1 3]

[1]Klinikum rechts der Isar der Technischen Universität München, Abteilung für diagnostische und interventionelle Neuroradiologie, München, Germany
[2]Technische Universität München, Chair for Computer Aided Medical Procedures & Augmented Reality, Garching, Germany
[3]Technische Universität München, Zentralinstitut für translationale Krebsforschung, München, Germany

Background: While automated glioma segmentation holds promise for objective assessment of tumor biology and response [1], its routine clinical use is impaired by missing sequences, e. g. due to motion artifacts. The aim of our study was to develop and validate a Generative Adversarial Network for synthesizing missing sequences to allow for a robust automated segmentation.
Methods: Our model was trained on data from The Cancer Imaging Archive [2] ($n=238$ WHO °II–°IV gliomas) to synthesize either missing FLAIR, T2w, T1w or contrast-enhanced T1w images from available sequences, using a novel tumor-targeting loss to improve synthesis of tumor areas. We validated performance in a test set from both the REMBRANDT repository and our local institution ($n=68$ WHO °II–°IV gliomas), using qualitative image appearance metrics, but also segmentation performance with state-of-the-art segmentation models. Segmentation of synthetic images was compared with two commonly used strategies for handling missing input data, entering a blank mask or copying an existing sequence.
Results: Across tumor areas and missing sequences, synthetic images generally outperformed both conventional approaches, in particular when FLAIR was missing. Here, for edema and whole tumor segmentation we improved the Dice score by 12 % and 11 %, respectively, over the best conventional method. No method was able to reliably replace missing contrast-enhanced T1w images.
Discussion: Our approach significantly outperforms conventional strategies of handling missing input data. Importantly, this outperformance is stable across two very different, challenging glioma data sets, highlighting the robustness and clinical applicability of our model.
Conclusion: Replacing missing non-enhanced MR sequences via synthetic images significantly improves segmentation quality over conventional approaches. This model is freely available and facilitates more widespread use of automated segmentation in routine clinical use, where missing sequences are common.

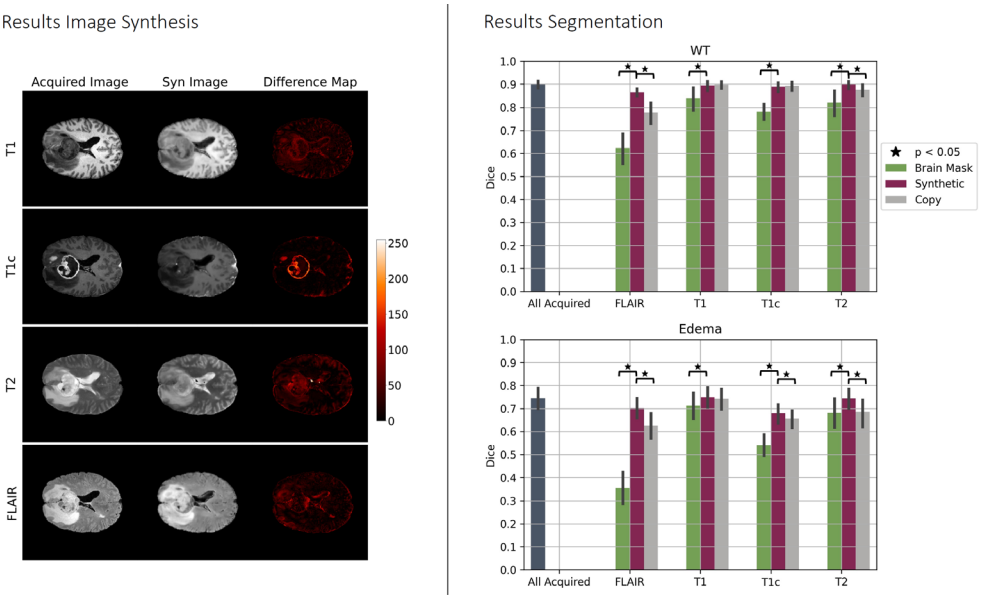

Fig. 1 | 127

References

1. Ghaffari M, Sowmya A, Oliver R. Automated Brain Tumor Segmentation Using Multimodal Brain Scans: A Survey Based on Models Submitted to the BraTS 2012–2018 Challenges. IEEE Rev Biomed Eng. 2020;13:156–68.
2. Bakas S, Akbari H, Sotiras A, et al. Advancing The Cancer Genome Atlas glioma MRI collections with expert segmentation labels and radiomic features. Sci Data. 2017;4:170117. https://doi.org/10.1038/sdata.2017.117.

[129] Virtuelle AVM Embolisation – ein Tool zur Verbesserung der Behandlungsplanung

Daniel Behme[1,2], Ulrike Sprengel[3], J Stahl[2], P Saalfeld[3], Benjamin Behrendt[3], Maximilian Thormann[1], Anastasios Mpotsaris[1], B Preim[3], Philipp Berg[2,4], Sylvia Saalfeld[2*,3]

[1]Klinik für Neuroradiologie, Universitätsklinik Magdeburg, Deutschland
[2]Forschungscampus STIMULATE, Magdeburg, Deutschland
[3]Department of Simulation and Graphics, Universität Magdeburg, Magdeburg, Deutschland
[4]Department of Fluid Mechanics and Technical Flows, Magdeburg, Deutschland

Hintergrund: Die Behandlung von AVM mit Flüssigembolisation bleibt eine Herausforderung, vor allem bei großen AVM mit multiplen Feedern. Insbesondere hier kann der vorzeitige Verschluss der drainierenden Vene zu einer Ruptur führen. Das Tool zur virtuellen AVM-Embolisation wurde entwickelt, um vor der Behandlung ein besseres Verständnis für hämodynamische Veränderungen durch partielle Embolisationsschritte zu gewinnen.
Methoden: 3-D-AVM-Oberflächenmodelle wurden von multimodalen Bilddaten (3-D-DSA und -MRT) extrahiert. Für die virtuelle Embolisation wurden alle Feeder identifiziert und separat verschlossen. Für die Anzahl Feeder (n) wird eine Gesamtzahl von n^2 Blutflusssimulationen mittels CFD durchgeführt. Ein Tool zur 3-D-Visualisierung des Flusses und seiner Veränderungen wurde die Game Engine Unity genutzt und der Fluss als Millionen kleiner Partikel dargestellt.
Ergebnisse: Das Softwartetool zur virtuellen AVM-Embolisation erlaubt es den behandelnden Neurointerventionalist*innen, spezifische AVM im 3-D-Modell zu simulieren; hierbei können einzelne Feeder selektiv verschlossen werden und Fluss- bzw. Druckveränderungen so im Vorhinein abgeschätzt werden.
Diskussion: Die Planung einer AVM-Embolisation beruht aktuell fast ausschließlich auf der Erfahrung von Behandler*innen, das Tool zur virtuellen AVM Embolisation gibt nun eine Möglichkeit, dedizierte Fragen an Fluss- und Druckveränderungen einer AVM während einer Intervention zu planen.
Fazit: Da der Behandlungserfolg und das Risikomanagement einer AVM-Embolisation mit der hämodynamischen Balance während der AVM-Embolisation zusammenhängen, kann das Tool zur virtuellen Embolisation wertvolle Unterstützung bieten, um die richtige Embolisationsstrategie anzuwenden.

[132] Einfluss von Feedback über das Outcome endovaskulär behandelter Schlaganfallpatienten auf die Arbeitszufriedenheit neuroradiologischen Personals

Charlotte Hager[1], Homan Taufik[1], Friederike Blum[1], Andrea Stockero[1], Rebecca May[1], Arno Reich[1], Martin Wiesmann[1], Omid Nikoubashmann[1*]

[1]Uniklinik RWTH Aachen, Aachen, Deutschland

Hintergrund: In der endovaskulären Schlaganfalltherapie sind Therapie und der weitere Verlauf von Patienten häufig entkoppelt. Daher gaben wir auf Wunsch unseres Personals dem gesamten neuroradiologischen Personal, einschließlich Ärzten, MTRAs und Forschern, über einen Zeitraum von 6 Monaten per E-Mail systematisches Feedback über den weiteren klinischen Verlauf (Entlassung und 90-Tage-Follow-up) von endovaskulär behandelten Schlaganfallpatienten. Wir analysierten die Auswirkungen dieses Feedbacks auf die Arbeitszufriedenheit, die Bewertung der Sinnhaftigkeit der Arbeit und die Bewertung der endovaskulären Therapie.
Methoden: Unsere Mitarbeiter füllten vor und nach dem Zeitraum von sechs Monaten mit systematischem Feedback jeweils einen Fragebogen bezüglich ihrer Arbeitszufriedenheit, der Bewertung der Sinnhaftigkeit ihrer Arbeit und die Bewertung der endovaskulären Therapie aus.
Ergebnisse: Mitarbeiter mit höherer Bewertung der Sinnhaftigkeit ihrer Arbeit und höherer Arbeitszufriedenheit bewerteten die endovaskuläre Schlaganfalltherapie als nützlicher ($p<0{,}001$). Ein gutes klinisches Ergebnis wurde als motivierender angesehen als ein gutes interventionelles Ergebnis ($p<0{,}001$). Das Erhalten von systematischem Feedback erhöhte weder die Arbeitszufriedenheit ($p=0{,}318$) noch die Sinnhaftigkeit der Arbeit ($p=0{,}178$). MTRAs bewerteten die Sinnhaftigkeit der interventionellen Therapie am schlechtesten von allen Mitarbeitern ($p\leq0{,}017$). Nach der Feedback-Phase schätzten 75 % der MTRAs den Schlaganfall als eine schwerere Erkrankung ein als zuvor. Auch ihr Wunsch nach Feedback nahm signifikant ab ($p=0{,}007$). Vor allem Fälle mit ungünstigem Ausgang blieben den Mitarbeitern im Gedächtnis.
Diskussion: Systematisches E-Mail-Feedback über den klinischen Verlauf endovaskulär behandelter Schlaganfallpatienten erhöht nicht per se die Arbeitszufriedenheit oder die Bewertung der Sinnhaftigkeit der Arbeit bei Mitarbeitern. Der Erhalt von Feedback ist jedoch lehrreich für die Mitarbeiter. Die Evaluierung der Arbeitszufriedenheit und der Wahrnehmung der Behandlung kann helfen, unerwartete Probleme zu identifizieren und spezifische Maßnahmen zu finden, welche die Arbeitszufriedenheit und Motivation erhöhen.
Fazit: Systematisches E-Mail-Feedback über den klinischen Verlauf endovaskulär behandelter Schlaganfallpatienten erhöht nicht per se die Arbeitszufriedenheit, kann aber dazu dienen, das Bild über die Erkrankung und die Möglichkeiten der Therapie besser einzuordnen.

[134] Start, stop, continue? Overlapping intravenous thrombolysis and mechanical thrombectomy: a matched case-control analysis from the German Stroke Registry

Egon Burian[1*], Dominik Sepp[1], Manuel Lehm[1], Kathleen Bernkopf[2], Silke Wunderlich[2], Christian Maegerlein[1], Claus Zimmer[1], Tobias Boeckh-Behrens[1]

[1]Abteilung für Neuroradiologie, Klinikum rechts der Isar, München, Germany
[2]Klinikum rechts der Isar der Technischen Universität München, München, Germany

Background: Intravenous thrombolysis is frequently started before mechanical thrombectomy in patients with large vessel occlusion. Reliable data on different clinical approaches regarding the temporal overlap of alteplase administration and the beginning of mechanical thrombectomy are scarce. Here we report the procedural and clinical outcome of patients undergoing thrombectomy with running thrombolysis to matched controls with completed intravenous therapy and no overlapping activity.
Methods: Patients' baseline characteristics (including ASPECTS, NIHSS and mRs), grade of reperfusion, and functional outcome 24 h and at day 90 after intervention were extracted from the German Stroke Registry ($n=2566$). In a case-control design we stepwise matched the groups due to age, sex and time to groin puncture and time to flow restoration. Surrogate parameters for early neurological improvement (ΔNIHSS baseline/NIHSS after 24 h and NIHSS 24 after hours of 0/1), procedural and functional outcome were compared between the two groups.
Results: In the initial cohort (overlap group $n=864$, control group $n=1702$) reperfusion status (median TICI in overlap group vs. control

group: 3 vs 2b), NIHSS after 24 h, early neurological improvement parameters, mRs at 24 h and at day 90 were significantly better in the overlap group ($p<0.001$) with a similar risk of bleeding (2,9 % vs. 2,4 %) and death (18 % vs. 22 %).

After adjustment for age, sex, baseline NIHSS, ASPECTS and time to groin puncture and time to flow restoration, mRs at day 90 still showed a statistical tendency for lower disability scores in the overlap group (3 IQR 4 vs 3 IQR 5, $p=0.09$). While comparable bleeding risk could be maintained (4 % in both groups), there were more deaths in the control group (18 % vs. 30 %).

Discussion: The presented results support the approach of continuing and completing a simultaneous administration of intravenous thrombolysis during mechanical thrombectomy procedures in patients with acute ischemic stroke.

Conclusion: Simultaneous administration of intravenous thrombolysis and initiation of mechanical thrombectomy is safe with comparable functional and procedural outcome as mechanical thrombectomy performed after completed alteplase treatment.

[138] Altered grey matter myelination in premature-born adults

Benita Schmitz-Koep[1*, 2], Aurore Menegaux[1, 2], Claus Zimmer[1, 2], Christian Gaser[3, 4], Dieter Wolke[5, 6], Peter Bartmann[7], Christian Sorg[1, 2, 8], Dennis Hedderich[1, 2]

[1]Abteilung für Diagnostische und Interventionelle Neuroradiologie, Klinikum rechts der Isar, Technische Universität München, München, Germany
[2]TUM-NIC Neuroimaging Center, Klinikum rechts der Isar, Technische Universität München, München, Germany
[3]Klinik für Neurologie, Universitätsklinikum Jena, Jena, Germany
[4]Klinik für Psychiatrie und Psychotherapie, Universitätsklinikum Jena, Jena, Germany
[5]Department of Psychology, University of Warwick, Coventry, United Kingdom
[6]Warwick Medical School, University of Warwick, Coventry, United Kingdom
[7]Abteilung für Neonatologie, Universitätsklinikum Bonn, Bonn, Germany
[8]Klinik und Poliklinik für Psychiatrie und Psychotherapie, Klinikum rechts der Isar, Technische Universität München, München, Germany

Background: Microscopic studies in newborns and animal models indicate impaired myelination after premature birth, particularly for cortical myelination; however, it is not clear whether myelination impairments of prematurity last into adulthood and–if so–are relevant for impaired cognitive performance. The ratio of T1w and T2w MRI signal intensity is a proxy for myelin content. We hypothesized altered grey matter (GM) T1w/T2w ratio in premature-born adults, which is associated with lower cognitive performance after premature birth.

Methods: We analyzed the T1w/T2w ratio in GM in 101 very premature-born adults (<32 weeks of gestation and/or birth-weight <1500 g, VP/VLBW) and 109 full-term (FT) controls at 26 years of age. Cognitive performance was assessed by verbal, performance, and full-scale intelligence quotient (IQ) using the Wechsler Adult Intelligence Scale.

Results: We found significantly ($p<0.05$, FDR-corrected, cluster size >10 voxels) higher T1w/T2w ratio in VP/VLBW subjects compared to FT controls in widespread cortical areas, particularly in frontal, parietal and temporal cortices, and in bilateral thalamus, putamen, pallidum, hippocampus and amygdala. Furthermore, we found significantly lower T1w/T2w ratio in bilateral superior temporal gyrus which was positively associated with gestational age and birth weight, and approximated a significant positive relationship with verbal IQ in the VP/VLBW group.

Discussion: In VP children, lower T1w/T2w ratio has been reported in the temporal lobes, occipital lobes, thalamus, putamen and amygdala. However, GM myelination is an ongoing process with an inverted U-shaped trajectory and a steep increase until the end of the 30s[6]. Hence, findings of increased T1w/T2w ratio could reflect reorganization of cortical myelin architecture, while lower T1w/T2w ratio might indicate particular vulnerability with lastingly reduced myelination after premature birth, possibly as a consequence of dysmaturational processes such as pre-oligodendrocyte death.

Conclusion: T1w/T2w ratio in GM is lastingly altered after premature birth, indicating aberrant GM myelination.

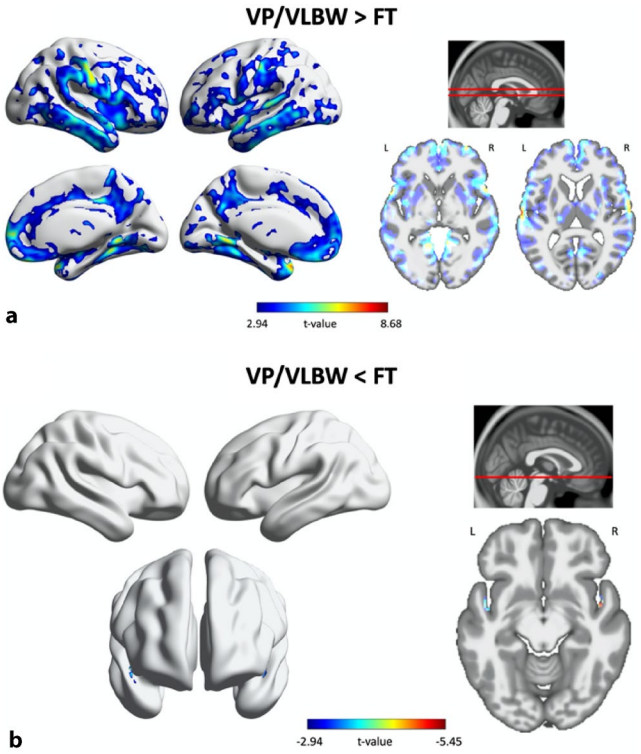

Fig. 1 | 138 Voxel-wise group comparison of T1w/T2w ratio controlling for GM volume in a voxel-wise way and with sex and scanner an additional covariates. **a** shows areas in which Tlw/T2w ratio was significantly higher in VP/VLBW subjects compared to FT controls. **b** shows areas in which T1w/T2w ratio was significantly lower in VP/VLBW subjects compared to FT controls. Significance was defined as $p<0.05$, FDR-corrected, cluster size >10 voxels

References

1. Ball G, Srinivasan L, Aljabar P, Counsell SJ, Durighel G, Hajnal JV, et al. Development of cortical microstructure in the preterm human brain. Proc Natl Acad Sci. 2013;110(23):9541–6. https://doi.org/10.1073/pnas.1301652110.
2. Dean JM, McClendon E, Hansen K, Azimi-Zonooz A, Chen K, Riddle A, et al. Prenatal cerebral ischemia disrupts MRI-defined cortical microstructure through disturbances in neuronal arborization. Sci Transl Med. 2013;5(168):168ra7–168ra7. https://doi.org/10.1126/scitranslmed.3004669.
3. Volpe JJ. Dysmaturation of Premature Brain: Importance, Cellular Mechanisms, and Potential Interventions. Pediatr Neurol. 2019;95:42–66. https://doi.org/10.1016/jpediatrneuro1.2019.02.016.
4. Ganzetti M, Wenderoth N, Mantini D. Whole brain myelin mapping using T1- and T2-weighted MR imaging data. Front Hum Neurosci. 2014; https://doi.org/10.3389/fnhum.2014.00671.

5. Vandewouw MM, Young JM, Shroff MM, Taylor MJ, Sled JG. Altered myelin maturation in four year old children born very preterm. Neurolmage: Clin. 2019;21:101635. https://doi.org/10.1016/j.nic1.2018.101635.
6. Grydeland H, Walhovd KB, Tamnes CK, Westlye LT, Fjell AM. Intracortical myelin links with performance variability across the human lifespan: results from T1- and T2-weighted MRI myelin mapping and diffusion tensor imaging. J Neurosci Off J Soc Neurosci. 2013;33(47):18618–30. https://doi.org/10.1523/JNEUROSCI.2811-13.2013.

[140] Flow diverter treatment of ruptured basilar artery perforator aneurysms: a pooled multi-center experience

Samer Elsheikh[1*], Markus Möhlenbruch[2], Fatih Seker[2], Ansgar Berlis[3], Christoph Maurer[3], Naci Kocer[4], Ala Jamous[5], Daniel Behme[5,6], Horst Urbach[1], Stephan Meckel[1,7]

[1]Neurozentrum der Uniklinik Freiburg, Freiburg im Breisgau, Germany
[2]Universitätsklinikum Heidelberg, Heidelberg, Germany
[3]Universitätsklinikum Augsburg, Augsburg, Germany
[4]İstanbul Üniversitesi-Cerrahpaşa, Radiology Department, Division of Neuroradiology, Turkey
[5]Institut für Diagnostische und Interventionelle Neuroradiologie–Universitätsmedizin Göttingen, Göttingen, Germany
[6]Otto-von-Guericke-Universität Magdeburg, Institut für Neuroradiologie, Magdeburg, Germany
[7]Johannes Kepler Universität Linz–JKU, Linz, Austria

Background: Ruptured basilar artery perforator aneurysms (BAPAs) represent a very rare cause of subarachnoid hemorrhage and under-reported subtype of cerebral aneurysm. There is no consensus for the optimal treatment strategy (conservative vs. surgical vs. various endovascular approaches). We aim to present a multicenter experience of BAPA treatment using flow-diverter (FD) stents.
Methods: At five large tertiary neurovascular centers, all cases of ruptured BAPAs treated by FD were retrospectively collected. Baseline imaging and clinical characteristics, complications, as well as early and long-term angiographic and clinical outcome (mRS) were analyzed.
Results: A total of 18 patients (mean age: 57; SD ±10.7 years) with acute SAH related to a BAPA were treated using 18 FD stents. Aneurysms were detected on initial imaging study in 28 %; delayed diagnosis was triggered by clinical deterioration due to rebleeding in 15 %. No rebleeding after FD was seen, 28 % developed FD-related ischemic complications. At long-term ($n=16$), overall mortality was 13 % (2/16), and favorable outcome (mRS 0–2) was 81 % (13/16). All BAPAs were completely occluded at long-term angiographic follow-up.
Discussion: In this pooled multi-center cohort is, to our knowledge, the largest published case-series of FD treatment of BAPAs. BAPAs are usually small and commonly not diagnosed in the acute neurovascular imaging. Early rebleeding is not uncommon. Treatment using FD mandates long-term antiplatelet therapy. The need for antiplatelet therapy may collide with acute operative procedures (e. g. drainage of acute hydrocephalus). Careful coordination is important to avoid bleeding complications. Ischemia is an important complication both in conservative and endovascular treatment of BAPAs. As spontaneous resolution is well documented in the literature, conservative treatment is a valid alternative strategy. Although the occlusion rate is lower compared to endovascular therapy, the outcome of both strategies is comparable. Due to the rarity of BAPAs, there is no clear evidence favoring conservative vs. endovascular treatment.
Conclusion: In our retrospective multicenter experience, FD was a safe and effective treatment for ruptured BAPAs exhibiting complete angiographic occlusion, protection from rebleeding, and a high rate of favorable outcome. Future studies comparing FD to conservative management are required to define the optimal treatment strategy.

[142] Ätiologie und klinische Relevanz von extravasalen Kontrastmittelakkumulationen in der kraniellen Computertomographie nach endovaskulärer Behandlung inzidenteller zerebraler Aneurysmen

Jenna Schellin[1]*, Hannes Schacht[1], Peter Schramm[1], Alexander Neumann[1]

[1]Lübeck, UKSH, Campus Lübeck, Lübeck, Deutschland

Hintergrund: Nach endovaskulärer Therapie (ET) von zerebralen Aneurysmen (CA) sind abweichende Befunde mit Kontrastmittelakkumulationen (KMA) in der kraniellen Computertomographie (CCT) beschrieben. Diese können eine Blutung vortäuschen und mit klinischen Symptomen einhergehen.
Methoden: Auswertung der postinterventionellen CCT und der Verlaufsbildgebung in Bezug auf extravasale Dichtesteigerungen (EDS) bei 58 Patienten (44 weiblich, 14 männlich; medianes Alter: 61 Jahre) mit insgesamt 68 behandelten CA in 62 Prozeduren (24 ACM, 21 ACI/PCOM, 14 ACA, 9 vertebrobasilär). Verteilung der Devices: $n=15$ Coils, $n=27$ Coils+Stent, $n=15$ intrasakkulärer Flowdisruptor (IFD), $n=6$ tubulärer Flowdiverter (TFD), $n=1$ IFD+Stent, $n=2$ TFD+Coil, $n=1$ IFD+Coil, $n=1$ IFD+Coil+Stent. Unterscheidung KMA/Blutung: EDS in der CCT mit deutlicher Regression innerhalb von 24–48 h definiert als KMA, bei Persistenz als Blutung. Untersuchung des Zusammenhangs von KMA mit den Faktoren Alter und Gender, Dauer der ET und Narkose, Lokalisation der CA, verwendete Devices, verabreichte KM-Menge und Thrombozytenaggregationshemmung (TAH). Zudem Erfassung von mit dem Auftreten von EDS verbundenen Symptomen.
Ergebnisse: Nach 17/62 ET von CA (27,4 %) zeigten sich extravasale KMA in der CCT; in 2 Fällen (3,2 %) zunächst unauffällige CCT, in der Verlaufsbildgebung Nachweis einer peripheren SAB. In der logistischen Regressionsanalyse signifikante Assoziation von KMA sowohl mit der Interventionsdauer ($p=0{,}038$) als auch mit der verwendeten TAH ($p=0{,}04$; häufiger KMA bei Mono- als bei dualer TAH). Signifikanter Zusammenhang von Symptomen und KMA ($p=0{,}01$), jeweils vollständig reversibel.
Diskussion: Bislang spärliche Literatur zu Befunden in der CCT unmittelbar nach ET von CA und Einflussfaktoren [1, 2]. Hier bislang größte Fallserie zu speziell ausnahmslos inzidentellen CA und Berücksichtigung erstmals auch moderner Devices (IFD, TFD).
Fazit: EDS im CCT sind nach der ET von CA ein häufiger Befund, in der Mehrzahl KMA entsprechend. Möglicher Zusammenhang mit Symptomen, die bei uns ausnahmslos reversibel waren. KMA sind als wichtige DD zu Blutung oder Infarkt zu bedenken.

Literatur

1. Brisman JL, Jilani M, McKinney JS. Contrast enhancement hyperdensity after endovascular coiling of intracranial aneurysms. Am J Neuroradiol. 2008;29(3):588–93.
2. Ozturk A, Saatci I, Pamuk AG, et al. Focal increased cortical density in immediate postembolization CT scans of patients with intracranial aneurysms. AJNR Am J Neuroradiol. 2006;27(9):1866–75. Oct.

[144] Effects of videogaming on dexterity while learning neurointerventional techniques

Sebastian Reder[1*], Annaïg Rohou[2], Naureen Keric[3], Carolin Brockmann[1], Mario Alberto Abello Mercado[1], Sebastian Altmann[4], Ahmed Othman[1], Marc A. Brockmann[1]

[1]Department of Neuroradiology, University Medical Center Mainz, Mainz, Germany
[2]Faculty of Psychology, University of Graz, Graz, Austria
[3]Department of Neurosurgery, University Medical Center Mainz, Mainz, Germany
[4]Department of Radiology, University Medical Center Mainz, Mainz, Germany

Background: Playing video games has been discussed to influence dexterity of individuals while learning and practicing medical techniques. There is no data available on the effects of video gaming experience on learning neurointerventional techniques.
Methods: Performance of 64 subjects (35 Gamer, 29 Non-gamer) naïve to neurointerventional techniques were analysed solving four neurointerventional tasks using a simulator. After a standardized short training sequence required time, number and pathway of catheter movements and tries to pass vascular branches were analysed. Afterwards, subjects had to answer a questionnaire regarding videogaming activities and other skills possibly influencing manual dexterity including NASA Task Load Index to rate individual workload.
Results: Gamer (G) required fewer tries to pass vascular branches with vertebralis- (V) and sidewinder-shaped (SW) catheters (5.03 ± 3.4 vs. 6.6 ± 3.6; $p = 0.035$ respectively 24.7 ± 16.6 vs. 34.4 ± 23.9; $p = 0.08$), V-pathway (25.1 ± 10.6 cm vs. 30.8 ± 15.5 cm; $p = 0.085$) and time (V+SW: 308.3 ± 227.4 s vs. 372.7 ± 215.2 s.; $p = 0.059$ respectively SW: 255.8 ± 222.2 s vs. 315.3 ± 206.9 s; $p = 0.079$) than Non-gamer (NG). For G, perceived stress-level correlated positive to pathway ($r = 0.43$; $p = 0.01$), tries ($r = 0.4$; $p = 0.017$) and catheter movements ($r = 0.37$; $p = 0.03$), but not for NG. Less G (1.7 ± 0.76) asked for help than NG (4.7 ± 2.7; $p = 0.029$). G playing ego-shooter/fighting-games (EF) needed less time in four tasks (in average 45 %; $p = 0.02$ to 0.06) than those playing strategic games (S). For EF, pathway correlated positive to stress-level ($r = 0.53$; $p = 0.076$). For S, tries correlated positive to stress-level ($r = 0.793$; $p = 0.034$).
Conclusion: Gamer, and here especially EF, needed less time, pathway, help and tries in simulated neurointerventional tasks than Non-gamer. Stress-level of G correlated positive to pathway, tries and movements, but not for NG. Stress-level of EF correlated positive to pathway. Stress-level of NG correlated positive to tries. Whether these findings should be transferred to selection and training of neuroradiologists remains to be elucidated.

[145] Kontrastmittelbolus-Interferenz in einem multimodalen CTA-CTP-Stroke-Protokoll

Elias Kellner[1*], Alexander Rau[1], Theo Demerath[1], Marco Reisert[1], Horst Urbach[1]

[1]Uniklinik Freiburg–Klinik für Neuroradiologie, Freiburg im Breisgau, Germany

Background: Whether CT perfusion (CTP) is performed before or after CT angiography (CTA) varies within multimodal CT stroke protocols. CTA after CTP might show venous filling and CTP metrics might be disturbed by prior CTA. Therefore, we compared CTP metrics conducted before and after CTA in a large cohort of stroke patients and analyzed interferences of the CTA bolus with the CTP measurement.
Methods: A total of 1980 patients (368 with CTP performed before CTA vs. 1602 patients with CTP performed after CTA) were analyzed. Mean curves, histograms of CTP baseline Hounsfield units (HU), CBF, CBV, Tmax, hypoperfusion, and core volumes were calculated using the software VEOcore. CTA and CTP interferences were rated and a correction method proposed (Fig. 1). The timing information was derived from the DICOM headers.
Results: Mean CTP baseline values were significantly different in both groups (41 vs. 45 HU), which cancelled out in calculation of tracer concentration curves. Perfusion metrics, hypoperfusion and core volumes showed no significant differences. In 49 patients, the descending flank of the CTA bolus interfered with the CTP-baseline, leading to erroneously CBV values. These errors vanished when applying a correction. Time gap between CTP and CTA, and vice versa was similar (60–90 s), but significantly shorter in the group showing bolus interference (18 s).
Discussion: These results are in line with [1]. A too short time gap between CTA and CTP is the major cause for bolus interference. Other confounding factors might be low cardiac output [2] and carotid stenosis.
Conclusion: CTP can be reliably performed after CTA without a significant net effect on perfusion metrics. However, when measuring CTP after CTA either a short pause in the order of 30 s should be respected or an appropriate correction method be applied.

References

1. Dorn F, et al. Order of CT stroke protocol (CTA before or after CTP): impact on image quality. Neuroradiology. 2012;54(2):105–12.
2. Konno M, et al. Cardiac output obtained from test bolus injections as a factor in contrast injection rate revision of following coronary CT angiography. Acta Radiol. 2012;53(10):1107–11. Dec 1.

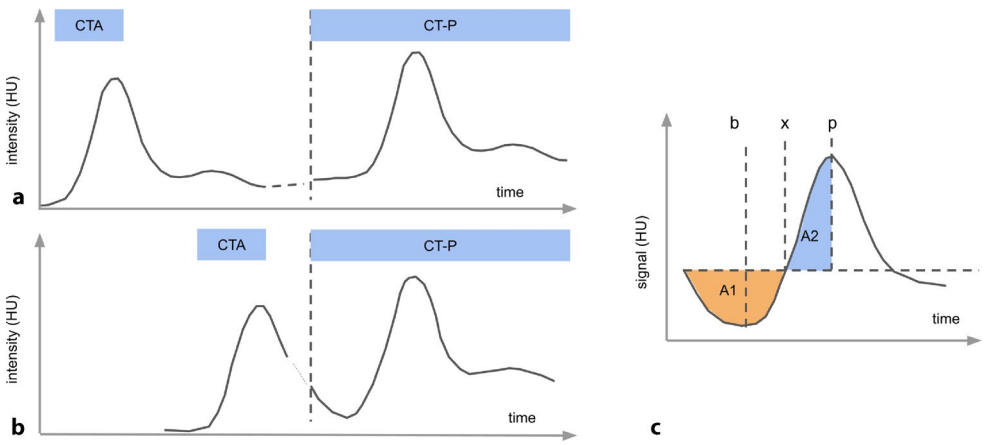

Fig. 1 | 145 **a** If there is a sufficiently long pause between CTA and CTP (>30 s), the CTA bolus is well-mixed in the vascular system. **b** For a short time gap, the trailing flank of the CTA bolus might interfere with the CTP baseline. **c** A simple correction based on comparing the areas A1 and A2, if above a certain threshold, the flank can be corrected by using point b as baseline

[151] Subcortical volume changes in glioma patients after radio(chemo)therapy

Felix Raschke[1*], Annekatrin Seidlitz[1,2], Tim Wesemann[3], Christina Jentsch[1,2], Ivan Platzek[4], Jörg Kotzerke[5], Jörg van den Hoff[6], Bettina Beuthien-Baumann[7], Michael Baumann[1,8], Jennifer Linn[3], Mechthild Krause[1,2], Esther Troost[1,2]

[1]OncoRay–National Center for Radiation Research in Oncology, Faculty of Medicine and University Hospital Carl Gustav Carus, Technische Universität Dresden, Helmholtz-Zentrum Dresden-Rossendorf, Dresden, Germany, Germany
[2]Department of Radiotherapy and Radiation Oncology, Faculty of Medicine and University Hospital Carl Gustav Carus, Technische Universität Dresden, Dresden, Germany
[3]Institute of Neuroradiology, Faculty of Medicine and University Hospital Carl Gustav Carus, Technische Universität Dresden, Dresden, Germany, Germany
[4]Department of Diagnostic and Interventional Radiology, Faculty of Medicine and University Hospital Carl Gustav Carus, Technische Universität Dresden, Dresden, Germany
[5]Department of Nuclear Medicine, Faculty of Medicine and University Hospital Carl Gustav Carus, Technische Universität Dresden, Dresden, Germany
[6]Helmholtz-Zentrum Dresden–Rossendorf, Institute of Radiopharmaceutical Cancer Research, Center for Positron Emission Tomography, Dresden-Rossendorf, Germany
[7]Radiology, German Cancer Research Center (DKFZ), Heidelberg, Germany
[8]German Cancer Research Center (DKFZ), Heidelberg, Germany

Background: Radiotherapy of brain tumor patients causes brain atrophy [1] and neurocognitive dysfunction [2]. The hippocampus is a suspected focal point of neurocognitive impairment, due to its known connection to dementia [3] and suspected increased radiosensitivity [4]. The goal of this study was to investigate volume changes of six subcortical structures in glioma patients after radio(chemo)therapy (RT) and compare the estimated atrophy rates.
Methods: The hippocampus, amygdala, putamen, thalamus, pallidum and caudate were automatically segmented from T1-weighted MR images (voxel size 1 mm^3) of 91 glioma patients before RT ($n=91$) and from longitudinal follow-ups acquired in three monthly intervals ($n=349$). Right and left structures were evaluated separately. Structures overlapping with or touching the clinical target volume or T2-hyperintensities were excluded from the analysis. Relative volumes were calculated as ratios to the pre-RT values. A multivariate linear mixed effects model was used to determine volume changes as function of time after RT, mean dose delivered to the corresponding structure and the interaction of time and dose.
Results: The linear mixed effects model revealed that the highest dose and time dependent atrophy occurs in the hippocampus, followed by the amygdala and thalamus. The caudate was the only structure that showed no significant volume changes with time and dose. Exemplarily, assuming a mean dose of 20 Gy and a follow-up time of 2 years, volume changes resulting from the mixed effects model were: hippocampus –6.1 %, amygdala –4.4 %, thalamus –3.5 %, pallidum –2.6 %, putamen –2.5 %, caudate –1.9 %.
Discussion: The six subcortical regions show very different levels of atrophy following RT. Further work is now needed to determine clinically relevant levels of hippocampal atrophy and subsequently calculate effective normal tissue complication probability models. This would be the basis to establish dose thresholds and dose sparing strategies.
Conclusion: The hippocampus showed the largest volume changes after RT, thus further strengthening the hypothesis that it is particularly radiosensitive.

References

1. Petr, et al. Radiother Oncol. 2018;128:121–7.
2. Douw, et al. Lancet Neurol. 2009;8:810–8.
3. Moodley, et al. Front Neurol Neurosci. 2014;34:95–108.
4. Seibert, et al. Int J Radiat Oncol Biol Phys. 2017;97:263–9.

[152] Mechanische Thrombektomie bei Patienten mit distalem Gefäßverschluss im vorderen Stromgebiet: eine Propensity-Score-Matching-Analyse

Dominik Sepp[1*], Moritz Hernandez Petzsche[1], Teresa Zarth[1], Claus Zimmer[1], Christian Maegerlein[1], Tobias Boeckh-Behrens[1], Jan Kirschke[1]

[1]Technische Universität München, Klinikum rechts der Isar, Abteilung für Diagnostische und Interventionelle Neuroradiologie, München, Deutschland

Hintergrund: Die mechanische Thrombektomie (MT) gehört beim akuten zerebralen Infarkt mit proximalem Gefäßverschluss zu den wichtigsten Therapieoptionen. Bei distalen Gefäßverschlüssen sind die Evidenzen jedoch schwächer und die Therapieentscheidung daher oft schwieriger zu treffen. Diese Studie vergleicht Patienten mit akutem distalem Gefäßverschluss im vorderen Stromgebiet, bei denen eine mechanische Thrombektomie durchgeführt wurde, mit Patienten, die ausschließlich „best medical treatment" (BMT) inklusive systemischer Thrombolyse erhalten haben.
Methoden: Eingeschlossen wurden Patienten mit primärem distalen Verschluss der A. cerebri media (MCA) im distalen M2- und M3-Segment sowie der A. cerebri anterior (ACA), die zwischen 01/2015 und 12/2020 in unserem Schlaganfallzentrum aufgenommen und behandelt wurden. Klinischer Endpunkt war die Verbesserung des NIHSS (National Institutes of Health Stroke Scale) zwischen Aufnahme und Entlassung.
Ergebnisse: Insgesamt konnten 148 Patienten eingeschlossen werden. Davon konnten 48 Patienten mit MT und 48 Patienten mit BMT mittels 1:1 Propensity-Score-Matching gematcht werden. Die Gefäßverschlüsse befanden sich bei 70 Patienten (72,9 %) in der MCA (distale M2 und M3), bei 21 Patienten (21,9 %) in der ACA und bei 5 Patienten (5,2 %) in beiden Gefäßen. Die MT war bei 33 von 48 Patienten erfolgreich (≥ TICI 2b). Die mediane Verbesserung des NIHSS bis Entlassung betrug 3,0 Punkte (Q1 = 0,0; Q3 = 6,0) bei den Patienten mit MT und nur 1,0 Punkte (Q1 = 0,0; Q3 = 5,0) bei den Patienten mit BMT ($p=0,16$). Bei ausschließlicher Berücksichtigung der Patienten mit einer erfolgreichen mechanischen Rekanalisation (≥ TICI 2b) war die Verbesserung des NIHSS im Vergleich zu der BMT-Gruppe noch relevanter (Median: 5,0 Punkte; Q1 = 1,0, Q3 = 8,5, $p=0,01$).
Diskussion/Fazit: Diese Studie zeigt, dass die mechanische Thrombektomie auch bei distalen Gefäßverschlüssen der MCA und der ACA angewendet werden kann und insbesondere bei erfolgreicher Rekanalisation den klinischen Verlauf signifikant verbessert.

[153] KI-basierte Volumetriealgorithmen zur Unterstützung bei der bildgebenden Epilepsiediagnostik

Anna-Lena Mayer[1*], Angelika Mennecke[1], Stefan W. Hock[1], Dominique Marterstock[1], Julie Rösch[1], Hajo Hamer[2], Burkhard Kasper[2], Arnd Dörfler[1], Manuel Schmidt[1]

[1]Universitätsklinikum Erlangen, Neuroradiologische Abteilung, Erlangen, Deutschland
[2]Universitätsklinikum Erlangen, Neurologische Klinik, Erlangen, Deutschland

Hintergrund: Die automatisierte Berechnung des Hirnvolumens aus MRT-3-D-Datensätzen erlaubt eine zeitsparende quantitative Beurteilung des Hirnvolumens in der klinischen Befundungsroutine. Ziel dieser Arbeit war es, zwei unabhängige Softwarelösungen hinsichtlich

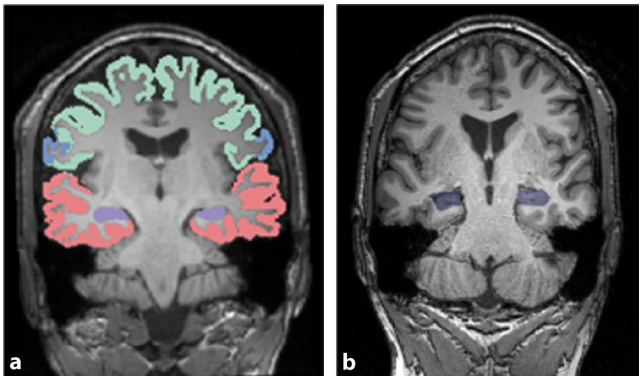

Abb. 1 | 153 **a**: Segmentierungskartierung der Software mdbrain. Hippocampusformation (*lila*), Temporallappen-Kortex (*rot*), Parietallappen-Kortex (*blau*), Frontallappen-Kortex (*grün*). **b**: mdbrain Hippocampus-Segmentierung (*lila*)

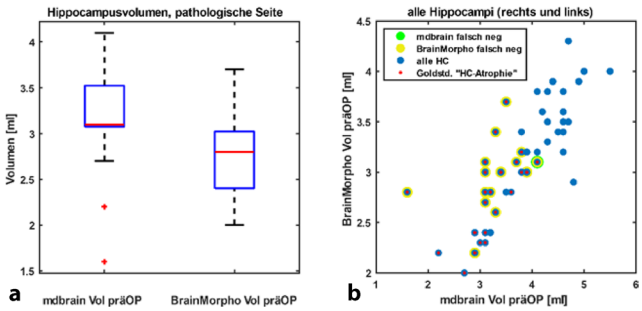

Abb. 2 | 153 **a**: Boxplots der absoluten Volumenangaben des pathologischen Hippocampus (HC) in Milliliter (ml). mdbrain vs. BrainMorphometry (3,2 ml vs. 2,7m1; $p<0{,}005$). **b**: Absolute Volumenangaben aller Hippocampi (HC) in ml (gesunde und pathologische Seite) für mdbrain- und BrainMorphometry (*blau*). Darstellung der Volumenbewertung: Goldstandard klassifizierte Hippocampusvolumenminderung (*rot*), falsch negativ bewertetes HC-Volumen durch mdbrain (*grün*), falsch negativ bewertetes HC-Volumen durch BrainMorphometry (*gelb*)

Sensitivität und Validität bei der Erkennung von volumengeminderten Hippocampussklerosen zu vergleichen.
Methoden: Präoperative MRT-Bilder (1,5 T und 3 T, T1w MPRAGE sag 3D) von 25 Patienten mit histologisch gesicherter Hippocampussklerose (Typ 1: $n=20$, Typ 2: $n=4$, Typ 3: $n=1$) wurden retrospektiv in die Untersuchung eingeschlossen. Es wurden die Softwareprogramme mdbrain Version 3.4.0 (Mediaire, Berlin) und BrainMorphometry VB50B (Syngo.via, Siemens Healthineers, Erlangen) zur automatischen Volumenmessung des Hippocampus verwendet und mit der Klassifizierung durch 3 unabhängige Neuroradiologen anhand eines kompletten MRT-Epilepsieprotokolls verglichen.
Ergebnisse: Die Sensitivität für die Erkennung einer Hippocampussklerose (anhand der Volumenminderung) lag bei 96,0 % für mdbrain und 32,0 % für BrainMorphometry. Die Spezifität war 100 % zum Goldstandard. Die berechneten Volumina unterschieden sich signifikant zwischen mdbrain und BrainMorphometry (3,2 ml vs. 2,7 ml; $p<0{,}005$). Es bestand eine signifikante positive Korrelation ($r=0{,}79$) zwischen den Volumina.
Diskussion: KI-basierte Algorithmen sind geeignet Hippocampussklerosen anhand der Volumenminderung zu detektieren. Da es jedoch deutliche Unterschiede in den absoluten Volumenangaben und Bewertungen bezüglich pathologischer Werte gibt, müssen die Programme vor einer Routineanwendung auf ihre Eignung für die jeweilige Fragestellung überprüft werden. Die unterschiedlichen Sensitivitäten könnten u. a. durch unterschiedliche Grenzwerte für den Volumennormbereich verursacht werden. Hippocampussklerosen ohne Volumenminderung können mit dieser Methode nicht detektiert werden.
Fazit: Abhängig von der gewählten Softwarelösung ist eine Hippocampussklerose (Volumenminderung) mit einer Sensitivität von bis zu 92,3 % bei einer Spezifität von 100 % detektierbar. So können KI-basierte Algorithmen den Radiologen unterstützen und die bildgebende Epilepsiediagnostik verbessern bzw. beschleunigen.

Literatur

1. Blümcke I. et al. Epilepsia. 2013 Jul.
2. Lehéricy S. et al. J Radiol. 1996 Nov.
3. Malmgren K. et al. Epilepsia. 2012 Sep.
4. Masaki H. et al. Jpn J Radiol. 2020 Nov.

[154] Standardisierte Klassifikation des zerebralen Vasospasmus nach subarachnoidaler Blutung in der digitalen Subtraktionsangiographie

Cindy Richter[1*], Helena Merkel[1], Jennifer Jentzsch[1], Ulf Quäschling[1], Dirk Lindner[2], Svitlana Ziganshyna[3], Stefan Schob[4], Karl-Titus Hoffmann[1], Khaled Gaber[5]

[1]Institut für Neuroradiologie Universitätsklinikum Leipzig, Leipzig, Deutschland
[2]Klinik und Poliklinik für Neurochirurgie Universitätsklinikum Leipzig, Leipzig, Deutschland
[3]Klinik und Poliklinik für Anästhesiologie und Intensivtherapie, Universitätsklinikum Leipzig, Leipzig, Deutschland
[4]Universitätsklinikum Halle Universitätsklinik und Poliklinik für Radiologie, Halle (Saale), Deutschland
[5]Klinik und Poliklinik für Neurochirurgie, Universitätsklinikum Leipzig, Leipzig, Deutschland

Hintergrund: Der zerebrale Vasospasmus (ZVS) nach einer aneurysmatischen, subarachnoidalen Blutung (SAB) ist eine Erkrankung, die mit einer hohen Letalität von mehr als 30 % einhergeht. Pharmakologische und mechanische Spasmolysen sind aktuelle Forschungsschwerpunkte, jedoch gibt es keine standardisierte ZVS-Klassifikation, die einen Vergleich der Wirksamkeit ermöglicht. In dieser Studie wurden Referenzwerte für eine Gefäßdurchmesser-basierte ZVS-Klassifikation erhoben. Weiterführend wurde die zeitliche und anatomische Manifestation des ZVS untersucht, um eine neue standardisierte, visuelle Klassifikation zu etablieren.
Methoden: Der Verlauf des prolongierten ZVS in der digitalen Subtraktionsangiographie wurde von 33 SAB-Patienten, welche intraarterielle, pharmakologische Spasmolysen erhielten, ausgewertet. Die Durchmesser der Gefäßsegmente C5–C7, A1, M1 und der proximalen A2 und M2 wurden an drei Zeitpunkten (Hospitalisierung, vor Spasmolyse, 6-Monats-Kontrolle) erhoben. Die Referenzwerte wurden an den gleichen Lokalisationen bei 301 weiteren Patienten bestimmt.
Ergebnisse: Die 6-Monats-Kontrollen der ZVS-Gruppe und die Referenzwerte unterschieden sich nicht signifikant, was die Genauigkeit unserer Ergebnisse bestätigt. Hingegen wichen die Gefäßdurchmesser bei Hospitalisierung am Tag der SAB signifikant von den Referenzwerten ab, wohingegen die Tage 1–2 physiologische Werte ergaben. Die initialen Messungen ab Tag 3 zeigten eine progrediente Gefäßverengung. Die frühe Manifestation von ZVS betrifft die distalen Segmente (besonders das A2-Segment), gefolgt von einer proximalen Ausbreitung bis zum C5-Segment.
Diskussion: Als Konsequenz dieses zeitlichen Verlaufes entwickelten wir eine neue visuelle Klassifikation, die auf der Ausbreitung des ZVS von den distalen zu den proximalen Gefäßsegmenten basiert. Referenzwertbasierte Klassifikationen sind umständlich und zeitaufwändig.
Fazit: Die vorgeschlagene Klassifikation ist als Standardbewertungsverfahren für einen geräteunabhängigen, interindividuellen und gruppenübergreifenden Vergleich geeignet.

[162] Absence of differences between male and female collegiate athletes after sports-related concussion: preliminary findings

Vivian Schultz[1*, 2, 3], Holly Carrington[2], Nico Sollmann[1, 2, 3, 4, 5], Paul Raffelhüschen[2, 3], Leonard Jung[2, 3], Lara Pankatz[2, 3], Katherine Breedlove[6], Scott Passalugo[7], Martha E. Shenton[2, 8, 9], Claus Zimmer[1], David Howell[10, 11], Alexander P. Lin[2, 6, 8], Inga K. Koerte[2, 3, 12]

[1]Department of Diagnostic and Interventional Neuroradiology, Klinikum rechts der Isar, Technische Universität München, Munich, Germany
[2]Psychiatry Neuroimaging Laboratory, Department of Psychiatry, Brigham and Women's Hospital, Harvard Medical School, Boston, MA, USA
[3]cBRAIN, Department of Child and Adolescent Psychiatry, Psychosomatic and Psychotherapy, Ludwig-Maximilian-University, Munich, Germany
[4]TUM-Neuroimaging Center, Klinikum rechts der Isar, Technische Universität München, Munich, Germany
[5]Department of Diagnostic and Interventional Radiology, University Hospital Ulm, Albert-Einstein-Allee 23, 89081 Ulm, Germany
[6]Center for Clinical Spectroscopy, Department of Radiology, Brigham and Women's Hospital, Harvard Medical School, Boston, MA, USA
[7]Division of Sports Medicine, Department of Orthopedics, Boston Children's Hospital, Harvard Medical School, Boston, MA, USA
[8]Department of Radiology, Brigham and Women's Hospital, Harvard Medical School, Boston, MA, USA
[9]VA Boston Healthcare System, Boston, MA, USA
[10]Sports Medicine Center, Children's Hospital Colorado, Aurora, CO, USA
[11]University of Colorado School of Medicine, Department of Orthopedics, Aurora, CO, USA
[12]Department of Psychiatry, Massachusetts General Hospital, Harvard Medical School, Boston, MA, USA

Background: There is evidence that female athletes are at increased risk for sustaining a sports-related concussion (SRC) compared to their male counterparts [1]. However, only a small number of studies have focused on sex differences following SRC and the results remain mixed [2]. This preliminary study investigates sex differences in white matter microstructure following acute SRC.
Methods: We included 18 (10 female and 8 male) collegiate contact-sport athletes (mean age: males 20.1 ± 0.9 years, females 20.1 ± 1.1 years) following SRC (24–72 h postinjury). We analyzed diffusion weighed MR images (dMRI) acquired at 3T. FA maps were calculated for each subject and tract-based spatial statistics (TBSS) were performed. Symptoms were assessed using the Post-Concussion Symptom Scale (PCSS). Time (in days) to symptom resolution (TSR) and return-to-play (TRP) was noted. Means were compared using an unpaired, two-sample t test. A p-value of <0.05 was considered statistically significant for all analyses with a correction for multiple comparisons being applied throughout.
Results: TBSS did not show statistically significant group differences in white matter FA between males and females. There were no statistically significant differences between sexes in PCSS total scores ($p = 0.20$), TSR ($p = 0.24$), or TRP ($p = 0.24$). However, a tendency for higher PCSS total scores and longer TSR and TRP were observed in females compared with males (mean (SD) PCSS scores: males: 11 (±7.9), females: 21 (±18.4); mean (SD) TSR: males: 9.7 (±2.5), females: 16.8 (±11.4); mean (SD) TRP: males: 12.2 (±3.5), females: 28.6 (±26.4).
Discussion: This is a preliminary analysis of collegiate athletes in an acute phase following SRC. Recruitment was paused due to the COVID-19 related pandemic. Sex showed no significant effect on white matter microstructure, symptom severity, TSR, or TRP. However, a trend for higher post-injury symptom loads, longer return to play, and symptom resolution times were observed in female athletes.
Conclusion: Our results correspond to previous findings in this field [2]. Finally, the small sample size may have precluded statistically significant results for some of the analyses.

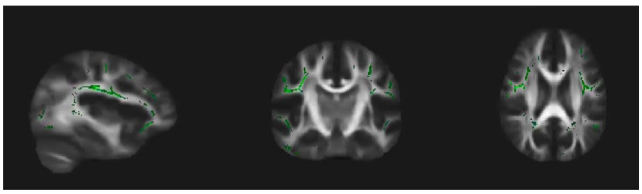

Fig. 1 | 162 Statistically non-significant differences in white matter FA between female and male athletes

References

1. Abrahams S, SM F, Patricios J, Posthumus M, AV S. Risk factors for sports concussion: an evidence-based systematic review. Br J Sports Med. 2014;48:91–7.
2. Koerte I, Schultz V, Sydnor V, et al. Sex-related differences in the effects of sports-related concussion: A review. J Neuroimaging. 2020;30:387–409.

[163] Tissue at risk is underestimated by admission NIHSS as a clinical marker for penumbra in right-sided large vessel occlusion (LVO) stroke

Adrian Mak[1* 2], Charles C. Matouk[3], Emily W. Avery[1], Jonas Behland[1 2], Dietmar Frey[2], Vince I. Madai[2], Peter Vajkoczy[4], Ajay Malhotra[1], Pina C. Sanelli[5], Guido J. Falcone[6], Nils Petersen[6], Lauren H. Sansing[6], Kevin N. Sheth[6], Seyedmehdi Payabvash[1]

[1]Yale School of Medicine, Department of Radiology, New Haven, USA
[2]Charité–Universitätsmedizin Berlin, Charité Lab for Artifical Intelligence in Medicine, Berlin, Germany
[3]Yale School of Medicine, Department of Neurosurgery, New Haven, USA
[4]Charité–Universitätsmedizin Berlin, Department of Neurosurgery, Berlin, Germany
[5]Feinstein Institutes for Medical Research, Department of Radiology, Manhasset, USA
[6]Yale School of Medicine, Department of Neurology, New Haven, USA

Purpose: The concept of clinical-core mismatch is applied to determine eligibility for endovascular therapy (ET) in the extended time window after large vessel occlusion (LVO), using the admission NIHSS as clinical surrogate for the total tissue-at-risk. It is however known that the NIHSS for an infarct of a given volume is higher in left compared to right-hemispheric stroke. We aimed to determine the effects of LVO side on final infarct volume and clinical outcome after ET with regards to admission NIHSS score.
Methods: We retrospectively identified anterior circulation LVO stroke patients that received ET and had follow-up MRI. Using a multivariate voxel-wise general linear model, we assessed the post-thrombectomy infarct distribution in relation to admission NIHSS, post-thrombectomy reperfusion success (mTICI) and discharge modified Rankin Scale (mRS) score. We identified independent predictors for final infarct volume and clinical outcome using multivariate regression models.
Results: We included a total of 469 patients (254 left, 215 right). Admission NIHSS was significantly lower among patients with right (median 11: IQR 8–16) versus left-sided LVO (16: 10–22, $p > 0.001$). In voxel-wise analysis, lower mTICI, lower admission NIHSS, and poor discharge outcome (mRS >2) were associated with right-hemispheric infarct lesions. Right-sided LVO was an independent predictor of larger final infarct volume ($\beta = 18.3$, $p = 0.003$). There was a significant three-way interaction between admission stroke severity (based on NIHSS), LVO side, and mTICI regarding final infarct volume ($F(7,440) = 2.11$,

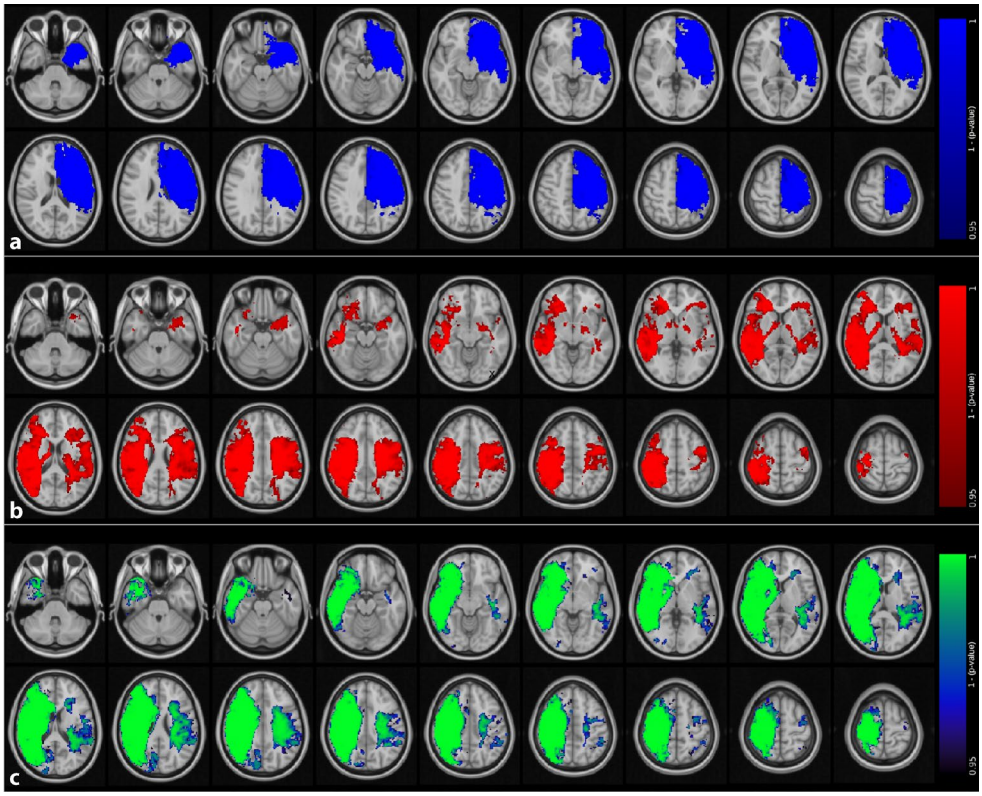

Fig. 1 | 163 **a** Final infarcts associated with higher admission NIHSS, after correction for reperfusion success. **b** Final infarcts associated with worse reperfusion, after correction for admission NIHSS. **c** Final infarcts associated with poor outcome and worse reperfusion, after correction for admission NIHSS

$p=0.041$). Specifically, in patients with moderate stroke (NIHSS 6–15), incomplete reperfusion (mTICI 0–2b) was associated with larger infarct volume (55.5 ± 76.6 ml vs. 30.0 ± 47.2 ml, $p<0.001$) and worse discharge mRS (4: 2–4 vs. 3: 1–4, $p=0.022$) in right compared to left-sided LVO. We found no differences in outcomes of patients with moderate stroke and complete reperfusion (mTICI 3).

Discussion: Incomplete reperfusion in the context of right-sided LVO was associated with larger loss of eloquent brain tissue, which led to worse clinical outcome for patients. These results likely represent larger tissue-at-risk in patients with right-sided LVO for a given admission NIHSS score.

Conclusion: Using admission NIHSS as clinical surrogate of tissue-at-risk may lead to underestimation and consequently undertreatment among patients with right-sided LVO. This highlights the need for more nuanced eligibility criteria for ET in the extended time window.

[168] Prediction of incident vertebral fractures in routine MDCT: Comparison of global texture features, 3D finite element parameters and volumetric BMD

Michael Dieckmeyer[1*], Nithin Manohar Rayudu[2], Long Yu Yeung[2], Maximilian Löffler[1 3], Anjany Sekuboyina[1], Egon Burian[1], Nico Sollmann[1 4], Jan Kirschke[1], Thomas Baum[1], Karupppasamy Subburaj[2]

[1]Abteilung für Diagnostische und Interventionelle Neuroradiologie, Klinikum rechts der Isar der Technischen Universität München, München, Germany
[2]Pillar of Engineering Product Development, Singapore University of Technology and Design, Singapur, Singapore
[3]Klinik für Diagnostische und Interventionelle Radiologie, Universitätsklinikum der Albert-Ludwigs-Universität Freiburg, Freiburg, Germany
[4]Klinik für diagnostische und interventionelle Radiologie, Universitätsklinikum Ulm, Ulm, Germany

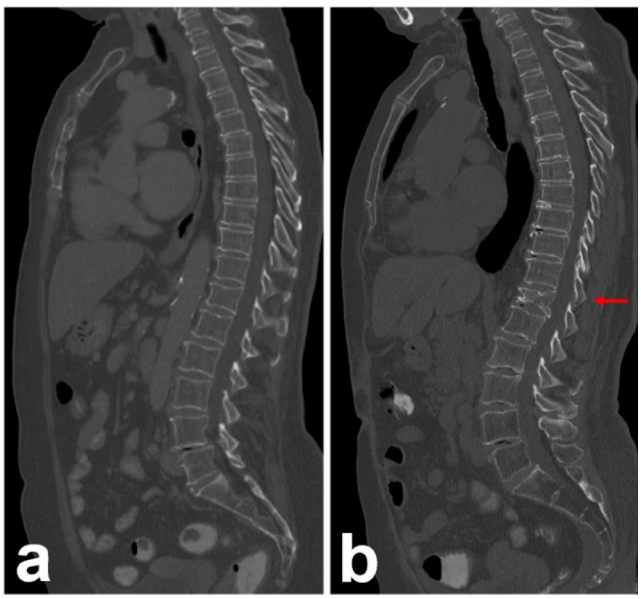

Fig. 1 | 168 Baseline (**a**) and FU (**b**) MDCT with incident VF of T12 (*arrow*)

Background: Osteoporosis is a systemic disorder of bone metabolism and has become a global healthcare problem [1]. The increased risk of vertebral fractures (VF) results in high morbidity, mortality and enormous socioeconomic costs [2]. To guide prevention and early treatment of osteoporotic fractures, an accurate diagnostic tool is more important than ever. In this case-control study, we evaluated different quantitative parameters derived from routine multi-detector computed tomography

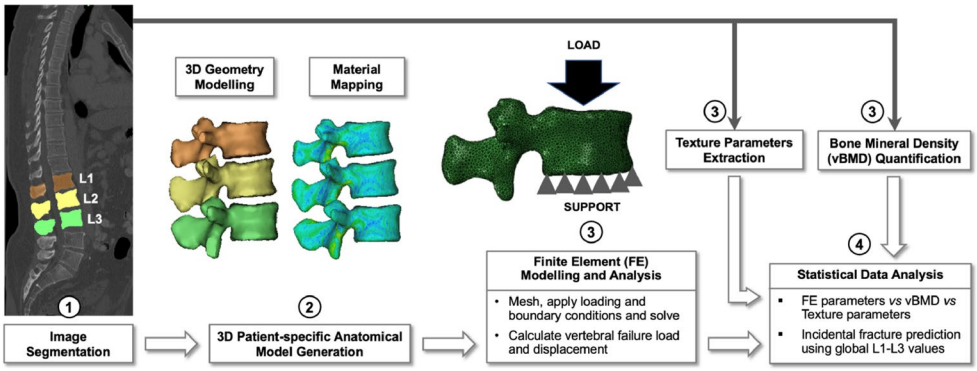

Fig. 2 | 168 Steps of the modeling and analysis methodology

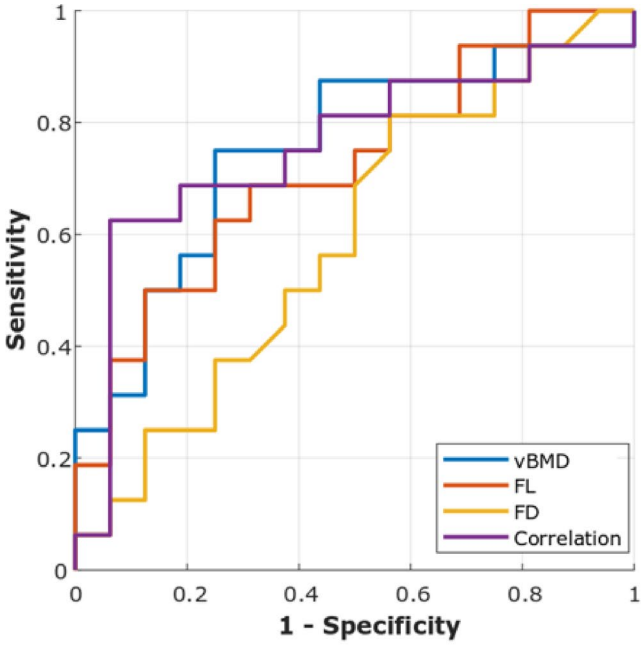

Parameter	AUC	SE	*p*
vBMD	.750	0.089	0.016
FL	.719	0.091	0.035
FD	.592	0.102	0.376
Correlation	.754	0.092	0.014

Fig. 3 | 168 ROC analysis results (*SE* standard error)

(MDCT) scans with respect to their ability to predict incident osteoporotic vertebral fractures of the thoracolumbar spine.
Methods: A total of 16 patients who received baseline and follow-up (FU) contrast-enhanced MDCT and were diagnosed with an incident osteoporotic VF at FU (Fig. 1), and 16 age-, sex-, and FU-time-matched controls were included. Vertebrae were labelled and segmented using a fully automated pipeline. Volumetric bone mineral density (vBMD), finite element analysis (FEA)-based failure load (FL) and failure displacement (FD), as well as 24 texture features (TF) were extracted from L1–L3 and averaged. Odds ratios (OR) with 95 % confidence intervals (CI), expressed per standard deviation decrease, receiver operating characteristic (ROC) area under the curve (AUC), and logistic regression, including all parameters as independent variables, were used to assess the prediction of incident VF (Fig. 2).
Results: The TF *Correlation* (AUC = 0.754, $p = 0.014$; OR = 2.76, CI = 1.16–6.58) and vBMD (AUC = 0.750, $p = 0.016$; OR = 2.67, CI = 1.12–6.37) classified incident VFs best, while the best FEA parameter FL showed AUC = 0.719 ($p = 0.035$; Fig. 3). *Correlation* was the only significant predictor of incident VF in the logistic regression ($p = 0.022$).
Discussion and conclusion: FEA parameters and vBMD have been investigated before, and the combination of different local parameters outperformed global parameters for the prediction of incident vertebral fractures[3]. In the present study, MDCT-derived FEA parameters and TFs, averaged from L1–L3, showed only a moderate, but no statistically significant improvement of incident VF prediction beyond vBMD, supporting that vertebra-specific parameters are superior for fracture risk assessment.

References

1. Drake et al. (2015).
2. Borgstrom et al. (2020).
3. Yeung et al. (2021).

[177] Der neuartige P64 HPC Flow Diverter – initiale klinische Erfahrungen und Kurzzeit-Follow-up-Daten

Victoria Hellstern[1*], Marta Aguilar Perez[1], Elina Henkes[1], Oliver Ganslandt[2], Hans-Jörg Bäzner[3], Hans Henkes[1]

[1]Klinikum Stuttgart, Neurozentrum, Klinik für Neuroradiologie, Stuttgart, Deutschland
[2]Klinikum Stuttgart, Neurozentrum, Klinik für Neurochirurgie, Stuttgart, Deutschland
[3]Klinikum Stuttgart, Neurozentrum, Klinik für Neurologie, Stuttgart, Deutschland

Hintergrund: Der p64 HPC-FD (Phenox GmbH, Bochum, Germany) ist ein neuartiger FD, der sich durch eine hydrophile Oberflächenbeschichtung auszeichnet und die Implantation unter Mono-Thrombozytenaggregation (SAPT) erlaubt. Wir berichten über die initiale klinische Erfahrung mit dem p64 HPC mit besonderem Augenmerk auf ischämischen Ereignissen und Kurzzeit-follow-up-Daten bezüglich Verschlussraten.
Methoden: Zwischen 04/2020 und 04/2021 wurden $n = 56$ Patienten mit 63 nicht rupturierten, sakkulären Aneurysmen mit mindestens einem p64 HPC unter SAPT behandelt. Die Aneurysmen konnten vorbehandelt gewesen sein, jedoch ohne vorangegangene FD-Implantation in das Trägergefäß.
Ergebnisse: Es wurden 56 Patienten mit 63 Aneurysmen mit mindestens einem p64 HPC behandelt. Die Implantation des p64 HPC war in allen Fällen technisch erfolgreich. In 55 Aneurysmen (87,3 %) wurde ein FD verwendet. In 7 Aneurysmen (11,1 %) musste aufgrund erheb-

licher Stentverkürzung nach Freisetzung ein weitere FD implantiert werden. Bei 2 Patienten (3,8 %) traten symptomatische ischämische Ereignisse nach der FD-Implantation auf, darunter in einem Fall eine In-Stent-Thrombose aufgrund insuffizienter TAH bei Non-Compliance. In dem ersten FU-DSA-Kontrollen (verfügbar für 43/63 Aneurysmen) zeigte sich ein adäquater Verschluss OKM C+D in 70 %.
Diskussion: Die Behandlung intrakranieller Aneurysmen mit FD hat sich als Standartmethode etabliert. Jedoch gilt die Notwendigkeit einer dualen Thrombozytenaggregationshemmung als großer Nachteil des Verfahrens. Mit der Einführung von oberflächenmodulierten FD wie dem p48 HPC (Phenox GmbH, Bochum, Germany) und dem Pipeline Shield (Medtronic, CA USA) ist erstmal die Verwendung von FD unter Mono-Antiaggregation möglich [1, 2]. Mit dem p64 HPC steht nun ein weiterer hydrophil beschichteter Stent zur Verwendung unter SAPT zu Verfügung.
Fazit: Implantation des p64 HPC unter SAPT ist sicher und effizient mit geringer Morbi-Mortalität und hohen Okklusionsraten.

Literatur

1. Bhogal P, Bleise C, Chudyk J, et al. The p48_HPC antithrombogenic flow diverter: initial human experience using single antiplatelet therapy. J Int Med Res. 2020; https://doi.org/10.1177/0300060519879580.
2. Manning NW, Cheung A, Phillips TJ, et al. Pipeline shield with single antiplatelet therapy in aneurysmal subarachnoid haemorrhage: multicentre experience. J NeuroIntervent Surg. 2019;11:694–8. https://doi.org/10.1136/neurintsurg-2018-014363.

[181] Local cerebral matrix metalloproteinase-9 concentrations correspond to the degree of bleeding complications and functional outcome following mechanical thrombectomy

Alexander Kollikowski[1*], Michael Schuhmann[2], Jörn Feick[1], Fabian Essig[2], Bernhard Nieswandt[3, 4], Marc Strinitz[1], Alexander G. März[1], Guido Stoll[2], Mirko Pham[1]

[1]Institut für Diagnostische und Interventionelle Neuroradiologie, Universitätsklinikum Würzburg, Würzburg, Germany
[2]Neurologische Klinik und Poliklinik, Universitätsklinikum Würzburg, Würzburg, Germany
[3]Institut für Experimentelle Biomedizin, Universitätsklinikum Würzburg, Würzburg, Germany
[4]Rudolf-Virchow-Zentrum, Universität Würzburg, Würzburg, Germany

Background: Numerous clinical and experimental studies have addressed the role of matrix metalloproteinases (MMPs) in blood-brain barrier degradation, the generation of vasogenic edema or hemorrhagic transformation following ischemic stroke, but local concentrations during occlusion condition have never been assessed in acute ischemic stroke patients [1].
Methods: We conducted a prospective observational study on 258 consecutive patients undergoing mechanical thrombectomy (MT) due to large-vessel-occlusion stroke of the anterior circulation (08/2018–05/2020). Intraprocedural microcatheter aspiration of 1 ml of cerebral-ischemic (occlusion condition) and systemic arterial blood samples was attempted according to a prespecified protocol. Plasma levels of MMP-9 and -2 were quantified by enzyme linked immune sorbent assay. Pappenheim-stained smears were used for white blood cell differential counting [2]. Biological relevance was assessed by analyses of hemorrhagic events on postinterventional brain CT scans at 24–48 h (Heidelberg Bleeding Classification, HBC), clinical outcome (modified Rankin Scale at discharge) and multivariable testing (molecular-cellular, clinical and interventional parameters).
Results: A total of 70 consecutive patients entered analyses. Mean cerebral MMP-9 (736 vs 543 ng/ml, $p=0.0008$) but not MMP-2 levels (139 vs 115 ng/ml, $p=0.56$) were increased compared with control samples. Among leukocytes, neutrophils had the strongest association with cerebral MMP-9 levels ($r=0.51$, $p<0.0001$). Mean cerebral MMP-9 levels corresponded to the degree of bleeding following intervention (no hemorrhage: 490 ng/ml vs hemorrhagic infarction [HBC 1a/b]: 603 ng/ml vs parenchymatous hematoma (HBC 1c/2): 1801 ng/ml, $p=0.0002$). Cerebral MMP-9 levels were lower in patients with favourable outcome (mRS≤2: 385 vs mRS>2: 987, $p=0.0011$). Multiple logistic regression revealed cerebral MMP-9 concentrations as independent predictor of functional outcome (mRS≤2: aOR = 0.9981, $p=0.0416$).
Conclusion: Our data for the first time show that MMP-9 is locally released into the ischemic cerebral vasculature in acute stroke and support the notion that MMP-9 contributes to hemorrhagic transformation and affects outcome.

References

1. Turner RJ, Sharp FR. Implications of MMP9 for Blood Brain Barrier Disruption and Hemorrhagic Transformation Following Ischemic Stroke. Front Cell Neurosci. 2016;10:1–13.
2. Kollikowski AM, et al. Local Leukocyte Invasion during Hyperacute Human Ischemic Stroke. Ann Neurol. 2020;87(3):466–79.

[183] Anterior chamber enhancement predicts optic nerve infiltration in retinoblastoma: stasis of the orbital glymphatic system?

Katerina Deike-Hofmann[1* 2], Paula von Lampe[3], Maija Eerikaeinen[3], Saskia Ting[4], Sabrina Schlueter[5], Heinz-Peter Schlemmer[2], Nikolaos Bechrakis[5], Michael Forsting[4], Alexander Radbruch[1]

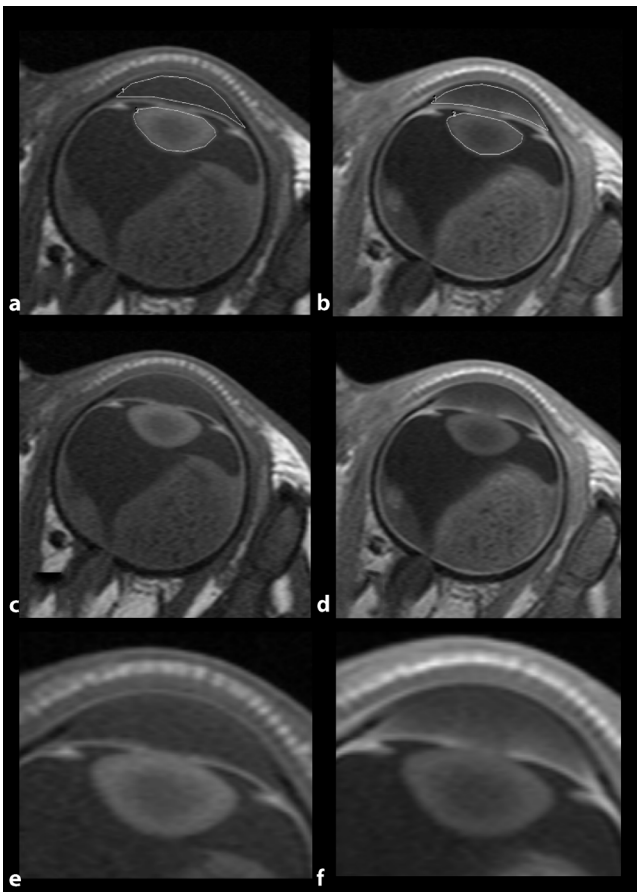

Fig. 1 | 183 Example of orbital MRI and applied image analysis

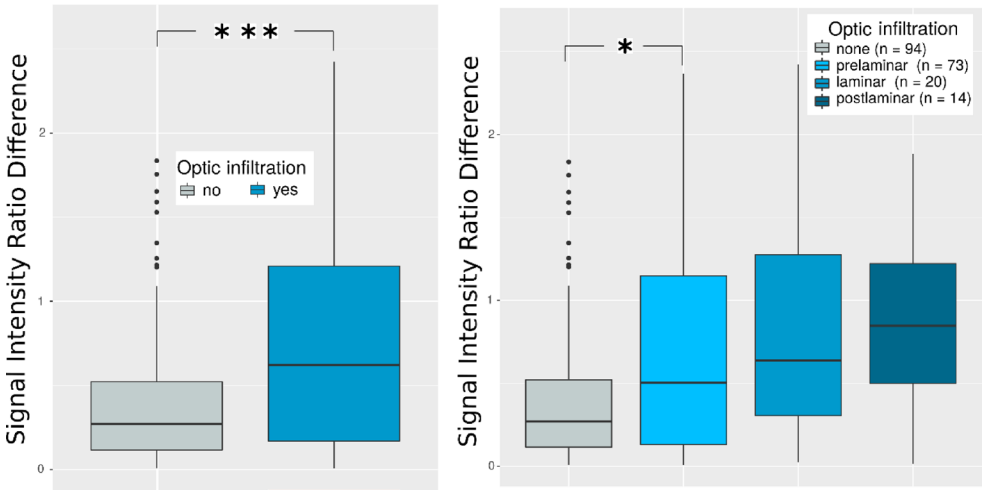

Fig. 2 | 183 Boxplots of anterior chamber-to-lens signal intensity ratio differences (ΔSIRs) depending on optic infiltration level

[1]Universitätsklinik Bonn, Neuroradiologie, Bonn, Germany
[2]Deutsches Krebsforschungszentrum, Radiologie, Heidelberg, Germany
[3]Universitätsklinikum Essen, Radiologie, Essen, Germany
[4]Universitätsklinikum Essen, Pathologie, Essen, Germany
[5]Universitätsklinikum Essen, Augenheilkunde, Essen, Germany

Background: Brain clearance imaging revealed penetration of gadolinium-based contrast agents (GBCAs) into the anterior eye chamber (AC) in healthy humans [1, 2]. We investigated whether the degree of GBCA enhancement of the AC predicts histopathologic tumor features in children suffering from retinoblastoma (RB).
Methods: This study encompassed 539 orbital MRIs performed between 2010 and 2019. MRI was performed with an orbital coil and with the children in a state of general anesthesia. Differences of signal intensity ratios of the AC to the lens (ΔSIRs) were determined between native and GBCA-enhanced T1-weightings (Fig. 1). Subsequently, ΔSIRs of RB eyes were correlated with histopathologic tumor features such as infiltration of the optic nerve (ON), choroid, ciliary body, sclera and AC.
Results: ΔSIRs were significantly higher in RB eyes compared to healthy eyes ($p<0.001$). ΔSIR of the RB eye was an independent, significant predictor for ON invasion in multivariate analysis with adjustment for tumor size ($p<0.05$) and increased with infiltration level (Fig. 2). ΔSIR was not predictive for any other assessed histopathologic tumor feature.
Discussion: Increased GBCA enhancement of the anterior eye chamber in retinoblastoma with optic infiltration might be explained by disturbed retinal homeostasis with consecutive neovascularisation of the iris due to dysfunction of the orbital glymphatic system (Fig. 3; [3]).
Conclusion: GBCA enhancement of the anterior eye chamber predicts optic nerve infiltration by retinoblastoma.

References

1. Deike-Hofmann K, Reuter J, Haase R, et al. Glymphatic Pathway of Gadolinium-Based Contrast Agents through the Brain: Overlooked and Misinterpreted. invest Radiol. 2019;54(4):229–37.
2. Deike-Hofmann K, von Lampe P, Schlemmer H, et al. The Anterior Chamber of the Eye: An Overlooked Entry of the Natural

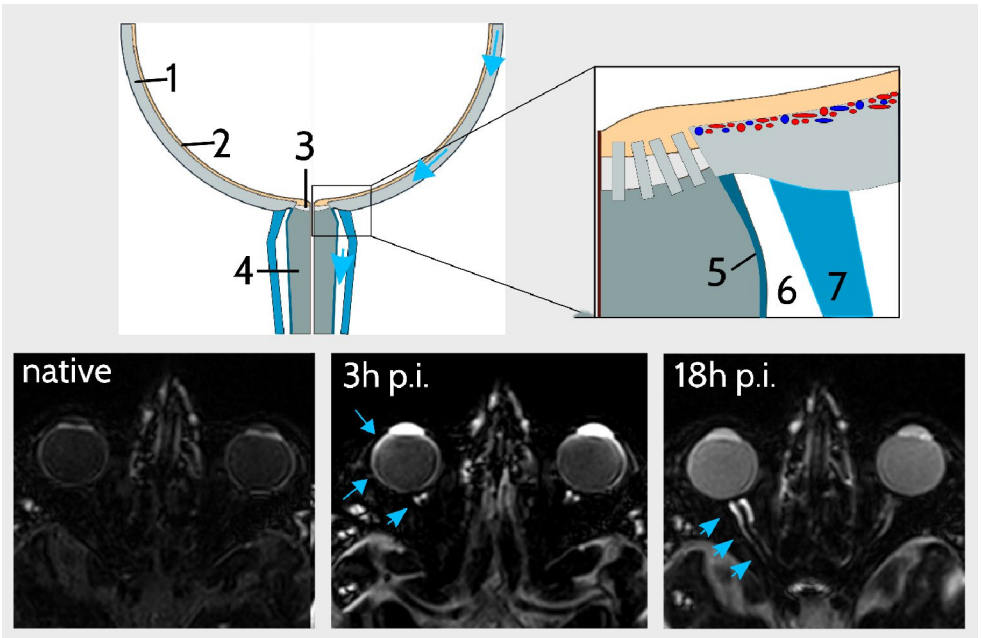

Fig. 3 | 183 Illustration of orbital GBCA distribution in healthy eyes following intravenous injection

Excretion pathway of Gadolinium Based Contrast Agents? Eur Radiol. 2020;30:4633–40.
3. Wang X, Lou N, Eberhardt A, et al. An ocular glymphatic clearance system removes beta-amyloid from the rodent eye. Sci Transl Med. 2020;12:3210.

[186] Synthetic DIR is superior to FLAIR for multiple sclerosis lesion detection: multi-center validation of a task-specific generative adversarial network

Tom Finck[1*], Sarah Schlaeger[1], Hongwei LI[2], Lioba Grundl[1], Nico Sollmann[3], Benjamin Bender[4], Eva Buerkle[4], Jan Kirschke[1], Björn Menze[2], Claus Zimmer[1], Mark Mühlau[5], Benedikt Wiestler[1]

[1]Klinikum rechts der Isar der Technischen Universität München, Abteilung für diagnostische und interventionelle Neuroradiologie, München, Germany
[2]Klinikum rechts der Isar der Technischen Universität München, Image-Based Biomedical Modeling, München, Germany
[3]Klinikum rechts der Isar der Technischen Universität München, Abteilung für diagnostische und interventionelle Neuroradiologie, Universitätsklinikum Ulm, Abteilung für diagnostische und interventionelle Radiologie, München, Germany
[4]Radiologische Universitätsklinik Tübingen–Abteilung für Diagnostische und Interventionelle Radiologie, Tübingen, Germany
[5]Klinikum rechts der Isar der Technischen Universität München, Abteilung für Neurologie, München, Germany

Background: Generative adversarial networks (GANs) create high-contrast magnetic resonance imaging (MRI) data from lower-contrast input. Targeted translation of lesions in multiple sclerosis (MS) augments their clinical value, provided that a GAN's performance remains robust for external data. Here, we investigate the external validity of a novel GAN framework aimed at improving MRI in patients with MS.
Methods: Our GAN synthesized double-inversion-recovery (DIR) from fluid-attenuated-inversion-recovery (FLAIR) and T1w of 50 prospectively acquired MS patients (training data). In another 50 patients (test data), two blinded readers (R1&R2) quantified lesions in synthetic DIR (synthDIR), acquired DIR (trueDIR), and FLAIR. Of these patients, 20 were investigated on the same scanner than training data (internal data), while 30 were scanned on different scanners (external data). Lesions were grouped according to the McDonald criteria. Contrast-to-noise ratios (CNRs) were compared.
Results: Higher counts of MS-specific lesions were found in synthDIR vs. FLAIR (R1: 26.7 ± 2.6 vs. 22.5 ± 2.2 $p < 0.0001$; R2: 22.8 ± 2.2 vs. 19.9 ± 2.0, $p = 0.0005$). Importantly, improvements in lesion counts were noted to similar degrees in internal and external data and synthDIR replicated the intrinsic strength of DIR to improve the depiction of juxtacortical lesions. SynthDIR had higher CNRs than FLAIR with respective medians of 46.2 (IQR: 26.5; 50.8) vs. 31.8 (IQR: 22.1; 44.9; [$p < 0.0001$]) in internal and 33.1 (IQR 18.4; 37.0) vs. 23.4 (IQR 17.7; 27.5; [$p < 0.0001$]) in external data.
Discussion: This multicentric study confirms the efficacy and external validity of a DL tool aimed at improving MRI in patients with MS.
Conclusion: GAN-mediated image synthesis can remain robust in external data and has the potential for vast scan time reductions.

[189] Qualitative and quantitative comparison of hippocampal volumetric software applications

Stephanie Mangesius[1*2], Lukas Haider[3 4], Lukas Lenhart[1 2], Ruth Steiger[1 2], Ferran Prados[3 5 6], Christoph Scherfler[7], Elke Ruth Gizewski[1 2]

[1]Medical University of Innsbruck, Department of Neuroradiology, Innsbruck, Austria
[2]Medical University of Innsbruck, Neuroimaging Core Facility, Innsbruck, Austria
[3]University College London Institute of Neurology, NMR Research Unit, Queen Square Multiple Sclerosis Centre, United Kingdom
[4]Medical University of Vienna, Department of Biomedical Imaging and Image Guided Therapy, Austria
[5]University College London, Centre for Medical Image Computing (CMIC), Department of Medical Physics and Biomedical Engineering, United Kingdom
[6]Universitat Oberta de Catalunya, e-Health Center, Spain
[7]Medical University of Innsbruck, Department of Neurology, Austria

Background: Brain volumetric software is increasingly suggested for clinical routine [1]. The present study quantifies agreement across different software applications.
Methods: Ten individuals were chosen based on hippocampal volume z-scores < –1.96 as measured by FreeSurfer (FS) based on an in-house gender and age-adjusted healthy control (HC) group, and 10 age-matched HCs, median age: 74 years (25–75 %, range: 66–77). Hippocampal volumes were computed based on 3 T T1-MPRAGE-sequences with FS, statistical parametric mapping (SPM; neuromorphometrics and Hammers atlases), Geodesic-Information-Flows (GIF),

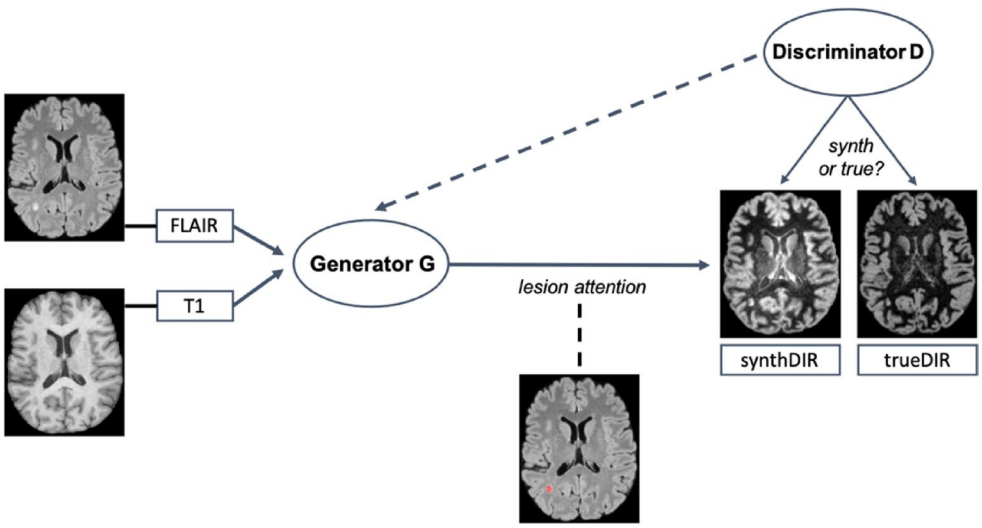

Abb. 1 | 186

Similarity-and-Truth-Estimation-for-Propagated Segmentations (STEPS), and a commercially available software application. Volumetric measures of each individual were compared against the mean of all applications with intraclass-correlation coefficients (ICC) and Bland-Altman plots.
Results: Comparing against the mean of all methods, moderate to low agreement was present considering categorization of hippocampal volumes into quartiles. Interclass correlation coefficients (ICC) ranged noticeably between software applications (left hippocampus, LH): from 0.42 (STEPS) to 0.88 (FS); right hippocampus (RH): from 0.36 (commercially available software application) to 0.86 (FS). The mean differences between individual methods and the mean of all methods (mm^3) was considerable (LH: FS –209, SPM-Neuromorphometrics –820; SPM-Hammers –1474; commercially available software application –680; GIF 891; STEPS 2218; RH: FS –232, SPM-Neuromorphometrics –745; SPM-Hammers –1547; commercially available software application –723; GIF 982; STEPS 2188).
Discussion: Consistency across centers is viable for any diagnostic test [2]. Our results reveal considerable variability in volumetric measurements between different established applications, even in a cohort with large spread in the data (normal aging vs. severe atrophy) and absence of structural lesions.
Conclusion: Interchangeable use of different volumetric software applications is not recommended.

References

1. Despotovic I, et al. Comput Math Methods Med. 2015;2015:450341.
2. Klauschen F, et al. Hum Brain Mapp. 2009;30:1310–27.

[190] Clinical utility of automatically derived acute ischemic volumes on native computed tomography in patients with anterior acute ischemic stroke and endovascular therapy

Peter Mihalicz[1*], Christian Herweh[1], Simon Nagel[2], Peter Arthur Ringleb[2], Martin Bendszus[1], Markus Möhlenbruch[1], Ulf Neuberger[1]

[1]Universitätsklinikum Heidelberg Neurologische Klinik: Neuroradiologie, Heidelberg, Germany
[2]Neurologische Klinik, Heidelberg, Germany

Background and purpose: The clinical utility and non-inferiority of electronically derived ASPECTS (eASPECTS) to quantify signs of acute ischemic infarction could be demonstrated. Here, we aimed to evaluate the clinical and predictive capabilities of a new parameter, automatically derived acute ischemic infarct volumes (AIV) from native computed tomography (NCT) images in patients undergoing endovascular therapy due do anterior acute ischemic stroke (AAIS).
Methods: We performed a retrospective analysis of $n=1132$ consecutive patients, with AAIS and subsequent endovascular therapy between 01/2013 and 01/2020. eASPECTS and AIV were generated from baseline NCT with the Brainomix software (www.brainomix.com, Version 9.0). Obtained data were correlated with clinical outcome (stroke severity measured by National Institute of Health Stroke Scale, NIHSS, at baseline and after 24 h, modified Rankin Scale, mRS, after 90 days). Furthermore, the predictive capabilities of AIV were tested using adjusted multivariate logistic regression and machine learning methods.
Results: Patients with a good clinical outcome (mRS 0–2 after 90 days) had a significant lower AIV (16.91 ± 16.68 ml vs. 24.56 ± 20.21 ml, $p<0.001$). AIV correlated significantly with NIHSS at baseline ($\rho=0.22$) and 24 h after therapy ($\rho=0.27$) as well as with mRS after 90 days ($\rho=0.20$; Fig. 1). In a multivariate logistic regression model, adjusted for important clinical parameters AIV was revealed as an independent predictor for good clinical outcome (aOR 0.98, 95 % CI 0.97–0.99). Prediction of clinical outcome with machine-learning using AIV showed a moderate accuracy (ROC-AUC = 0.64, 95 % CI 0.61–0.67), in comparison to ordinary eASPECTS (ROC-AUC = 0.62, 95 % CI = 0.59–0.65). However, a significant difference between of the predictive accuracy between the two models could not be shown with DeLong's test ($p=0.730$; Fig. 2).

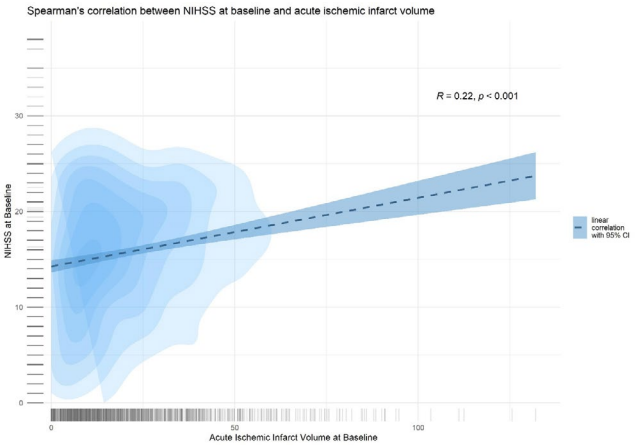

Fig. 1 | 190 Correlation between NIHSS and acute ischemic infarct volume at baseline

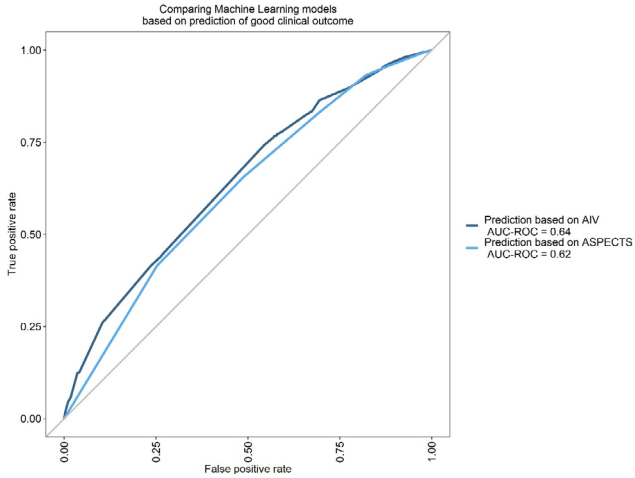

Fig. 2 | 190 Comparison of the predictive accuracy with area under the curve in operating characteristics curve derived in machine-learning models for acute ischemic stroke volume (AIV) and ASPECTS

Discussion and conclusion: AIV independently predicted clinical outcome in patients with AAI with a higher predictive accuracy than eASPECTS. In an era where acute stroke diagnosis and treatment eligibility is mainly performed with NCT, AIV might be a useful and easily applicable addition in stroke diagnostics to identify patients eligible for endovascular therapy, with a higher statistical power due to the continuous nature of the parameter, in comparison to the ordinal ASPECTS.

[191] Spatial correlation of resting state activity alterations in premature-born adults with nuclear imaging derived neurotransmitter maps

David Schinz[1*,2], Benita Schmitz-Koep[1,2], Aurore Menegaux[1,2], Claus Zimmer[1,2], Dieter Wolke[3,4], Peter Bartmann[5], Christian Sorg[1,2], Dennis Hedderich[1,2]

[1]Klinikum rechts der Isar der Technischen Universität München, Neuroradiologie, München, Germany
[2]TUM-NIC Neuroimaging Center, Technical University of Munich, München, Germany

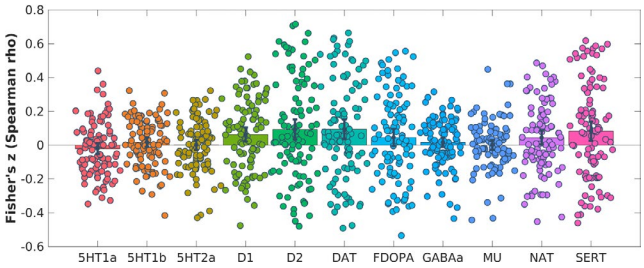

Fig. 1 | 191 Relative Fisher's z-transformed correlation coefficients comparing premature-born adults to FT controls with the respective neurotransmitter maps. Each dot represents the relative fALFF alterations in premature-born adults compared to FT controls per individual in correlation with the spatial distribution of neurotransmitter systems. Significant alterations between premature-born adults and FT controls can be seen for D1, D2, DAT, and Serotonin transporter (DASB PET) maps. Error bars represent the 95 % confidence interval. DAT Dopamine transporter, FDOPA Fluorodopa, GABAa γ-Aminobutyric acid type A, NAT Noradrenaline transporter, SERT Serotonin transporter

[3]University of Warwick, Warwick medical school, Coventry, United Kingdom
[4]University of Warwick, Department of Psychology, Coventry, United Kingdom
[5]Universitätsklinikum Bonn, Department of Neonatology, Bonn, Germany

Background: The brains of premature-born subjects show a wide range of structural and functional differences compared to full-term (FT) born controls [1, 2]. However, the effect of prematurity on neurotransmitter systems in humans remains largely unknown. Recently, a new tool for linking MRI data to neurotransmitter information based on nuclear imaging derived estimates was introduced [3].
Methods: We included 99 very-preterm/very-low-birthweight (VP/VLBW; <32 weeks of gestation/birth weight below 1500 g) and 107 FT born adults at 26 years of age in a prospectively acquired cohort. We investigated whether fractional amplitude of low-frequency fluctuations (fALFF) alteration patterns in VP/VLBW individuals compared to FT controls are correlated with specific neurotransmitter systems.
Results: Differences in fALFF of the two groups showed a spatial association with neurotransmitter maps of the dopaminergic (D1, D2, DAT) and serotonergic (SERT) transmitter systems (Fig. 1).
Discussion: We found significant correlations between spatial alteration patterns in the functional activity of premature-born adults with the dopaminergic and serotonergic systems. These findings suggest a particular vulnerability of the dopaminergic system that stands in line with previously shown alterations through perinatal brain damage as well as to changes in the structure and architecture of premature-born brains [4].
Conclusion: Prematurity is associated with functional resting state activity alterations that may reflect underlying neurotransmitter-level changes in dopaminergic and serotonergic pathways.

References

1. Volpe JJ. Dysmaturation of Premature Brain: Importance, Cellular Mechanisms, and Potential Interventions. Pediatr Neurol. 2019;95:42–66.
2. Shang J, et al. Decreased BOLD fluctuations in lateral temporal cortices of premature born adults. Hum Brain Mapp. 2018;39:4903–12.
3. Dukart J, et al. JUSPACE: A tool for spatial correlation analyses of magnetic resonance imaging data with nuclear imaging derived neurotransmitter maps. Hum Brain Mapp. 2021;42:555–6.
4. Froudist-Walsh S, et al. The effect of perinatal brain injury on dopaminergic function and hippocampal volume in adult life. Elife. 2017;6:e29088.

[200] High serum glucose in patients with acute ischemic stroke: quantification of the mediation effect of edema formation on poor functional outcome

Helge Kniep[1*], Lukas Meyer[1], Matthias Bechstein[1], Jens Fiehler[1], Uta Hanning[1], Gabriel Broocks[1]

[1]Klinik und Poliklinik für Neuroradiologische Diagnostik und Intervention, Universitätsklinikum Hamburg-Eppendorf, Hamburg, Germany

Introduction: Different risk factors for poor clinical outcome after endovascular thrombectomy with successful recanalization have been identified. Higher blood glucose levels were shown to be associated with worse clinical outcome and increased edema formation [1]. A better understanding of the pathophysiological pathways and a quantification of their effects might support targeted therapeutic approaches. We therefore conduct a mediation analysis to quantify the effect of edema formation on clinical outcome in patients with high blood glucose.
Methods: A total of 124 patients with acute ischemic stroke who underwent mechanical thrombectomy were included. Mediation analysis was performed to evaluate whether serum glucose associated edema formation has a significant effect on the probability of good outcome (mRS ≤2).
Results: The likelihood for poor outcome increased with increasing blood glucose levels (odds ratio [OR] 1.23 per 10 mg/dl increase; $p=0.005$), edema formation (OR 1.13 per % net water uptake; $p=0.02$) and poor collaterals (OR 1.64; $p=0.04$; Fig. 1). Edema formation was also associated with higher blood glucose (linear regression coefficient 0.033; $p=0.01$; Fig. 2). The mediation effect of edema formation on functional outcome was 15 % ($p=0.034$). The mediation model showed an increase of the probability for good outcome of 47 % ($p<0.005$) in

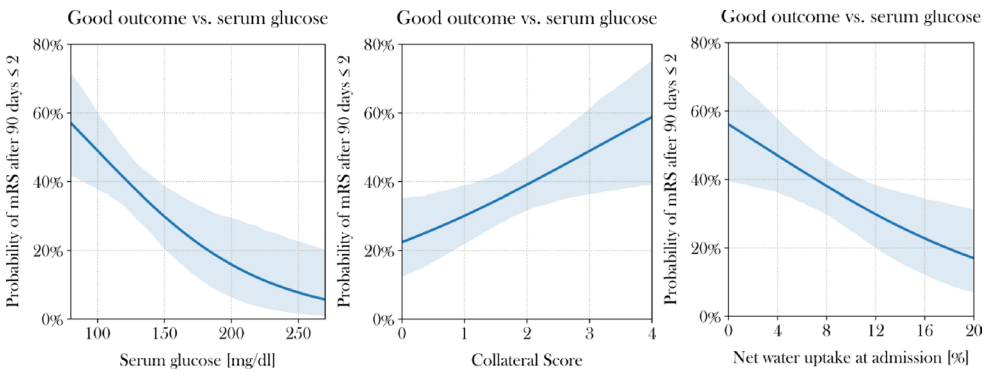

Fig. 1 | 200 Impact of serum glucose, edema formation (net water uptake) and collateral score on functional outcome (logistic regression)

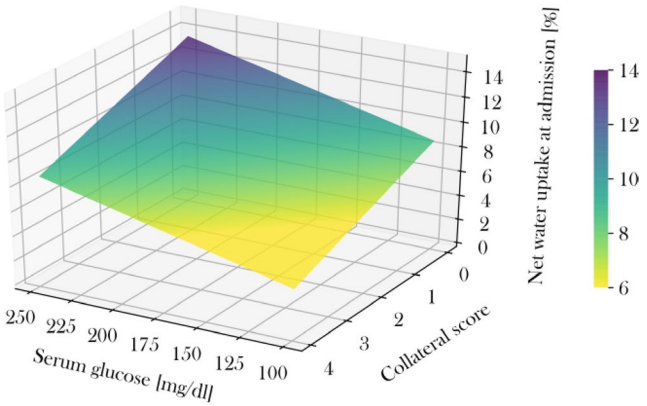

Fig. 2 | 200 Impact of serum glucose and collateral score on edema formation (linear regression)

patients with good collaterals and of 26 % ($p<0.005$) in patients with poor collaterals at blood glucose levels of 100 mg/dl vs. 200 mg/dl.
Discussion: In patients with poor functional outcome accompanied by high blood glucose, excessive edema formation accounts for 15 % of the total adverse effects. Hence, major pathways are also linked to other direct effects of high blood glucose, such as altered vessel wall and thrombus characteristics and higher thrombogenicity of the cerebral blood flow. Additional intermediation effects are introduced by the collateral status.
Conclusion: Targeted treatment approaches for patients with high blood glucose require a personalized multidimensional approach not only aiming at reducing edema formation but also considering other adverse effects of high serum glucose.

References

1. Thorén M, et al. Predictors for Cerebral Edema in Acute Ischemic Stroke Treated With Intravenous Thrombolysis. Stroke. 2017;48(9):2464–71.

[204] CSF venous fistulas: diagnostic work-up

Niklas Lützen[1*], Philippe Dovi-Akué[1], Christian Fung[2], Jürgen Beck[2], Horst Urbach[1]

[1]Uniklinik Freiburg–Klinik für Neuroradiologie, Freiburg im Breisgau, Germany
[2]Uniklinik Freiburg–Klinik für Neurochirurgie, Freiburg im Breisgau, Germany

Background: CSF venous fistulas–initially described in 2014 [1]–are a significant cause of spontaneous intracranial hypotension (SIH) in so-called head-positive, SLEC-negative (spinal longitudinal extradural contrast) patients. Here, we analyzed the diagnostic work-up to identify and locate these leaks.
Methods: Eight patients were studied with lateral decubitus (dynamic subtraction) myelography (ld DSM), lateral decubitus CT myelography (ld CTM), and/or intrathecal Gadolinium MR myelography (MRM).
Results: CSF venous fistulas were proven by ld DSM ($n=3$) and/or ld CTM ($n=7$), and/or MRM ($n=0$). CSF venous fistulas were located at the levels between Th 2/3 and Th 11/12 (6 dexter, 2 sinistral).
Discussion: Lateral decubitus DSM has a lesser and MRM no diagnostic sensitivity in our series.
Conclusion: Head-positive, SLEC-negative SIH patients should undergo lateral decubitus CT myelography.

References

1. Schievink WI, Moser FG, MM M. CSF-venous fistula in spontaneous intracranial hypotension. Neurology. 2014;83:472–3.

[205] CSF venous fistulas: endovascular treatment

Niklas Lützen[1*], Philippe Dovi-Akué[1], Christian Fung[2], Jürgen Beck[2], Horst Urbach[1]

[1]Uniklinik Freiburg–Klinik für Neuroradiologie, Freiburg im Breisgau, Germany
[2]Uniklinik Freiburg–Klinik für Neurochirurgie, Freiburg im Breisgau, Germany

Background: CSF venous fistulas are a significant cause of Spontaneous Intracranial hypotension (SIH) in so-called head-positive, SLEC-negative (spinal longitudinal extradural contrast) patients. Recently, transvenous embolization has been suggested as a less invasive therapeutic option than surgery [1].
Methods: Of eight patients with CSF venous fistulas, four were surgically ligated by clipping and four were occluded with Onyx. For embolization, a Scepter balloon occlusion microcatheter was navigated via the azygos or hemiazygos veins into the paravertebral veins at the levels Th 5/6 left, Th2/3 right, Th 10/11 right ($n=2$). Post-embolization CT slices confirmed the Onyx cast in the venous channels surrounding the leaking nerve root sleeve.
Results: Three patients showed a significant improvement (Fig. 1), while one woman with co-existing cerebral amyloid angiopathy died from a macrohemorrhage which was detected after the transvenous embolization.
Discussion: The definitive clinical outcome of both methods (surgical vs. endovascular) in comparison remains to be seen and more studies need to be done.

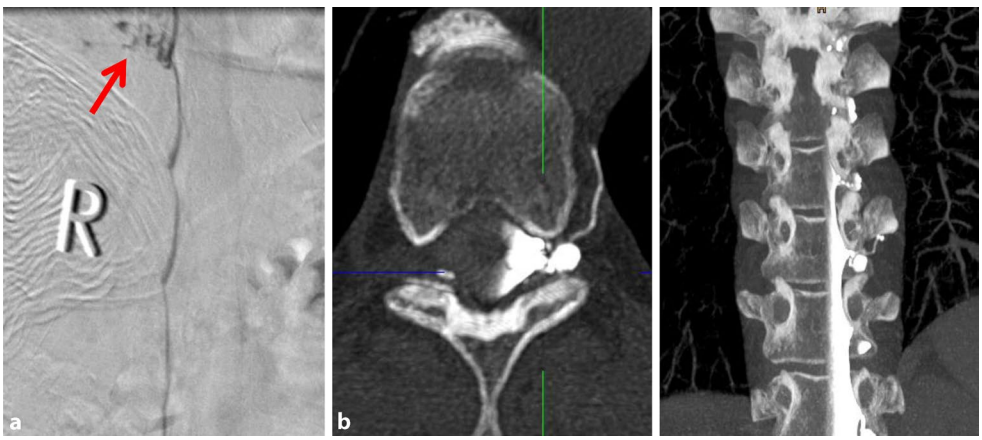

Fig. 1 | 204 Ld DSM shows CSF venous fistula (*arrow*) at the level Th 9/10 right (**a**); in another patient axial and coronal (*arrow*) ld CTM revealed the CSF venous fistula at the level Th 10/11left

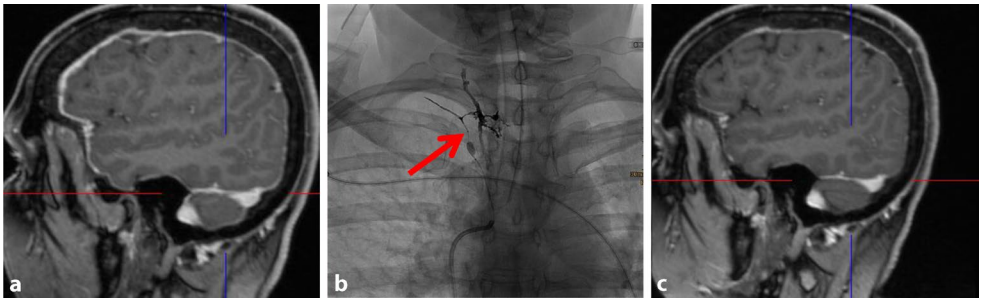

Fig. 1 | 205 MRI scans of a 53-year-old woman before (**a**) and 6 weeks after (**c**) transvenous embolization disclosing regression of pachymeningeal enhancement and sinus venous distension. The unsubtracted image (**b**) shows the Onyx cast in the veins surrounding the right-sided nerve root Th2 and the inflated Scepter balloon (*arrow*)

Conclusion: Transvenous Onyx embolization is an elegant therapeutic option to occlude CSF venous fistulas.

References

1. Brinjikji W, Savastano LE, Atkinson JLD, Garza I, Farb R, Cutsforth-Gregory JK. A Novel Endovascular Therapy for CSF Hypotension Secondary to CSF-Venous Fistula AJNR. Am J Neuroradiol. 2021; https://doi.org/10.3174/ajnr.A7014.

[208] Challenging cases for WMH segmentation comparatively processed by seven automated methods

Merita Aruci[1*], Max Dünnwald[2, 3], Frank Schreiber[3, 4], Alessandro Sciarra[3], Anne Maass[4], Stefanie Schreiber[3, 4, 5], Steffen Oeltze-Jafra[2, 3, 5]

[1]Otto-von-Guericke University Magdeburg, Faculty of Natural Sciences, Magdeburg, Germany
[2]Otto-von-Guericke University Magdeburg, Faculty of Computer Sciences, Magdeburg, Germany
[3]University Hospital Magdeburg, Department of Neurology, Magdeburg, Germany
[4]German Center for Neurodegenerative Diseases, Magdeburg, Germany
[5]Center for Behavioral Brain Sciences (CBBS), Magdeburg, Germany

Background: White matter hyperintensities of presumed vascular origin (WMH), a hallmark feature of cerebral small vessel disease (CSVD), are FLAIR/T2-hyperintense lesions that predict various clinical readouts, e. g., stroke or dementia [6, 8]. WMH are commonly determined according to their volume load [1], while capturing or classifying more subtle features such as different WMH patterns or "WMH mimics" is demanding. We aimed to compare automatic methods to segment challenging WMH patterns (e. g. multifocal spots, peri-basal ganglia WMH or WMH "mimics" surrounding lacunes/large hemorrhages) in clinical CSVD cases.

Methods: We applied seven different automatic WMH segmenting methods (LGA and LPA [7], SLS [5], MDbrain (Mediaire GmbH), BIANCA [2], FreeSurfer[4] and PGS–a Deep Learning approach [3]) in T1/FLAIR MRI sequences and compared their performance against gold standard manual segmentations in 10 CSVD patients with challenging WMH patterns aiming to identify the most suitable method to segment them. Segmentation accuracy was determined though Dice similarity coefficient and other metrics measuring sensitivity or precision.

Results: In our dataset, the PGS (DSC:0.6), LPA (DSC:0.59) and MDbrain (DSC:0.57) were superior in detecting periventricular and deep multifocal spot WMH with a high sensitivity and precision rate. However, similarly to other methods, on a variable scale, they falsely seg-

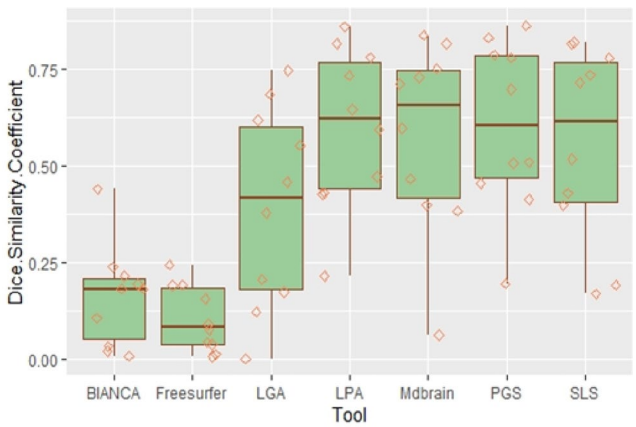

Fig. 1 | 208 Boxplot depicting Dice similarity coefficients for all methods. PGS (mean = 0.6), LPA (mean:D.59) and MDbrain (mean:D.57) score the highest DSC followed by SLS, LGA, BIANCA and SAMSEG Freesurfer. (boxplots depict the 25 %, 75 % percentile and the median for DSC distribution, *orange circles* represent each subject)

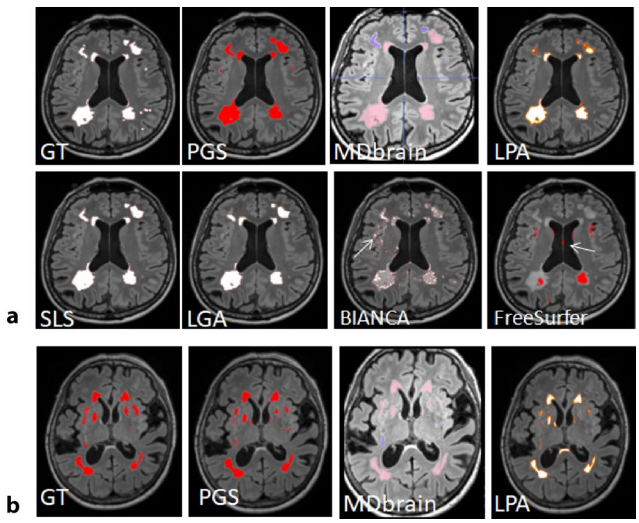

Fig. 2 | 208 (**a**) Example of the same axial FLAIR slice segmented by hand (GT) and with seven automatecl methods. All tools reach a good performante in detecting large confluent WMH surrounding the ventricular area, but their performante variably drops in detecting subcortical/deep WMH, especially when presenting as nonconfluent multifocal spots. For the latter, PGS and MDbrain are more sensitive compared to other tools. False positives are most commonly detected in the septum pelludicum (*white arrow*—FreeSurfer), choroidal plexus in the lateral ventricles, or in the sulci of temporal lobe regions (*white arrow*—BIANCA). (**b**) „WMH challenges" surrounding basal ganglia (depicted in a white arrow—GT) are more accurately detected by PGS, MDbrain and LPA. Images in both panels belang to two different patients

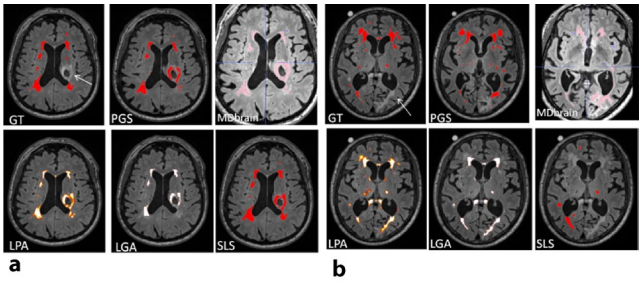

Fig. 3 | 208 WMH segmentation performance of different tools falsely detecting FLAIR hyperintense „WMH mimics" surrounding large hemorrhages (**a**) or post-hemorrhagic hyperintense changes (**b**). Pathological hyperintense FLAIR structures are depicted in *white arrow* in the GT panel

METHOD	DSC	IOU	SENSITIVITY	PRECISION	FPR	FDR
PGS (Park et al, 2021)	0.602	0.462	0.523	0.808	0.0002	0.192
SLS (Roura et al, 2015)	0.556	0.421	0.533	0.691	0.0004	0.309
MDbrain (Mediaire GmbH)	0.574	0.438	0.506	0.852	0.0003	0.148
LPA (Schmidt et al, 2012)	0.596	0.453	0.538	0.792	0.0003	0.208
LGA (Schmidt et al, 2012)	0.393	0.274	0.315	0.620	0.0002	0.280
BIANCA (Griffanti et al, 2016)	0.161	0.092	0.424	0.108	0.0057	0.892
FreeSurfer (Puonti et al, 2016)	0.104	0.057	0.091	0.176	0.0006	0.824

Sensitivity: TP / (TP + FN); Precision: TP / (TP + FP)
FDR-False Discovery Rate: FP / (FP + TP); FPR-False Positive Rate: FP/(FP+TN)

Fig. 4 | 208 Mean similarity metrics for each segmenting method

mented "WMH mimics" surrounding CSVD-related lesions as "true WMH" resulting in an overestimation of WMH volume. The volume of these "WMH mimics" segmentations is fluctuate on the method, but PGS performs better as it detects less false-positive-WMH-volume compared to other tools.

Discussion: Future WMH segmentation tools will need to detect more accurately challenging, highly relevant WMH patterns to move forward in the understanding of different CSVD subtypes and pathophysiology.

Conclusion: These results show weak points of common WMH segmentation methods in complex FLAIR/T2-hyperintense lesions and can be insightful in choosing the best performing tool in segmenting challenging WMH patterns.

References

1. Charidimou, A., et al. Neurology. 86.6 (2016)
2. Griffanti, L., et al. Neuroimage.141 (2016)
3. Park G, et al. Neuroimage. 2021;237
4. Puonti O, et al. Neuroimage. 2016;143
5. Roura E, et al. Neuroradiology. 2015;57(10)
6. Scheumann, V., et al. JNS. 419 (2020)
7. Schmidt P, et al. NeuroimageClin. 2019;23
8. Wardlaw JM, et al. Lancet Neurol. 2013;12(8)

[210] The Tigertriever 13 for mechanical thrombectomy in distal and medium intracranial vessel occlusions: initial experience from two high-volume stroke centers

Sebastian Fischer[1*], Volker Maus[1], Hannes Nordmeyer[2], Werner Weber[1]

[1]Institut für Diagnostische und Interventionelle Radiologie, Neuroradiologie und Nuklearmedizin, Knappschaftskrankenhaus Bochum, Bochum, Germany
[2]Neurozentrum Solingen, Radpax St. Lukas Hospital, Solingen, Germany

Background: To report our two-center initial experience using the Tigertriever 13 (a manually expandable low-profile stentretriever) in the treatment of acute stroke due to distal medium vessel occlusions (DMVO).

Methods: We performed a retrospective analysis of patients treated by mechanical thrombectomy using the Tigertriever 13 device due to an acute DMVO. Locations included the anterior, middle and posterior cerebral artery in the A2 and A3, the M3 and M4 and the P2 or P3 segment and the superior cerebellar artery.

Results: Forty-three patients with 45 DMVOs underwent MTE using the Tigertriever 13 on an intention to treat approach between May 2019 and December 2020. A median of two thrombectomy maneuvers resulted in a successful reperfusion rate (mTICI 2b-3) of 84.4 % (38/45) with a first pass effect of 26.7 % (12/45). The rate of symptomatic intracranial hemorrhages (sICH) and subarachnoid hemorrhages (SAH) was 7.0 % (3/43) and 14.0 % (6/43), respectively. At discharge, 53.5 % (23/43) of the patients had a favorable clinical outcome (mRS 0–2).

Discussion: To date only one study focuses on DMVOs exclusively treated with the Tigertriever 13. Rikhtegar et al. presented a series of 115 patients suffering from DMVOs treated with the Tigertriever 13 [1]. The concept of the Tigertriever offers the possibility to manipulate the expansion and by this, the radial force of the device. This might help to obtain a higher likelihood of capturing the clot compared to traditional stent retrievers [2].

Conclusion: MTE in DMVOs using the Tigertriever 13 is safe and effective with high recanalization rates. The incidence of clinically asymptomatic hemorrhagic events appears to be higher in comparison MTE procedures in LVOs.

References

1. Rikhtegar R, Mosimann PJ, Weber P, Wollocha M, Yamac E, Mirza_Aghazadeh-Attari M, et al. Effectiveness of very low profile thrombectomy device in primary distal medium vessel occlusion, as rescue therapy after incomplete proximal recanalization or following iatrogenic thromboembolic events. J NeuroIntervent Surg. 2021;0:1–6.
2. Will L, Maus V, Maurer C, Weber A, Weber A, Weber W, et al. Mechanical thrombectomy in acute ischemic stroke using a manually expandable stenttriever (Tigertriever): Preliminary single-center experience. Clin Neuroradiol. 2020.

[211] Latest artificial intelligence provides fast, accurate and consistent detection of multiple sclerosis lesions

Stefan Hock[1*], Dominique C. Marterstock[2], Anna-Lena Meyer[2], Clemens Bettray[2], Konstantin Huhn[1], Veit Rothhammer[1], Arnd Dörfler[2], Manuel Schmidt[2]

[1]Universitätsklinikum Erlangen, Neurologische Klinik, Erlangen, Germany
[2]Universitätsklinikum Erlangen, Neuroradiologische Abteilung, Erlangen, Germany

Background: Artificial intelligence (AI) algorithms have already had a major impact on medical imaging and opened a wide field of detec-

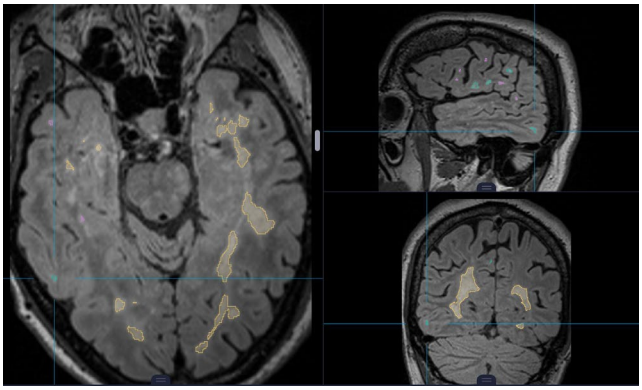

Fig. 1 | 211 Example of MS lesion detection by latest version AI

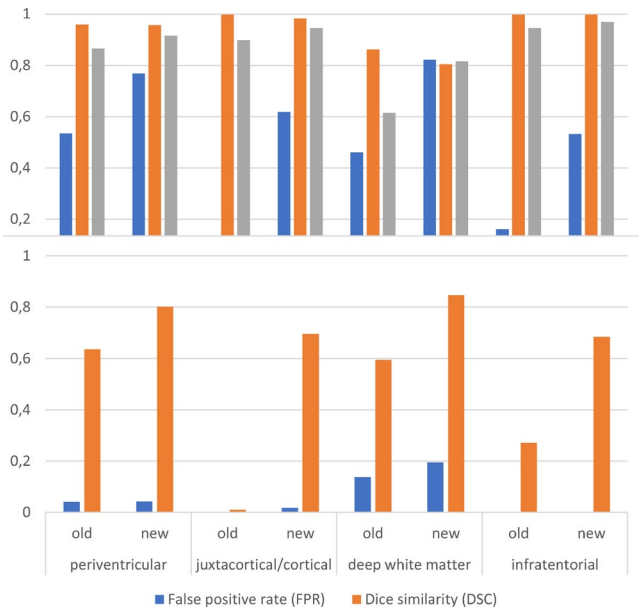

Fig. 2 | 211 Validation results illustrated as comparison of the two ANN according to region (periventricular, juxtacortical/cortical, deep white matter, infratentorial)

tion of textural and morphological patterns. Our aim was to evaluate the potential of latest AI regarding diagnosis and follow-up of Multiple Sclerosis (MS) in clinical radiology.

Methods: We included 101 patients who had undergone MRI at a single academic hospital to evaluate MS lesions according to McDonald criteria. T2w 3D FLAIR and T1w MPRAGE sequences were processed by two AI (Fig. 1)–deep learning ("latest") and traditional computer vision techniques ("previous")–and analyzed by three expert neuroradiologists (gold standard) independently. Statistical metrics were calculated and compared as follows: Sensitivity (TPR), specificity (TNR), overall accuracy (ACC), false positive rate (FPR) and Dice similarity score (DSC).

Results: A comparison of two artificial neuronal networks (ANN) corroborates the superiority of the latest generation AI in detection of MS lesions (Fig. 2). Overall sensitivity (77 % vs. 29 %) and DSC (0.81 vs 0.39) of the latest version AI were significantly higher as compared to previous version. In the periventricular compartment TPR (77 % vs. 53 %), ACC (92 % vs. 87 %) and DSC (0.8 vs 0.64) were higher, while TNR (96 % vs. 96 %) and FPR (0.043 vs. 0.041) did not change significantly. In the juxtacortical compartment TPR (62 % vs. 0.5 %), ACC (95 % vs. 90 %), FPR (0.018 vs. 0.001) and DSC (0.7 vs 0.01) were higher, while TNR (98 % vs. 99 %) was unaltered. In the deep white matter TPR (82 % vs. 46 %), ACC (82 % vs. 62 %) and DSC (0.85 vs 0.6) were higher, while TNR (80 % vs. 86 %) was lower. FPR (0.14 vs. 0.20) did not change significantly. Infratentorial TPR (53 % vs. 16 %) and DSC (0.69 vs 0.27) were higher, while TNR (99 % vs. 99 %), ACC (97 % vs. 95 %) and FPR (0.015 vs. 0.015) did not change significantly.

Conclusion: Preliminary data show that the latest generation AI provides consistent, automated and fully reproducible assessment of MS lesions without being influenced by intra- and/or interobserver intrinsic human variability–especially in the context of longitudinal patient follow-up. Thus, this novel tool may provide improved reliability and standardization in diagnosis and follow-up imaging of MS.

[215] Aberrant cholinergic basal forebrain functional connectivity in premature-born adults

Elin Brandes[1*,2], Juliana Zimmrmann[1,2], Aurore Menegaux[1,2], Claus Zimmer[1,2], Dieter Wolke[3,4], Peter Bartmann[5], Dennis M. Hedderich[1,2], Christian Sorg[1,2,6], Benita Schmitz-Koep[1,2]

[1]Technical University of Munich, School of Medicine, Department of Diagnostic and Interventional Neuroradiology, Munich, Germany
[2]Technical University of Munich, School of Medicine, TUM-NIC Neuroimaging Center, Munich, Germany
[3]University of Warwick, Department of Psychology, Coventry, United Kingdom
[4]University of Warwick, Warwick Medical School, Coventry, United Kingdom
[5]University Hospital Bonn, Department of Neonatology, Bonn, Germany
[6]Technical University of Munich, School of Medicine, Department of Psychiatry, Munich, Germany

Background: Studies in both animal models and in premature born adults suggest impaired development of the cholinergic basal forebrain (cBF) after premature birth [1–3]; however, these studies focused on local cBF changes only, ignoring effects on cBF connectivity. We hypothesized aberrant functional connectivity (FC) of ongoing cBF blood oxygenation fluctuations in premature-born adults.

Methods: Resting-state functional magnetic resonance imaging was used to determine whole brain seed connectivity from bilateral anteri-

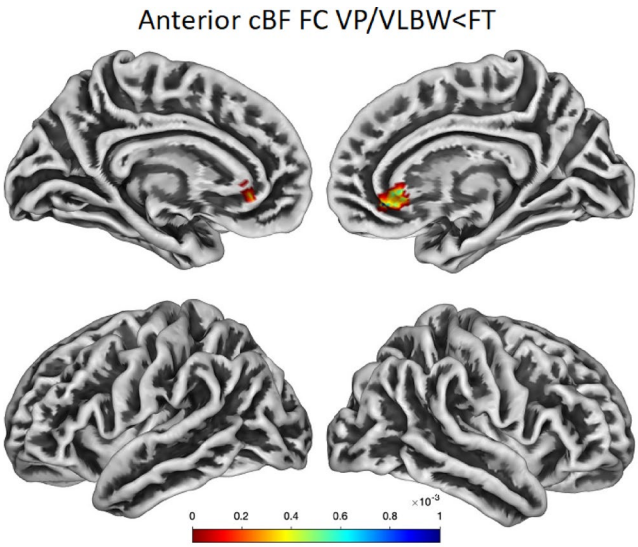

Fig. 1 | 215 Example of MS lesion detection by latest version AI

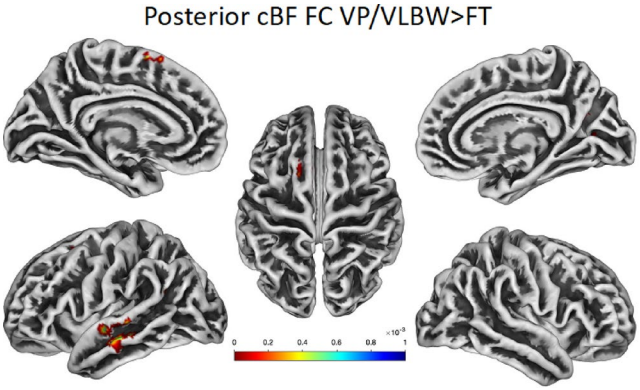

Fig. 2 | 215

or and posterior cBF [4] in a large and prospectively collected cohort of 79 very premature-born adults (<32 weeks of gestation and/or birth weight <1500 g, VP/VLBW) and 96 full-term born (FT) controls at 26 years of age. Group comparisons were performed with sex, scanner and cBF volume as covariates.
Results: While anterior cBF FC was significantly (p<0,001 uncorrected, cluster size >10) decreased in the anterior cingulate cortex (Fig. 1), posterior cBF FC was significantly increased in the left superior frontal gyrus, left superior temporal gyrus and middle temporal gyrus (Fig. B).
Discussion: Prematurity impacts cBF connectivity distinctively for anterior and posterior parts. It is unclear whether cBF volume loss interferes with these findings.
Conclusions: Results demonstrate impaired connectivity of the cBF into the forebrain in premature-born adults. Data suggest impaired cBF connectivity development in prematurity.

References

1. Aisa BG-B. FJ, Marcos B, Tordera R, Lasheras B, Del Río F, Ramírez -MJ. Neonatal stress affects vulnerability of cholinergic neurons and cognition in the rat: involvement of the HPA axis. Psychoneuroendocrinology. 2009;34(10):1495–505.
2. MV J. Neurotransmitter alterations in a model of perinatal hypoxic-ischemic brain injury. Ann Neurol. 1983;13(5):511–8.
3. Grothe MJ, Scheef L, Bäuml J, Meng C, Daamen M, Baumann N, et al. Reduced Cholinergic Basal Forebrain Integrity Links Neonatal Complications and Adult Cognitive Deficits After Premature Birth. Biol Psychiatry. 2017;82(2):119–26.
4. H-CJ FRN, Dyrba M, Sorg C, Teipel S, Grothe MJ. The corticotopic organization of the human basal forebrain as revealed by regionally selective functional connectivity profiles. Hum Brain Mapp. 2019;40(3):868–78.

[218] Semiautomatic reperfusion grading after endovascular therapy for acute ischemic stroke

Maximilian Thormann[1*], Muhannad Sabieleish[1], Axel Boese[2], Jonathan Metzler[1], Harald Paukisch[1], Mostafa Ergawy[1], Elie Diamandis[1], Anastasios Mpotsaris[1], Daniel Behme[1]

[1]Clinic for Neuroradiology, Magdeburg University Hospital, Magdeburg, Germany
[2]INKA HealthTec Innovation Laboratory, Otto-von-Guericke University Magdeburg, Magdeburg, Germany

Background: The degree of reperfusion after mechanical thrombectomy graded with mTICI score is an independent outcome predictor in acute ischemic stroke after endovascular treatment. However, the interrater reliability is low and operators tend to overestimate their own results. We therefore designed a fast, image-based grading for unbiased mTICI scoring.

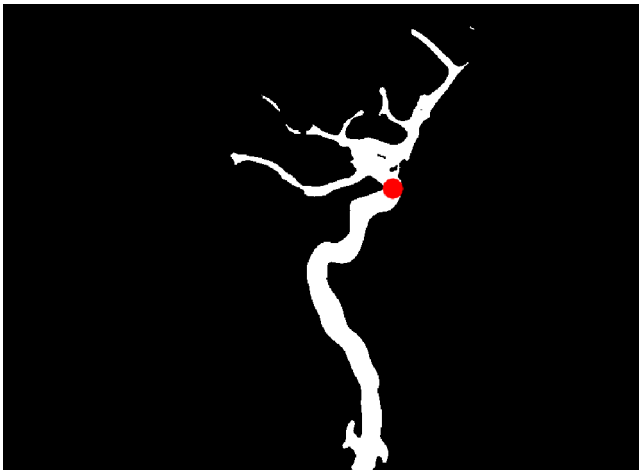

Fig. 1 | 218 ICA curve detection example (*red*)

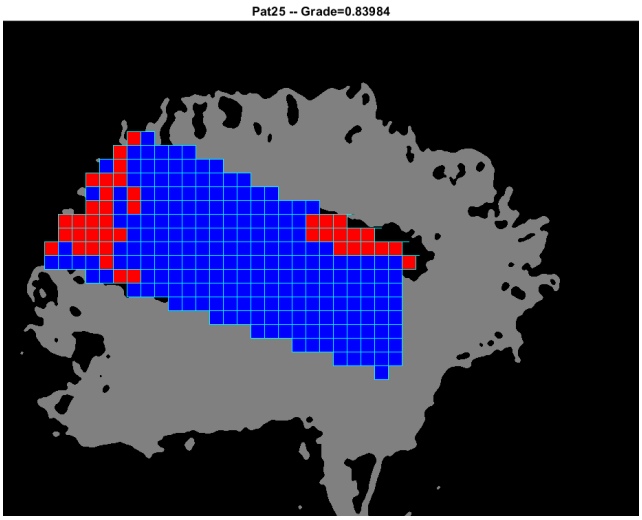

Fig. 2 | 218 Grid for „perfused“ (*blue*) and „unperfused“ (*red*) classification

Methods: A semiautomatic reperfusion grading on digital subtraction angiography (DSA) series was developed based on image processing techniques. After field of view adjustments, the internal carotid artery (ICA) curve was detected in the first “fill” image (Fig. 1) and used as a reference point. The region of interest (ROI) representing the target downstream territory (TDT) of the middle cerebral artery (MCA) was defined in the “capillary fill”-phase and divided into grid based check-zones classified as perfused or unperfused (Fig. 2). The percentage of reperfusion was calculated for each patient. Our approach was tested on 55 patients after thrombectomy in acute M1 occlusion. The mTICI grading as performed by our software was compared to the consensus scoring by two experienced neuroradiologists.
Results: Consensus reading mTICI scores in our cohort ranged from 2a to 3, with mTICI ≥2c in 63.6 % (35/55). Overall accuracy of the grading system was 47/55 (85.5 %), with 27/30 (90.0 %) mTICI 3 scored in agreement. Accuracy in mTICI >2c was 85.7 % (30/35). Differentiation into mTICI 2a/2b/2c was consistent in 20/25 patients (80.0 %). Five out of 8 disagreements occurred in mTICI 2c/3 gradings.
Discussion: Visual TICI scoring after mechanical thrombectomy is operator dependent and prone to interrater inconsistency. AI based approaches have been reported, but usually suffer from long computing

time and high GPU demand. A simpler method utilizing only post processing of angiographic images might be an adequate approach to develop an impartial grading standard. Our model presents an accurate and reliable semiautomated method for mTICI grading.
Conclusion: Semiautomated scoring of mTICI results for M1 occlusions is feasible, robust, and easy to integrate into routine reporting.

[219] Akzidentelle Läsionen des N. lingualis und N. alveolaris inferior – Einfluss der MRT auf das bisherige Managementkonzept

Monika Probst[1*], Egon Burian[1], Peter Cornelius[2], Florian Probst[2]

[1]Klinikum rechts der Isar, Neuroradiologie, München, Germany
[2]LMU Innenstadt Campus, Mund-, Kiefer- und Gesichtschirurgie, München, Germany

Hintergrund: Dentoalveolärchirurgische Eingriffe können zu mechanischen Verletzungen des N. lingualis (NL) oder des N. alveolaris inferior (NAI) führen. Diese Nervenverletzungen werden in der Regel intraoperativ nicht bemerkt, sondern erst bei Nachuntersuchungen durch bestehende neurosensorische Defizite apparent. Mit klinischen neurosensorischen Tests und neurophysiologische Untersuchungen wurde bisher versucht, den zugrundeliegenden Läsionstyp (Sunderland Grad) zu bestimmen und bei V. a. eine komplette Kontinuitätsunterbrechung die Indikation zur mikroneuralen Rekonstruktion zu stellen. Engmaschige Nachkontrollen mit wiederholter Sensibilitätstestung fanden in geplanten Intervallen statt, um innerhalb dieser Timeline das Zeitfenster für mikroneurale Interventionen zu bestimmen.
Methoden: Die MRT-Untersuchungen zur Neurographie erfolgten in einem 3.0-T-Scanner (Elition, Philips) mit einer 16-Kanal-Kopf-Hals-Spule. Die Scan-Protokolle beinhalteten spezifische hochauflösende Sequenzen (3-D-STIR, 3-D-DESS und 3-D-T1-FFE). Die MRT-Befunde wurden im weiteren Verlauf mit neurosensorischen Tests und mit intraoperativen Befunden korreliert.
Ergebnisse: Bei 15 Patienten mit unilateralen akzidentellen Läsionen der sensiblen Mandibularisäste (NL $n=10$; NAI $n=5$) gelang eine direkte Visualisierung der betroffenen Nerven in ihrem anatomischem Verlauf und nach der typischen Läsionstopographie. Es gelang keine Differenzierung axonaler, endo- und perineurialer Läsionen, d. h. von Läsionen mit erhaltener Kontinuität (Sunderland Grad I–IV). Dagegen ließ sich eine vollständige Kontinuitätsunterbrechungen und Neurombildungen (Sunderland Grad V und VI/Mackinnon-Dellon) zuverlässig erkennen, wie die anschließende intraoperative Korrelation in einigen Fällen (NL $n=5$; NAI $n=1$) zeigte.
Diskussion/Fazit: Das beschriebene MRT-Protokoll ermöglicht eine neurographische Darstellung bei NL- und NAI-Läsionen und kann schon in der Frühphase nach Verletzung eine Basis zur Differenzierung des Schädigungsausmaßes liefern. In der Konsequenz wird die MRT-Bildgebung damit zum Wegweiser in der Entscheidungsfindung für ein konservativ-abwartendes Verhalten versus operative Revision. Die Kontroll-Intervalle und Wartezeiten bis zu einer chirurgischen Intervention verkürzen sich, was Abänderungen im Managementkonzept nach sich zieht.

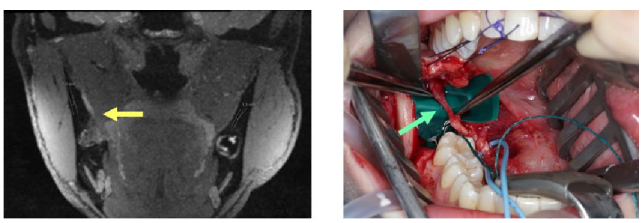

Abb. 1 | 219

[221] Automated quantification of vessel density in single- and multiphase CT angiography for EVT triage in stroke patients

Daniel Kaiser[1*2], Daniela Schoene[3], Johannes Gerber[1], Volker Puetz[3], Jennifer Linn[1], Matthias Gawlitza[1 2]

[1]Uniklinikum Carl Gustav Carus TU Dresden, Institut und Poliklinik für Diagnostische und Interventionelle Neuroradiologie, Dresden, Germany
[2] Technische Universität Dresden, Else Kröner-Fresenius Center for Digital Health, Dresden, Germany
[3]Uniklinikum Carl Gustav Carus TU Dresden, Klinik und Poliklinik für Neurologie, Dresden, Germany

Background: The assessment of the collateral vessel supply in stroke patients is a major criterion of the triage for endovascular thrombectomy (EVT). Collaterals are classified in single- or multi-phase/dynamic CT angiography (CTA) using scoring systems. However, visual scoring systems harbour the risk of not being precise and robust. We aimed to assess the performance of an automated quantification of the vessel density in comparison to established stroke triage parameters.
Methods: We prospectively included consecutive stroke patients who received CTA and CT perfusion (CTP) for EVT triage between April and May 2021. We used an artificial intelligence stroke software (Brainomix Ltd., Oxford, UK) to automatically assess ASPECT Score and infarct volume in non-contrast CT, location of target occlusion, collateral score and vessel density on single phase and dynamic CTA (Fig. 1) as well as infarct core (rCBF<30 %) and tissue-at-risk (Tmax >6 s) volumes on CTP images. Dynamic CTA was derived from 1.5 mm CTP source images. We recorded baseline data including baseline NIHSS, time-metrics, treatment strategy and NIHSS score at discharge. We compared vessel density on single and dynamic CTA with the Wilcoxon signed-rank test and determined Spearman's rank correlation coefficient for correlation with other parameters.
Results: A total of 18 patients (median age 83 [78–86] years, six male, baseline NIHSS 12 [5–19] and time from symptom onset to imaging 168 [84–448] min) met the inclusion criteria. Five patients did not qualify for EVT due to no large vessel occlusion ($n=4$) and low ASPECTS without CTP-mismatch ($n=1$). We achieved successful reperfusion in 11/13 patients. Median NIHSS score at discharge was 9 [3, 14]. The median vessel density on the single-phase CTA was significantly lower compared to the dynamic CTA (77 % vs 96.5 %; $p=0.001$) which resulted in a higher rate of collateral score 0–1 ($n=4$ vs $n=1$). Tab. 1 summarizes results of the correlation analysis.
Discussion: In stroke patients who are screened for EVT, collateral vessel supply can be automatically assessed by measurement of vessel density as a quantifiable parameter. Importantly, single-phase CTA may significantly underestimate the vessel density due to delayed filling of collaterals.

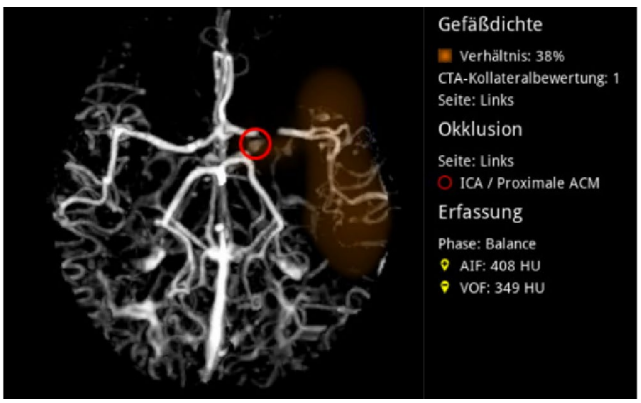

Fig. 1 | 221 Automated quantification of vessel density in a patient with carotid L occlusion

Fig. 2 | 221 Spearman's rank correlations

		onset to imaging	baseline ASPECTS	baseline infarct volume	collateral score	rCBF <30%	Tmax >6s	follow up ASPECTS	discharge NIHSS
single-phase CTA vessel density	coefficient	-.639	.633	-.600	.930	-.646	-.722	.608	-.380
	sig. (2-tailed)	.034	.005	.005	.000	.004	.001	.010	.120
dynamic CTA vessel density	coefficient	-.660	.666	-.662	.866	-.719	-.768	.630	-.407
	sig. (2-tailed)	.027	.003	.003	.000	.001	.000	.003	.093

Conclusion: The automated assessment of the vessel density could be a quantifiable and robust alternative to visual scoring systems in the triage of stroke patients for EVT.

[222] Machine learning on top of deep learning-based brain volumetry segmentation to support neuroradiologists in diagnosing neurodegenerative disorders

Chang Gyu Cho[1], Holger Wenz[1], Alex Förster[1], Markus Sebald[2], Thomas Ganslandt[3], Christoph Groden[1], Máté Maros[1*, 3]

[1]Universitätsklinikum Mannheim, Abteilung für Neuroradiologie, Mannheim, Germany
[2]Siemens Healthineers, Erlangen, Germany
[3]Medizinische Fakultät Mannheim, Abteilung für Biomedizinische Informatik, Mannheim, Germany

Background: We investigated whether supervised machine learning (ML) algorithms can be effectively applied to segmentation results of an FDA-approved deep learning-based brain morphometry algorithm in order to aid objective empirical neuroradiological scoring and comprehensive dementia diagnosis.
Methods: A single-center retrospective cohort of 275 patients (157F, 57.1 %; median age: 68 years, range: 17–95 years) with suspected neurocognitive disorders was retrieved from local RIS/PACS between 01/2012 and 08/2020. Brain volumetric segmentation (BVS) of 47 anatomical regions and structures was performed using the AI-Rad Companion MR Brain (Siemens Healthineers) software based on 3 T (Siemens, Trio) isotropic (1 mm) sagittal T1-weigthed MPRAGE (3D-MPRAGE) images. Three neuroradiologists generated consensus values of well-established empirical scoring systems including global cortical atrophy (GCA), medial temporal lobe atrophy (MTA), Koedam for parietal atrophy and Fazekas scale for white matter lesions (overall 12 features). Supervised ML algorithms such as dense neural networks (DNN), tree-based algorithms were trained on BVS values within 5x-fold nested cross validation setup [1] to suggest these empirical scores as target labels in a standardized manner [2].
Results: BVS values of key anatomical structures could be matched to the respective empirical scores based on correlation metrics. In contrast to automated segmented volumes (rsp = 0.68, $p < 0.001$), empirical scores demonstrated large variances and low correlation with age (rsp = 0.4, $p < 0.001$). DNNs achieved the highest classification accuracies (70–88 %) for all scores but suffered from overfitting and poor calibration. Feature importance metrics of tree-based algorithms selected the most sensible anatomical BVS features.
Discussion: Supervised ML algorithms on top of deep learning-based volumetric morphometry results can objectively aid radiological and clinical diagnosis of neurocognitive disorders while providing robust and reproducible measures for follow-up evaluation.
Conclusion: Multilayer ML setup is feasible to improve report quality and diagnostic accuracy of neurodegenerative disorders. Due to its anonymized nature, our study cohort could serve as benchmark data set for comparing algorithms of various vendors.

References

1. Maros ME, et al. Sci Rep. 2021;11:5529.
2. Cuingnet R, et al. Neuroimage. 2011;56:766–81.

[224] Identifikation hämodynamischer Parameter zur Vorhersage asymptomatischer Carotis-interna-Stenosen mittels Random Forest Machine Learning

Carina Gleißner[1*], Stephan Kaczmarz[1], Jan Kufer[1], Lena Schmitzer[1], Michael Kallmayer[2], Claus Zimmer[1], Benedikt Wiestler[1], Christine Preibisch[1], Jens Göttler[1]

[1]Technische Universität München, Klinikum rechts der Isar, Abteilung für Diagnostische und Interventionelle Neuroradiologie, München, Deutschland
[2]Technische Universität München, Klinikum rechts der Isar, Abteilung für Gefäßchirurgie und Endovaskuläre Chirurgie, München, Deutschland

Hintergrund: Eine Vielzahl von zerebralen hämodynamischen Parametern sind bei Patienten mit asymptomatischer Arteria-carotis-interna-Stenose (ACIS) verändert. Um die relevantesten Parameter und Regionen zu identifizieren, wurde ein Random-Forest-Klassifikator (RFK) [1] auf multimodale MRT-Daten angewandt. Individuelle Grenzzonen (iGZ) zwischen Gefäßterritorien sind hämodynamisch besonders anfällig [2], weshalb wir für die Parameterwerte in iGZ eine erhöhte Vorhersagegenauigkeit (VG) erwarten.
Methoden: Vierundzwanzig Patienten mit asymptomatischer, unilateraler, hochgradiger ACIS (>70 % nach NASCET; 70,6 ± 6,4y) und 24 gesunde Kontrollen wurden rekrutiert. Acht hämodynamische Parameter basierend auf ASL, mq-BOLD, Atemanhalte-fMRT und DSC gemäß [3] wurden jeweils inner- und außerhalb von iGZ [2] in grauer (GM) und weißer Substanz (WM) ipsi- und kontralateral zur Stenose extrahiert und die Seitendifferenz bestimmt (Abb. 1). Resultierende 96 Features (12 VOIs x 8 Parameter) wurden mit einem RFK gerankt. Durchschnittliche Feature-Relevanz-Scores und VG wurden berechnet [1].
Ergebnisse: Abb. 1 zeigt 1000-mal gemittelte Feature-Relevanz-Scores des mit 96 Features trainierten RFKs.
Nach Ausschluss von Redundanzen sind die wichtigsten Features in absteigender Reihenfolge: interhemisphärische Differenzen von TTP in WM und CBF in GM sowie ipsilaterale CVR in GM, jeweils innerhalb iGZ (Abb. 2). Trainiert man den RFK nur mit den vier sensitivsten Features, erreicht die VG 87,7 ± 2,3 % und wird durch weitere Features nicht wesentlich erhöht (Abb. 3). VOIs ohne Trennung nach iGZ erzielen signifikant geringere VG (Abb. 3). Unter Verwendung eines 10-fach Kreuzvalidierten AdaBoost-Klassifikators steigt die VG auf 92,3 ± 2,7 %.
Diskussion: Bereits wenige sensitive hämodynamische Features, wie die Seitendifferenz von TTP, CBF und die CVR ipsilateral zur Stenose, können ACIS-Patienten identifizieren. iGZ erhöhen dabei die VG.
Fazit: RFK ermöglichen es, die Relevanz von Parametern für die Vorhersage von ACIS zu ranken und könnten helfen, die Früherkennung von schweren hämodynamischen Einschränkungen bei ACIS-Patienten zu verbessern.

Literatur

1. Breiman, Machine Learning, 2001
2. Kaczmarz, Neuroradiology, 2018
3. Kaczmarz, JCBFM, 2020

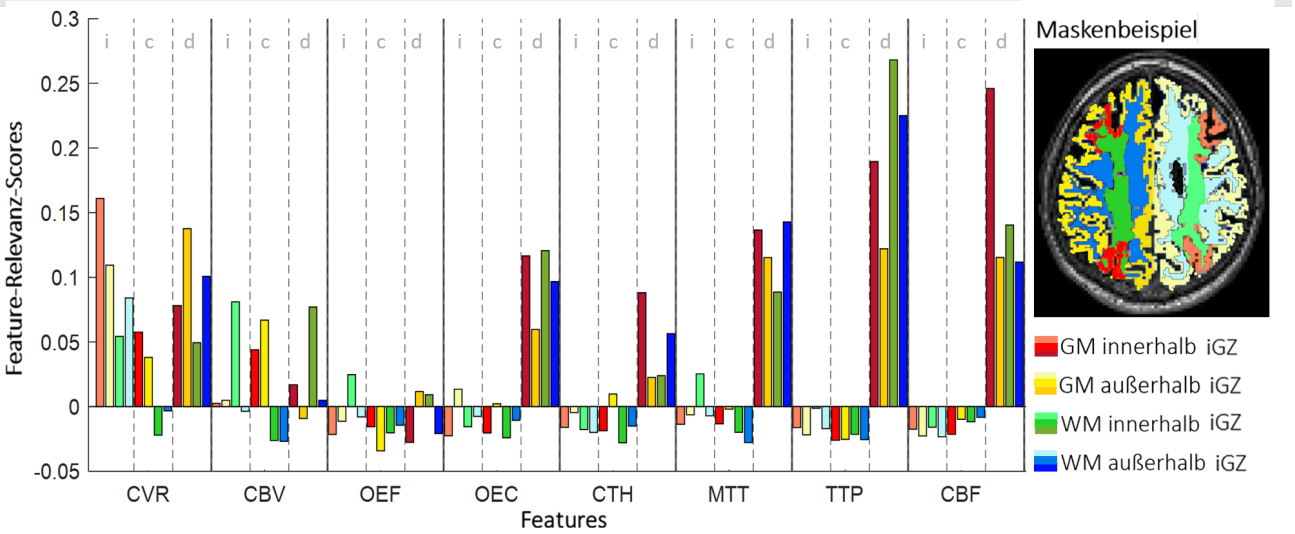

Abb. 1 | 224 Tausendfach gemittelte Feature-Relevanz-Scores des mit 96 Features trainiertem RFK. Acht MRT-Parameter (zerebrovaskuläre Reaktivität (CVR), zerebraler Blutfluss (CBF), zerebrales Blutvolumen (CBV), Sauerstoffextraktionsfraktion (OEF) und -kapazität (OEC), kapillare Transitzeit-Heterogenität (CTH), mittlere Transitzeit (MTT) und Zeit-zum-Peak (TTP)) in jeweils 12 VOIs. Die ersten vier Säulen je Parameter stellen ipsilaterale VOIs (i), die zweiten vier kontralaterale (c) und die dritten interhemisphärische Differenzen (d) dar. Je Gruppe ist GM innerhalb iGZs *rot*, GM außerhalb iGZs *gelb*, WM innerhalb iGZs *grün* und WM außerhalb iGZs *blau* markiert. Die Farbintensität steigt von Gruppe eins bis drei an

Abb. 2 | 224 Abb. 2: Zweihundertfach gemittelte Feature-Relevanz-Scores (± Standardabweichung) der sieben höchst gerankten Features. In der Tabelle sind der MRT Parameter und VOI Charakteristika je Feature angegeben

Rang	Parameter	Hemisphäre	Substanz	iGZ	Feature-Relevanz-Score ± Standardabweichung
1	TTP	Differenz	WM	innerhalb	0.60
2	CBF	Differenz	GM	innerhalb	0.53
3	CVR	ipsilateral	GM	innerhalb	0.38
4	CVR	Differenz	GM	außerhalb	0.31
5	MTT	Differenz	WM	außerhalb	0.26
6	OEC	Differenz	WM	innerhalb	0.22
7	CTH	Differenz	GM	innerhalb	0.18

[225] MR neurography in chemotherapy-induced peripheral polyneuropathy

Anastasia Priester[1*], Laura Michel[2], Philipp Romar[2], Michael Breckwoldt[1], Andreas Schneeweiss[2], Sabine Heiland[1], Martin Bendszus[1], Daniel Schwarz[1]

[1]Universitätsklinikum Heidelberg, Neuroradiologie, Heidelberg, Germany
[2]Universitätsklinikum Heidelberg, Gynäkologie, Heidelberg, Germany

Background: Chemotherapy-induced polyneuropathy (CIPN) is a common side effect of taxane-containing chemotherapies resulting in a pure sensory and painful, peripherally accentuated neuropathy. In up to 30 % of patients CIPN is irreversible [1] and can therefore require dose reduction or even discontinuation of the required chemotherapy. To date, hardly any preventive or therapeutic measures are available, with moderate effects reported for cooling or compression [2, 3]. The aim of this study was to investigate in vivo morphological and functional correlates of taxane-induced CIPN by means of magnetic resonance neurography (MRN) for early diagnosis and follow-up.
Methods: In this prospective study in progress, we performed a standardized high-resolution 3 Tesla (T) MRN on patients diagnosed with breast cancer undergoing taxane-containing chemotherapy. The protocol included imaging at baseline with two follow-ups. All patients underwent a clinical examination and detailed neurophysiological examination prior to neuroimaging. We examined the median, ulnar and radial nerves at the upper arm and wrist region using T2-weighted fat-saturated sequences and diffusion tensor imaging. Quantitative assessment included nerve T2-weighted (T2) signal (caliber), fractional anisotropy (FA) and apparent diffusion coefficient (ADC).
Results: Compared to baseline and age-matched controls, preliminary data indicate an increased T2 nerve-to-muscle signal ratio with corresponding elevated ADC. Surprisingly, these findings occur predominantly at upper arm level, although clinical symptoms are typically to be found at hand level.
Conclusion: We hypothesize that taxane-induced neurotoxicity leads to specific edematous nerve changes which underlie a distal neuropathic phenotype of CINP. These changes are readily picked up by high-resolution MRN and may show potential for early diagnosis and follow-up.

[228] MRI imaging of the glymphatic system after intrathecal gadolinium administration

Ikram Eda Duman Kavus[1*], Elias Kellner[2], Niklas Lützen[1], Philippe Dovi-Akué[1], Horst Urbach[1]

[1]Uniklinik Freiburg–Klinik für Neuroradiologie, Freiburg im Breisgau, Germany
[2]Uniklinik Freiburg–Klinik für Radiologie, Medizin Physik, Freiburg im Breisgau, Germany

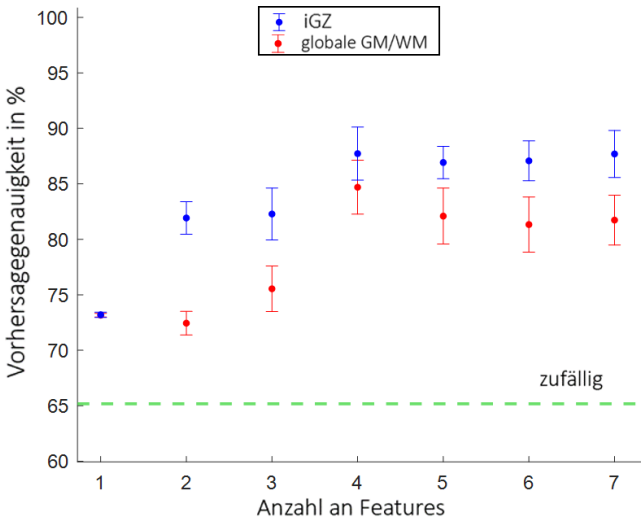

Abb. 3 | 224 Zweihundertfach gemittelte Vorhersagegenauigkeit (± Standardabweichung) von RFKs trainiert mit steigender Anzahl an Features. Hinzugefügte Features sind nach sinkender Relevanz sortiert (siehe Rang in Abb. 2). Bei zusätzlicher Trennung der VOIs nach inner- und außerhalb von iGZs (*blau*) ist die VG signifikant höher als unter Verwendung globaler GM und WM VOIs (*rot*). Um einen möglichen Feature-Selektions-Bias zu berücksichtigen, wurde die mittlere VG von RFKs berechnet, die mit zufällig gelabelten Probanden trainiert wurden (*gestrichelte grüne Linie*)

Background and purpose: The glymphatic (glia-lymphatic) system is a paravascular pathway for the clearance of waste metabolites including amyloid-β from the brain (Iliff et al. 2012). It can be visualized with serial Gadolinium cisternography (Ringstad et al. 2017). Here, we applied serial T1 relaxation time measurements in order to analyze the temporal dynamics of the glymphatic system.
Material and methods: 3D T1-weighted MP2RAGE sequences were acquired before and after intrathecal gadobutrol injections at 2–4, 6–8, and 24–48 h. MR scans were warped to the MNI space and serial scans were co-registered. T1 relaxation time measurements were performed in predefined ROIs including the perivascular spaces at the base of the basal ganglia. Five patients with spontaneous intracranial hypotension (SIH) and suspected spinal CSF leaks and four patients with frontobasal CSF leaks were studied so far.
Results: The time–T1-relaxation time curves indicate a flow e. g. through the perivascular spaces surrounding the lenticulostriate arteries. Compared to CSF in the ventricles, the decline is less extended and the return to baseline values obviously slower (Fig. 1).
Discussion: The decline and delayed return of T1-relaxation times when compared to CSF is compatible with a convective flow via perivascular spaces.
Conclusion: The glymphatic system can be visualized with serial Gadolinium cisternography.

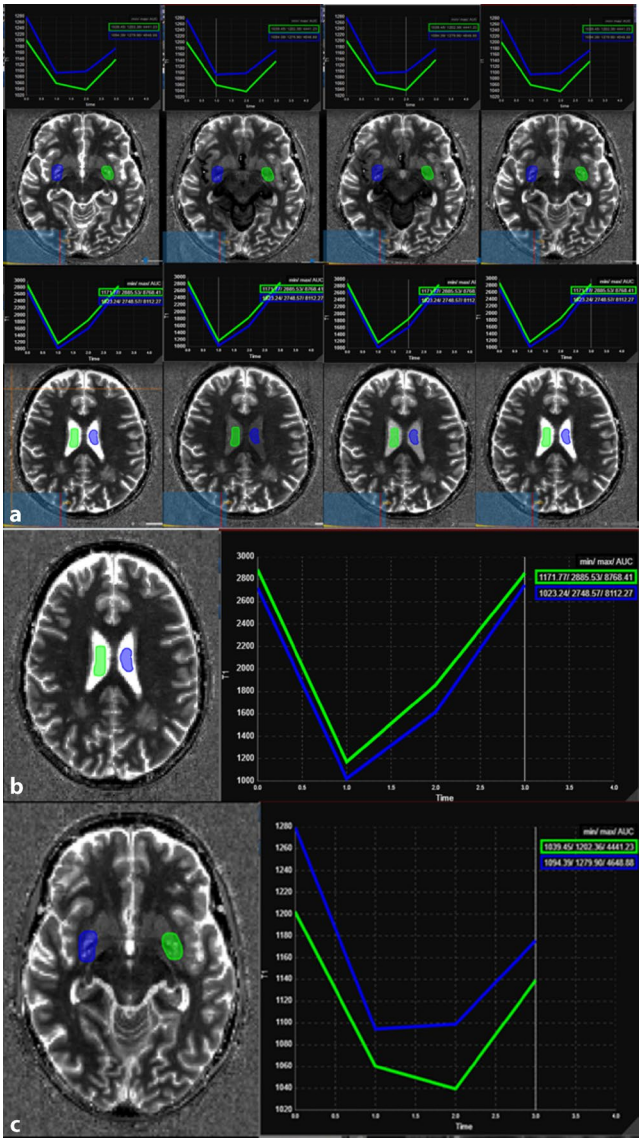

Fig. 1 | 228 In this 65-year-old woman with SIH, the Gadolinium uptake via the glymphatic system is measured with T1 relaxation time measurements at three time points following the pre Gadolinium examination. The top *rows show* ROIs covering the perivascular spaces at the level of basal ganglia. The *middle rows* show ROIs in the ventricles, where Gadolinium mixes with CSF and no brain parenchyma is present (**a**). The T1 relaxation times in the ventricles distinctly decline from around 2800 to 1000 ms and return to baseline values at 24 h (**b**). The T1 relaxation times in the perivascular spaces at the level of basal ganglia decline from around 1240 to 1080 ms. However, return to baseline values is obviously slower (**c**)

References

1. Iliff JJ WM, Liao Y, et al. A paravascular pathway facilitates CSF flow through the brain parenchyma and the clearance of interstitial solutes, including amyloid beta. Sci Transl Med. 2012;4:147ra111.
2. Ringstad G, Vatnehol SAS, Eide PK. Glymphatic MRI in idiopathic normal pressure hydrocephalus. Brain. 2017;140(10):2691–705. https://doi.org/10.1093/brain/awx191.

[232] Identification of arterial microaneurysm and micro venous abnormalities using susceptibility-weighted images (SWI) in perimesencephalic subarachnoid haemorrhage (PMSAH)

Silke Hopf-Jensen[1*], Ann-Kathrin Lohse[2], Michael Preiß[1], Rüdiger Buchalla[3], Jan Regelsberger[3], Stefan Müller-Hülsbeck[1]

[1]Department of Diagnostic and Interventional Radiology and Neuroradiology, DIAKO Hospital Flensburg, Flensburg, Germany
[2]Department of Radiology, University Hospital, LMU Munich, München, Germany
[3]Department of Neurosurgery, DIAKO Hospital Flensburg, Flensburg, Germany

Purpose: Perimesencephalic subarachnoid hemorrhage (PMSAH) is centered anteriorly to the pons and midbrain. The cause of the bleeding is still unknown, although a venous source is still discussed [1]. Susceptibility-weighted images (SWI) represent a powerful tool to visualize venous structures [2]. The purpose of the study was to assess the value of SWI MRI for visualization and characterization of vessel micro-angioarchitectur in PMSAH.
Methods: Analyses of clinical data and SWI sequences of 22 patients with PMSAH compared with 13 patients with aneurysmal SAH in perimesencephalic location (control group).
Results: PMSAH patients (mean age 53.6 years, ±11.3, fem. 10) showed a more favourable clinical course compared to the control group (56.8 years, ±8, fem. 9) with median of 15 on the Glasgow coma scale [IQR 15–15] at admission vs. 11 (IQR 3–15, $p=0.006$), with median HH 1 (1–2) vs. 4 (IQR 3–4), median Fisher-grad 3 (IQR 3–3.75) vs. 4 (IQR 3–4), 6 patients with vasospasm (27.3 %) without delayed ischaemic (DIC) vs. 7 patients with vasospasm (53.8 %) with 4 patients with DIC (30.8 %), 1 patient with ventriculoperitoneal shunt indication (4.5 %) vs. 5 patients (38.5 %, $p=0.035$) and a median of 1 on the Glasgow outcome scale (IQR 1–1) at discharge vs. 3 (IQR 3–3, $p<0.00001$). In SWI analysis of PMSAH one case of thrombosed basilar artery microaneurysm was identified. In three cases, petechial microbleedings beneath the uncal vein were detected. Microhemorrhages ventral to the interpeduncular vein (four cases) and eight enlarged Rosendahl veins have been described. These susceptibility artefacts were not seen in aneurysmal SAH.

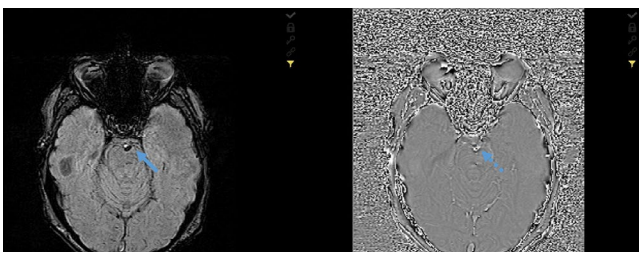

Fig. 1 | 232

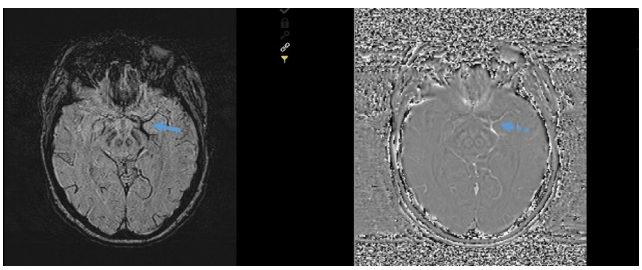

Fig. 2 | 232

Discussion: SWI sequences can visualize increased levels of deoxyhemoglobin in cortical vein thrombosis and are useful in visualization of arterial clots [2]. We show enlarged veins as a result of local venous high pressure suitable with micro-venous thrombosis. Petechial micohemorrhages beneath the uncal vein speak for local breakdown of the blood brain barrier and could indicative for venous inflammation. Thrombosed arterial or venous microaneurysm can change susceptibility by decreasing flow with increased level of deoxygenated blood.
Conclusion: Susceptibility-weighted images are feasible in PMSAH and might have significant impact on detection of thrombosed microaneurysms and identification of venous pathology.

References

1. van der Schaaf IC, et al. Venous drainage in perimesencephalic hemorrhage. Stroke. 2004;35:1614–8.
2. Mittal S, et al. SWI: technical aspects and clinical applications. Am J Neuroradiol. 2009;30:232–52.

[233] Acute central retinal artery occlusion: correlating DWI-MRI with OCT

Eberhard Siebert[1*], Mirjam Rossel-Zemkouo[2], Kersten Villringer[3], Konrad Neumann[4], Georg Bohner[1], Leon Danyel[5]

[1]Institut für Neuroradiologie, Charité–Universitätsmedizin Berlin, Berlin, Germany
[2]Klinik für Augenheilkunde, Charité–Universitätsmedizin Berlin, Berlin, Germany
[3]Center for Stroke Research, Charité–Universitätsmedizin Berlin, Berlin, Germany
[4]Institut für Biometrie und klinische Epidemiologie, Charité–Universitätsmedizin Berlin, Berlin, Germany
[5]Klinik für Neurologie, Charité–Universitätsmedizin Berlin, Berlin, Germany

Background: Retinal diffusion restrictions (RDR) have recently been identified as a regular finding on diffusion-weighted (DWI) MRI in patients with central retinal artery occlusion (CRAO). However, sensitivity for standard 1.5 T and 3 T brain stroke DWI sequences is limited. Optical coherence tomography (OCT) allows for noninvasive examination of retinal layers with a micrometer spatial resolution and has been shown to detect microstructural retinal changes in CRAO. In this study we investigated differences in retinal microstructure between CRAO patients with and without discernable RDR on DWI.
Methods: Consecutive CRAO patients with both MRI and OCT within 7 days after symptom onset between 2010 and 2019 were included in this retrospective cohort study. Standard stroke MRI including DWI, acquired at 1.5 or 3 T, was evaluated for RDR. OCT scans were evaluated for retinal ischemia related microstructural changes such as central, superior, inferior macular thickness (CMT, SMT, IMT) and inner retinal layer thickness (IRLT). OCT results were compared to the presence of RDR using Mann–Whitney U or Chi-squared testing. Nonaffected eyes were also evaluated for CMT. A p-value<0.05 was considered statistically significant. Descriptive statistics are presented as mean ± SD.
Results: A total of 58 patients were included in the study. RDR were seen in 39 patients (67.2 %, 75 % at 3 T and 57.7 % at 1.5 T). Retinal layer thickness measurements of RDR negative patients were significantly lower compared to RDR positive patients (CMT: 305 ± 45.9 vs. 345.4 ± 76.9 µm, $p=0.034$; SMT: 366.7 ± 45.6 µm vs. 418.5 ± 75.06 µm, $p=0.007$; IMT: 370.3 ± 45.2 µm vs. 428.9 ± 62.4 µm, $p=0.002$; IRLT: 233.9 ± 48.6 µm vs. 186,7 ± 34.7 µm, $p=0.001$). CMT of the fellow eye did not differ between RDR positive and negative cases (297.8 ± 96.58 µm vs. 291 ± 52.9 µm, $p=0.949$). DWI tended to be negative at higher IRLT values at 1.5 T compared to 3 T (199.8 ± 29.7 µm vs. 168.6 ± 32.8 µm; $p=0.057$) reflecting improved detectability of RDR at 3 T.

Discussion: The sensitivity of DWI in CRAO is dependent on retinal thickness that increases due to ischemic retinal edema formation and associated microstructural changes as determined by OCT. Differences in the extent of retinal cell edema appear to influence the ability to produce a perceivable DWI signal in affected voxels.
Conclusion: The sensitivity of DWI–MRI in CRAO is dependent on the extent of retinal ischemic edema that leads to an increase of the inner retinal thickness. This interrelation may explain false-negative DWI investigations.

[234] Transformation of stroke lesions after ischemic stroke: do inflammatory processes matter?

Simone Henze[1*], Kathleen Bernkopf[2], Christian Maegerlein[1], Claus Zimmer[1], Moritz Hernandez Petzsche[1], Benno Ikenberg[2], Tobias Boeckh-Behrens[1], Maria Berndt[1]

[1]School of Medicine, Technical University of Munich, Klinikum rechts der Isar, Department of Diagnostic and Interventional Neuroradiology, Munich, Germany
[2]School of Medicine, Technical University of Munich, Klinikum rechts der Isar, Department of Neurology, Munich, Germany

Background: The immune system plays an important role in the pathophysiological processes after ischemic stroke, both causing additional damage and stimulating remedial action. The direct impact of inflammation on brain tissue in the further course after ischemic stroke is not finally clarified. Aim of the study was to analyze the stroke lesions and their transformation in the follow-up imaging in relation to inflammatory occurrence in the acute stroke phase and to assess the impact on clinical outcome.
Methods: Stroke lesions were segmented in FLAIR-images in the acute post-stroke phase (3 days after reperfusion) and in the follow-up (3 months later) for 69 patients after mechanical recanalization. After coregistration and subtraction of lesion maps, volume change was quantified and patients were classified into two main groups: patients with a volume decrease of more than 50 % without increase (group A; $n=40$) and patients with a volume decrease of less than 50 % ($n=11$) or growth of stroke lesions ($n=18$, group B: $n=29$; Fig. 1). Inflammation values (C-reactive protein [CRP] and leukocytes) were gathered on admission (T0), 24 h later (24 h), three days after stroke (T1), and the maximum value (max). These values were compared between the two patient groups and correlated to clinical outcome (NIHSS after 90 days).
Results: Patients of group A have lower values of CRP and leukocytes in the acute phase than patients of group B (Fig. 2). CRP at T1 and maximum values are lower in group A (median/IQR of CRP-T1:1.3/1.3 and CRP-max:1.8/2.35) than in group B (2.1/3.8 and 3.9/8.6; $p=0.047/0.01$). Also, the maximum value of the leukocytes is

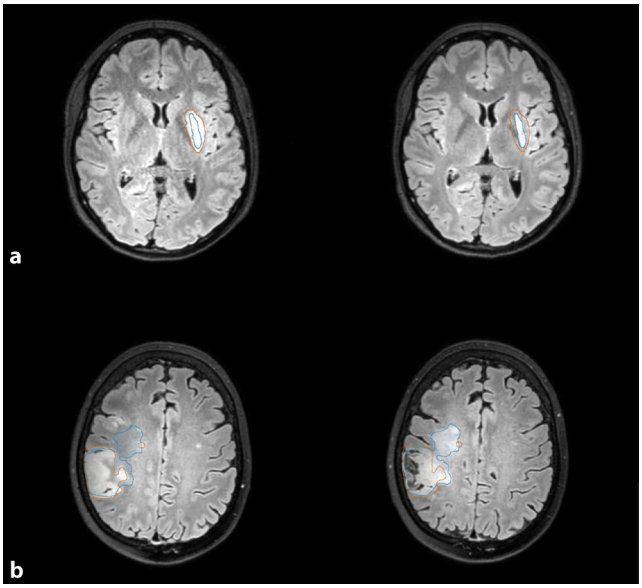

Fig. 1 | 234 Example of two patients three days after mechanical recanalization of an acute M1-occlusion (FLAIR, on the left) and in the follow-up after three months (FLAIR, on the *right*). In (**a**) the stroke lesion (segmented in FLAIR 3 days after stroke, in *orange*) shows a decrease of >50 % in the follow-up imaging (segmented in FLAIR after 3 months, in *blue*), in (**b**) the stroke lesion increases after 3 months

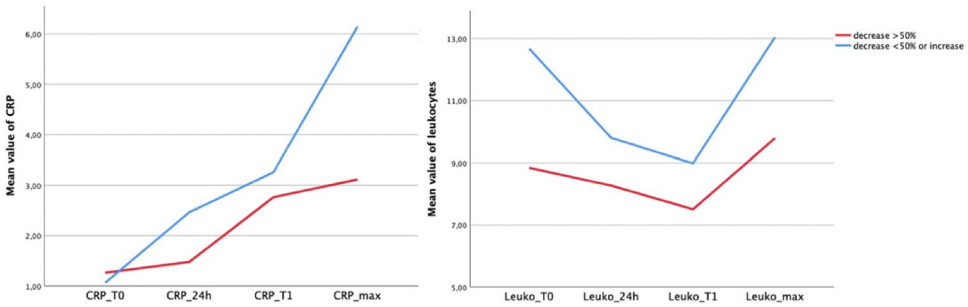

Fig. 2 | 234 The course of the mean values of C-reactive protein (CRP, on the *left*) and of the number of leukacytes (on the *right*) in group A (decrease of lesion volume >50 %, *red*) and B (decrease of lesion volume <50 % or growth of stroke lesions, *blue*) at admission (T0), 24 hours later (24 h), 3 days after strpke (T1) and the maximum value (max)

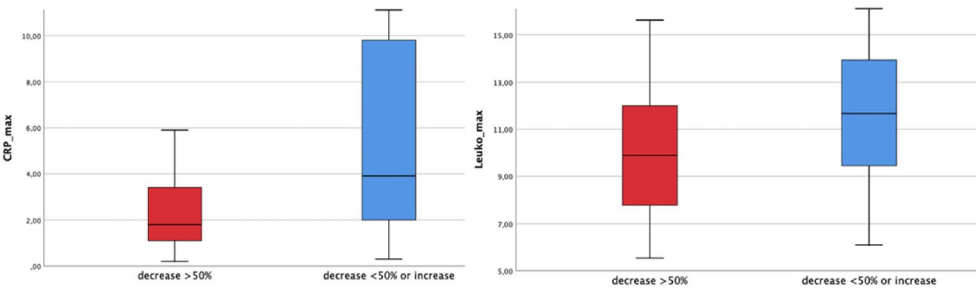

Fig. 3 | 234 Distribution af maximum values of CRP (on the *left*) and the number of leukocytes (on the *right*) for the two patient groups (A: decrease of lesion volume >50 %, B: decrease of lesion volume <50 % or growth of stroke lesions). There are significantly lower values in group A than in group B (for CRP_max/Leuko_max: $p=0{,}01/0{,}03$)

lower in group A (median/IQR: 9.9/4.25) than in group B (11.7/4.64; $p=0.03$; Fig. 3).
NIHSS score after three months is lower for patients in group A (median/IQR:1.0/1) than in group B (1.5/4; $p=0.03$) and is correlated to the maximum value of CRP ($r=0.21/p=0.04$) and leukocytes ($r=0.27/p=0.01$).
Discussion: Inflammatory processes assessed by CRP and leukocytes in the acute post-stroke phase seem to influence the transformation of stroke lesions in the follow-up imaging. Both inflammation and consecutive changes of the stroke lesions impact the clinical outcome.
Conclusion: Patients with signs of inflammation in the acute post-stroke phase should be further investigated. This could be of interest in terms of a specific therapeutic approach as inflammation seems to cause clinically relevant stroke lesion transformation. Additionally, the pathophysiological background of lesion increase must be studied.

[235] Beyond mean value analysis–a voxel-based analysis of the quantitative MR biomarkers water T2 and PDFF for assessment of skeletal muscle tissue of patients with neuromuscular diseases

Sarah Schlaeger[1*], Dominik Weidlich[2], Agnes Zoffl[1], Edoardo Aitala Becherucci[1], Elisabeth Klupp[1], Federica Montagnese[3], Marcus Deschauer[4], Benedikt G. H. Schoser[3], Claus Zimmer[1], Thomas Baum[1], Dimitrios Karampinos[2], Jan Kirschke[1]

[1]Klinikum rechts der Isar der Technischen Universität München, Neuroradiologie, München, Germany
[2]Klinikum rechts der Isar der Technischen Universität München, Radiologie, München, Germany
[3]Friedrich-Baur-Institut, München, Germany
[4]Klinikum rechts der Isar der Technischen Universität München, Neurologie, München, Germany

Background: The main pathologies in muscles of patients with neuromuscular diseases (NMD) are fatty and edematous changes [1–3]. Recently, quantitative magnetic resonance (MR) imaging for determination of the corresponding MR biomarkers proton density fat fraction (PDFF) and water T_2 (T_{2w}) has been advanced [4]. Biophysical effects or pathology can have counteracting effects on MR biomarkers, e. g. MR spectroscopy showed a dependency of T_{2w} on the fat fraction (FF) [5]. Thus, in heterogeneously affected muscles the routinely performed mean value analysis [6] is questionable. Our work proposes a voxel-based histogram analysis of PDFF and T_{2w} based on co-registered quantitative images to mitigate partial volume effects.
Methods: In 12 patients with NMD (LGMD2A $n=5$; DM2 $n=5$; Pompe $n=2$) chemical shift encoding-based water-fat imaging for PDFF and T_2 mapping with SPAIR [7] for T_{2w} determination were performed. Nine thigh muscles were segmented bilaterally ($n=216$). PDFF and T_2 maps were co-registered.
Results: A voxel-based comparison of PDFF and T_{2w} revealed a dependency of T_{2w} on the FF showing that T_{2w} is decreased with increasing FF (Fig. 1). A comparison of the T_{2w} value distribution in the semimembranosus muscle of a patient with [1] Pompe disease and [2] DM2 revealed different histograms. Both muscles have the mean T_{2w} of healthy muscles (≈32 ms). However, the Pompe patient's T_{2w} histogram has a broad distribution, and two peaks are present (at 22/35 ms) corresponding to T_{2w} of edematous and fatty voxels, whereas in the DM2 patient's T_{2w} histogram a single peak is present (at 31 ms) corresponding to T_{2w} of healthy voxels (Fig. 2).
Discussion: Partial volume effects can lead to misinterpretation of muscle health when only the mean T_{2w} of a heterogeneously affected muscle is assessed. A muscle with healthy muscle tissue that is simultaneously affected by fatty and edematous changes might have a mean T_{2w} like healthy muscles.
Conclusion: The assessment of muscle pathologies based on PDFF and T_{2w} requires an interpretation beyond mean value analysis to account for regional pathological differences. Histograms could be an alternative way of interpretation.

References

1. Mercuri E, Pichiecchio A, Allsop J, Messina S, Pane M, Muntoni F. Muscle MRI in inherited neuromuscular disorders: past, present, and future. J Magn Reson Imaging. 2007;25(2):433–40. https://doi.org/10.1002/jmri.20804.
2. Wattjes MP, Kley RA, Fischer D. Neuromuscular imaging in inherited muscle diseases. Eur Radiol. 2010;20(10):2447–60. https://doi.org/10.1007/s00330-010-1799-2.
3. Mercuri E, Jungbluth H, Muntoni F. Muscle imaging in clinical practice: diagnostic value of muscle magnetic resonance imaging in inherited neuromuscular disorders. Curr Opin Neurol. 2005;18(5):526–37. https://doi.org/10.1097/01.wco.0000183947.01362.fe.
4. Carlier PG, Marty B, Scheidegger O, Loureiro de Sousa P, Baudin PY, Snezhko E, Vlodavets D. Skeletal Muscle Quantitative Nuclear Magnetic Resonance Imaging and Spectroscopy as an Outcome Measure for Clinical Trials. Neuromuscul Dis. 2016;6(4):10–20. https://doi.org/10.17650/2222-8721-2016-6-4-10-20.
5. Schlaeger S, Weidlich D, Klupp E, Montagnese F, Deschauer M, Schoser B, et al. Decreased water T 2 in fatty infiltrated skeletal muscles of patients with neuromuscular diseases. NMR Biomed. 2019;32(8):e4111. https://doi.org/10.1002/nbm.4111.
6. Willcocks RJ, Arpan IA, Forbes SC, Lott DJ, Senesac CR, Senesac E, et al. Longitudinal measurements of MRI-T2 in boys with Duchenne muscular dystrophy: effects of age and disease progression. neuromuscul Disord. 2014;24(5):393–401. https://doi.org/10.1016/j.nmd.2013.12.012.
7. Schlaeger S, Weidlich D, Klupp E, Montagnese F, Deschauer M, Schoser B, et al. Water T2 Mapping in Fatty Infiltrated Thigh Muscles of Patients With Neuromuscular Diseases Using a T2-Prepared 3D Turbo Spin Echo With SPAIR. J Magn Reson Imaging. 2020;51:1727–36. https://doi.org/10.1002/Jmri.27032.

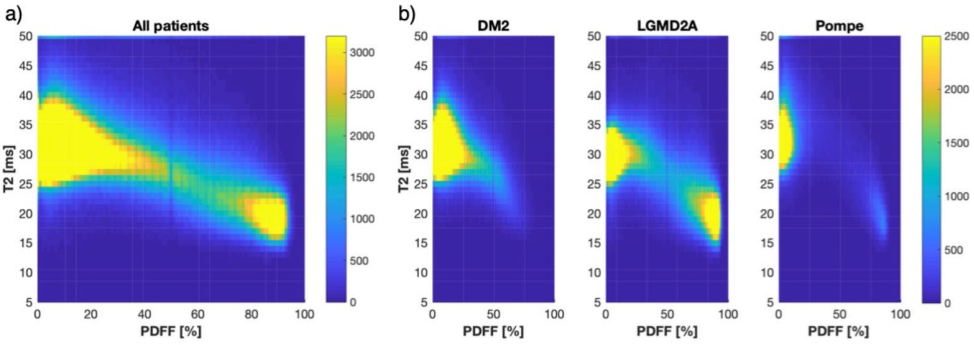

Fig. 1 | 235 Histogram of certain PDFF/T_{2w} value combinations (the brightness encodes the probability). **a**) Decreased T_{2w} with increasing PDFF in 216 muscles of patients with neuromuscular diseases. **b**) Behavior of T_{2w} with increasing PDFF separated for three different patient groups (LGMD2A, DM2 and Pompe disease)

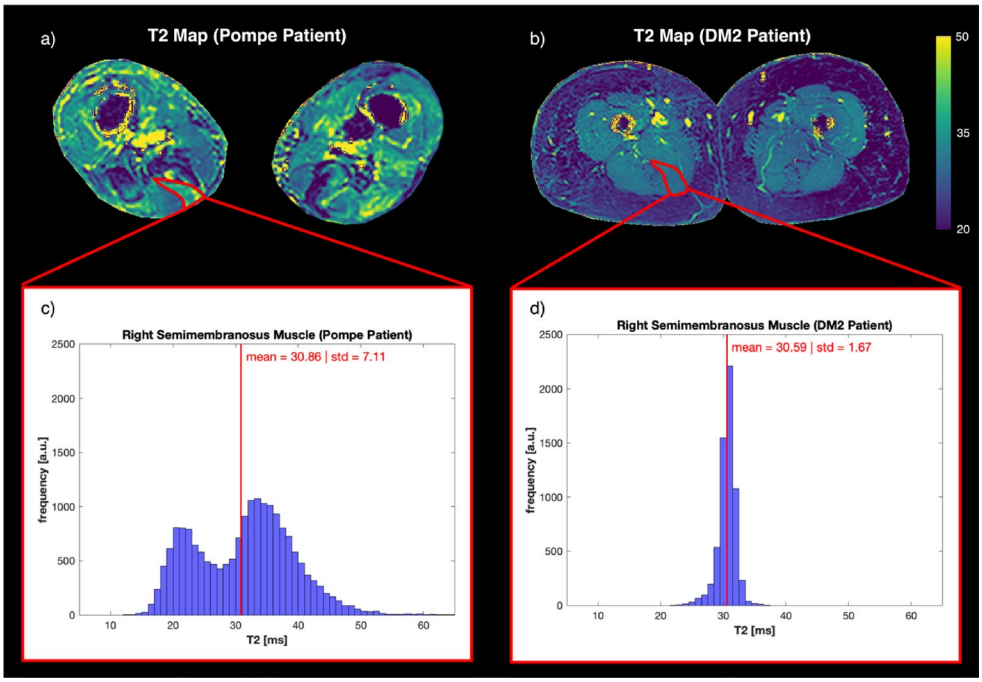

Fig. 2 | 235 T_2 maps of the thigh muscles of **a**) a patient with Pompe disease and **b**) a patient with DM2. Segmentation masks of the right semimembranosus muscle are depicted in *red*, respectively. Corresponding histograms of T_{2w} in the right semimembranosus muscle of **c**) the patient with adult Pompe disease and **d**) the patient with DM2. In the *left* histogram two peaks are present (at 22/35 ms), whereas in the *right* histogram only one peak is present (at 31 ms), however both muscles have approximately the same mean T_{2w} (=31 ms)

[236] Occupation-related effects on motor cortex thickness among older, cognitive healthy individuals

Lukas Lenhart[1*], Melanie Nagele[1], Ruth Steiger[1], Vincent Beliveau[1], Elisabeth Skalla[1], Laura Zamarian[1], Elke Ruth Gizewski[1], Thomas Benke[1], Margarete Delazer[1], Christoph Scherfler[1]

[1]Medizinische Universität Innsbruck, Innsbruck, Austria

Background: Both, decline of sensorimotor functions and decrease of cortical thickness are known processes in healthy aging [1]. Physical activity has been suggested to have a positive effect on the execution of daily routine activities and to extend the time of functional independence in advanced age [2]. We hypothesized that cortical thickness of motor areas in retired individuals would be related to physical demands of the profession carried out during the working life period.
Methods: The study population consisted of 69 healthy participants (range from 70–85 years) without signs of cognitive impairment as assessed by neuropsychological testing (MMSE value>25, GDS score<5 and z-values>–2 CERAD). Participants' former occupations were divided into higher physically complex occupations and lower physically complex occupations (HPCO, $n=27$ and LPCO, $n=42$) according to the international standard classification of occupations (ISCO-08).
Results: Surface-based morphometry analyses revealed higher cortical thickness in the left precentral ($p=0.001$) and postcentral gyrus ($p<0.001$) and right postcentral gyrus ($p=0.001$) for the HPCO relative to the LPCO group (corrected for multiple comparisons, sex, age, and leisure activities in the past 20 years). Physical leisure activities associated with exertion were positively correlated with cortical thickness in the left pre- and postcentral gyrus ($p=0.037$) of the LPCO group. Time since retirement was negatively associated with cortical thickness in the left postcentral gyrus ($p=0.004$) of the HPCO group.
Discussion: Executing a physical complex occupation before retirement was related to increased cortical thickness in motor regions supporting the hypothesis that exercise contributes to neural reserve in these regions. However, neural reserve and assumed protective effects appear to vanish when physical activity is reduced because of retirement.
Conclusion: Increased understanding of reserve capacity and age-related motor decline in older adults may help to design appropriate rehabilitation strategies to improve everyday needed motor abilities, which in turn lead to better health and quality of additional lifetime.

References

1. Seidler RD, Bernard JA, Burutolu TB, et al. Motor control and aging: links to age-related brain structural, functional, and biochemical effects. Neurosci Biobehav Rev. 2010;34(5):721–33.
2. Erickson KI, Leckie RL, Weinstein AM. Physical activity, fitness, and gray matter volume. Neurobiol Aging. 2014;35(Suppl 2):20–S8.

[237] Altered dynamics connectivity patterns in multiple sclerosis at rest: a case-control and a longitudinal study

Xiaojing Fang[1*, 2], Michael Marxen[2], Bruce Morton[3], Paul Kuntke[1], Hagen H. Kitzler[1]

[1]Technische Universität Dresden, University Hospital Carl Gustav Carus, Institute for Diagnostic and Interventional Neuroradiology, Dresden, Germany
[2]Technische Universität Dresden, University Hospital Carl Gustav Carus, Department of Psychiatry and Neuroimaging Center, Dresden, Germany
[3]University of Western Ontario, Department of Psychology, Cognitive Development and Neuroimaging Laboratory, Canada

Background: Neural functional connectivity (FC) dynamics at rest may be linked to cognitive and behavioural deficits in multiple sclerosis (MS) [1]. However, it is still unclear how FC network dynamics can be differentially characterized for MS versus healthy controls (HC) and during the cause of the disease. Here, we investigate properties of two mutually exclusive dynamic FC brain states: functional segregation (I) and integration (II).
Methods:
Results: Dynamic functional connectivity (DFC) analyses.
Statistical analyses: There was no significant linear time effect on the parameters. We observed an increasing trend of the effect on DMT of state I (F-value: 0.352, p-value: 0.071; Fig. 5). In the group comparisons, we observed significant group differences in the MDT of state I (p-value: 0.002) and prevalence of state I (p-value: 0.0002).

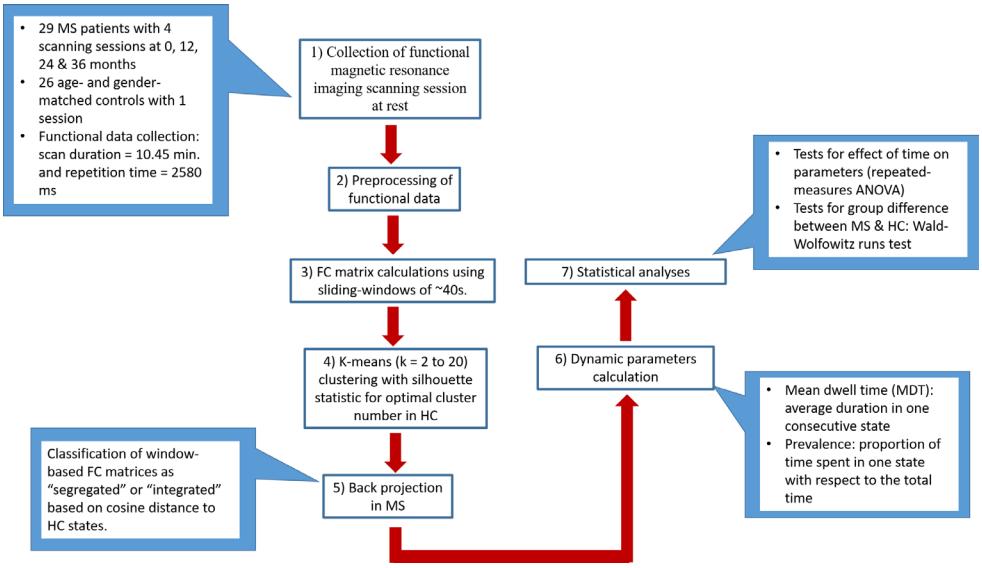

Fig. 1 | 237 Flow chart of methods

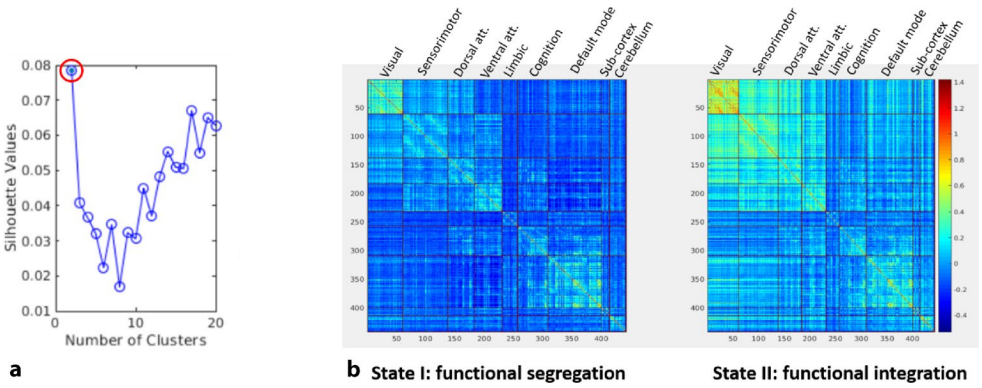

Fig. 2 | 237 Results of clustering analyses for HC. **a**) Silhouette indices for k-means clustering results based on the 1-IC data. **b**) Averaged DFC for each state in HC when k = 2

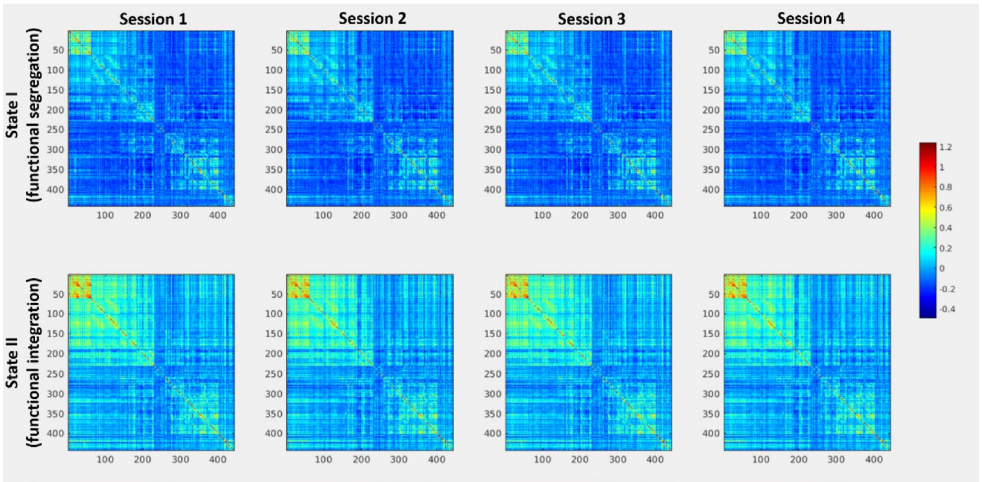

Fig. 3 | 237 Averaged DFC for each state of patients based on back projection

Discussion: 1) The two patterns in the HC confirm that functional segregation versus integration is a useful organizational principle of brain function [2].
2) We found no linear effect of time on our dynamic FC parameters over a time scale of 3 years in MS.
3) Altered MDT and prevalence of the states may help to explain cognitive impairments in MS [1].

Conclusion: Our analyses show that dynamic FC parameters may show differences in MS as compared to HC but are not sensitive enough to track longitudinal decline. Additional analysis to investigate correlations with clinical severity and other imaging measures are in progress.

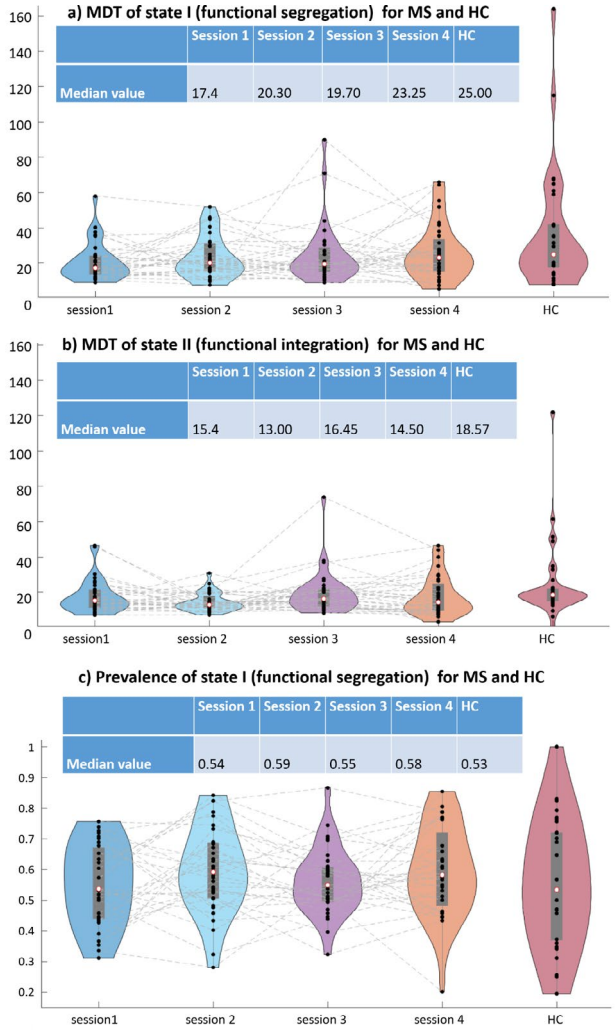

Fig. 4 | 237 Longitudinal development of dynamic properties for HC and MS. The median and interquartile range was plotted for the four sessions for patients and one session for HC. Prevalence of state II was not calculated since h was equal to 1 – prevalence of state I and thus had the same statistical significance as state I

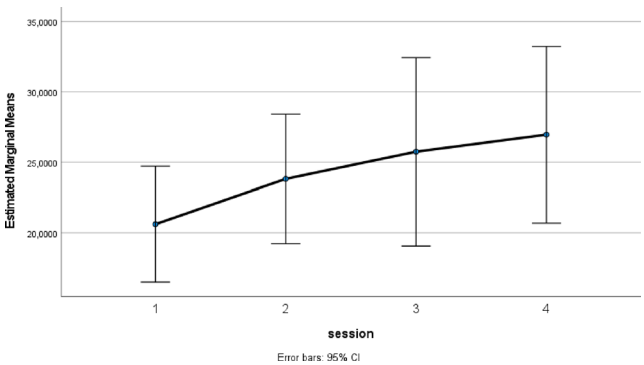

Fig. 5 | 237 Repeated-measures ANOVA results for MDT of state I

References

1. Rocca MA, et al. Impaired functional integration in multiple sclerosis: a graph theory study. Brain Struct Funct. 2016;221(1):115–31.
2. Fox PT, Friston KJ. Distributed processing; distributed functions? Neuroimage. 2012;61(2):407–26.

[238] Gender aspects in interventional neuroradiology (INR) training

Sebastian Reder[1*], Annaïg Rohou[2], Naureen Keric[3], Marc A. Brockmann[1], Sebastian Altmann[4], Ahmed Othman[1], Mario Alberto Abello Mercado[1], Carolin Brockmann[1]

[1]Department of Neuroradiology, University Medical Center Mainz, Mainz, Germany
[2]Faculty of Psychology, University of Graz, Graz, Austria
[3]Department of Neurosurgery, University Medical Center Mainz, Mainz, Germany
[4]Department of Radiology, University Medical Center Mainz, Mainz, Germany

Background: Gender-differences have been discussed for various surgical techniques. We aimed at investigating gender differences in training of INR techniques using a silicone model.
Methods: After a standardized training sequence, performance of 64 subjects (26 women, 38 men) naïve to neurointerventional techniques was analysed. Analysing four different, simulated, neurointerventional tasks to required time, number of catheter movements, covered pathway and tries to pass vascular branches. Afterwards, subjects had to answer a questionnaire regarding video gaming activities and a NASA Task Load Index to rate individual perceived workload.
Results: Women required more time to solve the tasks (688 ± 363 vs. 501 ± 230 s; $p = 0.019$) and more female participants ($n = 19$) asked earlier for help than men ($n = 8$; 203 ± 94 vs. 305 ± 142 s; $p = 0.049$). Women perceived higher stress-levels (8.9 ± 4.9 vs. 6.3 ± 4.4; $p = 0.037$) and tasks more difficult (11.5 ± 4.2 vs. 9.6 ± 3.3; $p = 0.016$). They subjectively rated their own performance lower than men (9.12 ± 3.3 vs. 11.3 ± 3.3; $p = 0.009$). There were no significant gender-based differences for catheter movements, covered pathway, number of tries or objective performance (except time). In females, subjective performance correlated to movements (r = –0.555; $p = 0.004$), pathway (r = –0.469; $p = 0.018$), time (r = –0.513; $p = 0.009$), tries (r = –0.394; $p = 0.051$) and objective performance (r = –0.383; $p = 0.059$). Perceived difficulty correlated to time (r = 0.459; $p = 0.021$), objective performance (r = –0.469; $p = 0.018$) and number of tries (r = 0.379; $p = 0.061$). Stress-level correlated to objective performance (r = –0.429; $p = 0.033$). In males, stress level correlated to number of movements (r = 0.587; $p < 0.001$), number of tries (r = 0.399; $p = 0.013$), catheters pathway (r = 0.459; $p = 0.004$) and time (r = 0.469; $p = 0.003$).
Conclusion: Women were slower, asked earlier and more frequently for help than men. There were no gender-based differences in objective performance otherwise. Since perceived stress level and objective parameters in men and women differ, these aspects should be considered in training of future neurointerventionalists.

[240] Subtraction of 3D-FLAIR for monitoring disease progression in multiple sclerosis using a clinically approved medical product

Mario Alberto Abello Mercado[1*], Andrea Kronfeld[1], Sebastian Altmann[2], Ahmed Othman[1], Felix Lüssi[3], Marc A. Brockmann[1], Sebastian R. Reder[1]

[1]Department of Neuroradiology, University Medical Center Mainz, Mainz, Germany
[2]Department of Radiology, University Medical Center Mainz, Mainz, Germany

[3]Department of Neurology, University Medical Center Mainz, Mainz, Germany

Background: MR-imaging results significantly influence therapy of multiple sclerosis (MS). Image interpretation in MS can be time-consuming. We aimed at simplifying and accelerating image analysis using an approved medical product, such as image fusion with subtraction.
Methods: MRI studies of 73 patients with MS were retrospectively analyzed. Every case included a baseline and a follow-up scan (incl. T2 SPACE dark fluid). Images were analyzed by unexperienced (R1) and experienced (R2) neuroradiology resident. Using an automatic matching software (Syngo via; Siemens Healthineers), the follow-up images were co-registered and subtracted from the baseline images, hereby more clearly showing differences between both scans. Both readers analyzed the unsubtracted and the subtracted images separately for new lesions in independent readings blinded to each other's findings. Primary outcomes were reading time, diagnostic confidence (visual analog scale, VAS), sensitivity and specificity to detect new MS plaques for each reader and both methods (standard and with post-processed images). Reading sessions were timed two weeks apart.
Results: In analyzing standard images R1 was slower than R2 (186.6 ± 72.6s vs. 159.1 ± 49.3s, $p = 0.026$), same was observed analyzing post-processed image reading (90.3 ± 22.7s vs. 80.2 ± 14.7s, $p = 0.008$). The experienced reader analyzed all images significantly faster (both $p < 0.001$). Sensitivity increased for both readers analyzing post-processed images, while specificity decreased (standard images: R1/R2: sensitivity = 0.72/0.81, specificity = 0.32/0.91 vs. post-processed images: R1/R2: sensitivity = 1.0/1.0, specificity = 0.16/0.71). Confidence increased while analyzing post-processed images, which affected the unexperienced reader stronger (VAS = 5.6 ± 1.9 vs. 6.4 ± 1.7, $p = 0.011$) than the experienced reader (VAS = 7.4 ± 0.72 vs. 8.06 ± 0.72, $p \leq 0.001$).
Conclusion: Using an approved medical product, image fusion with subtraction significantly reduces reading time in MS-imaging. Due to the increased sensitivity it appears to be a helpful tool in daily routine, despite its reduced specificity.

[241] Synthetic T2-weighted fat sat delivers valuable information for pathology assessment in the spine: validation of a task-specific generative adversarial network

Sarah Schlaeger[1*], Katharina Drummer[1], Malek Husseini[1], Nico Sollmann[1], Claus Zimmer[1], Benedikt Wiestler[1], Jan Kirschke[1]

[1]Klinikum rechts der Isar der Technischen Universität München, Neuroradiologie, München, Germany

Background: Generative adversarial networks (GAN) based on deep learning (DL) can create novel contrasts in magnetic resonance imaging data [1]. The purpose of this study was to compare a GAN-based synthetic (syn) T2-weighted (w) fat saturated (fs) sequence with its true counterpart regarding (1) ability to detect spinal pathologies not seen on non-fs T2-w and T1-w images, (2) diagnostic agreement, and (3) image quality.
Methods: We retrospectively identified 173 patients with sagittal T1-w TSE, T2-w TSE and fs T2-w TSE images of the spine. A GAN was trained to synthesize T2-w fs images from T1- and T2-w images in 129 scans of 72 patients (Fig. 1). This GAN was used to create syn T2-w fs images from the remaining, previously unseen 101 sagittal spine scans (Fig. 2). Diagnostic performance of syn images was assessed in 6 pathologies (Fig. 3). Pathologies were first assessed on T1-w and T2-w images only, then (randomized syn or true) T2-w fs was blindly added. This approach was repeated with the remaining syn or true T2-w fs. We evaluated (1) the additional diagnostic information of syn vs. true T2-w fs, (2) the agreement of syn vs. true T2-w fs using Cohen's Kappa, and (3) the grading of image and fs quality.
Results: (1) Assessment of syn T2-w fs allowed detection of abnormalities not seen on non-fs images, comparable to true T2-w fs (Fig. 3). (2) Agreement of syn vs. true T2-w fs ranked between moderate to almost perfect (Fig. 4). Of note, it was equal or higher than intrarater agreement of T1- and T2-w based ratings. (3) Image quality was higher for syn than for true T2-w fs (99,9 % vs. 88,1 % graded at least acceptable). Fat sat quality was comparable.
Discussion: The syn T2-w fs delivers valuable additional information on spine pathologies, showing excellent intra-method agreement and an overall better image quality compared to true T2-w fs. Additional

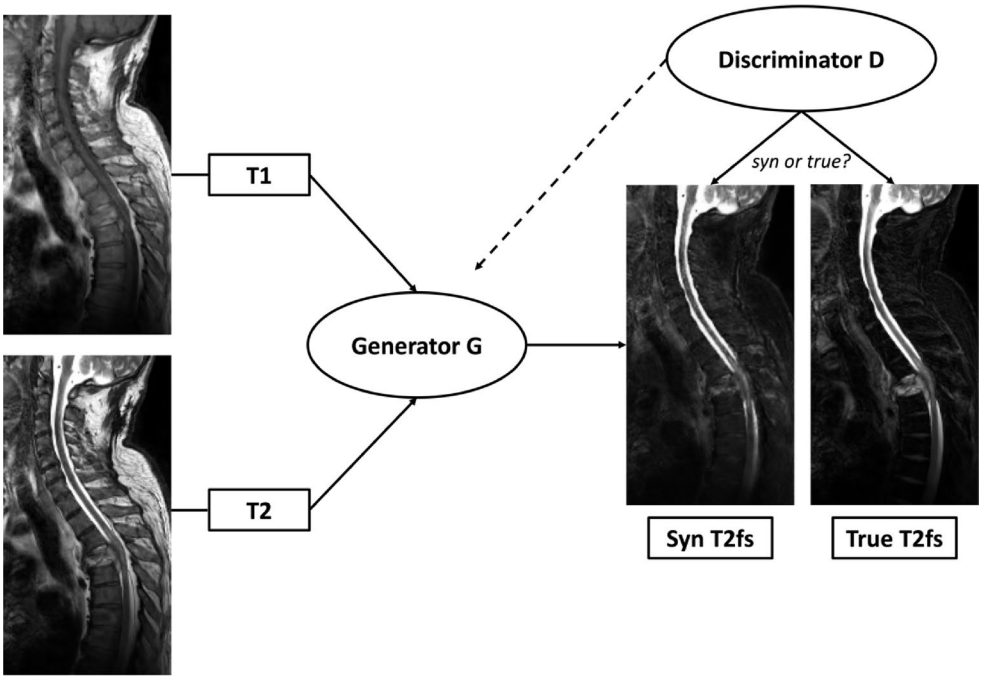

Fig. 1 | 241 Diagram of architecture and training process of the Synthesis task. The Generator G uses T1- and T2-w images to generate syn T2-w fs images. Feedback on the similarity between syn T2-w fs and true T2-w fs is offered by the Discriminator **D** and causes modifications in network weightings until the lass of function to discriminate between both images is minimal

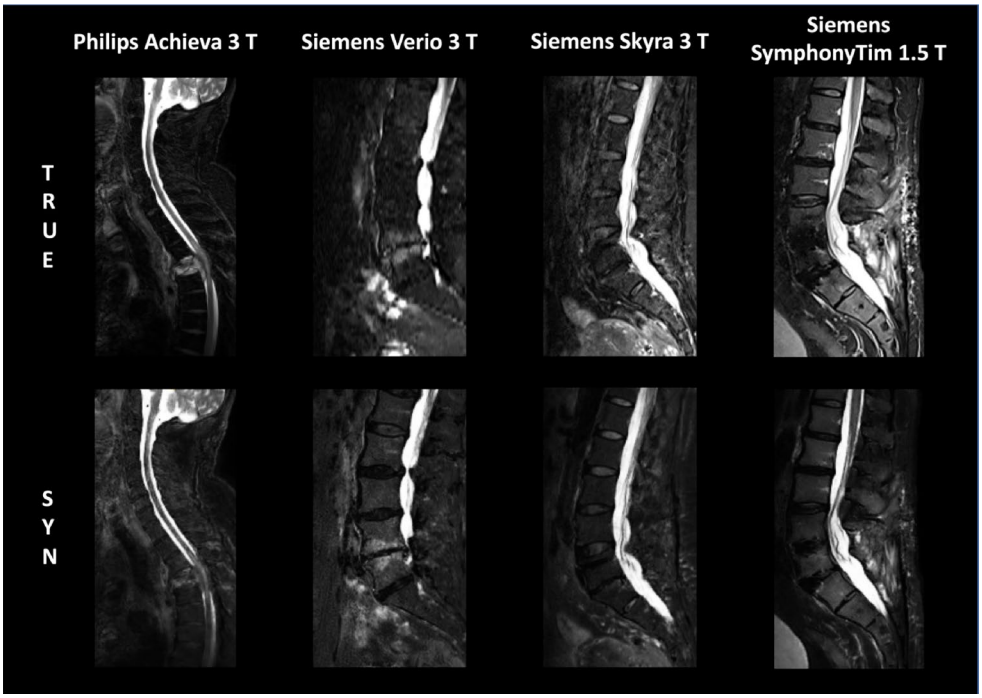

Fig. 2 | 241 Exemplary images of true and syn T2-w fs for different scanner hardware

Pathology	Syn T2-w fs	True T2-w fs
Bone marrow abnormalities	5/54 (9.3 %)	8/51 (15.7 %)
Spondylodiscitis expansion	1/3 (33.3 %)	3/4 (75.0 %)
Juxtadiscal Modic changes	28/66 (42.4 %)	29/68 (42,6 %)
Vertebral fracture	5/21 (23.8 %)	5/16 (31,3 %)
Cord lesions	5/10 (50.0 %)	8/13 (61,5 %)
Paravertebral tissue abnormalities	15/25 (60.0 %)	16/28 (57,1 %)

Fig. 3 | 241 Absolute (and relative) number of abnormalities, in which the syn or true T2-w fs offered additional diagnostic information compared to the rating based on T1- and T2-w images only

Pathology	Cohen's Kappa Syn vs. True T2-w fs	Cohen's Kappa T1-w/T2-w 1. vs. 2. rating
Bone marrow abnormalities	0.76	0.76
Spondylodiscitis expansion	0.85	0.49
Juxtadiscal Modic changes (inflammatory)	0.75	0.70
Vertebral fracture	0.78	0.78
Cord lesions	0.56	0.65
Paravertebral tissue abnormalities	0.79	0.76

Fig. 4 | 241 First column: Cohen's Kappa values for inter-method agreement of true T2-w fs vs. syn T2-w fs for grading of six different pathologies. The pathology grading was based on the combined information of T1-/T2 w and T2 fs images, respectively. Second column: Cohen's Kappa values for intra-rater agreement of first and second pathology rating round based on Tl-w and T2-w images only

advantages are shorter scan protocols and the possibility for a retrospective generation of T2-w fs images from T1- and T2-w images.
Conclusion: Our work underlines the potential of a GAN based syn T2-w fs for MR spine examinations.

References

1. Nie D, Trullo R, Lian J, Petitjean C, Ruan S, Wang Q, et al. Medical image synthesis with context-aware generative adversarial networks. IEEE Trans Biomed Eng. 2018;65(12):2720–30. https://doi.org/10.1109/TBME.2018.2814538.
2. Jakobsson U, Westergren A. Statistical methods for assessing agreement for ordinal data. Scand J Caring Sci. 2005;19:427–31. https://doi.org/10.1111/j.1471-6712.2005.00368.x.

[246] Identifikation stabiler und instabiler intrakranieller Aneurysmen mittels bildbasierter Blutflusssimulation

Daniel Behme[1, 2], Samuel Voß[2, 3], Jana Korte[2, 3], Maximilian Thormann[1], Anastasios Mpotsaris[1], Sylvia Saalfeld[2, 4], Gabor Janiga[3], Philipp Berg[2*, 3]

[1]Klinik für Neuroradiologie, Universitätsklinik Magdeburg, Magdeburg, Deutschland
[2]Forschungscampus STIMULATE, Magdeburg, Deutschland
[3]Department of Fluid Mechanics and Technical Flows, Universität Magdeburg, Magdeburg, Deutschland
[4]Department of Simulation and Graphics, Universität Magdeburg, Magdeburg, Deutschland

Hintergrund: Die Unterscheidung von hämodynamisch stabilen und instabilen Aneurysmen bleibt herausfordernd. Neuere Studien legen nahe, dass intraaneurysmale Fluktuationen des Blutflusses mit hohen Frequenzen existieren könnten. Da diese Flussalterationen das Remodeling der Aneurysmawand beeinflussen könnten, ist das Phänomen der Hochfreuquenz-Fluktuationen von potenziellem Interesse als neuer Biomarker für Aneurysmastabilität.
Methoden: Zur Quantifikation instabiler Hämodynamik wurden zunächst Blutflusssimulationen für ein rupturiertes PICA-Aneurysma, mit angiographisch bekannter Rupturstelle durchgeführt. Neben der Analyse zeitabhängiger Flussalterationen wurden der „shear stress" und die Wirbelbildung analysiert. Darüber hinaus wurde die spektrale Flussentropie mittels orthogonaler Dekomposition untersucht. Abschließend wurden alle Simulationen in einem unrupturierten Media-Aneurysma mit vergleichbaren Größendimensionen wiederholt.
Ergebnisse: Hochauflösende Blutflusssimulation bestätigt die Existenz komplexer Flussmuster, welche zusammen mit Hochfrequenz-Fluktuationen auftreten. Diese treten vorwiegend direkt nach dem Peak des systolischen Einstroms auf und bestehen bis zur Diastole. Die Wall-shear-stress-Verteilung zeigt zudem eine starke Oszillation und

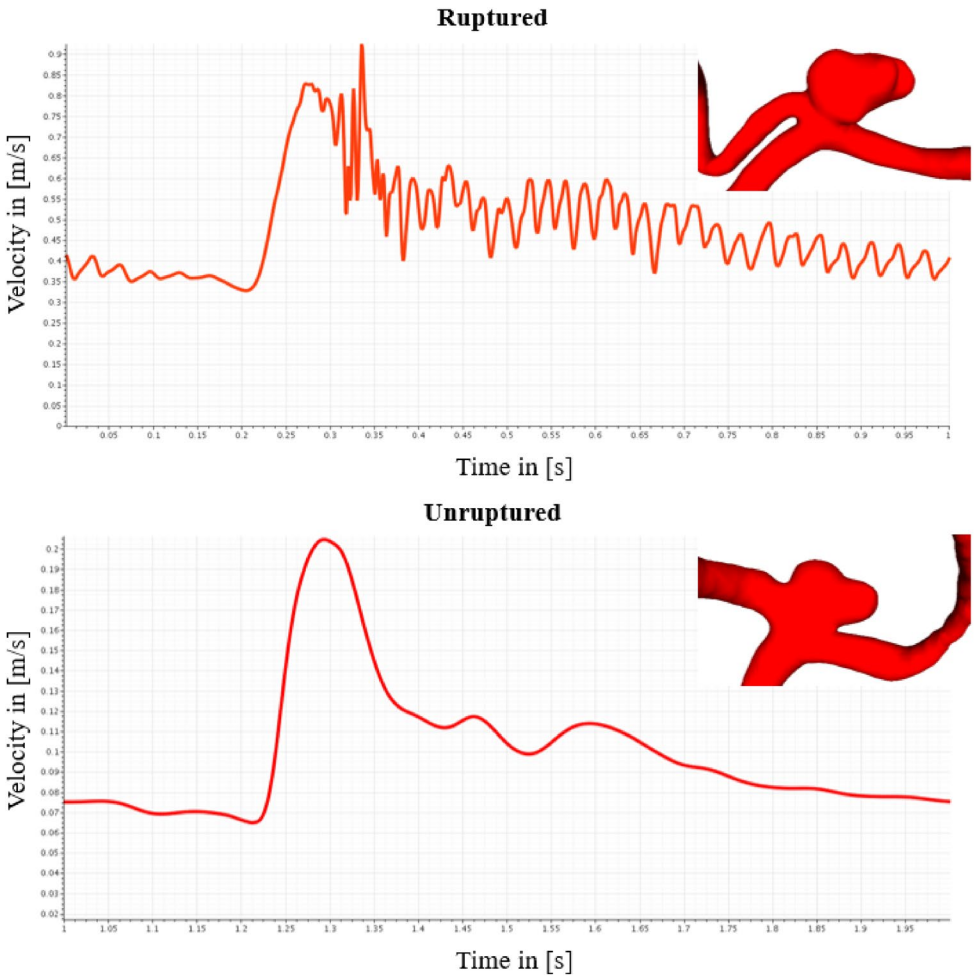

Abb. 1 | 246

die spektrale Flussentropie zeigt einen Wert von 0,76. Diese Beobachtungen konnten im unrupturierten Aneurysma nicht gemacht werden (Entropie von 0,12 – wobei 0 konstanten Fluss repräsentiert).
Diskussion: Multiple Biomarker bestehen für das Rupturrisiko von intrakraniellen Aneurysmen, Hochfrequenz-Fluktuationen könnten ein weiterer, wichtiger Baustein im Risikoassessment von Aneurysmen werden, wie die Analyse unserer Beispiele nahelegt. Eine Validierung ist allerdings an größeren Kohorten notwendig, zudem sollte eine Analyse der Beziehung zu den angrenzenden Gefäßen und deren Blutfluss durchgeführt werden.
Fazit: Hochfrequenz-Fluktuationen des Blutflusses in Aneurysmen existieren und könnten sich als guter Biomarker für Aneurysmastabilität etablieren.

[247] Multiparametrische MRT-Signaturen von Response und Resistenz unter Immuntherapie mit dem Nanopartikel Konjugat CDNP-R848 im experimentellen Gliommodell

Verena Turco[1], Kira Pfleiderer[2], Jessica Hunger[2], Kianush Karimian-Jazi[2], Katharina Schregel[2], Gianluca Brugnara[2], Kristine Jähne[1], Manuel Fischer[2], Theresa Bunse[1], Wolfgang Wick[3], Sabine Heiland[2], Christopher Rodell[4], Philipp Vollmuth[2], Martin Bendszus[2], Michael Breckwoldt[2*], Michael Platten[1]

[1]Klinische Kooperationseinheit Neuroimmunologie und Hirntumorimmunologie, Deutsches Krebsforschungszentrum DKFZ, Deutschland
[2]Abteilung Neuroradiologie, Uniklinik Heidelberg, Deutschland
[3]Abteilung Neurologie, Uniklinik Heidelberg, Heidelberg, Deutschland
[4]School of Biomedical Engineering, Drexel University, Philadelphia, Vereinigte Staaten

Hintergrund: Die Therapieresistenz von Gliomen liegt u. a. am immunsuppressiven Tumormikromileu (TME). Neue immuntherapeutische Ansätze induzieren proinflammatorische Veränderungen in der TME. CDNP-R848 ist ein β-Cyclodextran-Nanopartikel, welcher den Toll-like-Rezeptor (TLR) 7/8 Agonisten, R848 komplexiert. Neue MRT-Ansätze versuchen, eine frühzeitige Vorhersage zwischen Therapieansprechen und -resistenz zu erreichen. Zur Etablierung einer entsprechenden Signatur nutzen wir die multiparametrische MRT (T2, T1 CE, Diffusion, Perfusion), die Phagozyten-spezifische USPIO-Bildgebung und Radiomics-basiertes prädiktives Modeling im experimentellen Gliommodell.
Methoden: Gl261Gliome wurden in C57Bl/6J Mäuse implantiert. Hochfeld-MRTs (9.4T) erfolgten zu Woche 2 (Randomisierung), 3 und 4. Die Response wurde im Verlauf mittels zuvor etablierter Kriterien verfolgt. Die „ultrasmall iron oxide"(USPIO)-Bildgebung erfolgte mit Ferumoxytol i. v. (30 mg/kg, quantifiziert über Multigradienten-Echo [MGE]"). Die radiomische Analyse erfolgte analog zu (Aslan et al., 2020).
Ergebnisse: Unter CDNP-R848 Gabe zeigte sich eine Responserate von 80 % (2,5 % CR, 52,5 % PR und 25 % SD, $n=52$ Mäuse), während unter CDNP Vehikel-Gabe der Tumor exponentiell wuchs

($n=12$). 25 % ($n=8/32$) der Responder-Tiere zeigten eine Pseudoprogression (PsPD). Eine gesteigerte Aufnahme von USPIOs ging mit einer Tumorprogression einher (Δ T2*: –11,7 ms±4,2 vs. –4,0 ms±2,8, $p=0{,}01$, $n=9$). Der USPIO-Uptake war auf den vermehrten Influx von Tumormakrophagen in die TME zurückzuführen (R2: 0,78, $p=0{,}004$). Mittels Radiomics konnte das Ansprechen mit einer Genauigkeit von 84,7 % vorhergesagt werden (Sensitivität: 80,8 %; Spezifität: 86,9 %). Das Top-Radiomic-Merkmal für die Vorhersage des Therapieversagens war der Unterschied in der volumetrischen Kompaktheit zwischen Woche 2 und Woche 3.

Diskussion: Neben der präklinischen Effizienz dieses immuntherapeutischen Ansatzes zeigen wir, dass die USPIO-MRT im Gegensatz zu konventionellen Sequenzen (Perfusion, Diffusion) die CDNP-R848-Wirksamkeit monitorieren kann und dadurch eine Responseprädiktion vor Beginn der Tumorregression möglich ist. Unsere Radiomics-Analyse ist kohärent mit unseren früheren Analysen unter

Abb. 1 | 247

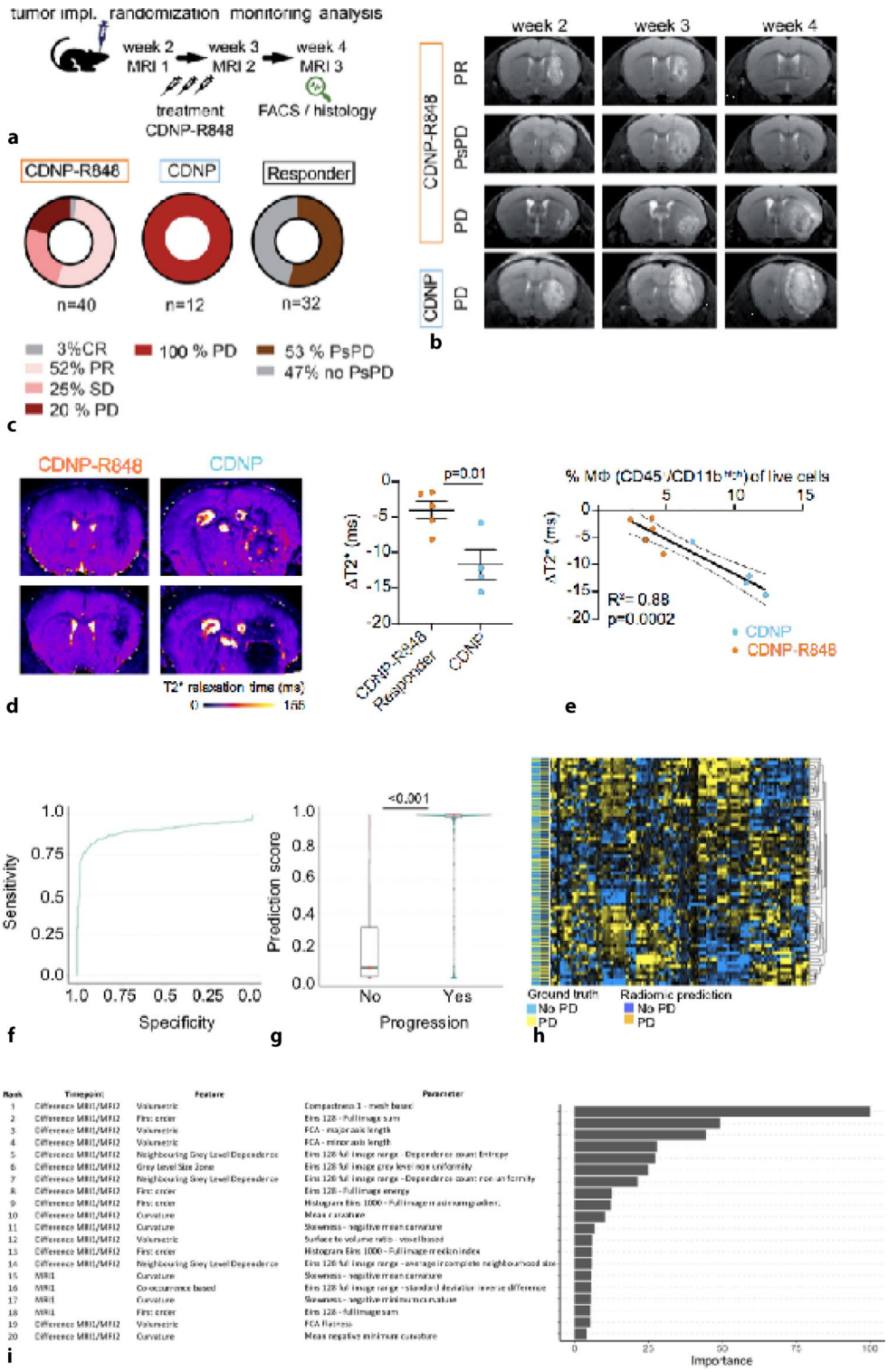

Checkpoint-Blockade. Somit scheint die Entwicklung einer therapieunabhängigen radiomischen Signatur für das Therapieansprechen möglich.
Fazit: Dieser Ansatz ermöglicht die zelluläre Visualisierung und Analyse von Veränderungen der TME durch multiparametrische MRT.

[250] Noninvasive perfusion territory mapping and time-resolved angiography by ASL is clinically applicable in cerebrovascular diseases

Jens Göttler[1*], Hans Liebl[1], Miriam Reichert[1], Moritz Hernandez Petzsche[1], Maria Berndt[1], Kim van de Ven[2], Christine Preibisch[1], Jan Kirschke[1], Makoto Obara[3], Michael Helle[4], Claus Zimmer[1], Nico Sollmann[1, 5], Stephan Kaczmarz[1]

[1]Department of Neuroradiology, Technical University of Munich (TUM), München, Germany
[2]Philips Healthcare, Best, The Netherlands
[3]Philips Japan, Tokyo, Japan
[4]University Hospital Schleswig-Holstein Campus Kiel, Kiel, Germany
[5]Department of Radiology, University Ulm Medical Center, Ulm, Germany

Background: Collateralization status in cerebrovascular diseases (CVD) is crucial to assess stroke risk. Recently, two noninvasive imaging tools based on arterial spin labeling (ASL) have been proposed to depict collateral flow: 4D-sPack [1] enables time-resolved angiography and super-selective ASL (ss-ASL) [2] maps individual perfusion territories. Here we assessed their clinical feasibility in combination with a novel automated vessel planning tool [3] in patients with different CVDs and healthy controls (HC) in comparison with digital subtraction angiography (DSA) and perfusion weighted imaging.
Methods: A total of 14 CVD patients, including 10 with arteriovenous malformations, 3 with moyamoya and 1 with internal carotid artery (ICA) dissection, and 10 HCs (Table 1) underwent MRI on 3T Philips scanners. Sequence parameters are summarized in Fig. 1. Labeling positions of ss-ASL and 4D-sPack were set automatically [3]. In selected patients, intracranial DSA was obtained.
Results: The automated planning tool successfully identified labeling positions in 20/20 HC and 26/29 CVD patients (Fig. 5). Two of three failed attempts were caused by motion, the third was the dissected ICA (Fig. 2). Collateral flow patterns in patients were reliably depicted by ss-ASL and 4D-sPack (Fig. 2 and 3). Comparisons of 4D-sPack with DSA showed excellent spatial correspondence even for distal contralateral collaterals (Fig. 4).
Discussion: 4D-sPack and ss-ASL were successfully applied in CVD patients and HC, highly facilitated by the automated labeling tool. Rare labeling failures were associated with motion and vessel disease. 4D-sPack angiography was comparable to DSA and may be a diagnostic substitute in some cases. Ss-ASL could spatially localize shifted vascular territories and border zones explaining regional perfusion delays.
Conclusion: Noninvasive vascular territory mapping and time-resolved angiography based on super-selective ASL combined with automated planning is clinically applicable and can assess collateralization status in a number of CVDs. Thus, it may guide revascularization therapy in the future.

References

1. Obara; ISMRM2018,#185
2. Helle, et al. MRM. 2010;64(3):777–86.
3. Helle et al.; ISMRM2018,#302

[252] Safety profile and complication rates in emergency off-label use of tirofiban in interventional neuroradiology: an observational study

Sebastian Altmann[1*], Daniel Dillinger[1], Anastasios Mpotsaris[2], Annette Spreer[3], Stephan Waldeck[4], Ahmed Othman[1], Florian Ringel[5], Thomas Kerz[5], Marc A. Brockmann[1], Carolin Brockmann[1]

[1]Universitätsmedizin Mainz, Klinik und Poliklinik für Neuroradiologie, Mainz, Germany
[2]Universitätsklinikum Magdeburg A. ö. R., Universitätsklinik für Neuroradiologie, Magdeburg, Germany
[3]Städtisches Klinikum Braunschweig gGmbH, Neurologische Klinik, Braunschweig, Germany
[4]Bundeswehrzentralkrankenhaus Koblenz, Klinik VIII–Radiologie und Neuroradiologie, Koblenz, Germany
[5]Universitätsmedizin Mainz, Neurochirurgische Klinik und Poliklinik, Mainz, Germany

Background: Tirofiban is approved for treatment of acute coronary syndrome. Meanwhile, however, tirofiban is frequently applied in various emergency situations in INR despite contraindications (CI). This study aimed at evaluating the safety profile of tirofiban when used off-label in patients with CI.
Methods: Data of 86 patients undergoing neurointerventional therapy and being treated with tirofiban in two neuroendovascular centres between January 2016 and July 2017 were retrospectively analysed: $n=18$ without CI and 67 with off-label use due to one or more CI, such as recent stroke (<30 days; $n=45$), recent haemorrhage, thrombocytopenia (<150.000/microl; $n=6$), aPTT>1.3-fold, INR<1.5 ($n=15$), severe liver or renal insufficiency (Child-Pugh C; $n=2$), and preceding intravenous thrombolysis ($n=28$). Haemorrhage between the beginning and up to 10 h after infusion of tirofiban was considered tirofiban-related (incl. gastrointestinal bleedings and macrohematuria). CI and treatment were evaluated using subgroup and multivariate analysis.

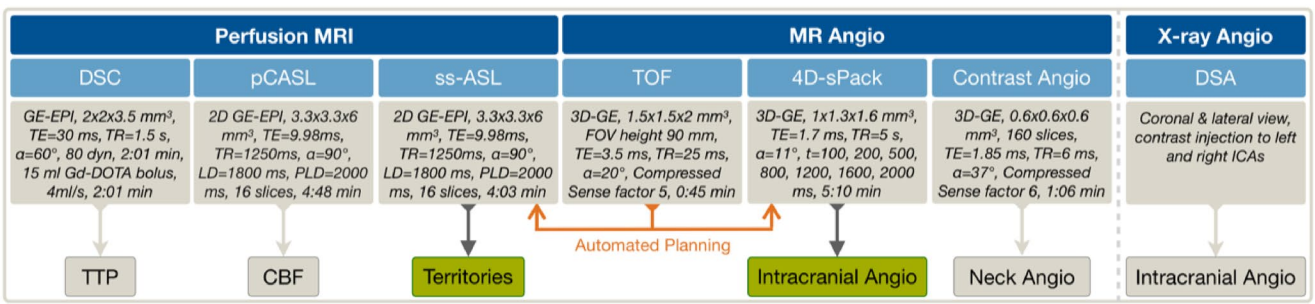

Fig. 1 | 250 Imaging protocol and derived parameters. Dynamic susceptibility contrast (DSC) MRI was applied to derive time-to-peak (TTP) maps, pseudo-continuous arterial spin labeling (pCASL) for cerebral blood flow (CBF), super-selective ASL (ss-ASL) for perfusion territories and 4D-sPack for timeresolved intracranial angiography. Vessel-selective labeling was repeated for each brain feeding artery (*green*) and automatically planned (*orange*) using time-of-flight (TOF). For comparisons, MR neckangiography and digital subtraction angiography (DSA) were applied

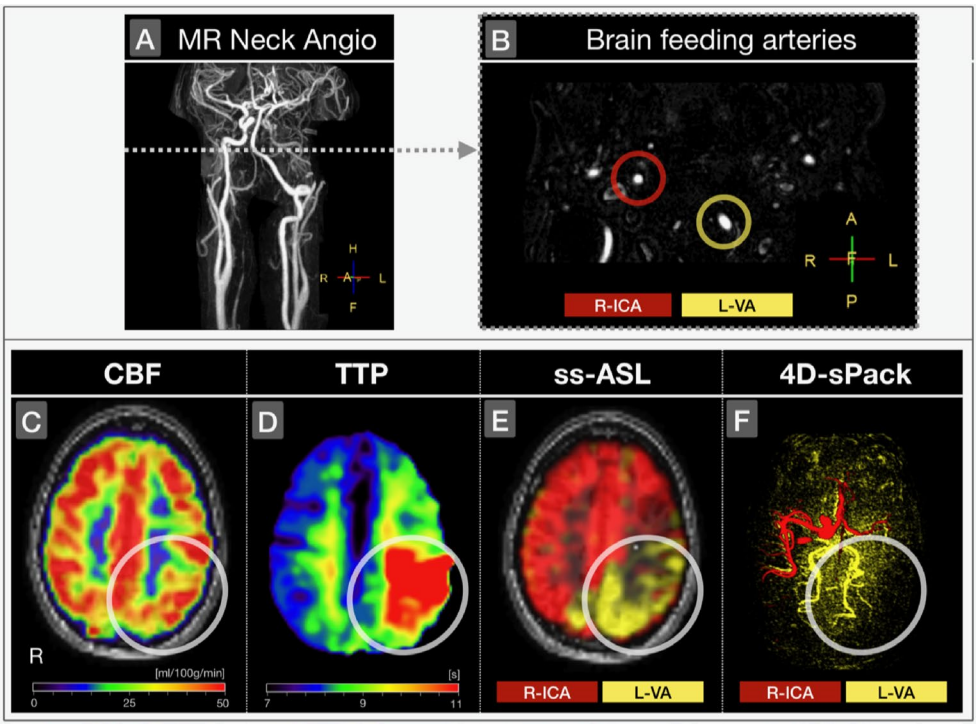

Fig. 2 | 250 Perfusion and angiography in a patient with left-sided ICA (L-ICA) dissection and ipsilateral M1 occlusion. Conventional MR neck angiography (A and B) shows occlusion of the L-ICA. Brain perfusion is mainly preserved by the right-sided ICA (R-ICA, *red circle* in B) and left-sided vertebral artery (L-VA, *yellow circle* in B); the R-VA is hypoplastic. There is slightly decreased CBF (*circle*, C) and substantially prolonged TTP (*circle*, D) in the left parietal border zone. Ss-ASL reveals that the left middle cerebral artery territory is collateralized via the L-VA and R-ICA and that the region with prolonged TTP is mainly supplied by the L-VA (*circle*, E). Accordingly, 4D-sPack demonstrates that the L-VA supplies the posterior parts of the left brain regions (*circle*, F), while RICA supplies the left anterior and proximal middle cerebral arteries

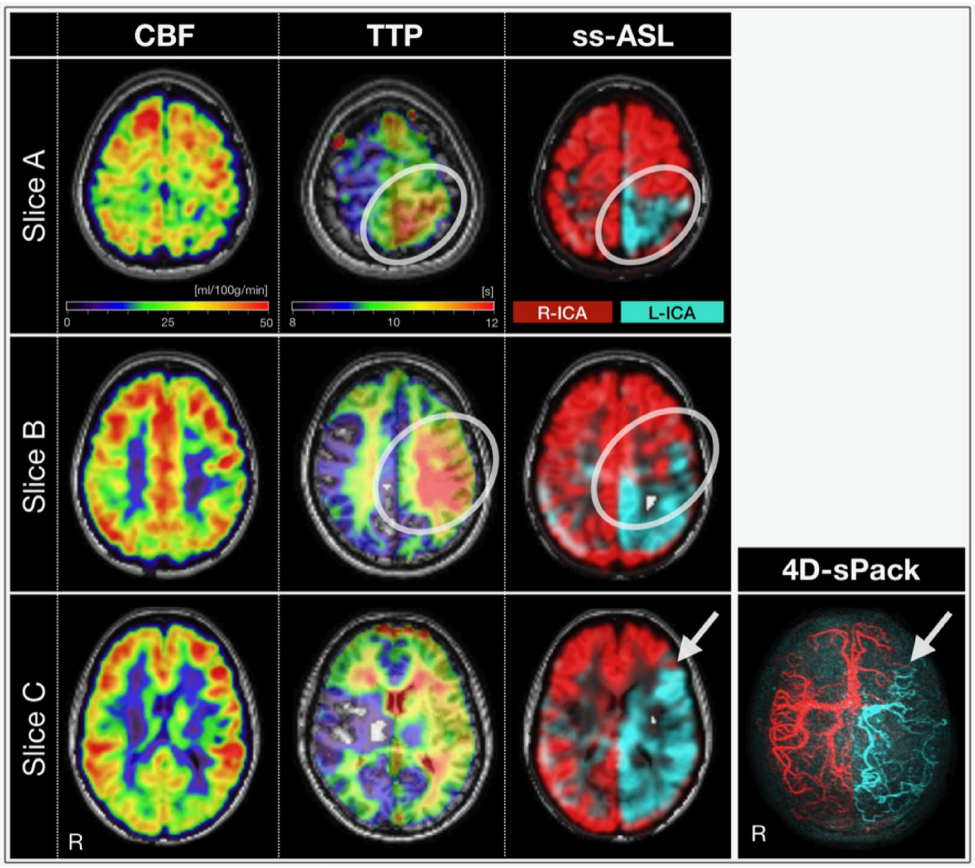

Fig. 3 | 250 Perfusion in a patient with moyamoya disease. Cerebral blood flow (CBF), time-to-peak (TTP) and both ICA territories visualized by ss-ASL (*red* & *cyan*) are compared in three axial slices (A,B,C). White no severe hypoperfusion is apparent, the R-ICA territory is shifted contralaterally and supplies the left anterior cerebral artery. The perfusion delay is severely prolonged in the left hemisphere were territories of L-ICA and R-ICA meet (*circles*). Note the excellent spatial correspondence of non-invasive perfusion territory mapping and angiography by 4D-sPack (*arrows*; see Fig. 4 for time-resolved results)

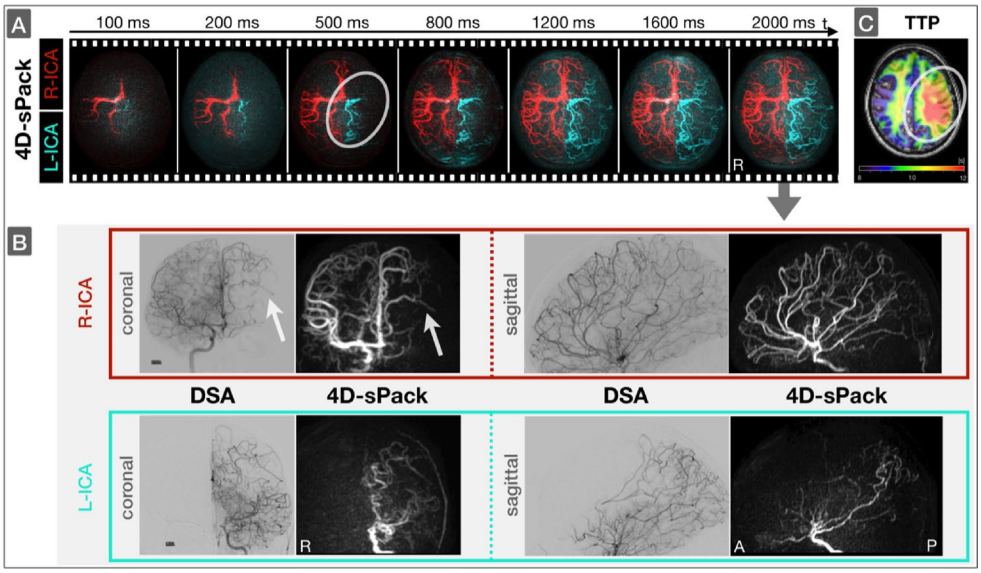

Fig. 4 | 250 Angiography of a patient with moyamoya disease. (A) Non-invasive time resolved angiography by 4D-sPack of R-ICA (*red*) and L-ICA (*cyan*) are shown in axial view with maximum intensity projections (*top row*). Note that delayed filling of the left middle cerebral artery is in agreement with delayed perfusion depicted by elevated time-to-peak (TTP) (*circles*). (B) The noninvasive angiogram at t = 2000 ms is compared to conventional DSA in the same patient in coronal and sagittal view for R-ICA and L-ICA, respectively. Note, 4D-sPack can even depict small pial collaterals originating from R-ICA in agreement with DSA (*arrows*)

Group	Number of participants	Number of female participants	Age	Success rate of automated labelings
Young Healthy Controls	10	3	24.3±0.9 y	20/20
AVM	10	3	39.6±21.6 y	18/20*
Moyamoya	3	3	35.0±2.6 y	6/6
ICA Dissection	1	0	36 y	2/3**

Fig. 5 | 250 Study cohort and success rate of labeling. The study included young healthy controls and patients with arteriovenous malformations (AVM), moyamoya disease and an unilateral internal carotid artery (ICA) dissection. The number of female participants and average age with standard deviation is given for each group. Automated labeling of both ICAs and a vertebral artery (VA) was successful for most participants, but failed twice in the same AVM patient because of severe motion (see *asterisk*) and for a dissected ICA of another patient (*double asterisk*, see Fig. 2)

Results: Tirofiban effectively prevented thrombotic events in 81/86 patients (94.2 %). Relevant tirofiban-associated complications occurred in 14 patients (16.3 %), of which nine received IV thrombolysis. Twelve of 86 patients died, while the overall tirofiban-related mortality was 2.3 % (two patients with ICH). Overall, we could show no significant differences for tirofiban-related complication between the control group and Patients with CI. Multivariate analysis revealed age as the only parameter significantly associated with development of tirofiban-associated complications ($p = 0.026$).
Discussion: Off-label use of tirofiban in INR is feasible at a low rate of adverse events. Highest risk for relevant tirofiban-associated complications is observed in older patients treated by emergency stent-PTA for acute stroke and thus requires even more precise benefit-risk assessment.

[256] Ausprägung von Zeichen einer idiopathischen intrakraniellen Hypertension in der MRT bei Adipositas

Schekeb Aludin[1], Sönke Peters[1], Julia Juhasz[1], Olav Jansen[1], Matthias Laudes[2], Lars-Patrick Schmill[1*]

[1]Klinik für Radiologie und Neuroradiologie, Universitätsklinikum Schleswig-Holstein, Campus Kiel, Kiel, Deutschland
[2]Klinik für Innere Medizin I, Universitätsklinikum Schleswig-Holstein, Campus Kiel, Abteilung für Endokrinologie, Diabetologie und klinische Ernährungsmedizin, Kiel, Deutschland

Hintergrund: Die idiopathische intrakranielle Hypertension (IIH) tritt insbesondere bei jungen, adipösen Frauen im gebärfähigen Alter auf. Entsprechend der häufigen Koinzidenz besteht der Verdacht darauf, dass Adipositas einen Risikofaktor für IIH darstellt. Da die Adipositas in der Bevölkerung zunehmende epidemiologische Relevanz erfährt, kann angenommen werden, dass ebenfalls die Inzidenz der IIH künftig zunehmen wird. In dieser Studie soll das Auftreten typischer MR-Zeichen der IIH bei Personen mit einem BMI>30 kg/m^2 gegenüber normalgewichtigen Personen verglichen werden.
Methoden: Zerebrale MRT von 85 Teilnehmern (53 Teilnehmer mit BMI<30; 50,75 ± 10,24 Jahre; 32 Teilnehmer BMI>30; 48,97 ± 10,28 Jahre) der Food-Chain-Plus-Kohorte (FoCus) wurden retrospektiv hinsichtlich typischer MR-Zeichen der IIH untersucht. Drei verblindete Radiologen mit unterschiedlichem Erfahrungsniveau quantifizierten dabei drei MR-Hauptzeichen: (1) Stenosierung des Sinus transversus, (2) Höhenminderung der Hypophyse und (3) Erweiterung der Sehnervenscheide. Neben der Quantifizierung wurden die drei MR-Zeichen mit einem neu konzipierten Score bewertet und zwischen den Gruppen verglichen.
Ergebnisse: Adipöse Personen weisen im Vergleich zu den normalgewichtigen einen signifikant höheren Score der Hauptzeichen auf ($p = 0{,}0006$). Ebenso der quantitative Vergleich der einzelnen Hauptzeichen ergab bei adipösen Personen ein signifikant häufigeres und ausgeprägteres Auftreten von Stenosen des Sinus transversus ($p < 0{,}0005$), einer Erweiterung der Sehnervenscheide ($p < 0{,}05$) und einer Höhenminderung der Hypophyse ($p < 0{,}05$). Weiterhin bestehen signifikante Korrelationen zwischen der Ausprägung der Hauptzeichen und dem BMI der Patienten ($p < 0{,}05$).
Diskussion: Adipöse Personen weisen gegenüber normalgewichtigen signifikant häufiger zerebrale MR-Zeichen der IIH auf, was die Rolle der Adipositas als Risikofaktor für die IIH unterstützt. Es ist zu evaluieren, ob lediglich ein erhöhter intraabdomineller Druck zu einem verminderten zerebralvenösen Abfluss und hierüber zu einem erhöhten intrakraniellen Druck führt oder ob auch andere Faktoren wie Veränderungen der hormonellen Achsen eine Verstärkung von Adipositas und IIH bedingen.
Fazit: Adipositas ist mit der Ausprägung von Zeichen einer IIH im MRT assoziiert, was verstärkt auf ihre Rolle in der Pathophysiologie der IIH hinweist. Den genauen Pathomechanismus gilt es in zukünftigen Studien weiterhin zu klären.

[265] Fluid-structure interaction for the simulation of intracranial aneurysm after endovascular flow diverter stent implantation

Elie Hachem[1*], Aurelien Larcher[1], Nemer Ramy[1], Augusto Fava Sanches[2], Yigit Özpeynirci[2], Thomas Liebig[2], Meliga Philippe[1]

[1]PSL Mines ParisTech, CFL Research Group at CEMEF, Sophia Antipolis, France
[2]Institute of Neuroradiology, University Hospital LMU, Munich, Germany

Background: Modeling the flow in intracranial aneurysms after flow diverter stent implantation is of particular interest to understand the relationship between treatment outcomes and the induced flow and hemodynamics modifications. In practice, however, the high-fidelity simulation of such complex systems remains especially challenging due to the need to realistically deploy the stent in patient-specific vascular models, adequately mesh and resolve the thin wires and gaps between the stent and the vascular wall, and account for vessel wall deformations via relevant fluid-structure interaction (FSI) modeling.
Methods: A novel FSI computational framework based on the Adaptive Immersed Mesh (AIM) method is proposed for the simulation of stented intracranial aneurysms. It combines a finite element solid dynamics solver and a fully Eulerian fluid-solid framework. The Navier-Stokes equations with non-Newtonian blood rheology and hyperelastic solid dynamics equations (valid for compressible/incompressible material) are solved with the Variational Multi Scale (VMS) method, to stabilize the advection dominated regime for the flow problem and damp out spurious pressure oscillations for the solid problem. The approach accurately describes the mechanical exchanges between the blood flow, the vessel wall and the stent, without requiring body-conforming meshes around the stent wires and their contacts with the wall.
Results: Results obtained from a patient-specific model of unruptured aneurysm (including inflow conditions measured by phase contrast magnetic resonance imaging) show that the sac significantly deforms under the action of the hemodynamic forces. The aspect ratio increases by up to 10 % at peak systole, and the wall shear stress (commonly used to assess the risk of rupture) decreases by 20 % with respect to rigid wall modeling.
Conclusion: The results assess the relevance of FSI modeling for intracranial aneurysm hemodynamics prediction, but must be confirmed with large sample sizes. We also plan to push forward the method using patient-specific wall thickness and locally tunable stress-strain relations (to account for the abrupt change in tissue structure between the parent vessel and the sac).

[266] Long-term outcomes of wide-necked intracranial bifurcation aneurysms treated with stent-assisted coiling using low-profile Acandis Acclino stents

Katharina Melber[1*], Dominik Grieb[1], Frederik Boxberg[1], Martin Schlunz-Hendann[1], Friedhelm Brassel[1]

[1]Sana Kliniken Duisburg, Duisburg, Germany

Background: Little data exists on endovascular treatment of intracranial aneurysms with the Acandis Acclino low-profile self-expanding closed-cell stent systems and is mainly limited to short- or midterm results. We report our long-term experience with the Acandis Acclino stent systems in the treatment of complex intracranial aneurysms.
Methods: A total of 64 aneurysms were treated electively using 91 Acclino stents. Single stent-assisted coiling was the preferred treatment in 40 and the kissing-Y stenting technique in 24 cases. We analyzed demographic data and long-term results.
Results: All stents were successfully deployed with immediate complete (RROC I) or near complete (RROC II) occlusion achieved in 92,2 %. Follow-up was available in 57 cases (89,1 %) with a mean follow-up of 37 months (range: 6–80 months). Long-term RROC I or II was achieved in 49 cases (86 %). Eight residual aneurysms (14 % RROC III) were noted (4 cases of stable residual aneurysmal filling and 4 of aneurysmal recanalization). Two of those recurrent aneurysms were retreated by coilembolization. The directly procedural-related complication rate was 4,7 %, including one death. Seven cases of in-stent-stenosis (12,3 %; morbidity $n=0$) were detected on follow-up with 6 of them when using the kissing-Y stenting technique.
Discussion: Our high long-term follow-up occlusion rates and overall in-stent stenosis rate are comparable to short- and midterm results of other low-profile stents. However, we detected a noteworthy number of clinically silent in-stent stenosis when using the kissing-Y stenting technique, possibly attributable to the stent configuration. Our data included long term follow-up of the latest Acclino stent generation also associated with low-complication and aneurysmal recurrence rates.
Conclusion: Endovascular treatment of various complex intracranial aneurysms using the Acandis Acclino stent systems is safe and efficient with high aneurysm occlusion rates combined with low complication rates at long-term follow-up. Overall, rates of in-stent-stenosis are low but seem to depend on the treatment technique (single stent-assisted vs. kissing-Y stenting with coiling).

References

1. Brassel F, et al. Endovascular treatment of complex intracranial aneurysms using Acandis Acclino stents. J Neurointerv Surg. 2017;9(9):854–9.
2. Goertz L, et al. Low-Profile Laser-Cut Stents for Endovascular Treatment of Intracranial Aneurysms: Incidence, Clinical Presentation and Risk Factors of Thromboembolic Events. Clin Neuroradiol. 2021;31(1):107–15.

[267] Mechanical thrombectomy for basilar artery occlusion stroke: analysis of the German Stroke Registry-Endovascular Treatment (GSR-ET)

Katharina Feil[1], Maria Berndt[2*], Silke Wunderlich[3], Christian Maegerlein[2], Kathleen Bernkopf[3], Moriz Herzberg[4], Manuel Lehm[2], Steffen Tiedt[5], Clemens Küpper[6], Johannes Wischmann[6], Sonja Schönecker[6], Konstantin Dimitriadis[5], Thomas Liebig[4], Marianne Dieterich[6], Claus Zimmer[2], Lars Kellert[6], Tobias Boeckh-Behrens[2]

[1]Department of Neurology and Stroke, Eberhard-Karls University Tübingen, Germany
[2]Department of Diagnostic and Interventional Neuroradiology, Klinikum rechts der Isar, School of Medicine, Technical University of Munich, Germany
[3]Department of Neurology, Klinikum rechts der Isar, School of Medicine, Technical University of Munich, Germany
[4]Institute of Neuroradiology, Ludwig-Maximilians-University Munich, Germany
[5]Institute for Stroke and Dementia Research (ISD), Ludwig-Maximilians-University Munich, Germany
[6]Department of Neurology, Ludwig-Maximilians-University Munich, Germany

Background: Stroke due to basilar artery occlusion (BAO) causes the most severe strokes with poor prognosis. Data regarding efficacy of mechanical thrombectomy (MT) in BAO are sparse.
Methods: Patients enrolled between 06/2015 and 12/2019 in the German Stroke Registry-Endovascular Treatment (GSR-ET) were analyzed. The GSR-ET is an independent, prospective, multicenter, observational registry with 25 participating stroke centers in Germany enrolling patients treated with MT. Primary outcomes were successful reperfusion (mTICI score of 2b-3) and good functional outcome at 3 months (mRS of 0–2).
Results: A total of 640 (9.6 %) of the 6635 patients in the GSR were strokes due to BAO. Successful reperfusion was observed in 86.6 %. At 3 months' follow-up, 31 % of patients showed a good function-

Fig. 1 | 267 Shift analysis of clinical outcome (mRS (modified Rankin Score) at three months follow-up) in BAO patients. CHnicol outcome in all BAO-patients is displayed in (**a**). In (**b**), mRS values are compared between the subgroups of successful anglographic outcome (good reperfusion (mTICI 2b) versus complete reperfusion3))

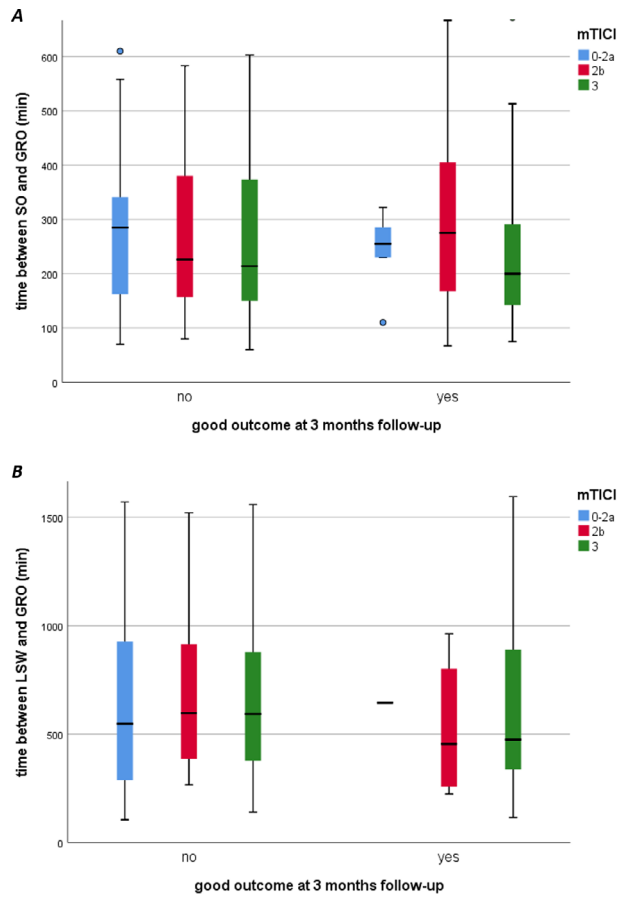

Fig. 2 | 267 Distribution of time values (in minutes) between SO (Symptom onset, in **a**)/LSW (last seen well, in **b**) and GRO (groin puncture) for outcome groups (good clinical outcome is defined as mRS (modified Rankin Scale) of 0-2 at three months follow-up). A further division into angiographic outcome groups (m77Cl 0-2a, 2b and 3) was made. No significant differences were observed

al outcome, mortality was 39 %. Analysis of mTICI3 vs. mTICI2b showed considerable better outcomes (good outcome in 38.9 % vs. 24.4 % $p=0.005$; Fig. 1). Strongest predictor for good functional outcome were IVT treatment (OR 3.04, 95 % CI 1.76–5.23) and successful reperfusion (OR 4.92, 95 % CI 1.15–21.11), while the effect of the time between symptom onset and start of reperfusion seems to be low (Fig. 2).

Discussion: Acute reperfusion strategies of BAO are common in daily practice and can be performed safely with high rates of successful reperfusion. Our data suggest that successful, and especially complete reperfusion predicts good outcome, while the time since symptom onset has a low impact.

Conclusion: The study reinforces the importance of reperfusion success in acute BAO. Future clinical trials should address acute reperfusion strategies of BAO patients.

[269] Endovaskuläre Schlaganfallversorgung auf dem Lande – liefert der „flying/driving doctor" hier eine vergleichbare technische Qualität wie im Zentrum?

Christian Maegerlein[1*], Alexander Kettner[2], Claus Zimmer[2]

[1]Klinikum rechts der Isar der Technischen Universität München, Abteilung für Neuroradiologie, München, Deutschland
[2]Klinikum rechts der Isar der Technischen Universität München, München, Deutschland

Hintergrund: Das klinische Outcome von Schlaganfallpatienten mit großem Gefäßverschluss (LVO) ist zu einem wesentlichen Ausmaß abhängig von der Onset-to-groin-Zeit. Falls die MT exklusiv an überregionalen Schlaganfallzentren (CSC) angeboten werden kann, verzögert sich die Therapie für Patienten im ländlichen Raum potenziell erheblich, da die Patienten erst sekundär in ein CSC verlegt werden müssen. Durch Flying- oder Driving-doctor-Konzepte kann die MT auch Patienten im PSC angeboten werden. Dort müssen die Eingriffe jedoch unter technisch und personell potenziell erschwerten Bedingungen durchgeführt werden. Ob sich diese besonderen Umstände negativ auf das technisch-prozedurale Ergebnis auswirken, soll in dieser Studie untersucht werden.

Methoden: Zwischen 2/2018 und 10/2020 wurden 100 Patienten mit LVO durch einen Neuroradiologen (CM) im Rahmen eines Flying-doctor-Konzeptes behandelt. Im gleichen Zeitraum wurden von dem-

selben Arzt (CM) 138 Patienten im CSC mittels MT behandelt. Die beiden Gruppen wurden hinsichtlich technisch-prozeduraler Parameter miteinander verglichen.
Ergebnisse: Eine erfolgreiche Reperfusion des Verschlusses (mTICI≥2b) wurde beim Flying-doctor-Konzept in 95,0 %, im CSC bei 94,5 % (p=0,728) erreicht. Komplikationen traten in der FIT-Gruppe in 3,0 %, im CSC in 1,6 % auf (p=0,473). Die Onset-to-groin-Zeiten lagen beim Flying-doctor-Konzept im Median bei 234 min, bei den im CSC behandelten Patienten bei 231 min (p=0,275).
Schlussfolgerung: Das Flying-doctor-Konzept stellt beim akuten Schlaganfall ein alternatives Versorgungskonzept dar, welches die MT mit der gleichen technischen Qualität und Sicherheit im PSC verglichen zum CSC gewährleisten kann.

[270] Diagnostic performance of ultra-high-resolution CT angiography for the detection of angiographically proven intracranial aneurysms: comparison with normal-resolution CT angiography

Marius Frenzel[1*], Sebastian Altmann[1], Oliver Korczynski[1], Marc A. Brockmann[1], Sebastian R. Reder[1], Carolin Brockmann[1], Ahmed Othman[1]

[1]Universitätsmedizin der Johannes Gutenberg-Universität Mainz, Klinik und Poliklinik für Neuroradiologie, Mainz, Germany

Purpose: Ultra-high-resolution CT angiography (UHR-CTA) is a newly developed technology and may increase the detectability of small abnormalities. We aimed to compare image quality and diagnostic accuracy of UHR-CTA and normal-resolution CT angiography (NR-CTA) for detection of intracranial aneurysms.
Methods: A total of 62 patients (age 58.2 years; 24.5–87.7 years; F=38, M=24) who underwent CT angiography and cerebral DSA for suspected aneurysmatic subarachnoid hemorrhage (aSAH) were included in this study. 32 patients underwent NR-CTA (Toshiba Aquillion 32; detector element size: 0.5 mm; matrix: 512), and 30 patients underwent UHR-CTA (Canon Aquillion Precision; detector element size: 0.25 mm; matrix: 1024). Image quality, sharpness, noise, contrast and diagnostic confidence were evaluated for CTA datasets by two neuroradiologists on a 4-point Likert-scale. Readers assessed also CTA-datasets for presence and localization of intracranial aneurysms. An interventional neuroradiologist assessed DSA datasets for presence and localization of intracranial aneurysms. Diagnostic accuracy for CTA was calculated with DSA serving as reference standard. Comparative analyses of UHR-CTA and NR-CTA were then performed.
Results: UHR-CTA revealed significantly superior overall image quality, sharpness, noise, contrast and diagnostic confidence as compared to NR-CTA (p<0.001). DSA revealed 53 aneurysms in 43 of the 62 included patients (20 patients with NR-CTA; 23 patients with UHR-CTA). UHR-CTA categorized patients correctly, identified all positive patients (patient-based sensitivity=1; specificity=1) and enabled the detection of 25 of 27 angiographically proven intracranial aneurysms (segment-based sensitivity=0.963). On the other hand, on NR-CTA 6 patients were misclassified as negative; 1 patient was misclassified as positive (patient-based sensitivity=0.700; specificity=0.917) and 15 of 26 angiographically proven aneurysms were detected (segment-based sensitivity=0.577). Comparative analysis revealed significantly higher diagnostic accuracy for UHR-CTA as compared to NR-CTA (p<0.01).
Discussion: Compared to NR-CTA, UHR-CTA has superior image quality and remarkably enhances diagnostic accuracy for the detection of angiographically proven intracranial aneurysms in patients with suspected aSAH.
Conclusion: UHR-CTA enhances the detection of intracranial aneurysms in patients with suspected aSAH.

[271] Preoperative IDH mutation prediction in glioma using 2-Hydroxyglutarate magnetic resonance spectroscopy

Tareq A. Juratli[1*], Amir Zolal[1], Mirko Peitzsch[2], Graeme Eisenhofer[2], Gabriele Schackert[1], Jennifer Linn[3], Annett Werner[3]

[1]Universitätsklinikum Carl Gustav Carus, Klinik und Poliklinik für Neurochirurgie, Dresden, Germany
[2]Universitätsklinikum Carl Gustav Carus, Institut für Klinische Chemie und Laboratoriumsmedizin, Labor Klinische Neurochemie, Dresden, Germany
[3]Universitätsklinikum Carl Gustav Carus, Institut und Poliklinik für Diagnostische und Interventionelle Neuroradiologie, Dresden, Germany

Background: Noninvasive and accurate diagnostic techniques to detect isocitrate dehydrogenase (*IDH*) mutant glioma have great potential in routine clinical practice. To date, only a few centers worldwide were able to establish 2HG detection by magnetic resonance spectroscopy (MRS) in glioma. Here, we report on the results of 2-Hydroxyglutarate (2HG) single-voxel spectroscopy (SVS) in a large glioma patient's cohort.
Methods: A total of 72 glioma patients were prospectively investigated using point-resolved spectroscopy at 3 T in parallel with standard clinical magnetic resonance imaging and assessment. The *IDH1/2* mutation status was determined using next generation sequencing or/and immunohistochemistry in the glioma tissue. In addition, in a subset of patients (n=8), 2HG concentrations were measured in the tissue by liquid chromatography-tandem mass spectrometry (LCMS).
Results: Only cases with histologic confirmation were included in the analysis (n=50). The cohort persisted of 36 *IDH* mutant gliomas (17 astrocytomas, 13 oligodendrogliomas and 6 glioblastomas), 8 *IDH* wild-type glioblastomas, three radiation-associated necrosis and three other pathologies. All patients underwent a histologic tumor conformation with consecutive *IDH* mutation assessment. The 2HG concentration in the spectroscopy varied between 0.45 and 6.9 mM. *IDH* mutations were correctly predicted with 90.5 % sensitivity and 70.6 % specificity. The test accuracy was 84.7 %. Three out of five false positive cases and two out of four false negative cases were observed during the early period of establishing the study protocol. Importantly, all cases with a radiation-associated necrosis in *IDH* mutant gliomas were predicted correctly
Discussion: Our findings suggest that 2HG spectroscopy is a reliable and reproducible method in *IDH* mutation prediction in gliomas, from indolent disease through post-treatment follow-up. We envision that 2HG MRS can be used as a biomarker for clinical trials in glioma.

[272] Diagnostic value of water and fat Dixon reconstructions and CT-like images extracted from a single ultra-short echo time sequence for the evaluation of vertebral fractures and degenerative changes of the spine

Georg Constantin Feuerriegel[1*], Sophia Kronthaler[1], Christof Boehm[1], Yannik Leonhardt[1], Martin Renz[2], Kilian Weiss[1], Thomas Liebig[3], Dimitrios Karampinos[1], Claus Zimmer[2], Marcus Makowski[1], Benedikt Schwaiger[2], Alexandra Sophia Gersing[1 3]

[1]Klinikum rechts der Isar der Technischen Universität München, Institut für diagnostische und interventionelle Radiologie, München, Germany
[2]Klinikum rechts der Isar der Technischen Universität München, Institut für Neuroradiologie, München, Germany
[3]LMU Klinikum, Institut für Neuroradiologie, München, Germany

Background: The aim of this study was to evaluate whether vertebral fractures including fracture age and morphology as well as degenerative bone changes of the spine can be accurately assessed on water and fat single echo Dixon reconstructions and computed tomography

Fig. 1 | 272 **a**, **c** STIR and T1w sequences with bone marrow edema of an acute fracture. **b**, **d** UTE derived water and fat-only Dixon sequences showing an edema equivalent

(CT)-like images extracted from a single echo ultra-short echo time sequence (UTE) compared to conventional CT and MR sequences.
Methods: CT and 3T MRI including short-tau inversion recovery (STIR) and T1-weighted sequences as well as a single echo UTE sequence were acquired of the spine of 30 patients and evaluated for semiquantitative and quantitative morphological features of fractures and degenerative changes. During post-processing single echo Dixon-like water and fat images as well as CT-like susceptibility-weighted images were reconstructed from the UTE. Two radiologists evaluated morphological features on CT and MR images. Agreement between the modalities was assessed using weighted Cohen's κ.
Results: Of 54 fractures detected, 21 were identified as being acute fractures in the STIR and T1w sequence, and 19 by UTE water and fat-only reconstructions (κ 0.86 [95 % confidence interval 0.56–1.00] and κ 0.75 [0.46–1.00]). For morphological assessment of fractures and degenerative changes, the agreement between UTE-derived CT-like and CT images was substantial to excellent (Genant: κ 0.77 [0.48–1.00]; AO/Magerl: κ 0.75 [0.28–1.00]; Osteophytes: κ 0.78 [0.49–1.00]; Sclerosis: κ 0.74 [0.34–1.00]). Overall inter-reader agreement was substantial to almost perfect (κ 0.86 [0.65–1.00]).
Discussion: Detection of vertebral fractures as well as the morphological assessment of fractures and degenerative bone changes was feasible and accurate using a single-echo UTE sequence with water- and fat-Dixon reconstructions as well as CT-like images derived from the same sequence.
Conclusion: Acquiring all diagnostic important information from one sequence could be highly useful in clinical routine, since it could potentially replace STIR, T1w as well as a CT for initial assessment of certain spine pathologies, thus substantially reducing overall examination durations and radiation exposure.

[273] Utility of drug-eluting Coroflex ISAR stent in intracranial atherosclerotic disease: a single center experience in 147 patients

Amgad El Mekabaty[1*], Victoria Hellstern[1], Marta Aguillar Perez[1], Hans Henkes[1]

[1]Katharinenhospital Stuttgart Klinik für Diagnostische und Interventionelle Neuroradiologie, Stuttgart, Germany

Introduction: Intracranial atherosclerotic disease (ICAD) is a major cause of stroke and particularly recurrent strokes worldwide. Different treatment regimen for ICAD, including medical treatment (e. g. dual antiplatelet inhibition) and endovascular treatment (e. g. balloon- and stent angioplasty). In this study we aim to investigate the safety and efficacy of the drug-eluting balloon-mounted Coroflex ISAR stent in treatment of ICAD.
Methods: A retrospective analysis of patients with attempted implantation of Coroflex ISAR stent suffering from ICAD in our institution from 2014 to 2020 was performed. Available demographic, angiographic, imaging and follow-up data were analyzed.
Results: A total of 147 patients were included (74.1 % males, average age: 70 years). Median baseline modified Rankin score (mRS) was 0 (IQR 0–1) and median pretreatment mRS was 2 (IQR 1–4). Treated Lesions were located in the ICA (42.9 %), V4 segment (36.1 %), basilar artery (12.2 %) and M1 segment (8.8 %). The stent was successfully implanted in 92.6 % (137/147) and the vessel stenosis was reduced from a mean of 76 % "range 50–99" to 36 % "range 0–82". Short-term follow-up was available in 77.7 % after a median of 3 months "IQR 1–5" and long-term follow-up was available in 63.3 % (93/147) after a median of 24 months "IQR 14–40". In-stent stenosis occurred in 13.9 % (16/115), recurrent stroke in 9.5 % (11/115) and asymptomatic intracranial hemorrhage in 3.4 % (5/147). Overall mortality was 4.1 % (6/147), of which 50 % (3/6) were in-hospital and 50 % (3/6) on follow-up.
Discussion: Treatment of ICAD remains controversial. While, aggressive medical management, including dual antiplatelet inhibition and tight control of blood pressure and cholesterol level, is the standard of care, our data show an acceptable outcome of Coroflex ISAR for ICAD.
Conclusion: The drug-eluting, balloon-mounted Coroflex ISAR is a safe and effective treatment option for ICAD. The overall recurrent stroke rate was 9.5 % and mortality was 4.1 %. Further work is needed to better delineate eligible ICAD patients for intracranial stenting.

References

1. Ye G, et al. Efficacy and safety of drug-eluting stent for the intracranial atherosclerotic disease: A systematic review and meta-analysis. J Clin Neurosci. 2019;59:112–8.
2. Vajda Z, et al. Treatment of intracranial atherosclerotic disease with a balloon-expandable paclitaxel eluting stent: procedural safety, efficacy and mid-term patency. Clin Neuroradiol. 2012;22(3):227–33.

[274] Developments in stent-retriever technology and their potential impact on safety and effectiveness in mechanical thrombectomy of large vessel occlusion stroke

Marius Vogt[1*], Alexander Kollikowski[1], Jörn Feick[1], Marc Strinitz[1], Franziska Weidner[1], Fabian Essig[2], Hermann Neugebauer[2], Karl Georg Häusler[2], Mirko Pham[1], Alexander März[1]

[1]Institut für diagnostische und interventionelle Neuroradiologie, Universitätsklinikum Würzburg, Würzburg, Germany
[2]Neurologische Klinik und Poliklinik, Universitätsklinikum Würzburg, Würzburg, Germany

Background: To investigate whether current developments in stent retriever technology have an impact on effectiveness and safety in mechanical thrombectomy (MT) of large vessel occlusion (LVO) stroke.
Methods: Retrospective data analysis of consecutive patients with LVO stroke treated with MT using either the APERIO® or the new generation APERIO® Hybrid stent-retriever device in the University hospital Würzburg between 01/19 and 09/20. Primary effectiveness endpoint was successful recanalization (mTICI ≥2b), primary safety endpoint was occurrence of hemorrhagic complications after MT.
Results: We enrolled 298 consecutive patients: 148 patients (49.7 %) treated with AP device vs. 150 patients (50.3 %) treated with new generation APH device. In the APH group, the pre-interventional ASPECT score was lower and there was a higher proportion of occlusions in the posterior circulation. In the AP group, more patients received stenting of the internal carotid artery. Other baseline characteristics were without significant differences. Rates of successful recanalization were not different between both groups (86.5 % for AP vs. 82.7 % for APH; $p=0.361$) but postinterventional hemorrhage, particularly subarachnoid hemorrhage (AP: 44 [29.7 %] vs. APH: [16.0 %]; $p=0.005$) occurred significantly less frequent in the APH group. Rates of postinterventional hemorrhage with associated clinical deterioration (sICH) and in domo mortality were not statistically different between groups.
Discussion: Both the APERIO® and the APERIO® Hybrid achieved high rates of successful recanalization (mTICI≥2b) in MT of LVO. Detection of hemorrhage on the post-interventional CT scan regardless of its clinical relevance was significantly less frequent in the group treated with the new generation APH. This may be associated in part with refinements of the stent-retriever device, that come with better visibility under fluoroscopy. But when it comes to evaluation of post-interventional hemorrhage after MT, the clinical/neurological course of the patient has to be taken into consideration. By applying different definitions of sICH concomitant with clinical deterioration we found no statistical differences between the two groups.
Conclusion: Technological developments and refinements of new generation stent-retriever devices did not alter typical observational indicators of effectiveness but may have a positive impact on safety.

[275] Risk for additional infarction in emergency carotid artery endarterectomy in thrombectomy acute stroke patients

Ehsan Yousefian Jazi[1]*, Martin Wiesmann[1], Arno Reich[2], Alexander Gombert[3], Drosos Kotelis[3], Omid Nikoubashman[1]

[1]Uniklinik RWTH Aachen, Klinik für diagnostische und Interventionen Neuroradiologie, Aachen, Germany
[2]Uniklinik RWTH Aachen, Klinik für Neurologie, Aachen, Germany
[3]Uniklinik RWTH Aachen, Klinik für Gefäßchirurgie, Aachen, Germany

Background: Thromboembolic occlusion of the middle cerebral artery (MCA) with tandem occlusion of the internal carotid artery (ICA) is a life-threatening condition with unfavorable neurological outcome. We perform emergency carotid endarterectomy (CEA) in the same anesthesia session as thrombectomy in our angiography suite whenever needed, despite the absence of electrophysiological neuromonitoring and selective shunt.
Methods: We evaluated 47 thrombectomy patients with emergency CEA in our clinic between June 2013 and November 2020. To determine whether there were additional infarctions due to the surgical procedure, we assessed the initial diagnostic CT imaging for previously infarcted areas, cerebral perfusion, and vascular anatomy, including collateralization in the Circle of Willis (CoW). We then analyzed follow-up imaging with respect to new infarctions that could not be explained by the initial stroke.
Results: Five of 47 (11 %) patients had a complete CoW. There was contralateral internal carotid artery (ICA) stenosis or occlusion in 18/47 (38 %) patients. Surgical procedure was eversion CEA in 34 (72 %) and with a patch graft CEA in 13 (28 %) cases. Shunts were used during surgery in 17/47 (36 %) patients. Two patients suffered from an additional infarction in a new territory, however this was due to embolism during cerebral thrombectomy. The final infarction size was significantly larger in patients with contralateral ICA stenosis or occlusion ($p=0.038$). Neither CoW anatomy nor the absence of a shunt during surgery could be identified as risk factors for additional infarction.
Conclusion: Emergency surgery in the angiography suite without neuromonitoring did not lead to additional stroke risk in our study.

[280] Clinical outcome after endovascular thrombectomy in 3 Triage concepts: a prospective, observational study (NEUROSQUAD)

Fatih Seker[1]*, Jens Fiehler[2], Markus Möhlenbruch[1], Friederike Heimann[1], Christian Herweh[1], Fabian Flottmann[2], Peter Arthur Ringleb[3], Götz Thomalla[4], Thorsten Steiner[5], Christoffer Kraemer[6], Caspar Brekenfeld[2], Martin Bendszus[1]

[1]Neuroradiologie, Universitätsklinikum Heidelberg, Germany
[2]Neuroradiologie, Universitätsklinikum Hamburg-Eppendorf, Germany
[3]Neurologie, Universitätsklinikum Heidelberg, Germany
[4]Neurologie, Universitätsklinikum Hamburg-Eppendorf, Germany
[5]Neurologie, Klinikum Frankfurt-Höchst, Germany
[6]Neurologie, Klinikum Lüneburg, Germany

Background: NEUROSQUAD is a prospective, observational, bicenter study comparing 3 triage pathways in endovascular stroke treatment: mothership, drip and ship (DS) and transferring a neurointerventionalist to a remote hospital for thrombectomy (drive the doctor [DD]).
Methods: Patients with anterior circulation stroke and premorbid mRS 0–3 that underwent thrombectomy within 24 h after stroke onset were included. Primary outcome measure was good clinical outcome defined as 90 day mRS 0–2 or clinical recovery to the status before stroke onset (i. e. equal premorbid mRS and 90 day mRS). Secondary outcome measures were successful reperfusion, NIHSS at discharge and mRS shift.
Results: In total, 360 patients were included in this study, of which 111 patients (30.8 %) were in the mothership group, 204 patients (56.7 %) were in the DS group, and 45 patients (12.5 %) were in the DD group. Good clinical outcome was achieved similarly in all three groups (mothership 45.9 %, DS, 43.1 %, DD 40.0 %, $p=0.778$). Likewise, frequency of successful reperfusion was similar in all three groups (mothership 86.5 %, DS 85.3 %, DD 82.2 %, $p=0.714$). There was no significant difference among the groups regarding NIHSS at discharge ($p=0.115$) and mRS shift ($p=0.342$). In the multivariate analysis, triage concept was not an independent predictor of good outcome (unadjusted odds ratio 0.89, confidence interval 0.64–1.23, $p=0.479$).
Discussion: Our data suggest that clinical outcome after thrombectomy is similar in mothership, DS and DD.
Conclusion: Hence, "drive the doctor" can be a valuable triage option in acute stroke treatment.

[281] CT-like MR-derived images for the assessment of craniosynostosis and further pathologies of the skull in children

Yannik Leonhardt[1*], Sophia Kronthaler[1], Dimitrios C. Karampinos[1], Benedikt J. Schwaiger[2], Georg Feuerriegel[1], Marcus R. Makowski[1], Inga K. Koerte[3, 4], Thomas Liebig[5], Klaus Wörtler[1], Marc-Matthias Steinborn[6], Alexandra S. Gersing[1, 5]

[1]Department of Radiology, Klinikum rechts der Isar, Technical University of Munich, Munich, Germany
[2]Department of Neuroradiology, Klinikum rechts der Isar, Technical University of Munich, Munich, Germany
[3]Psychiatric Neuroimaging Laboratory, Brigham and Women's Hospital, Harvard Medical School, Boston, United States

Fig. 1 | 281 Axial T1SGRE MR-sequence of a 5-months-old male patient with a metopic synostosis and trigonocephalus (**a** and **b**) and a 6-months-old male with a patent metopic suture (**c**)

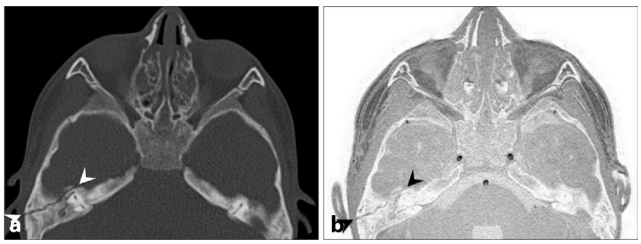

Fig. 2 | 281 Axial CT (**a**) and axial T1SGRE sequence (**b**) of a 6-year-old patient with a fracture of the right temporal bone (indicated by the *arrows*). The inverted MR-image shows the CT-like impression of the osseous structures

[4]Department of Child and Adolescent Psychiatry, Psychosomatic, and Psychotherapy, University Hospital of Munich (LMU), Munich, Germany
[5]Department of Neuroradiology, University Hospital of Munich (LMU), Munich, Germany
[6]Department of Pediatric Radiology, Städtisches Klinikum Munich Schwabing, Munich, Germany

Background: To evaluate the diagnostic value of CT-like images derived from a 3D T1w spoiled gradient echo (T1SGRE) MRI sequences for the detection and assessment of craniosynostosis and other pathologies of the pediatric skull.
Methods: In 20 patients with suspected craniosynostosis (mean age: 1.26 ± 1.38 years, 10 females), 3-T MR imaging was performed including CT-like images derived from a 3D T1SGRE sequence. Additionally, the skull of all patients was assessed for pathologies using either a radiograph, CT or ultrasound. The features overall image quality, contrast of bone and soft tissue, deformities, craniosynostosis and other pathologies of the skull were evaluated by two radiologists, blinded to the clinical information. Interrater agreement was calculated using Cohen's κ.
Results: Of the 20 patients included in this study, 8 patients had a metopic, 4 a coronal and 2 a sagittal synostosis. Two patients showed a complex combination of craniosynostoses as manifestation of the Crouzon syndrome. One patient presented with a "ping pong" skull fracture and one patient with a fracture of the temporal bone. The affected synostotic sutures could be identified in all patients. Interrater agreement for rating the calvarial sutures was high (κ = 0.81 [95 % confidence interval 0.70–1.00]).
Discussion: The assessment of craniosynostosis, sutures and fractures of the pediatric skull using the CT-like T1SGRE MR-sequence was feasible and comparable to other imaging modalities.
Conclusion: The MRI protocol with the T1 GRE-sequence used in this study poses a promising alternative to CT when imaging children with suspected or confirmed craniosynostosis or fractures.

References

1. Saarikko, et al. Comparison of Black Bone -MRI and 3D--CT in the preoperative evaluation of patients with craniosynostosis. J Plast Reconstr Aesthetic Surg. 2020;73(4):723–31.
2. Gersing, et al. Evaluation of -MR-derived -CT-like images and simulated radiographs compared to conventional radiography in patients with benign and malignant bone tumors. Eur Radiol. 2019;29(1):13–21.

[282] Prediction accuracy of Derivo Embolization Device implanted length with PreSize neurovascular and comparison of device size selection between conventional manual planning and software simulations

Ngoc Tuan Ngo[1*], Fabian Flottmann[1], Francesco Iori[2], Mirko Bonfanti[2], Katerina Spranger[2], Jens Fiehler[1], Maxim Bester[1]

[1]Universitätsklinikum Hamburg-Eppendorf, Klinik und Poliklinik für Neuroradiologische Diagnostik und Intervention, Hamburg, Germany
[2]Oxford Heartbeat Ltd, London, United Kingdom

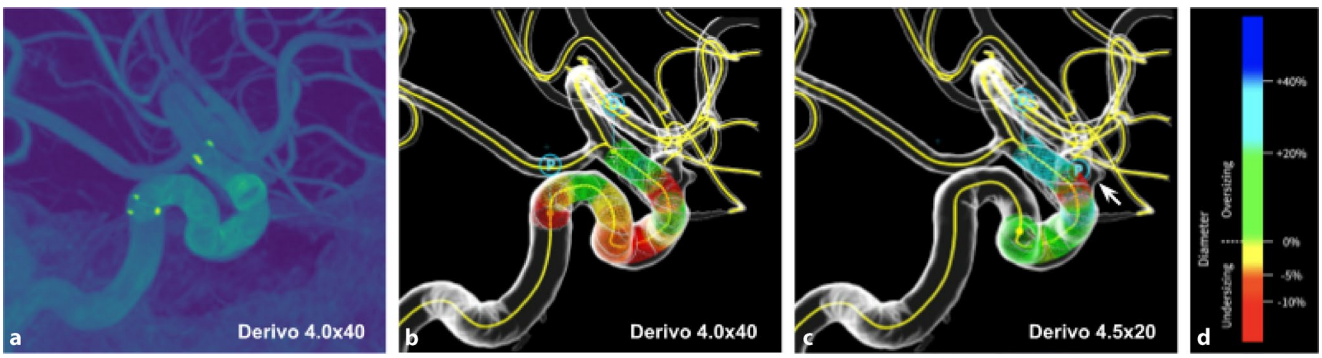

Fig. 1 | 282 (**a**) Maximum intensity projection of a pre-operative 3DRA co-registered with a post-operative VasoCT showing the deployed FD (Deriva 4.0 × 40: nominal length: 4.0 mm, nominal diameter: 40 mm). (**b**) Same FD deployed in the same case study using PreSize Neurovascular, showing an excellent comparison with the clinical data. (**c**) Optimal device (Deriva 4.5 × 20) chosen for the same case with the aid of PreSize Neurovascular. The shorter length of the optimal device led to a lower number of vessel bends covered by the device, while providing sufficient aneurysm coverage (*white arrow*). (**d**) Color-bar of the FD colouring in PreSize, indicating the oversizing of the stent diameter relative to the diameter of the blood vessel

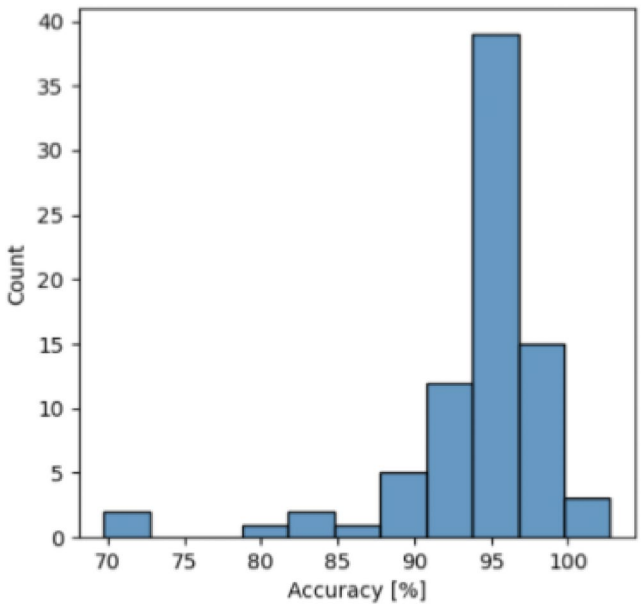

Fig. 2 | 282 Distribution of the deployment accuracy

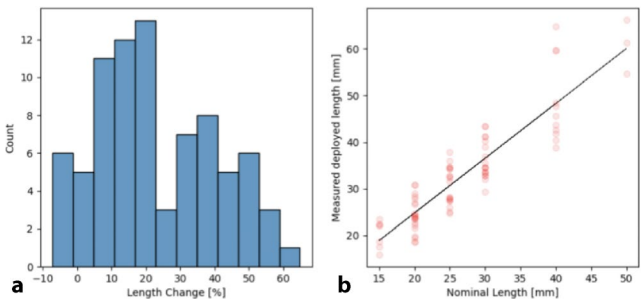

Fig. 3 | 282 (**a**) Distribution of relative length change between the measured deployed length and the nominal stent length, (**b**) linear regression between the measured deployed length and the stent nominal length

Background: Evaluating the final length and positioning of flow diverting (FD) stents inside patient arteries for optimal device size selection remains a challenging, yet crucial, task in complex aneurysm treatment. This study reports the accuracy of PreSize Neurovascular software in predicting FD deployed length and impact of PreSize's use on device size selection. PreSize (Oxford Heartbeat Ltd) is a visualisation/simulation software for neurovascular FD intervention planning in aneurysm treatment.
Methods: Imaging data from 80 FD cases using Derivo Embolisation Device (Acandis GmbH), collected from University Medical Center Hamburg-Eppendorf, were retrospectively analysed. Prediction accuracy was defined as agreement between PreSize simulation and actual deployed FD length measured in angiography. Two experienced interventional neuroradiologists (INRs), blinded to post-deployment angiographies, selected optimal sizes using PreSize in a subset (25 cases). PreSize-informed device choices (diameter/length) were compared to deployed devices (informed by conventional planning).
Results: Investigated FDs had a mean nominal length of 26.9 mm (15–50 mm). Mean change of 23 % (up to 62 %) was observed between actual deployed and nominal FD length. PreSize predicted deployed FD length with a mean accuracy of 94 % (95 % confidence interval [93 %, 95 %]). PreSize-informed devices were shorter (Wilcoxon signed-rank test, $Z = 27.5$, $p < 0.01$) by 6.6 mm on average (up to 25 mm) compared to conventionally chosen devices. In 35 % of cases, shorter PreSize-informed devices would have resulted in fewer FD-covered vessel bends while achieving sufficient aneurysm coverage. In 70 % of cases, PreSize's automatic size suggestion was INR's selection.
Discussion: Discrepancy between nominal and deployed FD length illustrates the sizing challenge with conventional planning. Conventionally choosing longer devices might prevent undersizing but could lead to inserted metal unnecessary for aneurysm coverage.
Conclusion: PreSize predicted deployed FD lengths with high accuracy. Results indicate INRs' propensity to select shorter devices with PreSize, supported by its precise deployment simulation and visualisation.

[287] Vertebral bone marrow T2*mapping using chemical shift encoding-based water-fat separation in the quantitative analysis of lumbar osteoporosis and osteoporotic fractures

Yannik Leonhardt[1*], Florian T. Gassert[1], Georg Feuerriegel[1], Felix G. Gassert[1], Sophia Kronthaler[1], Christof Boehm[1], Alexander Kufner[1], Stefan Ruschke[1], Thomas Baum[2], Claus Zimmer[2], Marcus R. Makowski[1], Dimitrios C. Karampinos[1], Benedikt J. Schwaiger[2], Alexandra S. Gersing[1 3]

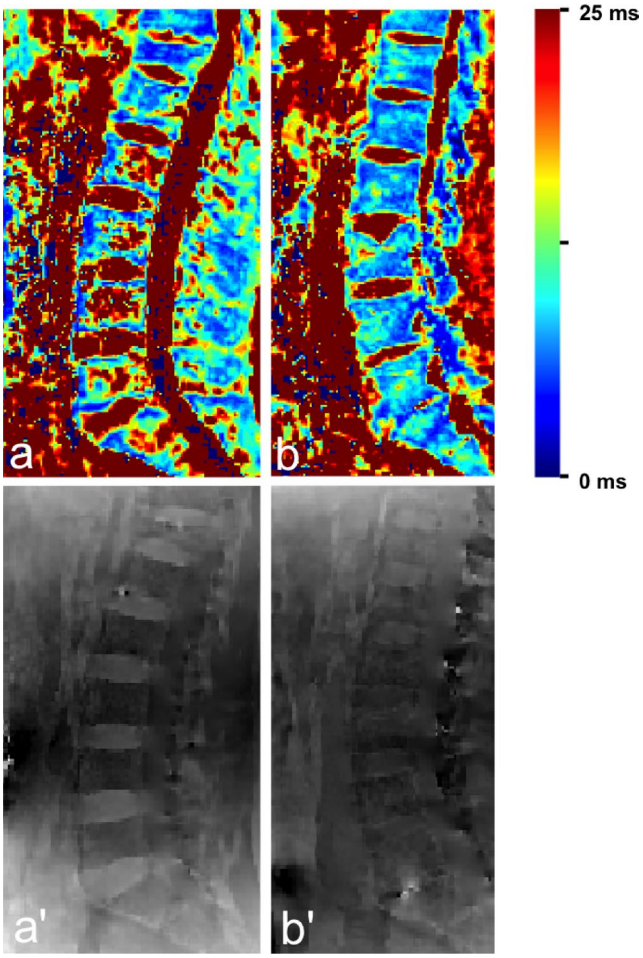

Fig. 1 | 287 Color-coded T2* maps of the thoracolumbar spine of a 70-year-old female patient with a low-energy fracture of Th12 (**a**) and a 49-year-old male patient with a high-energy fracture of L3 (**b**). Panels **a'** and **b'** show the corresponding B0 field maps

[1]Department of Radiology, Klinikum rechts der Isar, Technical University of Munich, Munich, Germany
[2]Department of Neuroradiology, Klinikum rechts der Isar, Technical University of Munich, Munich, Germany
[3]Department of Neuroradiology, University Hospital of Munich (LMU), Munich, Germany

Background: Chemical shift encoding-based water-fat separation techniques have been used for fat quantification, but they also enable the assessment of bone marrow T2*, which has previously been reported to be a potential biomarker for osteoporosis and may give insight into the cause of vertebral fractures (i.e. osteoporotic vs. traumatic).
Methods: The 32 patients (78.1 % with low-energy fractures, mean age 72.3 ± 9.8 years, 76 % women; 21.9 % with high-energy traumatic fractures, 47.3 ± 12.8 years, no women) were frequency-matched for age and sex to subjects without vertebral fractures ($n = 20$). All patients underwent 3T-MRI of the lumbar spine including sagittally acquired spoiled gradient echo sequences for chemical shift encoding-based water-fat separation. BMD and trabecular bone parameters describing the three-dimensional structure of trabecular bone were derived from qCT.
Results: Mean T2* values of nonfractured vertebrae showed a significant correlation with BMD (r = –0.65, $p < 0.001$), trabecular number (TbN; r = –0.56, $p < 0.001$) and spacing (TbSp) (r = 0.61, $p < 0.001$); patients with low-energy fractures showed significantly higher mean T2* values than those with traumatic fractures (13.6 ± 4.3 ms vs. 8.4 ± 2.2 ms, $p = 0.01$) and a significantly lower TbN (0.69 ± 0.08 mm^{-1} vs. 0.93 ± 0.03 mm^{-1}, $p < 0.01$) and a significantly larger TbSp (1.06 ± 0.16 mm vs. 0.56 ± 0.08 mm, $p < 0.01$). When comparing the mean T2* of the fractured vertebrae, no significant difference could be detected between low-energy and high-energy fractures (12.6 ± 5.4 ms vs. 8.1 ± 2.4 ms, $p = 0.10$).
Discussion: T2* mapping of vertebral bone marrow using CSE-MRI allows for assessing osteoporosis as well as the trabecular microstructure.
Conclusion: T2* mapping enables a radiation-free differentiation between patients with low-energy osteoporotic and high-energy traumatic vertebral fractures, suggesting its potential as a biomarker for bone fragility.

References

1. Wu, et al. Correlation of bone mineral density with MRI T2* values in quantitative analysis of lumbar osteoporosis. Arch Osteoporos. 2020;15(1):18.
2. Schmeel, et al. Quantitative evaluation of T2* relaxation times for the differentiation of acute benign and malignant vertebral body fractures. Eur J Radiol. 2018;108:59–65.

[289] Region-specific ASPECTS ratings of 100 investigators from the TENSION study: hypodensity thresholds and decision spread

Helge Kniep[1*], Noel van Horn[1], Gabriel Broocks[1], Lukas Meyer[1], Fabian Flottmann[1], Matthias Bechstein[1], Jens Fiehler[1], Uta Hanning[1], Andre Kemmling[2]

[1]Klinik und Poliklinik für Neuroradiologische Diagnostik und Intervention, Universitätsklinikum Hamburg-Eppendorf, Hamburg, Germany
[2]Klinik für Neuroradiologie, Westpfalzklinikum-Kaiserslautern, Kaiserslautern, Germany

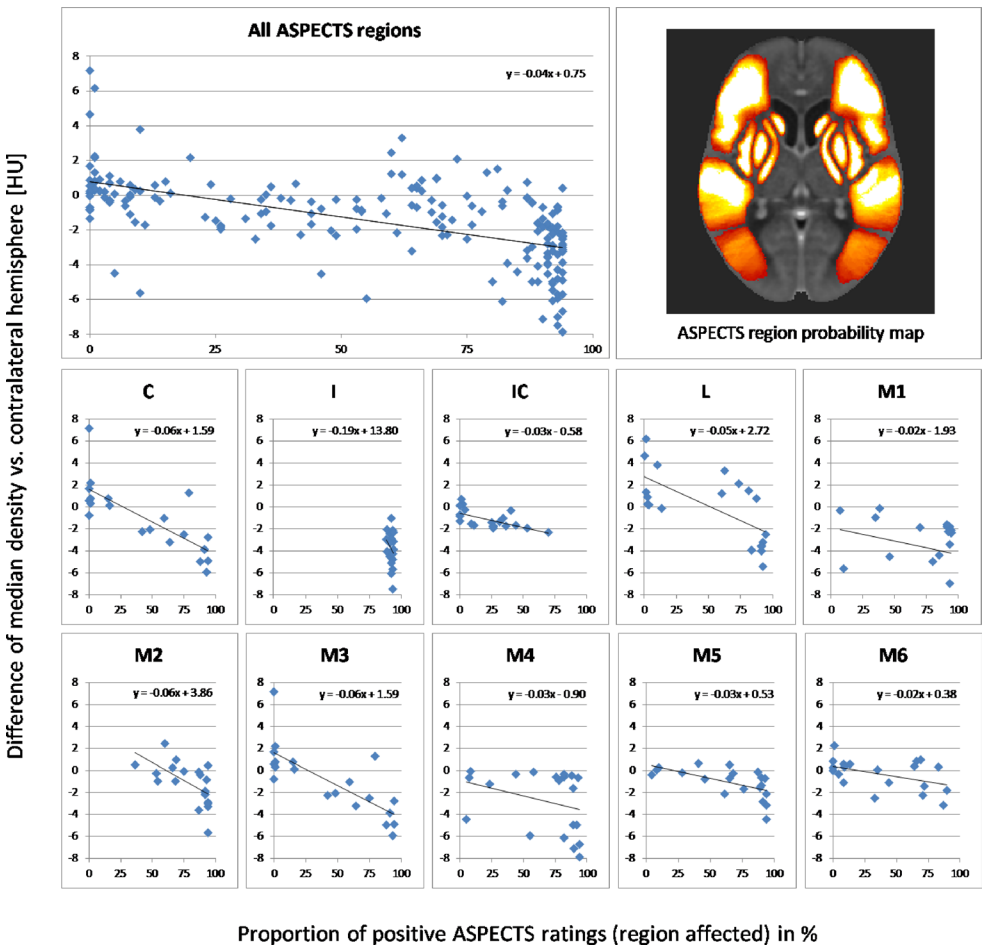

Fig. 1 | 289 Median hypodensity (HU) vs. share of positive ratings (ischemic changes)

Introduction: Patients with acute ischemic stroke are often triaged according to the Alberta Stroke Program Early CT Score (ASPECTS). ASPECTS is assessed for therapeutic decision making and as inclusion criterion for clinical trials. However, studies have shown relatively low interrater reliability [1]. We aim to establish a better understanding of quantitative thresholds and spread in human visual ASPECTS assessments.
Methods: We analyzed ASPECTS ratings of 100 investigators who independently evaluated 20 NCCT scans as part of the TENSION study. Quantitative assessment of early signs of infarctions was performed through measuring the density difference of each ASPECTS region compared to the contralateral hemisphere in median Hounsefield Units (HU). The proportion of raters who evaluated a specific region as affected was plotted against the median hypodensity in HU and linear regression analysis was performed.
Results: We observed a significant linear relationship between the median hypodensity and the probability for raters to evaluate a region as affected. For all ASPECTS regions combined, a decrease of 0.4 HUs vs. the contralateral hemisphere resulted in an increase of 10 % of infarction ratings ($p<0.001$, $R^2=0.32$, Fig. 1). The plot shows that for the majority of regions the proportion of positive ratings was located in the continuum between 0 % and 100 %. It furthermore suggests a relatively broad distribution which might be due to region-specific effects.
Discussion: Our study shows a significant relationship between the degree of hypodensity and the proportion of positive (region is affected) ratings. The observed continuum between 0 % and 100 % positive ratings confirms the relatively low interrater reliability. Region specific patterns were observed with different sensitivities for quantitative density alterations. In addition, these patterns suggest different levels of rater confidence depending on the anatomic region and the region-specific assumed a-priori probability for ischemic affection.
Conclusion: Our results enhance the understanding of visual ASPECTS ratings. More objective decision making through establishing of specific hands-on guidelines for improved visual ASPECTS readings might increase reliability of clinical trials and patient benefit in clinical practice.

References

1. van Horn N, et al. ASPECTS Interobserver Agreement of 100 Investigators from the TENSION Study. Clin Neuroradiol. 2021

[290] Safety and clinical outcome after endovascular treatment of aneurysmal subarachnoid hemorrhage since the evolution of the EVT devices in a 14-year series from a single high-volume center

Ali Khanafer[1*], Marta Aguilar Perez[1], Victoria Hellstern[1], Hansjörg Bäzner[2], Oliver Ganslandt[3], Hans Henkes[1]

[1]Katharinenhospital Stuttgart, Neuroradiologie, Stuttgart, Germany
[2]Katharinenhospital Stuttgart, Neurologie, Stuttgart, Germany
[3]Katharinenhospital Stuttgart, Neurochirurgie, Stuttgart, Germany

Background: Endovascular treatment (EVT) of ruptured cerebral aneurysms has evolved significantly over the past 15 years with the rapid development of new treatment modalities and devices, such as flow diversion or bifurcation stents. We sought to evaluate the safety and outcome of EVT, especially after the use of the new devices in the treatment of ruptured aneurysms, based on a 14-year series from a single center with EVT-first strategy.
Methods: We retrospectively studied all patients with aneurysmal subarachnoid hemorrhage (aSAH), managed in a single center between 2007 and 2020 and divided them into a conservative, microsurgical (MSC), and an EVT group according to treatment decision and requirements. Clinical and radiological findings at admission, discharge, and after long-term follow-up were studied. Since several new devices were mainly introduced from 2012 in the treatment of aSAH, the outcome was compared between four groups of treated patients, namely MSC and EVT before and after 2012.
Results: A total of 983 patients with aSAH were studied (694 EVT, 205 MSC, 84 conservative). There were no significant differences in mean age or the Hunt and Hess grades between the four groups. The rate of EVT of ruptured aneurysms increased after 2012 from 67 % to 72.2 %, the MSC and conservative groups showed a slight decrease after 2012 from 23 % to 19.7 % and from 9.6 % to 8 %, respectively. There was no significant difference in clinical outcomes between the MSC groups before and after 2012. Both EVT groups showed a favorable and comparable outcome at discharge; more than 50 % of aSAH patients were discharged with an mRS 0–2 (51 % 2007–11 and 55.3 % 2012–20). The long-term outcome of both EVT groups shows a significant decrease of morbidity (mRS 3–5) after 2012 from 25.9 % to 18.3 % ($p=0.015$); mortality was comparable. Retreatment rates were higher in EVT than in MSC regardless of time periods.
Discussion: Our data show that the introduction of the new EVT devices and techniques allows the treatment in aneurysms that were not treatable with coiling alone, MSC, or both, while providing a good outcome.
Conclusion: With the introduction of new endovascular devices, EVT treatment continues to offer an excellent safety profile and good outcomes

[293] In-vitro-Analyse der Zusammensetzung definierter Thromben mittels spektraler Computertomographie-Bildgebung

Julia Rozanka[1*], Nico Münnich[1], Ana Moya[2], Stephanie Ritter[1], Stefan Rohde[1]

[1]Klinikum Dortmund gGmbH, Klinik für Radiologie und Neuroradiologie, Dortmund, Deutschland
[2]Department of Business Intelligence and Data Science, Dortmund, Deutschland

Hintergrund: In der endovaskulären Therapie des ischämischen Schlaganfalls ist der histologische Aufbau der Thromben potenziell wichtig. Die spektrale Computertomographie (CT) mit dem Dual-Energy-Prinzip erlaubt die Unterscheidung von Geweben durch spezifische Analyse der materialeigenen keV-Absorption. In der vorliegenden Studie sollte anhand der Analyse von künstlichen Thromben mit definierten Erythrozyten- („red blood cells“, RBC) und Fibrinanteilen die Machbarkeit und Genauigkeit der spektralen CT-Bildgebung in der Thrombusbestimmung untersucht werden.
Methoden: Unter In-vitro-Bedingungen wurden 5 Gruppen von Schafsblutthromben mit definierten RBC- (<5 %–100 %) und Fibrinanteilen (>95 %–0 %) verwendet. Diese wurden mit einem spektralen Computertomographen mit kV-Switch-Technik (40 bis 140 keV) gescannt. Die Dichtewerte wurden dabei in Hounsefield Units gemessen, woraufhin spezifische Absorptionskurven erstellt werden konnten. Ein statistischer Vergleich erfolgte paarweise mit dem Kolmogorow-Smirnow-Test.
Ergebnisse: Die Absorptionskurven zeigten einen exponentiellen Abfall der Dichtewerte im Bereich zwischen 40 keV und 75 keV (Abb. 1). Die Differenzierbarkeit der Gruppen nahm mit hohen keV-Werten (ab ca. 80 keV) stetig zu. Statistisch signifikante Unterschiede zeigten die Absorptionskurven von Thromben der Gruppe 2 und 3 (p-Wert <0,05), der Gruppe 3 und 4 (p-Wert <0,001) sowie der Gruppe 4 und 5 (p-Wert <0,01). Die Unterscheidung von Thromben der Gruppe 1 und 2 war nicht zuverlässig.
Diskussion: Mittels der spektralen CT mit kV-Switch-Technik können spezifische spektrale Absorptionskurven für jede Thrombusgruppe erstellt werden. Somit kann theoretisch der RBC-Anteil eines Thrombus CT-morphologisch abgeschätzt werden. Ein neuer Aspekt dieser Studie ist die Analyse des gesamten keV-Spektrums und die Erstellung von Absorptionskurven, was die Differenzierung der Thromben er-

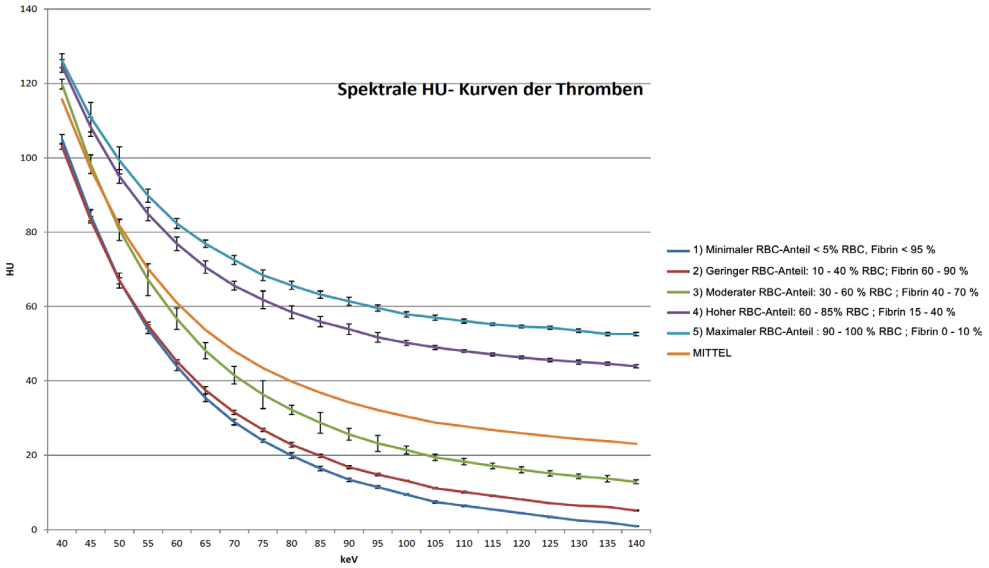

Abb. 1 | 293 Spektrale Absorptionskurven der Thrombusgruppen

leichtern soll. Die Kenntnis über die Histologie vor der Intervention ermöglicht die gezielte Materialwahl zur Therapieoptimierung bei unterschiedlichen mechanischen Thrombuseigenschaften je nach Aufbau.
Fazit: Mit der spektralen CT mit kV-Switch-Technik können Thromben mit einem definierten Anteil von RBC und Fibrin differenziert werden. Die bestmögliche Unterscheidung erfolgt bei Thromben mit einem RBC-Anteil von >40 % sowie auf Energieniveaus >80 keV. Diese Ergebnisse können als methodische Grundlage für weitere Studien mit dieser Technik dienen.

Autorenverzeichnis